9/26/95

SANDIA REPORT

SAND94–0244 • UC–814
Unlimited Release
Printed September 1995

Yucca Mountain Site Characterization Project

Stochastic Hydrogeologic Units and Hydrogeologic Properties Development for Total-System Performance Assessments

A. R. Schenker, D. C. Guerin, T. H. Robey, C. A. Rautman, R. W. Barnard

Prepared by
Sandia National Laboratories
Albuquerque, New Mexico 87185 and Livermore, California 94550
for the United States Department of Energy
under Contract DE-AC04-94AL85000

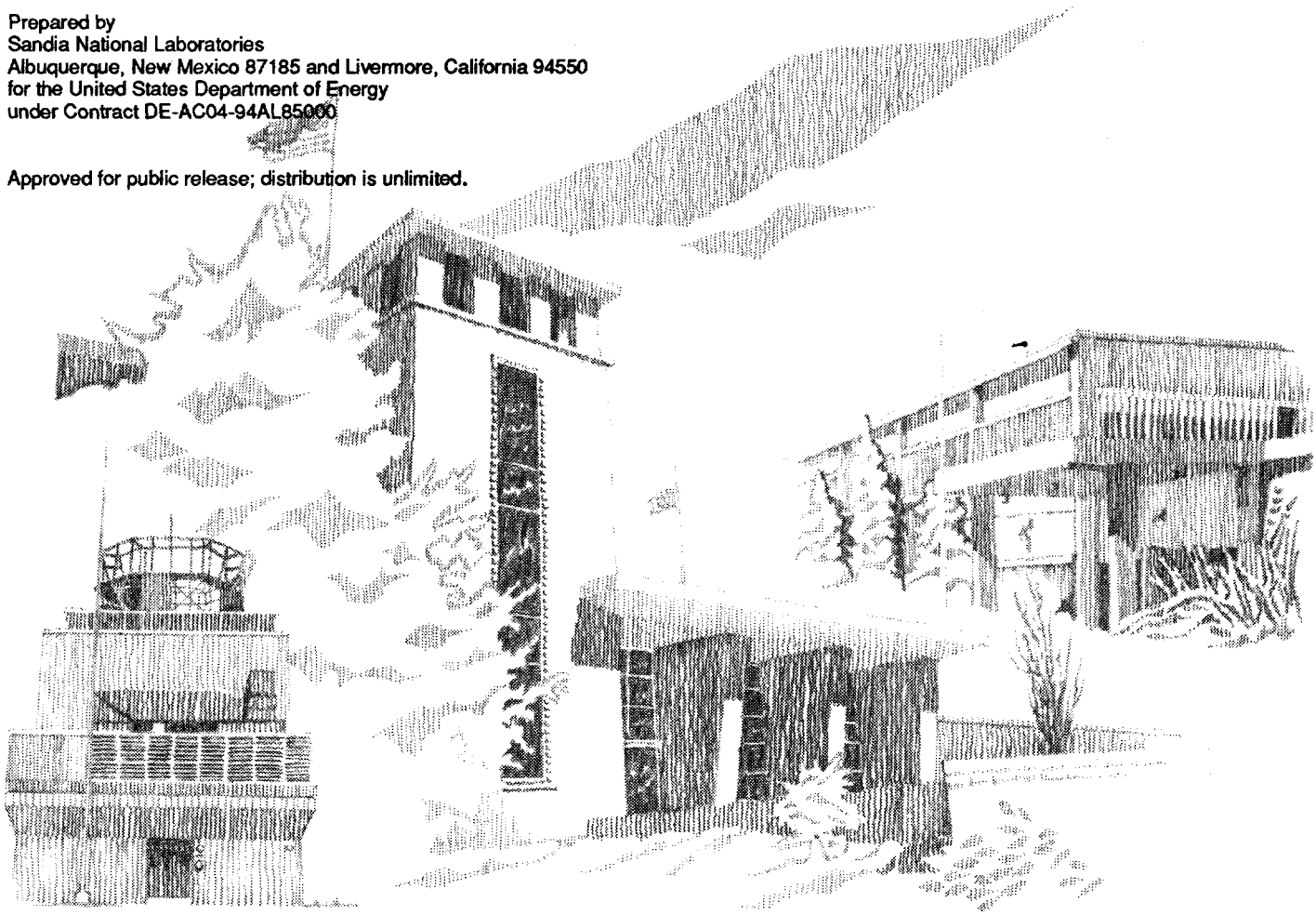

SF2900Q(8-81)

"Prepared by Yucca Mountain Site Characterization Project (YMSCP) participants as part of the Civilian Radioactive Waste Management Program (CRWM). The YMSCP is managed by the Yucca Mountain Project Office of the U.S. Department of Energy, DOE Field Office, Nevada (DOE/NV). YMSCP work is sponsored by the Office of Geologic Repositories (OGR) of the DOE Office of Civilian Radioactive Waste Management (OCRWM)."

Issued by Sandia National Laboratories, operated for the United States Department of Energy by Sandia Corporation.

Available to DOE and DOE contractors from
Office of Scientific and Technical Information
PO Box 62
Oak Ridge, TN 37831

Prices available from (615) 576-8401, FTS 626-8401

Available to the public from
National Technical Information Service
US Department of Commerce
5285 Port Royal Rd
Springfield, VA 22161

NTIS price codes
Printed copy: A09
Microfiche copy: A01

DISCLAIMER

Portions of this document may be illegible in electronic image products. Images are produced from the best available original document.

Distribution Category
UC-814

SAND94-0244

Unlimited Release
Printed September, 1995

STOCHASTIC HYDROGEOLOGIC UNITS AND HYDROGEOLOGIC PROPERTIES DEVELOPMENT FOR TOTAL-SYSTEM PERFORMANCE ASSESSMENTS

A. R. Schenker and D. C. Guerin
Los Alamos Technical Associates
Albuquerque, NM 87110

T. H. Robey
Spectra Research Institute
Albuquerque, NM 87102

C. A. Rautman
Geohydrology Department
R. W. Barnard
Yucca Mountain Project
System Performance Assessments Department
Sandia National Laboratories
Albuquerque, NM 87185

ABSTRACT

A stochastic representation of the lithologic units and associated hydrogeologic parameters of the potential high-level nuclear waste repository are developed for use in performance-assessment calculations, including the Total-System Performance Assessment for Yucca Mountain–SNL Second Iteration (TSPA-1993). A simplified lithologic model has been developed based on the physical characteristics of the welded and nonwelded units at Yucca Mountain. Ten hydrogeologic units are developed from site-specific data (lithologic and geophysical logs and core photographs) obtained from the unsaturated and saturated zones. The three-dimensional geostatistical model of the ten hydrogeologic units is based on indicator-coding techniques and improves on the two-dimensional model developed for TSPA-91. The hydrogeologic properties (statistics and probability distribution functions) are developed from the results of laboratory tests and in-situ aquifer tests or are derived through fundamental relationships.

Hydrogeologic properties for matrix properties, bulk conductivities, and fractures are developed from existing site specific data. Extensive data are available for matrix porosity, bulk density, and matrix saturated conductivity. For other hydrogeologic properties, the data are minimal or nonexistent. Parameters for the properties are developed as beta probability distribution functions. For the model units without enough data for analysis, parameters are developed as analogs to existing units. A relational, analytic approach coupled with bulk conductivity parameters is used to develop fracture parameters based on the smooth-wall–parallel-plate theory. An analytic method is introduced for scaling small-core matrix properties to the hydrogeologic unit scales.

This work was supported by the United States Department of Energy under Contract DE-AC04-94AL85000, and was performed under WBS 1.2.5.4.1

The data in this report were developed subject to the controls in QAGR S124212A, Revision 0, PCA 2.0, Task 2.1. The data are not to be used for licensing.

ACKNOWLEDGMENTS

The SNL94-0224 authors would like to thank all those individuals who contributed to the successful completion of this document. First and foremost we acknowledge the encouragement and direction of Holly Dockery of Sandia National Laboratories (SNL). Her interest and leadership were instrumental in the completion of this document and are greatly appreciated. Particular thanks go to Paul Kaplan, SNL, whose interest and expertise aided in the initial scoping and definition of the purpose and objectives for this analysis. The two primary customers and modelers for this analysis, Mike Wilson, SNL, and Jack Gauthier, Spectra Research, provided immensely helpful guidance and review of the data and parameter development for input to the TSPA models.

USGS personnel were extremely helpful during the evaluation and interpretation of the hydrogeologic properties. Alan Flint was most helpful in providing clarification and background information on porosity and conductivity data. Ed Weeks, Art Gelden, and Dave Apple provided background information that helped interpret the published barometric pumping data. Lennart Anderson provided background information on the range of values obtained for saturated hydraulic conductivity and the possibility of influence from microfracturing in drillhole UE25a #1. Additionally, Bob Nilson, S-Cubed, provided background information and clarification for the barometric-pumping section of the report.

The formal technical reviewers of this document were Lorraine Flint of FEC (now at USGS) and William Zelinski of Spectra Research. Their comments contributed to substantially improving this document. Significant review comments were also provided by the reviewers of TSPA-93 who referred to this document during their technical review. Laurence Costin, SNL, provided valuable comments with regards to the logical organization and technical discussion of the parameter development. Dwight Hoxie, USGS, provided comments that helped clarify and elaborate discussion on the Yucca Mountain hydrogeology and stratigraphy. Polly Hopkins provided numerous technical review comments that also helped clarify the technical content.

Leo Scully of Los Alamos Technical Associates provided critical review of the early draft of the document that provided substantial suggestions for improvement. Early editorial and format support were provided by Judith Reynolds and Barbara Gilles, also of Los Alamos Technical Associates. Dominic Martinez and Isaac Block of SNL contributed to the production of artwork and assembling the document.

CONTENTS

Section Page

FIGURES

TABLES

Table Page

ACRONYMS

CDF	cumulative distribution function
CV[x]	coefficient of variation
E*[x]*	expected value
GENISES	Geographic Nodal Information and Scientific Evaluation System
GWTT	Groundwater Travel Time
LHS	Latin Hypercube Sampler
Max*[x]*	maximum value
Min*[x]*	minimum value
OFR	Open File Report
PA	Performance Assessment
PAWDS	Performance Assessment Working Data Set
PDF	probability density function
SCV*[x]*	scaled coefficient of variation
SD	standard deviation
SEPDB	Site Engineering Properties Database
SNL	Sandia National Laboratories
TSPA	Total-System Performance Assessment
TSPA-91	TSPA, 1991 version
TSPA-93	TSPA, 1993 version
USGS	U.S. Geological Survey
YMP	Yucca Mountain Site Characterization Project

Note: Hydrologic parameter terms are defined in Table 3-1.

1.0 Introduction

The Yucca Mountain Site Characterization Project is evaluating the suitability of Yucca Mountain, Nevada as a site for a potential underground nuclear-waste repository. Evaluation of the long-term performance of an underground repository requires understanding the important natural processes, including those associated with groundwater and gas flow. These processes are modeled with varying degrees of sophistication, ranging from detailed process models to abstracted system-level performance-assessment (PA) models. Process models attempt to mechanistically describe phenomena such as unsaturated groundwater flow. The models for total-system performance assessment (TSPA) analyses are abstractions of the process models that try to capture the important features of the detailed models. The abstracted models are used in stochastic simulations to evaluate performance regulations. Examples of such regulations are the EPA repository post-closure system performance requirements given in 40 CFR Part 191 (EPA, 1985), or the geohydrology disqualifying condition (i.e., the groundwater travel time condition) in the DOE's site-suitability guidelines for geologic repositories given in 10 CFR 960 (DOE, 1984). Although the two cited regulations address different aspects of repository performance, they both will be resolved largely by groundwater-flow modeling.

The purpose of using stochastic models is to investigate the range of outcomes resulting from randomly selected sets of input values. This requires that the model parameters be expressed as ranges of values. Ranges for parameters can arise from two sources: One would expect that geologic properties would have an intrinsic variability. In addition, without an exhaustive sampling effort, there will also be uncertainties associated with unknown parameter values at the unsampled locations. Given our uncertainty in properties values, we try to develop parameter distributions from the properties data that reflect the probability that a value occurs within certain intervals. Normally, we want the parameters to be developed directly from basic data that are representative of the physical range that the properties actually encompass.

The parameters for the numerical hydrologic models range from observable properties data to derived quantities. These models rarely are equipped to accept hydrogeologic properties data directly as input. In most cases, many parameters (and large ranges of parameter values) are required by a model, and a simplified expression of data is necessary.

The model inputs require us to reduce numerous properties data while maintaining the variability and recognizing the uncertainty. To do this, the data are classified in some manner and are summarized in terms of probability density functions (PDFs). The PDFs reflect the probability that a value of a property occurs within a range. We define "properties" as the hydrologic characteristics described by the raw source data (the quantitative measurements). A "parameter" is the resulting statistical descriptive value derived from the properties data. The PDFs are then developed from the hydrogeologic parameters.

1.1 Prior parameter-development work

Prior groundwater-flow modeling efforts for performance assessments of Yucca Mountain have used limited site-specific data. PACE-90 (Barnard and Dockery, 1991) was a preliminary attempt to perform a total-system performance assessment with calculational models that used site data. PACE-90 developed deterministic hydrogeologic and associated parameters required for one- and two-dimensional flow and transport models.

The next performance assessment, TSPA-91 (Barnard *et al.*, 1992), used a limited amount of site data from the potential repository. Because TSPA-91 calculations made stochastic estimates of performance, the hydrogeologic parameters were described by PDFs. These parameters consisted of matrix and fracture properties from limited site-specific data.

Future iterations of performance assessments will have expanded and more sophisticated models of the processes occurring within the areas of interest. The modeling domains and model parameters therefore must be similarly enhanced. One of the needs recognized from previous performance-assessment analyses is the necessity of having more extensive site-specific data. Model parameters must reflect not only the variability inherent in the data but also the uncertainty in our estimations of the completeness of the data. In addition to considering not only variability of properties within a hydrogeologic unit, we must also model the uncertainty in the geometry of the unit. These steps have been undertaken in the work described here.

The first opportunity to provide enhanced parameters and modeling domains has been the recent total-system performance assessment (TSPA-93), (Wilson *et al.*, 1994). To meet the needs of this effort, we have developed a more comprehensive data set and a geostatistical rock model for use in stochastic analyses. Although this effort has directly provided information for TSPA-93, these data are available in a

general format and are intended to be available for application to similar analyses, such as the ongoing groundwater travel time (GWTT) effort.

1.2 Description of the current effort

In the process of developing the hydrogeologic parameter data base, we have applied new tools to the data-reduction process and have applied new models for interpretation of the properties data. In addition, the PDFs have been derived from the properties data in a more systematic and rigorous fashion.

The three-dimensional lithologic model of the site is based on the observed geological structure at Yucca Mountain. The model attempts to reflect the uncertainty in the geometry of the various lithologic units. The hydrogeologic units, for which the hydrogeologic parameters are determined, are identified from the lithologic components of the model. To improve the stochastic modeling we have also used geostatistical simulations to model variations in thicknesses of hydrogeologic units.

1.3 Approach

A modeling domain has been defined for which hydrogeologic units are developed. The hydrogeologic units are generated from a three-dimensional stochastic lithologic model; this model uses available data describing the degree of welding of the tuffs at limited locations. The model allows us to relate differences in rock types to differences in hydrologic properties so that the various properties values can be stochastically assigned to the modeling domain. The model reflects the uncertainties in knowledge of the degree of welding in areas where data have not been collected. Chapter 2 discusses the development of the lithologic model and the association of the hydrogeologic units with the lithologic components. Hydrogeologic parameters are assumed to depend strongly on the degree of welding of the tuffs comprising the geologic setting. The hydrogeologic model of Yucca Mountain has been constructed using degree of welding as the fundamental discriminator of the different units.

The hydrologic parameters required by the performance-assessment models depend on the choice of model. In general, the groundwater-flow models require parameters describing the hydrologic properties of the rock matrix (such as porosity, hydraulic conductivity, and water-retention behavior) and the hydrologic properties of the fractures (fracture spacing, hydraulic aperture, hydraulic conductivity, etc.). In addition, gas-flow models require bulk permeability and hydraulic con-

ductivity properties of the rock mass. Parameter development is discussed in detail in Chapter 3.

The origins of a large amount of the hydrogeologic data used for this document came from the Site Engineering Properties Data Base (SEPDB). The SEPDB was discontinued and transferred to the Yucca Mountain Site Characterization Project Office to become the core for the official project repository of site data, the Geographic Nodal Information and Scientific Evaluation System (GENISES). Although we started with information from the SEPDB, we also have made an extensive effort to identify additional geologic and hydrogeologic information available for Yucca Mountain. As data are identified, most have been assembled into a Sandia National Laboratories (SNL) performance-assessment working data set (PAWDS), which gives us the capability to locally format and prepare data for performance-assessment models. It is expected that the PAWDS and GENISES will remain closely coupled, with GENISES data included in the PAWDS and most of the new PAWDS data submitted to GENISES.

2.0 The Stochastic Lithologic Model

The modeling domain used for performance-assessment analyses is based upon a lithologic model. As performance-assessment analyses have evolved, the requirements for the model domain (and thus the lithologic model) have changed. TSPA-93 provided an opportunity to develop more sophisticated modeling capabilities. Of particular interest was increasing the realism of the performance-assessment model domain. (1) We have made an effort to represent the entire areal and vertical extent of the potential repository, which has required the development of a three-dimensional model; (2) we have attempted to incorporate in an objective manner as much drill-hole information as possible in order to represent the three-dimensional spatial variability of the repository block; (3) we have emphasized the most significant features of Yucca Mountain in the model of lithologic geometry, because total-system performance evaluation is necessarily conducted on an abstract level; (4) we want to treat uncertainty in the results in a quantitative manner.

Geostatistical methods help to assess the uncertainty in the geometry of unit contacts and thicknesses of stratigraphic units in a rigorous, quantitative manner; starting from available data, realizations of the lithology for the entire domain can be constructed in a manner that includes uncertainty in the locations and extent of individual units. Uncertainty in the site description will then be propagated to the outputs of the flow and transport models.

A geostatistical modeling method is discussed here for producing internally consistent three-dimensional models of hydrologic properties using a fundamental lithologic subdivision of the rocks present at Yucca Mountain. The application of this work is described in Wilson *et al.* (1994) and Rautman and Robey (1994).

2.1 Prior performance-assessment models of Yucca Mountain

Models used in previous performance-assessment calculations were limited in that they did not reflect the complete geographic and geometric variability and uncertainty of hydrologic properties at Yucca Mountain. Representation of the hydrogeologic subdivisions and models of hydrologic properties used in TSPA computations have evolved considerably over time. Many of the changes result from an increasing recognition of the variability of the properties of the tuffs at Yucca Mountain and efforts to incorporate this heterogeneity into models of site performance. Very limited data were used in the early assessments. For example, Dudley *et al.* (1988) simply used drillhole USW G-4 as the basis for their calculations. PACE-

90 (Barnard and Dockery, 1991) again was scoping in nature; the study defined 19 hydrogeologic units (from the land surface to the water table) derived from information from four boreholes located in the northeast portion of the Yucca Mountain site (USW G-1, USW H-1, UE-25a #1 and USW G-4). This area was considered fairly representative of the range of properties to be used in performance-assessment models.

The next iteration, TSPA-91 (Barnard *et al.*, 1992), used a composite stratigraphic profile developed by subjective interpretation of spatially distributed drillhole information. The site model is represented by a stratigraphic cross-section between drillholes USW H-5, USW G-4, and UE-25a #1 in the northern portion of Yucca Mountain. Because the PACE-90 calculations were not sensitive to the small contrasts in the hydrologic properties between hydrogeologic units, TSPA-91 combined a number of PACE-90 hydrogeologic units into five layers to model the unsaturated zone from the repository to the water table.

2.2 The TSPA-93 lithologic model

The three-dimensional lithologic model of the site has been constructed using a coding process (an "indicator" transform) that defines major lithologic boundaries. We classify the hydrogeologic units according to the relative vertical positions of lithologic units. Lithologic models can be constructed using estimation (i.e., kriging; Huijbregts and Matheron, 1971), which results in a deterministic model, or simulation (Montogolou and Wilson, 1982), which results in a stochastic model of the lithologic categories. The stochastic approach is used in this study because it explicitly evaluates uncertainty in the geometry of the various lithologic units. Other three-dimensional models have been developed (Wittwer *et al.*, 1992; Buesch *et al.*, 1993). However, these models portray lithologic units in a deterministic fashion and do not quantitatively address the uncertainty associated with the position of lithologic unit contacts in three-dimensional space. Uncertainty in geometry may potentially be important to performance assessment, and thus important in our modeling.

The fundamental lithologic distinction modeled is that between nonwelded and more-or-less densely welded tuffs; the former are porous and permeable while the latter have low-porosity and are less permeable. The product of this first-order modeling is a three-dimensional layered volume of alternating welded and nonwelded intervals consistent with data from the existing drillholes at the site. This binary lithologic model of Yucca Mountain is then modified to include additional site-characterization information, which indicates that the different welded and nonwelded intervals in any particular vertical sequence tend to have somewhat dif-

ferent hydrologic properties. These modifications transform the binary representation of major rock types into a geometric description of material-property, or hydrogeologic units. The simulated models are constructed in such a way that the individual models are equally likely "realizations" of the incompletely known reality that is Yucca Mountain. Variability among a suite of realizations quantitatively represents uncertainty that results from limited observation and sampling of the entire three-dimensional volume of the repository block.

2.2.1 Geologic basis of model

The volcanic rocks at Yucca Mountain consist of thick sequences of generally densely welded ash-flow tuff separated by thinner, nonwelded intervals of mixed ash-fall tuff, small-volume ash flows, and reworked or bedded tuffaceous materials. The generally recognized lithostratigraphic subdivisions applied to the tuff sequence at Yucca Mountain are shown in Figure 2-1, Column A (based upon Scott and Bonk, 1984). The principle underlying this stratigraphic subdivision is genetic. Specifically, the first-order nomenclature (e.g., Crater Flat Tuff, Paintbrush Tuff) is applied to materials of common petrologic character, perhaps indicating derivation from a common underlying magma chamber. Smaller-scale subdivisions (e.g., Bullfrog Member, Tiva Canyon Member) focus on materials produced by a single (although perhaps multi-stage) eruptive cycle, generally termed a cooling unit for welded tuffs. The boundaries between the deposits of these major eruptive events presumably represent extended periods of quiescence, and these time intervals may have produced thin intervals of reworked ("bedded") deposits or unreworked ash-fall tuffs.

Column B of Figure 2-1 illustrates a stratigraphic subdivision that focuses on identifying lithologic units comprised of materials with interpreted similar thermal/mechanical/hydrologic properties (Ortiz *et al.*, 1985). The subdivision is based principally upon the bimodal distinction between welded large-volume ash flows and nonwelded intervals of mixed origin (indicated by the "w" and "n" in the unit identifiers). Secondary distinctions are based upon the presence or absence of locally significant geologic features related to cooling, reworking, or late-stage alteration (specifically, zeolitization). This subdivision has been used as the major basis for hydrogeologic models in several prior performance-assessment analyses (e.g., PACE-90, TSPA-91).

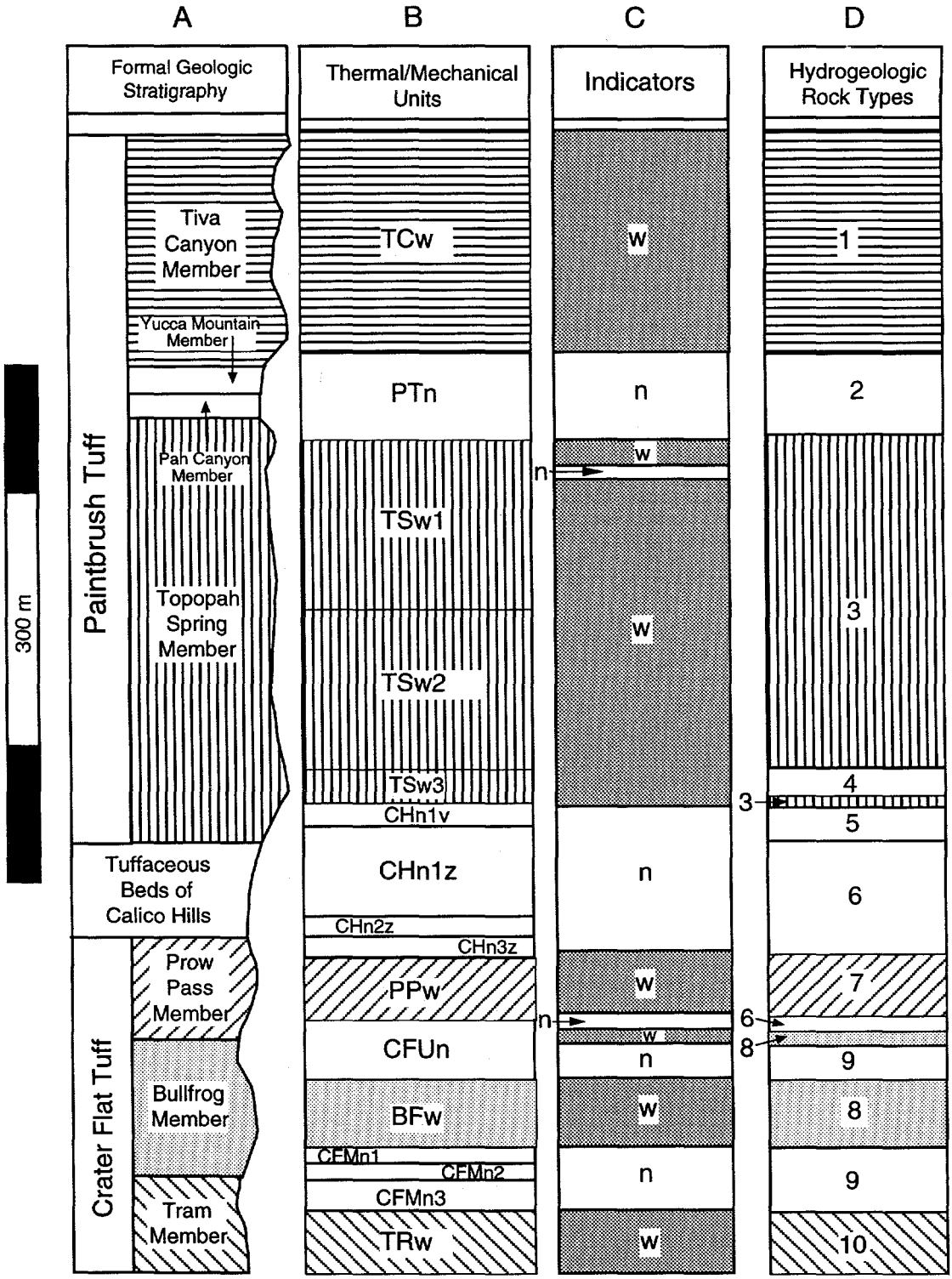

Figure 2-1. Composite vertical profile of Yucca Mountain showing approximate correspondence of lithologic indicators and hydrogeologic units with formal geologic nomenclature (Byers *et al.*, 1976), and thermal/mechanical units (Ortiz *et al.*, 1985). Note that between the subdivisions of Column A generally thin layers of bedded tuff are found.

The current lithologic model of Yucca Mountain is also based upon the bimodal distinction between welded and nonwelded rock types. However, in contrast to the subdivision of Ortiz *et al.*, the current model is (1) more detailed, allowing for the incorporation of thinner units of contrasting lithology, and (2) stochastic in nature, implying that the various units are created "randomly" consistent with the surface observations and that they need not be completely stratiform or continuous across the entire repository region. The assignment of initial lithologic classifications to a vertical column (e.g., a drillhole) through the upper part of the volcanic sequence at Yucca Mountain is illustrated in Figure 2-1, Column C.

Evaluation of reported hydrologic-property measurements on core samples from Yucca Mountain indicates that not all welded or nonwelded units possess the same physical properties. This point is developed in Chapter 3. Generally, however, there is a certain degree of consistency within a particular lithostratigraphic interval (i.e., Column A in Figure 2-1). Variations in the degree of welding, post-emplacement cooling, devitrification, and development of secondary alteration minerals interact to give rise to several relatively distinctive hydrogeologic units that fit within the binary classification of welded and nonwelded rock types. This model of Yucca Mountain identifies ten such units meriting separation within the unsaturated zone and the shallow saturated portion of the groundwater-flow system. Development of the units is discussed in Section 2.3.5 below and is shown in Figure 2-1, Column D.

2.3 Model development

Development of the three-dimensional stochastic model of the Yucca Mountain lithology involves several steps: (1) Available data from descriptive and geophysical logs of drillholes are extracted; (2) intervals from each drillhole are coded as being either welded or nonwelded; (3) a model of spatial correlation for the binary lithologic data is developed; (4) three-dimensional simulations of the two rock types are made; and (5) the welded and nonwelded intervals are further refined by consideration of hydrologic-property data to create distinctive hydrogeologic units.

The simulations of the rock-type spatial distributions honor the data at the drillholes. Away from drillhole observations, the simulations reflect the lack of information in a manner consistent with the spatial-correlation model. Correspondence of the simulated lithologic units with the intervals coded in step (2) allows the assignment of hydrogeologic unit identifiers and associated hydrologic

properties; such assignments are discussed in more detail in Chapters 6 and 7 of TSPA-93 (Wilson *et al.*, 1994).

2.3.1 Sources of information

Twenty-three drillholes exist in the immediate vicinity of the potential Yucca Mountain repository (Figure 2-2). The spatial distribution of drilling is uneven, with fewer holes located west of the Ghost Dance Fault. Drillholes in the eastern part of the area tend to be clustered in the washes at lower elevations. Only ten drillholes reach the water table, which leads to more sparse data at deeper levels within the repository block. Hydrologic data from drillhole USW GU-3 are available; however, the hole is farther away from the repository region than the other drillholes, so the data are not used in the lithologic model.

Published drillhole lithologic logs have been used as the primary sources of information. The information provided by the lithologic logs consists of descriptions and distributions of rock types taken from the boreholes. The data available from lithologic logs used for this work include type of rock, physical condition, structural features, color, and mineralogy present. Generally, the geologic descriptions in the logs were used to identify welded and nonwelded intervals. Following the practice of Scott *et al.* (1983), any interval described as "moderately" or "densely" welded was classified as welded for this analysis. Intervals described as "nonwelded" or only "partially" welded were classified as nonwelded, as were intervals of "bedded" or "reworked" tuff. Intervals described as "partially to moderately" welded are ambiguous, and could be categorized as either welded or nonwelded by this practice. To resolve these questions, other references (such as geophysical logs and color photographs of the core) were consulted. The supporting evidence from these futher observations was then used to categorize the ambiguous samples.

Color core photographs are available for some of the drillholes, and these photographs were used to provide additional information to clarify the welded/ nonwelded classification of intervals described in the published lithologic logs as variable rock type. Welded and nonwelded tuffs typically appear quite different in the core photographs, and the detailed foot-by-foot record allows introduction of much more detail into the current model than was incorporated in the thermal/mechanical stratigraphic model of Ortiz *et al.* (1985). Generally speaking, core from welded sequences is generally smooth on the cut surface and may be somewhat shiny in the photographs for the highly vitric units. Flattened pumice clasts

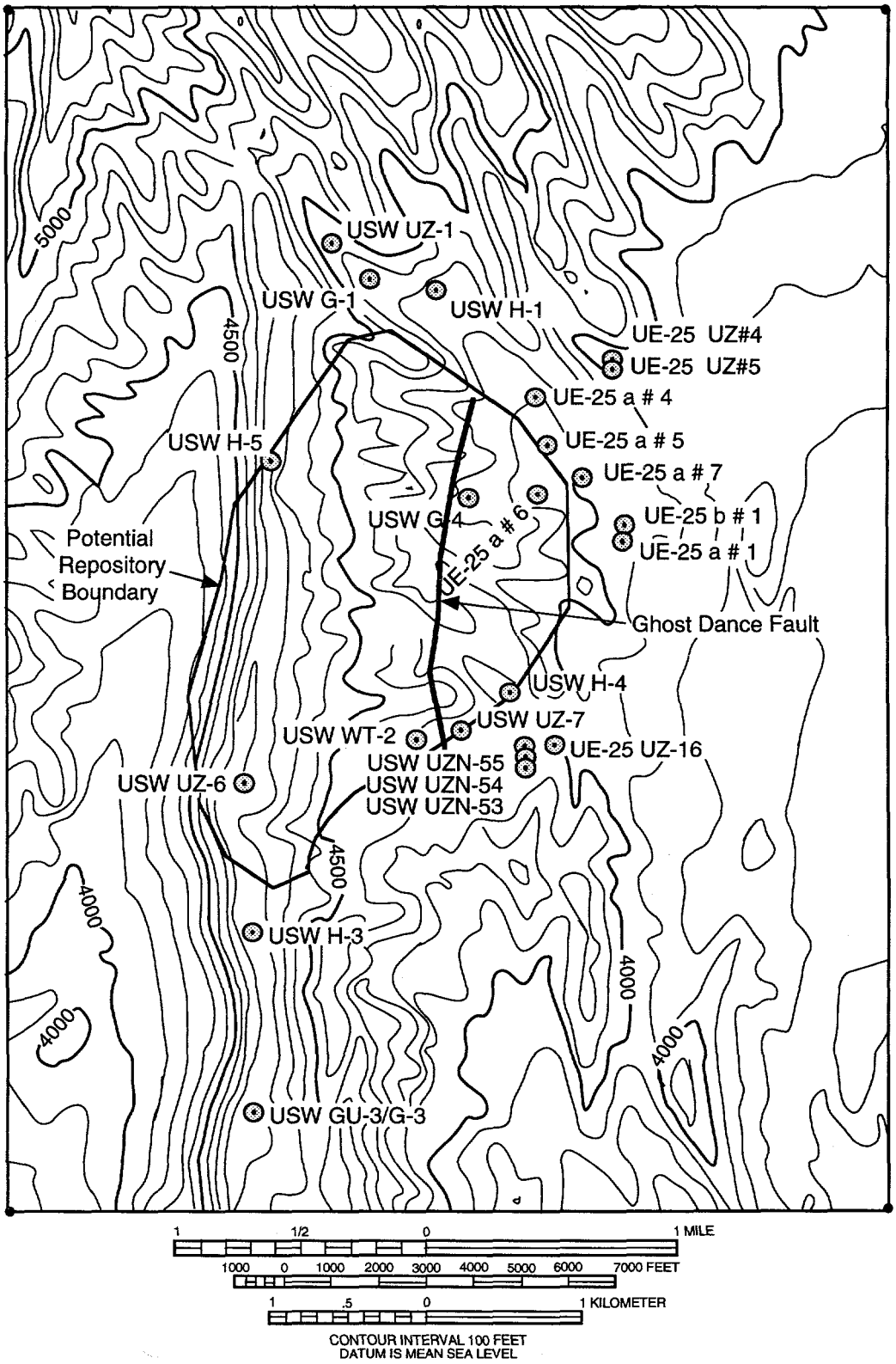

Figure 2-2. Yucca Mountain region at the potential repository site, showing drillholes from which data were available.

may be visible. Fracturing is typically prominent. Core from nonwelded intervals is typically more rough on the cut surface, unfractured, and more "earthy" in appearance. Some nonwelded intervals are completely disaggregated.

Geophysical logs (Nelson *et al.*, 1991) provide another, somewhat qualitative, cross check of the lithologic classifications. These logs were reviewed and the major lithologic contrasts confirmed wherever possible. The most useful geophysical data include density and neutron logs, which respond to changes in rock density (an indication of welding), and caliper logs, which reflect local drillhole enlargement. In some cases, the correlation between geophysical and descriptive geologic logs is excellent; for other intervals the correlation is weak or absent.

Table 2-1 lists the data available for each drillhole and the sources of data. The resulting rock-type classifications for each drillhole are provided in Appendix I.

Table 2-1. Summary of data sources for lithologic model.

Drillhole	Lithologic Log Data References	Geophysical Log Data Available?[a]	Core Photograph Negative Numbers
UE-25a #1	Spengler *et al.* (1979)	yes	W217 – W301
UE-25a #4	Spengler & Rosenbaum (1980)	yes	W1530 – W1545
UE-25a #5	Spengler & Rosenbaum (1980)	yes	W1448 – W1461
UE-25a #6	Spengler & Rosenbaum (1980)	yes	W1482 – W1493
UE-25a #7	Spengler & Rosenbaum (1980)	yes	W 1560 – W1592
UE-25b #1	Lobmeyer *et al.* (1983)	yes	W800 – W883
USW G-1	Spengler *et al.* (1981)	yes	W554 – W742
USW G-3/GU-3	Scott & Castellanos (1984)	yes	W1096 – W1282
USW G-4	Spengler *et al.* (1984)	yes	W088 – W195
USW H-1	Rush *et al.* (1983)	yes	W1466 - W1479/ W1602 – W1635
USW H-3	Thordarson *et al.* (1984)	yes	—
USW H-4	Whitfield *et al.* (1984)	yes	—
USW H-5	Bentley *et al.* (1983)	yes	—
USW UZN-53	Voss (1992c)	no	—
USW UZN-54	Voss (1992a)	no	—
USW UZN-55	Voss (1992a)	no	—
USW UZ-1	Whitfield *et al.* (1990)	yes	—
UE-25 UZ-4	Loskot & Hammermeister (1992)	no	—
UE-25 UZ-5	Loskot & Hammermeister (1992)	no	—
USW UZ-6	Whitfield *et al.* (1993)	yes	—
USW UZ-7	Kume & Hammermeister (1990)	no	—
UE-25 UZ-16	Buesch (1993)	no	—
USW WT-2	—	yes	—

[a] Geophysical log and core data from Nelson *et al.* (1991).

In one hole for which no published geologic log exists (specifically drillhole USW WT-2), the geophysical logs are the primary source of lithologic information. The interpretation for hole WT-2 was supplemented by correlation with the published geologic logs for drillholes USW H-4 (670 m to the northeast) and USW UZ-7

(305 m to the northeast). UZ-7 provided the most information for the upper portion of the hole (through the welded Topopah Spring Member); H-4 was used as guidance for the deeper units below the total depth of UZ-7.

2.3.2 Indicator coding

Geostatistical techniques can simulate continuous variables, such as most hydrologic properties measured in a laboratory, or categorical variables, such as a descriptive classification. Because first-order changes in hydrologic properties are related to the bimodal welded/nonwelded lithologic description, the current stochastic model of Yucca Mountain is based upon simulation of these two categories.

The bimodal descriptive classification of rock types at Yucca Mountain as welded or nonwelded (Column C of Figure 2-1) can, with some simplification, be transformed to a binary classification of zeros and ones through use of the indicator transform described by Journel (1983). The approach substitutes an indicator variable, $I(\mathbf{x})$, for the original category or verbal classification, $Z(\mathbf{x})$, for each observed spatial position, $\mathbf{x}$. Thus:

$$I(\mathbf{x}) = \begin{cases} 1 : Z(\mathbf{x}) \text{ is welded} \\ 0 : Z(\mathbf{x}) \text{ is not welded} \end{cases} . \qquad (2.1)$$

In the current model, rock type is categorized at regular downhole intervals as "welded" or "nonwelded" based on the information in Appendix I. Each such categorization is then transformed using Equation 2.1, and the resulting sets of spatially located indicators are used to condition the subsequent simulations.

2.3.3 Models of spatial correlation

Only a very small fraction of the volume of Yucca Mountain has been directly observed (e.g., the actual core samples from drillholes). Thus there is uncertainty associated with respect to the rock type existing at any unsampled spatial location. In stochastic modeling, the uncertainty associated with the rock type likely to exist at an unsampled location "near" an actual observation is intuitively less than the uncertainty associated with a similar location "far" from any data. Geostatistical simulation requires a quantitative description of what constitutes "near" and "far" and of how much uncertainty is associated with each. This description is provided mathematically by the interpreted model of spatial correlation (or spatial continuity), generally referred to as the **variogram**, and is represented by γ.

A sample variogram is computed from a set of data by examining the relationship between the variance of the difference between all sample pairs separated by a given distance, h, as a function of that separation distance. At short separations, the variability of the observed values (i.e., the variance of the difference between the two values) is expected to be small if the observations are spatially correlated. At larger separations, that variability is expected to be larger. This intuition translates into greater uncertainty when simulating the property for an unsampled location at that larger distance. Beyond a certain separation distance, generally referred to as the **range of spatial correlation**, the observations are typically uncorrelated, and the best measure of the variability of samples spaced at (or beyond) that distance—or of the uncertainty associated with simulating an unsampled point located beyond that distance from an observation—is simply the overall (univariate) sample variance.

Spatial correlation may not be identical in all directions. In geologic settings involving layered rock sequences such as Yucca Mountain, significant anisotropy may exist when spatial correlation is evaluated in different directions. Quantitatively, anisotropy is accommodated by evaluating separation distance as a vector, $\mathbf{h}$, instead of a simple scalar quantity, h. Conceptually, spatial correlation in three dimensions can be thought of as forming an ellipsoid in which the degree of flattening of the original sphere (i.e., the isotropic shape) and tilting of the major and minor axes describe spatial anisotropy.

The computational formula for the variogram is expressed mathematically (Journel and Huijbregts, 1978) as:

$$2\gamma(\mathbf{h}) \equiv Var\{I(\mathbf{x}+\mathbf{h}) - I(\mathbf{x})\} = E\left\{\left[I(\mathbf{x}+\mathbf{h}) - I(\mathbf{x})\right]^2\right\} = \frac{1}{N}\sum_{i=1}^{N(\mathbf{h})}\left[I(\mathbf{x}+\mathbf{h}) - I(\mathbf{x})\right]^2 , \qquad (2.2)$$

where $\mathbf{x}$ is a particular spatial location, $Var\{...\}$ is the variance operator and $I(\mathbf{x})$ is the indicator observed at that location. $E\{...\}$ is the expectation operator and N is the number of samples. The computed variogram data (sample variogram) are used to construct a variogram model that reproduces the observed spatial continuity.

In order to simulate all possible unsampled locations at all possible vector distances with respect to a complex set of data, the explicitly determined sample variogram must be replaced with a fitted **variogram model** from which the proper variability at arbitrary positions may be computed. Certain mathematical functions are generally selected to represent the model variogram for computational reasons.

Generally, variogram models are described by reference to the **type** of model (the specific functional relationship), the **range** of spatial correlation (a), the **sill** (C) or maximum level of variability, and potentially a **nugget** effect (C_0), which captures unresolved spatial variability at very small separation distances. Figure 2-3 illustrates the difference between a sample variogram and its variogram model. The various defining parameters of the variogram model are also indicated.

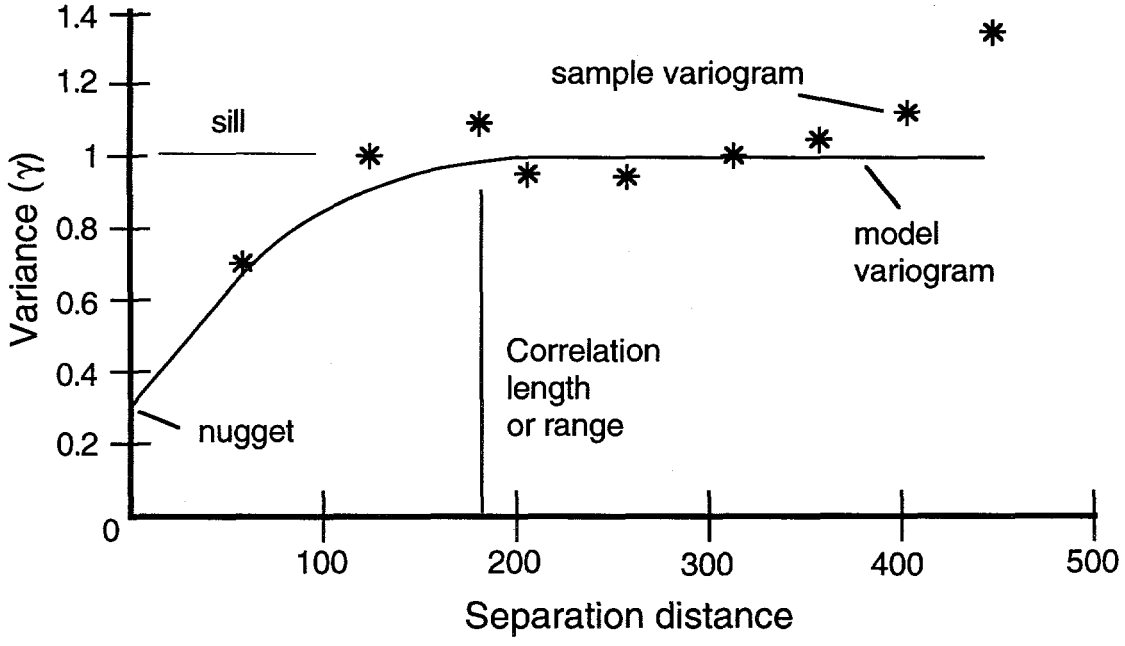

Figure 2-3: A typical sample variogram and model variogram.

Normal geostatistical practice in a simulation study is to compute sample variograms directly from the conditioning data. However, the density of drilling at Yucca Mountain is inadequate—and the inter-drillhole distances typically too great —to derive the required three-dimensional model of spatial correlation. As a surrogate for drillhole information, a more densely distributed set of indicator data was constructed from published geologic cross-sections of Yucca Mountain (Scott and Bonk, 1984), which specifically focus on the welded/nonwelded lithologic distinction that forms the basis for the current stochastic model. The locations of these cross-sections are shown in Figure 2-4, and Table 2-2 describes the panels from each cross-section that were digitized.

The boundaries of the welded and nonwelded units indicated on the cross-sections were digitized to capture the necessary three-dimensional coordinate system. A regular two-dimensional grid was then imposed on each digitized cross-

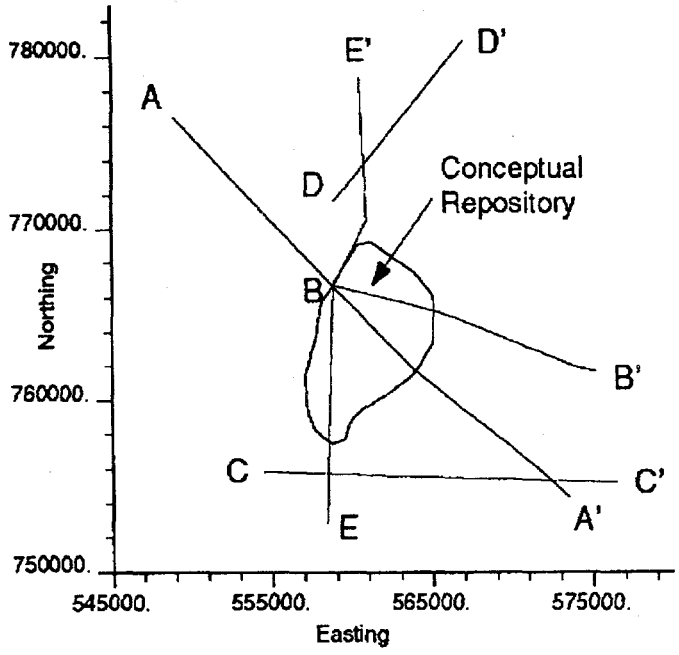

Figure 2-4. Locations of digitized cross-sections (after Scott and Bonk, 1984).

Table 2-2. Descriptions of digitized cross-sections.

Cross-Section	Panel		Deepest Unit Included in Cross-Section
	From	To	
A–A'	Solitario Canyon Fault	USW H-4	Tram Member, welded
	USW H-4	Paintbrush Canyon fault	Tram Member, welded
B–B'	USW H-5	USW G-4	Tram Member, welded
	USW G-4	UE-25a #1	Tram Member, welded
	UE-25a #1	Paintbrush Canyon fault	Bullfrog Member, welded
C–C'	Solitario Canyon Fault	Paintbrush Canyon fault	Tram Member, welded
D–D'	Yucca Crest	Past Yucca Wash fault	Tram Member, welded
E–E'	USW G-3	USW H-3	Lithic Ridge tuff, welded
	USW H-3	USW H-5	Nonwelded below Lithic Ridge tuff
	USW H-5	USW G-1	Lava flows and breccias
	USW G-1	USW G-2	Nonwelded below lava flows and breccias

section, and each grid node was associated with the appropriate indicator-transformed lithologic category. Minor units composed of lava flows and breccias, which occur principally at deeper stratigraphic levels, were excluded from consideration. Finally, a composite data file containing the true three-dimensional coordi-

nates of each grid node on all cross-sections and the relevant indicator value was generated in a format suitable for computing sample variograms.

Computation of sample variograms from the surrogate data set followed standard geostatistical practice. Because development of a variogram model in three dimensions is difficult by virtue of the many possible orientations of the anisotropy axes, geologic knowledge of the Yucca Mountain site was used to guide development of the sample variograms and fitted model. Across the region of interest, stratigraphic units strike more or less north-south and dip gently eastward at approximately 5 to 10 degrees. The geologic cross-sections are arranged spatially to capture this geologic context. Initially, the search strategy used in computing the sample variograms focused on these principal directions. Later, the search directions were systematically varied to derive the final sample variograms, to which the necessary model of spatial continuity could then be fitted.

Figure 2-5 presents sample variograms computed from the digitized cross-section data, looking horizontally in the north–south direction and at dips of 5° toward N 90° E and of 85° toward N 90° W. These directions are essentially parallel and perpendicular to the typical stratification. Figure 2-5 also presents the results of a single, nested, three-dimensional variogram model computed in the same three mutually perpendicular directions. Given the assumptions involved in the cross-section surrogate data and in the indicator coding of this thick, composite stratigraphic interval, the model is judged a rather good fit to the sampled data.

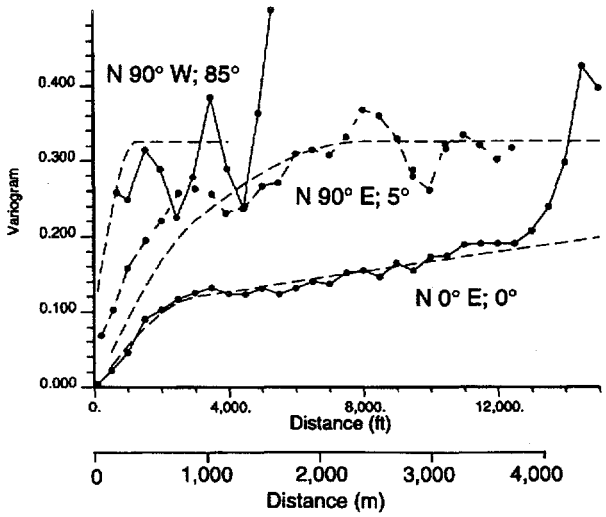

Figure 2-5. Sample variograms and fitted variogram models computed in indicated directions.

Parameters of the fitted model are given in Table 2-3. The nested, anisotropic variogram model given in Table 2-3 is presented in Figure 2-6. A reasonable explanation of the various spatial continuity parameters can be found in the geologic context of Yucca Mountain. The shorter of the two structures appears to be related principally to the stratigraphically vertical extent of the lithologic units. The 90-m vertical range of correlation (i.e., the 910-m major axis range of correlation times the 0.1 anisotropy ratio) seems to be a composite value related to the presence of thick (100-300 m) welded units interbedded with significantly thinner (6-60 m) nonwelded tuffs. For comparison, Rautman and Flint (1992) reported the following ranges of correlation for porosity: 30 m for a vertical composite of the Paintbrush Tuff, and 60 m for the Topopah Spring Member welded unit. The shorter range presumably represents a first-order degree of continuity related to the degree of welding. This correlation structure is perhaps accentuated by the smaller-volume, welded ash-flow tuffs, the Pah Canyon and Yucca Mountain Members of the Paintbrush Tuff, which are present in the northern portion of the Yucca Mountain region. No obvious anisotropy is apparent for this structure in plan view; hence the anisotropy factor of 1.0. The longer-range structure (approximately 15 km) appears to be related to the overall extent of the ash-flow sheets, which extend southward some tens of kilometers from a northern source caldera. The specific anisotropy observed in plan (0.16) may be partially a function of the extent of these units in the dip direction, which is limited both by Basin-and-Range normal faulting and by the construction

Table 2-3. Model variogram parameters.

	Major Axis Range (m)	Sill	Anisotropy Ratio 1[a]	Anisotropy Ratio 2[a]
Nugget	—	0.000	—	—
Structure 1	914	0.100	1.00	0.10/0.025[b]
Structure 2	15239	0.225	0.16	0.04/0.025[b]
		Rotation Angles[c]		
Angle 1			0°	
Angle 2			0°	
Angle 3			-5°/-6.7°	

[a] The length of the secondary and minor axes relative to the major axis for a conceptual ellipsoid.

[b] In "*nn*/*mm*," *nn* is the value obtained through variogram modeling and *mm* is the modified value used in the final simulations (see Section 2.3.4).

[c] Angles 1 and 2 are applied to the major (y) axis of the continuity ellipsoid, first in the x–y plane and then in the horizontally rotated x′–z plane. Angle 3 is then a clockwise rotation about the major axis, applied to the resultant y′–z′ plane.

of the cross-sections. The extreme anisotropy ratio for this longer structure in cross-sectional view (0.04) reflects the layered nature of the tuffs themselves. Without vertical exaggeration, an ash flow sheet is exactly that: a thin sheet of large lateral extent. The limited east-west extent of the modeled region limits the practical effect of this long-range structure in all directions other than those close to north-south, as indicated by the modeled variograms of Figure 2-5. (The sill is not reached even at the greatest E–W intersample distances.)

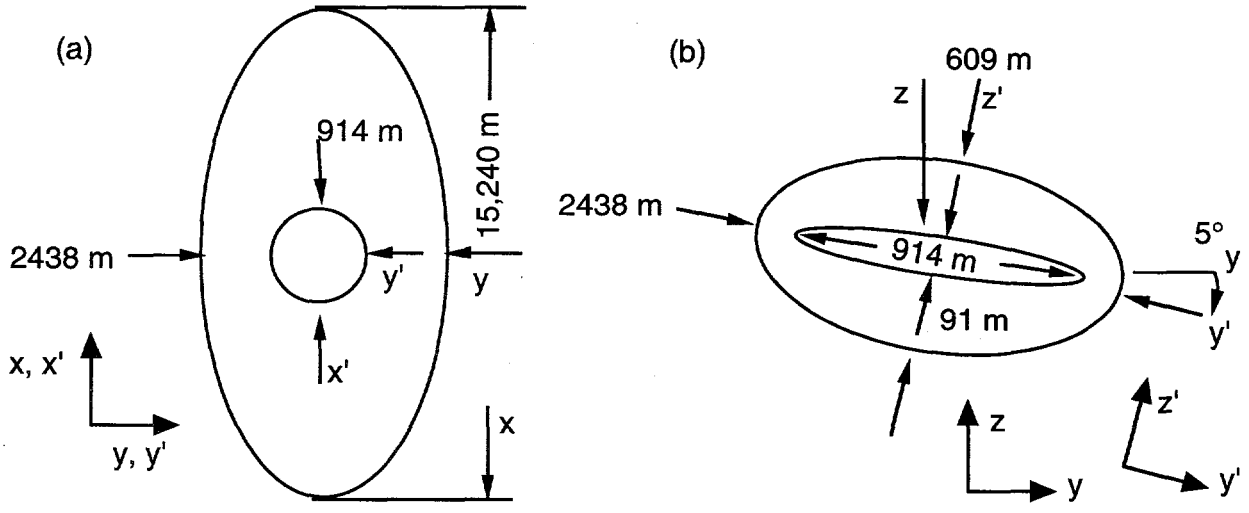

Figure 2-6. Schematic representation in two directions of the fitted, two-part nested variogram model: (a) plan view; (b) cross-sectional view from west to east. Ranges and degree of anisotropy are schematic and not to scale.

The choice of angle 3 (Table 2-3; this angle is essentially equivalent to the "average" dip of the tuffs at Yucca Mountain) affects the ability of the simulation algorithm to project conditioning information into unsampled volumes. The angle derived directly from the sample variogram reflects the final position of the various rock units in space after they have been offset by faulting. Accordingly, the measured dip angle is an *apparent* dip. The actual dip of the rock units between bounding faults is greater, and it is this dip that should control the propagation of information into unsampled regions. Measurements of actual dips in the field (Scott and Bonk, 1984) and experiments with different values for angle 3 in the geostatistical simulation led to a choice of 6.7° as the final anisotropy angle 3.

The vertical-to-horizontal anisotropy ratio (ratio 2) is not as great as might be expected considering that the horizontal extent of a stratigraphic layer should be very much greater than its vertical extent; a thin, layer-cake conceptual model im-

plies a degenerate ellipse with a very long principal axis. An ellipse with a large anisotropy ratio is particularly subject to magnification of error in measuring the spatial continuity of the principal axis (Deutsch and Journel, 1992). Possible sources of error include the lack of detail in the Scott and Bonk (1984) interpretation, cumulative errors related to discretization of the cross-sections, and the orientation of the Scott and Bonk cross-sections at a slight angle to the principal axis. Test runs of the simulations with half the number of nodes (twice the spacing) in each direction were used to evaluate ratio 2. The results were compared qualitatively with the Scott and Bonk cross-sections to arrive at an adjusted ratio 2. Figure 2-7 shows a simulated cross-section using the measured anisotropy and a simulated cross-section with 40:1 judged as the smallest anisotropy ratio that qualitatively matches the Scott and Bonk cross-sections.

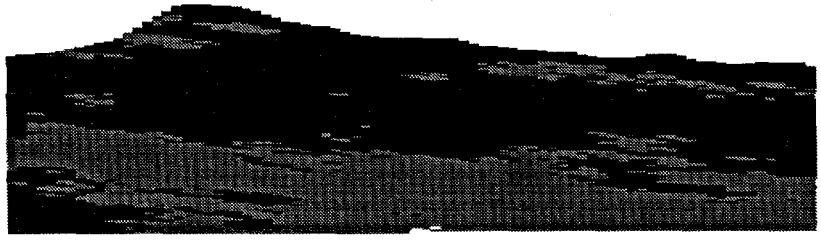

(a) original ratios

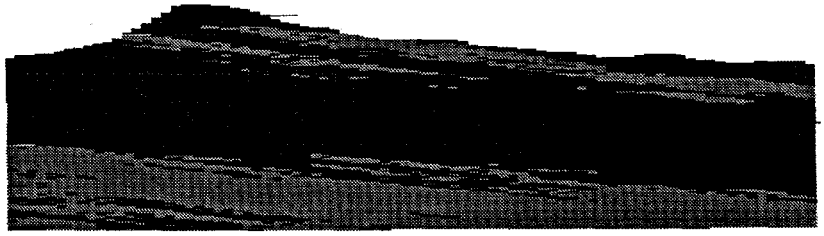

(b) adjusted ratios

Figure 2-7. Simulated cross-section of Yucca Mountain illustrating the tendency of simulated welded and nonwelded lithologies to pinch and swell and to interfinger in a more complex fashion than is believed reasonable based on field observations. (a) Profile simulated using original anisotropy; note discontinuous nonwelded unit in upper part of section; (b) the same profile after adjustment of anisotropy ratio.

2.3.4 Simulations

The simulated model domain is a three-dimensional gridded representation of the potential Yucca Mountain repository region, extending from Solitario Canyon on the west to beyond the east edge of the proposed perimeter drift and from the surface to below the static water level. Boundaries of the model are Nevada State Plane Coordinates 555,205 feet and 565,155 feet East, and 757,620 feet and 769,520 feet North. Elevations within the model range from 2350 to 4840 feet. Grid spacings of 100 feet N-S, 50 feet E-W, and 10 feet vertically, define 6 million nodes.

To construct a specific simulation, a random path that will visit each grid node is defined through the model. At each unsampled location, the probability of encountering a welded or a nonwelded rock type is estimated, given the surrounding conditioning data and the inferred model of spatial continuity. That location is then randomly assigned a rock type based on the locally conditioned probability of rock types. The simulation process then moves to the next node along the random path. At each point, the local probability is conditioned both to the original "measured" lithologic indicators and to any nearby previously simulated grid values. If there is no information of either kind within the range of spatial correlation specified by the spatial continuity model, a rock type is assigned randomly, respecting the overall proportion of different rock types. The marginal percentages for each rock-type category in the current model are 61% welded, 36% nonwelded, and 3% Prow Pass welded (Scott and Bonk, 1984)[1].

As the grid is filled in during the simulation, grid nodes in regions near conditioning data will tend to be assigned rock types resembling those data; an unsampled node stratigraphically near a thick welded unit observed in a drillhole generally will be simulated as welded. However, there is a nonzero probability of generating a nonwelded value at the same location. Conversely, at grid nodes in regions remote from any conditioning data, the probability of generating a particular lithology is initially very close to the overall proportion of that lithology defined for the model. As the simulation proceeds, subsequent nodes in that same region will be constrained by the values generated earlier, reflecting the identified spatial continuity model.

[1] The simulations produced for this modeling exercise are intended to include two lithologic types—welded and nonwelded. Because hydrologic properties must eventually be assigned to these lithologies for use in flow and transport calculations, and because the specific hydrologic properties vary with the member-level subdivisions, the welded category has been subdivided into two subclasses to distinguish a particular interval in which two different stratigraphic units (i.e., the welded phases of the Prow Pass and Bullfrog Members of the Crater Flat Tuff) may come into contact.

This simulation mechanism produces individual realizations that collectively reflect geologic uncertainty. Close to measured data, there is little uncertainty, and replicate simulations will appear similar. Far from data, uncertainty is great, and images extracted from the models may appear substantially different in character. Because of anisotropy, **near** and **far** refer to the geologic context: a point 100 m away along the plane of depositional layering from the type of volcanic ash falls or flows typical of Yucca Mountain depositional history is generally much nearer than a point 10 m away and perpendicular to that layering.

The search radius determines how far away to search for data in computing the indicator for each node and also greatly affects the amount of time required for computing the geostatistical simulation. The search radius used for these simulations is 2440 m in the direction of strike (direction with the maximum range). Eight total data (either from boreholes or nodes previously simulated) are used in the calculation of each simulated node. A maximun of two data points from each octant are allowed to ensure consideration of data in all directions with respect to the node being simulated. This helps eliminate undesired effects of spatially clustered information (such as along a drillhole).

Ten three-dimensional realizations of the welded/nonwelded rock material have been generated. The ten realizations are shown in Appendix II as four east-west vertical cross-sections, approximately equally spaced within the model domain (see Figure 1 of Appendix II for the locations of the cross-sections).

The geologic reasonableness of the simulations appears to deteriorate west of the crest of Yucca Mountain, especially at lower elevations within the model. The principal reason is that there is little actual information (i.e., conditioning drillhole data) in this region. With little conditioning information available, there is a high likelihood that no data will be found initially within the search radius and that the simulation algorithm will be forced to rely on the marginal proportions of the different rock types. Because simulated values are added to the set of conditioning data for subsequently simulated grid nodes, values sampled from the marginal distribution early in the simulation will necessarily be propagated though a particular realization for some surrounding distance. As the simulation progresses, true conditioning data will also propagate into the unsampled region and counteract (or reinforce) the early marginal choice. Sampling from the marginal distribution can lead to the production of geologic artifacts; however, the likelihood of that same artifact occurring in alternate simulations is relatively small. Good examples of such sampling artifacts are found in the unrealistic appearance of the Prow Pass welded

category at high elevations in the fourth cross-section from simulation 4 in Appendix II.

The ten simulations agree with geologic knowledge of Yucca Mountain in several respects. For example, the nonwelded interval near the top of the model (approximately equivalent to unit PTn in Figure 2-1) generally appears thicker in the north and thinner in the south (see Appendix II). The Paintbrush nonwelded interval does, in fact, thin from north to south as the nonwelded tuffs assigned to the Yucca Mountain and Pah Canyon Members thin and become essentially indistinguishable as map units (Scott and Bonk, 1984). All the simulations in Appendix II indicate that a thick, massive interval of welded tuff occurs below the level of the Paintbrush nonwelded interval; this unit corresponds to the welded portion of Topopah Spring Member of the Paintbrush Tuff. Below the "Topopah Spring unit" is a nonwelded interval that corresponds to the nonwelded tuffs of Calico Hills and similar nonwelded rock types in the upper portion of the Prow Pass Member of the Crater Flat Tuff. Welding within the Prow Pass Member (geologic unit, column A of Figure 2-1) is better developed lower in the section and in the more northern portions of Yucca Mountain.

The reasonableness of the simulated welded and nonwelded intervals below this "Calico Hills/upper Prow Pass" unit is more difficult to evaluate, as the stochastic model indicates considerable variability among simulations. This greater geologic uncertainty has two sources. First, fewer drillholes reach these deeper stratigraphic levels; thus, less information is available to determine the outcome of the stochastic model. Second, the distinction between welded and nonwelded rock types is less clear-cut in the subunits of the Crater Flat Tuff. Thus, greater variability and also greater uncertainty in coding the geologic descriptions are reflected in the conditioning data. This uncertainty subsequently is propagated into the various realizations.

Uncertainty related to the uneven spatial distribution of drilling (and thus of conditioning observations) is also reflected in the shallower units. For example, comparisons of the northernmost cross-sections (near the well-drilled and aptly named Drill Hole Wash) from the various realizations (see Appendix II) reveal relatively little variability. The relative thicknesses of the various rock types is essentially constant from one simulation to another. Indicated surface "exposures" are invariably welded tuff, corresponding to the widespread outcrops of the welded Tiva Canyon Member in this northern area. The appearance of the "Paintbrush nonwelded interval" is as a distinct, single unit that comes to the "surface" in the

model in the vicinity of the major topographic depression corresponding to Drill Hole Wash on the cross-section. Outcrops of thermal/mechanical unit PTn are frequently found at wash level in the real Drill Hole Wash. Throughout the vertical extent of this northernmost cross-section, contacts between simulated rock types are generally well defined.

In geologic contrast to the north, comparisons of cross-sections taken in the less intensely drilled southern portion of the modeled region indicate that variability is significantly greater throughout the entire vertical extent of the model. The "Paintbrush nonwelded interval," in addition to being much thinner (as it should be; see above) appears to pinch out locally, something that is not observed in the field. Nonwelded rock types have been simulated capping some ridges in this southern region (simulation 2, northing 761620, in Appendix II), despite the fact that these geomorphic features invariably are underlain by welded portions of the Tiva Canyon Member in the field. Generally speaking, the "contacts" or transitions from one rock type to another are less clearly defined in the sections from the southern part of Yucca Mountain; geologically unreasonable "interfingering" of the two lithologies is prominent locally.

Although much of the increased variability observed among the more southern cross-sections originates in geologic uncertainty related to spacing of drillholes, the simulation algorithm itself can work to accentuate variability and uncertainty in some instances. In particular, the prominent interfingering of welded and nonwelded rock types is an artifact related both to a lack of sufficient conditioning data and to the mechanics of the sequential simulation process. Sampling of non-reasonable rock types from the marginal distribution in regions without conditioning data is the worst contributor to the interfingering problem. Additional contributions arise from the use of a composite spatial continuity model to propagate conditioning information into regions affected by numerous closely spaced faults. As described earlier, anisotropy angle 3 (Table 2-3) identified from the sample variogram is an apparent dip; empirical adjustments were required to obtain a more geologically reasonable dip angle for this modeling parameter in order to project conditioning data along the true structural dip of the rock units. The spatial continuity model is not constant, but in reality is a function of location. However, determining the spatial dependencies introduces a complexity that is perhaps impossible to resolve. For example, in regions affected by closely spaced and poorly documented faulting, information may be better propagated along the faulting-induced apparent dip. Note, for example, the apparent "flattening" of the average dip of the strata

shown on the more east-west-trending cross-sections of Scott and Bonk (1984). The existence of this geologically unreasonable numerical phenomenon is evidence that the distribution of rock types in the affected regions is "uncertain." Indeed, any geologic interpretation in the vicinity of intense, poorly constrained faulting is inherently uncertain.

2.3.5 Development of hydrogeologic units

Laboratory measurements on core samples indicate that not all welded (or nonwelded) units at Yucca Mountain possess identical hydrologic properties (Chapter 3). Variations in the degree of welding and in the post-depositional history of cooling, devitrification, and development of secondary alteration minerals interact to produce a range of material properties within rocks coded either as "welded" or as "nonwelded" in the stochastic model. These variations in material properties are correlated to some extent with general, vertical stratigraphic position within the volcanic sequence; thus there is a tendency to maintain a gross correspondence with the formally named geologic units at the site (Column A of Figure 2-1). This correlation is more for referential convenience, however, than a strict correspondence. Integration of the available material-properties data with the indicator-coded lithologic model and with the overall vertical sequence of genetic units results in ten distinct hydrogeologic units that can be identified more or less throughout the current modeled volume. These units were introduced as Column D of Figure 2-1. An expanded description of each unit is provided in Table 2-4. Additional discussion of the character, origin, and reasons for distinguishing each unit from its neighbors is provided following a description of the mechanics by which the various units were identified within the stochastic models.

In order to define reasonably homogeneous hydrogeologic units, it is necessary to segregate the various three-dimensional, indicator-coded grid nodes into separate, identifiable volumes, each of which is then assigned a set of appropriate material properties. Interpreting these volumes in three dimensions poses visualization and selection difficulties, even under the best of circumstances. In addition, the presence of various numerical artifacts and uncertainties in the stochastic model (reflected principally by interfingering) induces even greater difficulty in the issue of identifying the appropriate three-dimensional hydrogeologic bodies.

For various computational and other reasons, total-system performance assessment activities for TSPA-93 focus on essentially one-dimensional flow and transport within the unsaturated zone (Wilson, *et al.*, 1994). This reduction in the

Table 2-4. Descriptions of the ten hydrogeologic units developed from the stochastic lithologic model.

Unit Number	Hydrogeologic Unit	Description
1	Tiva Canyon welded	Moderately to densely welded, devitrified ash-flow tuffs belonging to the Tiva Canyon member of the Paintbrush Tuff
2	Paintbrush nonwelded	Nonwelded to partially welded, vitric and locally devitrified tuffs belonging to the lowermost Tiva Canyon Member, Yucca Mountain Member, Pah Canyon Member and uppermost Topopah Spring Member of the Paintbrush Tuff; also includes air-fall tuffs, "bedded tuffs," and intercalcated reworked tuffaceous sediments. The Yucca Mountain and Pah Canyon Members are locally welded in the northern part of the modeled area.
3	Topopah Spring welded	Moderately to densely welded, devitrified ash-flow tuffs including the upper vitrophyre belonging to the Topopah Spring Member of the Paintbrush Tuff.
4	Topopah Spring vitrophyre	Densely welded basal vitrophyre belonging to the Topopah Spring Member of the Paintbrush Tuff.
5	Calico Hills/Prow Pass nonwelded vitric	Nonwelded to partially welded, vitric and argillic ash-flow, bedded, and reworked tuffs belonging to the lowermost part of the Topopah Spring Member of the Paintbrush Tuff, the tuffaceous beds of Calico Hills, and the nonwelded portion of the Prow Pass Member of the Crater Flat Tuff.
6	Calico Hills/Prow Pass nonwelded zeolitic	Same as unit 5, but specifically identifying the zeolitized portions of these units.
7	Prow Pass welded	Partially to moderately welded, devitrified and locally zeolitic ash-flow tuffs belonging to the Prow Pass Member of the Crater Flat Tuff.
8	Bullfrog welded	Moderately to densely welded, devitrified ash-flow tuffs belonging to the Bullfrog Member of the Crater Flat Tuff.
9	Bullfrog nonwelded	Nonwelded to partially welded, argillic, zeolitic, and devitrified ash-flow tuffs and minor "bedded tuffs" belonging to the upper and lower portions of the Bullfrog Member of the Crater Flat Tuff.
10	Tram welded	Moderately to densely welded, devitrified ash-flow tuffs belonging to the Tram Member of the Crater Flat Tuff.

dimensionality of the analysis provides a simple and effective, if not altogether satisfying, mechanism for dealing with the complexity of the full, three-dimensional, stochastic indicator model. One-dimensional columns were overlain on the appropriate east–west cross-sections extracted from the stochastic model at each of the chosen column locations. "Contacts" between the most obvious hydrogeologic

units in each one-dimensional profile were then interpreted from the indicator-coded rock types, based on the overall appearance of the entire cross-section. Many contacts are relatively straightforward. For example, the contact between a "Tiva Canyon" welded (unit 1) and a "Paintbrush nonwelded" (unit 2) hydrogeologic unit is quite obvious and unique in much of the northern part of the area (see discussion above in Section 2.3.4). In such cases, an effort was made to leave the proportion of each rock type unchanged when picking the contact. Essentially, welded and non-welded pixels at the profile location were swapped (visually), aggregating stray welded lenses with massive welded bodies and collecting nonwelded rock types in a similar manner. More ambiguous contacts characterized by severe interfingering of welded and nonwelded rock types posed more of a challenge. These contacts were resolved, arguably somewhat subjectively, by considering the specific setting of the contact. If a known fault (or zone of faulting) appeared to contribute to the uncertainty, the appearance of the cross-section on the appropriate side of the fault would be weighted (visually) more heavily in projecting a definite contact for the profile than the simulated lithologic character on the other side of the fault. A similar heuristic was employed for columns located near the margin of a cross-section, in which case the general trend from within the data-rich side of the section would take precedence over artifacts obviously related to marginal-distribution sampling problems in an undrilled area. In areas with indistinct units, the Ortiz model (Ortiz *et al.*, 1985) was used to provide guidance in the interpretation.

Following definition of discrete contacts in zones of lithologic ambiguity, the now segregated welded and nonwelded intervals in each TSPA-93 column were assigned to hydrogeologic units. Units 1, 2, 8, 9, and 10 were assigned based solely upon their respective lithologic category and vertical position within the overall sequence (Figure 2-1). The remaining hydrogeologic units required additional consideration. Units 3 and 4 correspond to a single welded interval (Figure 2-1). A thin but prominent vitrophyre near the base of the Topopah Spring Member has hydrologic properties that are distinctly different from the remainder of the welded portion of this stratigraphic unit (Chapter 3); accordingly, it is distinguished in subsequent TSPA-93 analyses from unit 3 (Figure 2-1), the welded devitrified portion of the Topopah Spring Member. Unit 4 was deterministically assigned a thickness indicated by the Ortiz model.

The nonwelded interval corresponding to the combination of hydrogeologic units 5 and 6 is subdivided based upon the dominant presence of zeolites in the lower portion of this nonwelded, originally vitric interval. The relationship of these

two hydrogeologic rock types to more conventional stratigraphic assignments is complex. Although the nonwelded portions of the Crater Flat Tuff are petrologically distinct from the equally nonwelded tuffaceous beds of Calico Hills, these two units were grouped together under the supposition that the hydrologic properties are quite similar. The more important hydrologic difference is whether or not the rocks have been zeolitized. Zeolitic materials exhibit significantly lower permeabilities for a given porosity than does the original, vitric tuff. Thus, the upper nonwelded portion of Prow Pass may be aggregated with the tuffs of Calico Hills, either as vitric (unit 5) or as zeolitic (unit 6) materials. The division (contact) between the vitric and zeolitic units is taken deterministically from Ortiz *et al.* (1985). A similar aggregation of genetically separate but hydrologically similar material forms hydrogeologic unit 9 (the upper part of the Tram Member is combined with the lower part of the Bullfrog Member); however, in this case, the entire interval is zeolitized because of its position deep within the (current and paleo-) saturated zone, and the defining character of the interval is simply its nonwelded nature.

Hydrogeologic unit 7 is perhaps the most interesting rock type, and the definition of this unit marks one of the most significant departures of the current model from prior modeling practice. Unit 7 is defined as representing welded material within the Prow Pass Member of the Crater Flat Tuff (Table 2-4). As shown in Figure 2-8, there are multiple instances of this hydrogeologic rock type shown within more extensive nonwelded tuff, ascribable, in part, also to the Prow Pass Member. Evaluation of all available data suggests that there are, in fact, two distinctly separate welded intervals of similar hydrologic character within this genetic unit in the modeled region. Note that the lower occurrence of hydrogeologic unit 7 is hydrologically distinct from the welded material of hydrogeologic unit 8 in terms of material properties. It is the juxtaposition of these hydrologically different materials (Chapter 3) that necessitated the use of a third indicator category in the simulation runs (see footnote on page 21). The origin of these multiple intervals within what is generally interpreted to be a single cooling unit is unclear. Uncertainty (ambiguity) resulting from the generally less-welded nature of the Crater Flat Tuff in the published geologic descriptions given in Scott and Bonk (1984) (compared with the very densely welded Paintbrush Tuff units) may have led to misinterpretation and incorrect indicator coding (Appendix I).

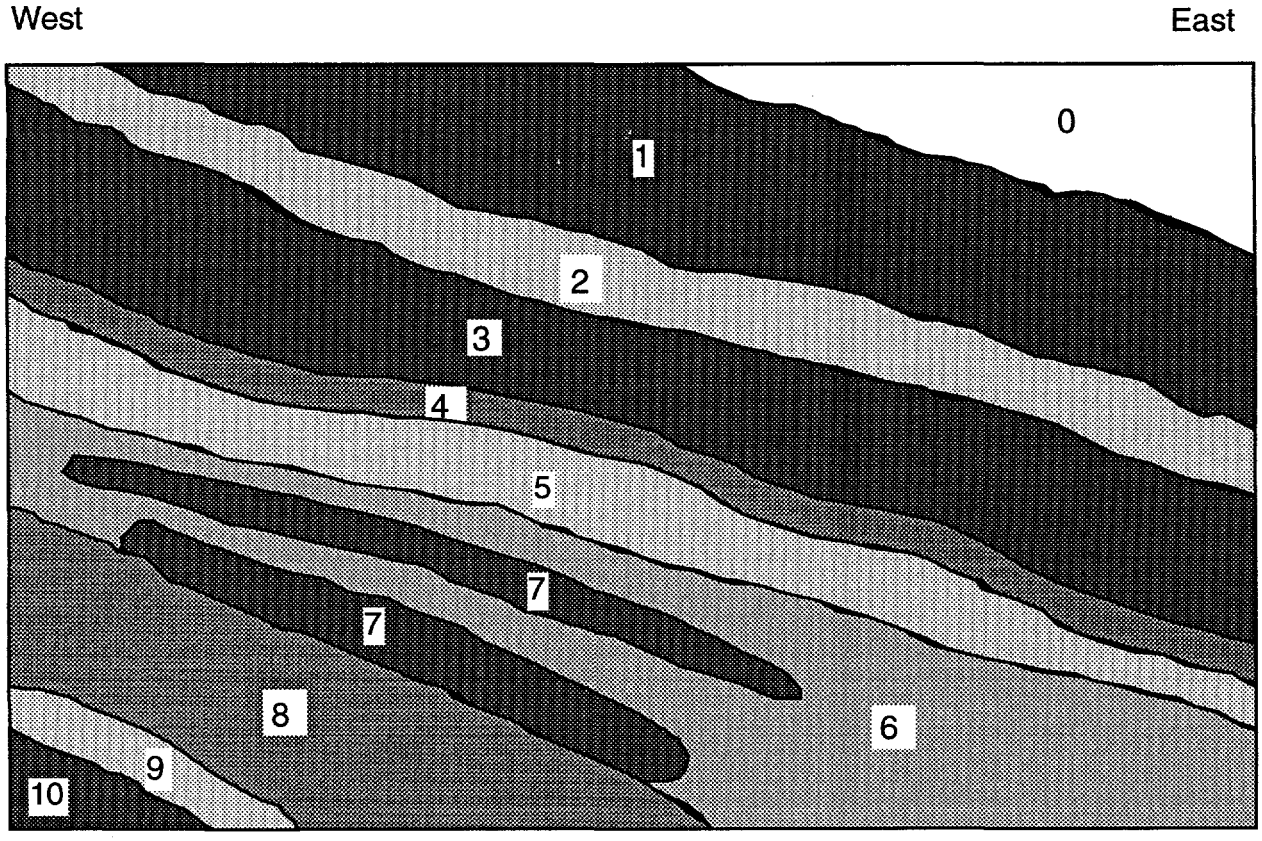

0 Unsimulated
1 Tiva Canyon welded
2 Paintbrush nonwelded
3 Topopah Spring welded
4 Topopah Spring basal vitrophyre
5 Calico Hills/Prow Pass vitric nonwelded
6 Calico Hills/Prow Pass zeolitic nonwelded
7 Prow Pass welded
8 Bullfrog welded
9 Bullfrog nonwelded
10 Tram welded

Figure 2-8. Conceptual cross-section used in the interpretation of three-dimensional lithologic simulations.

The two intervals may merge into a single welded zone outside the modeled region, indicating that the Prow Pass Member actually is a composite cooling unit. In any event, the two welded subzones are compatible with the assumptions of the modeling process, and these intervals have been respected in the simplified, simulated computational columns for TSPA-93. The interesting aspect of the two welded lenses is whether they have any impact on the flow and transport calculations; i.e., the performance of the site. Note that in the data used for this simulation, the Prow Pass welded unit is found northeast of Drill Hole Wash (and in the wash), but does not appear in drillholes within the repository region.

This page left intentionally blank.

3.0 Hydrogeologic Parameter Development

The hydrogeologic units developed in Chapter 2 are the physical description of the model of Yucca Mountain. To use this domain for hydrologic modeling of the effects of a potential repository at the site requires the assignment of hydrogeologic parameters to the units. These parameters are derived from hydrologic and other physical properties of the units. The parameters represent the statistical interpretation of the properties. "Properties" are considered to be the hydrologic characteristics described by the source data, while "parameters" are the resulting interpreted values derived from those data. Throughout the rest of this document, the term "parameter" is interpreted as the statistical parameters. The parameter probability density functions (PDFs) are developed from the hydrogeologic parameters. A PDF gives the likelihood of a value when the function is randomly sampled.

The PDFs discussed here were first developed for use with TSPA-93. Derivation of the PDFs is based on the approach developed for TSPA-91 (Barnard *et al.*, 1992). The PDFs used in TSPA-91 were not constrained by the observed data ranges, due to the scarcity of data. Instead, those PDFs attempted to reflect both the data and the analysts' estimates of the variability and uncertainty of those data. In contrast, for TSPA-93, we have analyzed an extensive range of hydrogeologic data from the Yucca Mountain site. The parameters developed here are descriptive of the actual geology and hydrogeology at Yucca Mountain to the extent that the underlying data are representative. Where there are insufficient data to derive PDFs with acceptable confidence, appropriate site data have been used as analogs.

As data have been compiled for this effort, they have been incorporated into the Performance Assessment Working Data Set (PAWDS), created by SNL to support TSPA needs. The PAWDS is a SNL database used to facilitate data management for performance assessment. It provides a means to format, prepare, and trace data for performance-assessment calculations. The PAWDS does not replicate the Yucca Mountain Site Characterization Project Office's database (GENISES), but provides a means to locally manage specific data. The information in the PAWDS is predominantly hydrologic and geologic parameters from Yucca Mountain. It includes the information formerly maintained in the Site Engineering Properties Database (SEPDB), as well as additional published data. It is expected that the parameters derived from these data, and the PDFs developed for performance-assessment analyses, will eventually be coordinated with the YMP GENISES database.

Hydrologic information used in the analysis that is not currently in the PAWDS is from published sources, such as SAND reports and U.S. Geological Survey (USGS) Open File Reports (OFRs). These additional data consist primarily of properties for matrix porosity, permeability, saturated hydraulic conductivity, bulk density, grain density, and water retention. In each of the sections in this report on the development of specific PDFs for properties, a table lists the sources for that particular property and indicates whether or not the data are in the PAWDS.

3.1 Overview of parameter development

Most of the parameter distributions derived in this chapter are used for the simulation of unsaturated-zone groundwater flow and transport using the composite-porosity model (see TSPA-93, Chapter 14 Wilson *et al.*, 1994). The fracture-aperture distributions are used in the modeling of unsaturated-zone groundwater flow using the weeps model (see TSPA-93, Chapter 15). The bulk hydraulic conductivity distributions are used in the gas-flow modeling (see TSPA-93, Chapter 12). Additionally, equivalent-porous-medium bulk hydraulic-conductivity values are used as starting values in the saturated-zone modeling (see TSPA-93, Chapter 11).

As is discussed in TSPA-93, the repository area for flow and transport modeling is described by several columns, (five or eight, depending on the analysis), each representing an equal portion of the repository, and each with stratigraphies characteristic of that portion. The TSPA calculations are one-dimensional that require uniform hydrogeologic properties for each unit for each realization. The hydrogeologic parameters developed in this chapter are used to characterize the eight analysis columns. Each column contains up to ten hydrogeologic units from the land surface of Yucca Mountain to the water table. (The undifferentiated overburden or alluvium is not modeled in the transport simulations and is therefore not included in the columns.) Only five layers (from the repository to the water table) are used for the unsaturated flow and transport modeling; however, the units from the repository to the surface are used for the gas-flow analyses. Figure 3-1 shows the units from near the surface, through the repository, to the water table. These units are used to construct the analysis columns, each of which is described using the hydrogeologic parameters developed in this report.

Hydrogeologic properties data are available from numerous sources. There are many properties data for some hydrogeologic units. For other properties at other locations the data are much more sparse. In the cases where there are many

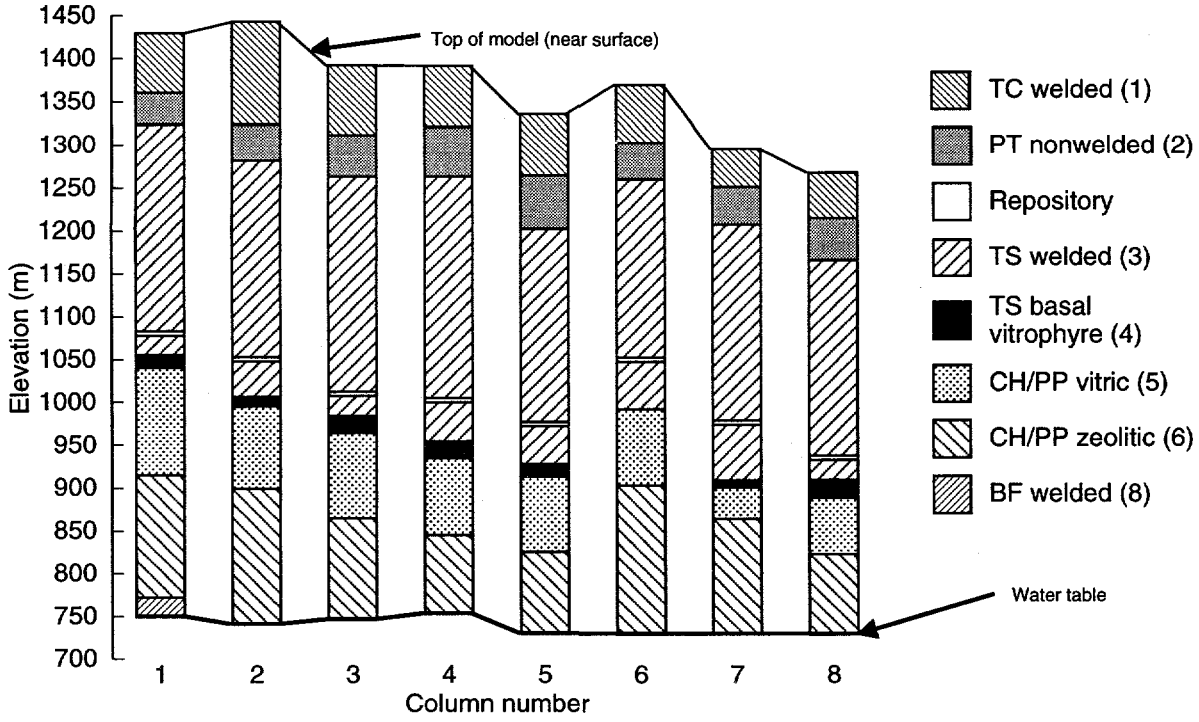

Figure 3-1. The unsaturated-zone hydrostratigraphy, from near surface through the potential repository horizon to the water table. Note that the water table elevation varies because the columns are located at different points within the repository area.

data, the parameters can be derived directly. Where data are minimal, we use a fitting routine that develops a population distribution from the sample data.

In Chapter 2, geostatistical techniques are used to develop spatial distributions of the thicknesses of the hydrogeologic units. Although the thicknesses of the units can vary by up to 50% between realizations, the hydrologic parameters associated with the units are assumed to be almost independent of thickness. Thus, all materials properties are grouped according to hydrogeologic unit and are analyzed without regard to specific location of the measurement. Each hydrogeologic unit is considered to be homogeneous, and one PDF is developed for each property in each of the ten hydrogeologic layers listed in Table 2-4.

3.1.1 Hydrologic properties considered

The hydrogeologic properties used to develop the parameter distributions fall in three major categories: matrix, bulk hydraulic, and fracture. The parameters are determined from the properties listed in Table 3-1.

Each of the specific parameter subsections in this report contains a table that includes the following data:

- the hydrogeologic units;
- the basic statistics, which include the number of observations (n), the expected value ($E[x]$), the coefficient of variation ($CV[x]$), the minimum (Min[x]) and maximum (Max[x]) values of the parameter;
- the beta exponents (α and β); and
- additional parameters for matrix properties: the scaled parameters for PDFs (the scaled coefficient of variation (SCV) and the scaled exponents α and β).

Table 3-1. Hydrogeologic properties used to determine PDFs.

Matrix Properties	Bulk Properties	Fracture Properties
Porosity (ϕ)	Bulk saturated hydraulic conductivity (K_{bs})	Frequency (F_f)
Rock bulk density (ρ_b)	Gas permeability (K_{bg})	Orientation (θ_f)
Saturated hydraulic conductivity (K_s)	Combined saturated hydraulic conductivities (bulk and gas)	Spacing (a_f)
Water retention (van Genuchten): air-entry (α_{vG}), saturation/desaturation (β_{vG}), and residual degree of saturation (S_r)		Hydraulic aperture (b_f)
		Porosity (ϕ_f)
		Saturated hydraulic conductivity (K_f)
		Water retention (van Genuchten): air-entry (α_{vGf})

3.1.2 Development method

The goal in developing PDFs is to represent the data with the least possible amount of interpretation to minimize the chance of biasing the results. Five steps are performed to develop the required PDFs for input to the flow and transport models. These are: identification of data, inclusion of the data in the PAWDS, preparation for analysis, statistical reduction to determine parameters, and definition of probability density functions from the parameters.

3.1.2.1 Data manipulation

The basic data, as identified from different sources, are sorted and grouped to correspond with each of the modeled hydrogeologic units. As data are entered into the PAWDS, they are evaluated for reasonableness. If there are questions of inter-

pretation, an attempt has been made to confirm their validity. As the data are prepared for analyses, they are converted to consistent units. The parameters calculated for each data set are the expected value, $E[x]$ (the mean), the high and low values (*Max* and *Min*), and the standard deviation *(SD)*. The coefficient of variation (*CV*) is also determined:

$$CV = \left| SD / E[x] \right| . \tag{3.1}$$

3.1.2.2 Description of probability density functions

The functional form of the PDFs is given by the beta function (Harr, 1987). The beta function is defined by (1) the minimum value, (2) the maximum value, (3) the mean, and (4) the coefficient of variation of the variable. The beta function can produce PDFs with many shapes (e.g., uniform, exponential, normal, bathtub). When combined with the principle of maximum informational entropy (Jaynes, 1957), the shape of the beta function is dictated by the data available. For example, knowing only the minimum and maximum values of a property requires that the PDF be a uniform distribution across the minimum-to-maximum range.

3.1.2.2.1 Normal distributions

Hydrologic properties such as matrix porosity and matrix bulk density that have large, normally distributed data sets produce distribution shapes that are approximated by normal curves. Such a distribution is presented in the following form (Gogg and Mott, 1992):

$$f(x) = \frac{1}{\sqrt{2\pi\sigma^2}} e^{-(x-\mu)^2/2\sigma^2} \text{ , for all } x. \tag{3.2}$$

An example of an approximation to a normal distribution is shown in Figure 3-2 for porosity in hydrogeologic unit 3. The solid line shows the histogram of 1234 data properties and the dashed line shows the distribution function for the data set. This data set represents a large population well distributed around a mean, with a strong central tendency. A data set such as this is the easiest and most straightforward to use.

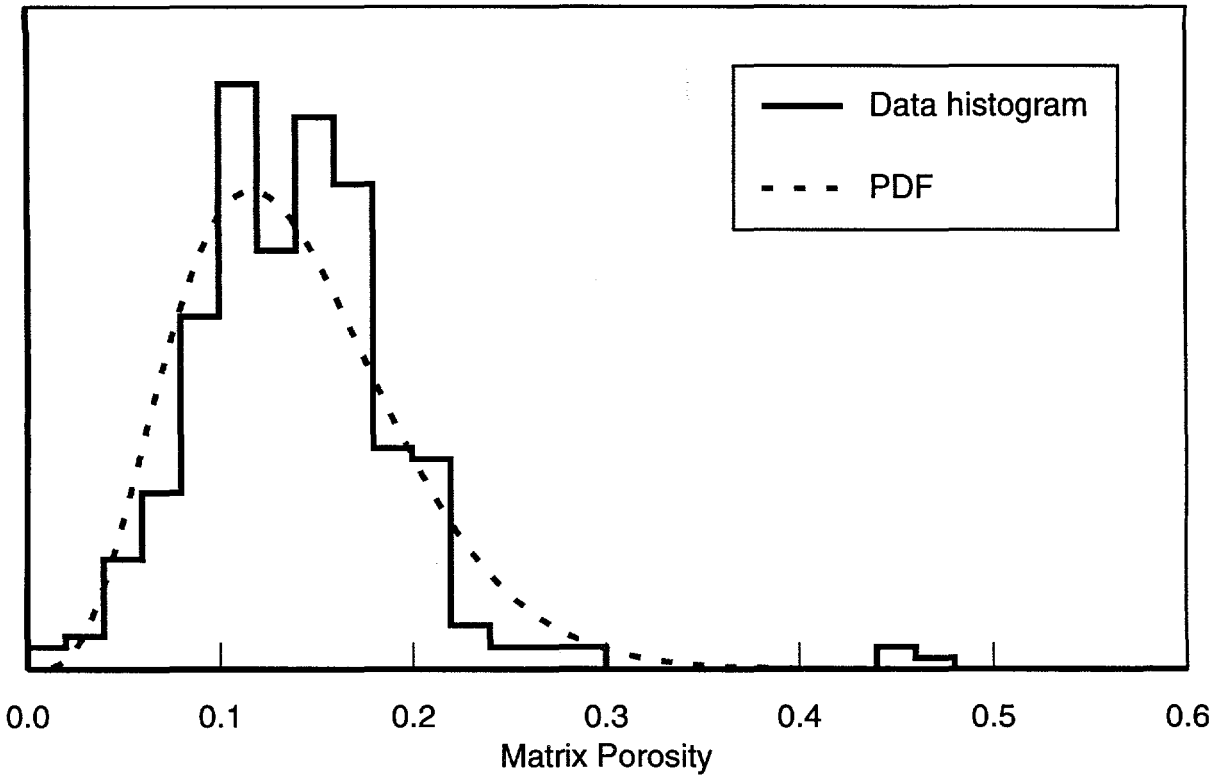

Figure 3-2. Representative normal distribution for matrix porosity for unit 3.

3.1.2.2.2 Lognormal distributions

Another common distribution is the lognormal distribution. A lognormal distribution is represented in the form (Gogg and Mott, 1992):

$$f(x) = \begin{cases} \dfrac{1}{x\sqrt{2\pi\sigma^2}} e^{-(\ln x-\mu)^2/2\sigma^2}, & x > 0 \\ , \textit{otherwise } 0. \end{cases} \quad . \tag{3.3}$$

The lognormal distribution is used for data sets such as permeability and conductivity that span many orders of magnitude. Note that some physical conditions follow lognormal distributions (Krumbein and Graybill, 1965). Figure 3-3 illustrates the use of a lognormal interpretation of matrix saturated conductivity data for unit 3. When plotted on a linear scale (Figure 3-3a), the data are closely grouped near zero. When converted to log values, Figure 3-3b, the data are represented by a slightly right-skewed normal distribution. The resulting logarithmic distribution curve for the data is superimposed on the data in Figure 3-3b.

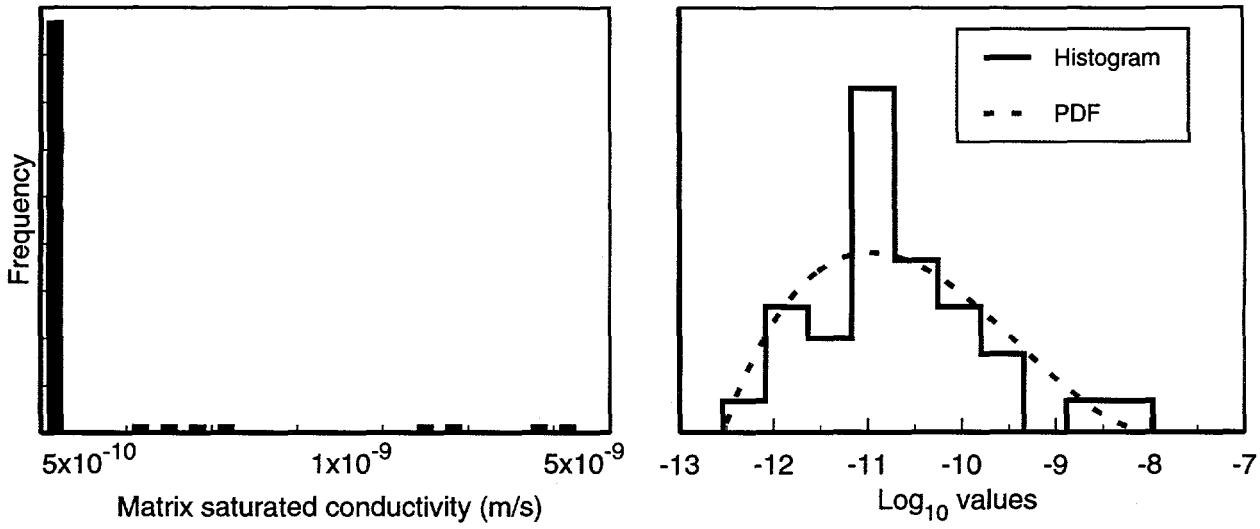

Figure 3-3a. Normal distribution for unit 3, matrix saturated conductivity.
Figure 3-3b. Lognormal distribution for unit 3, matrix saturated conductivity.

3.1.2.2.3 Exponential distributions

Exponential distributions are used for two reasons: for data that are skewed to one end of the range, or for limited amounts of data. For some parameters, the data are so sparse that only a mean value is known. Consistent with the maximum entropy formalism, the exponential distribution is used to define a PDF. The exponential distribution is in the form (Gogg and Mott, 1992):

$$f(x) = \begin{cases} \frac{1}{b} e^{-x/\beta}, x \geq 0 \\ \quad\quad , \text{otherwise } 0 \end{cases} . \tag{3.4}$$

As Figure 3-4 illustrates, even with a very large data set, if the data are strongly skewed toward one end of the range, an exponential PDF is appropriate.

3.1.2.2.4 Beta-function distributions

Because of the ability of the beta function to represent all these distribution types, we have chosen to use this function to generate all the PDFs. Over the range $[a,b]$, the beta function produces a PDF, $p(x)$, given by

$$p(x) = C(x-a)^{\alpha}(b-x)^{\beta} , \tag{3.5}$$

where α and β define the shape of the distribution, and C is a normalizing constant. The normalizing constant is undefined for values of α and β less than -1. When the α and β parameters are less than 0, this often is an indication that the range of the pa-

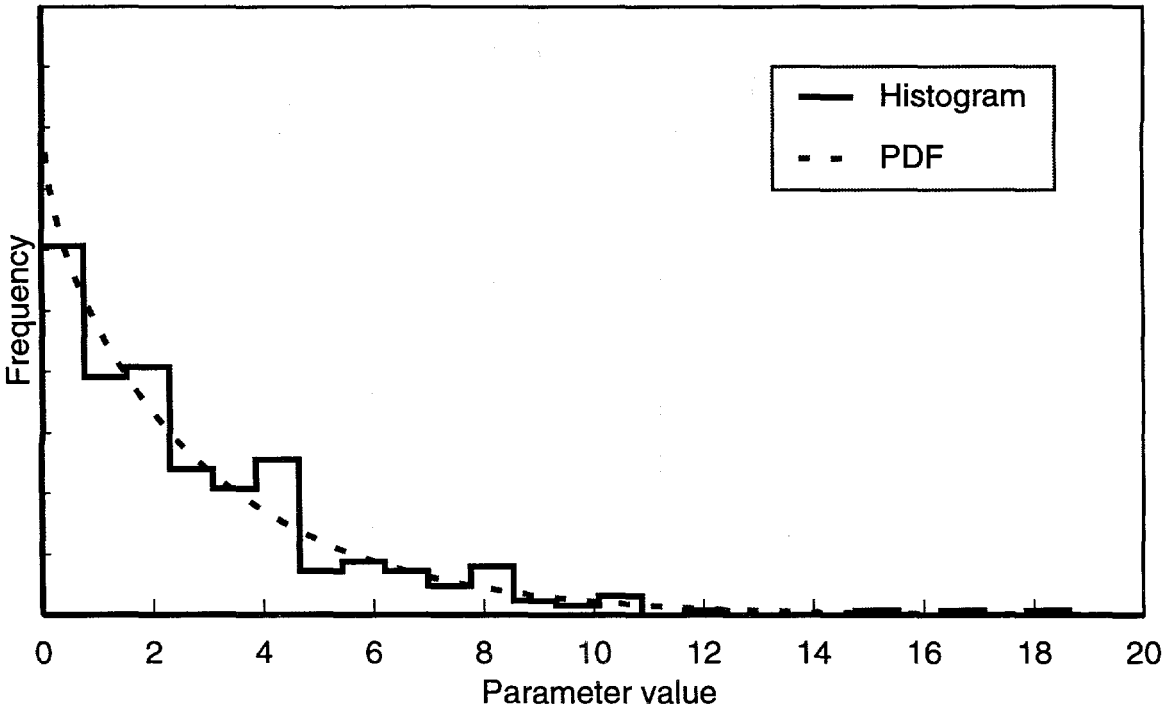

Figure 3-4. Fracture frequency histogram, unit 3.

rameter is underestimated; in this case, the PDF does not have a mode in the interior of the range, but the greatest probability density occurs at one or both extremes.

3.1.2.3 Considerations when describing data with PDFs

Where data are numerous, the parameters of the data set can be used directly to determine a beta-function PDF. It is possible that the range of the properties values actually measured may not encompass the physically possible range of values; thus, this approach may not be appropriate for all large data sets. Some properties, such as porosity, have a physical range that can be determined independently of the available data; the minimum and maximum values of porosity are defined to be 0.0 and 1.0. This extension of the range of data to the theoretical range is intended to recognize that the finite sample size is not exhaustive and that values outside the sample are possible. Note that the probability of sampling a value near the theoretical maximum or minimum may be very unlikely, if the area under the PDF near those points is insignificant. For properties where the data are not extensive and no physical restrictions exist on the range of the parameter, a beta distribution is fit using a nonlinear entropy fitting program.

3.1.2.3.1 Numeric fitting of distributions

Given a set of continuous data $x_1 < ... < x_i < ... < x_n$, a density function can be constructed:

$$f_n(x) = \frac{1}{(n-1)(x_{i+1} - x_i)}, \; x_i < x < x_{i+1}. \tag{3.6}$$

The formula can easily be adjusted for nonunique data ($x_i = x_{i+1}$ for some i). This function discretizes the continuous data into a histogram. The heights of the histogram elements are proportional to the closeness of adjacent data (x_i and x_{i+1}); thus, the continuous data are represented as a probability distribution.

A quantitative measure is required to evaluate the fit between the function $f_n(x)$ given by Equation (3.6) and the probability model. One common technique for fitting data to a model is least squares:

$$L = \sum_{i=1}^{n-1} \int_{x_i}^{x_{i+1}} [f_n(x) - p(x)]^2 dx + \int_{a}^{x_1} p(x) dx + \int_{x_n}^{b} p(x)^2 dx \;, \tag{3.7}$$

where L is the measure of goodness of fit (i.e., the least-squares residual), and $p(x)$ is the probability density function. Another technique is Shannon's entropy function (Shannon, 1948):

$$S = \sum_{i=1}^{n-1} f_n(x) \int_{x_i}^{x_{i+1}} ln[f_n(x)/p(x)] dx \;, \tag{3.8}$$

where S is the maximum-entropy measure of the goodness of fit.

This work has used the maximum-entropy formalism to develop PDFs. The advantage of this formalism can be seen from a typical situation occurring for data to be fitted with a PDF. If $p(x) = 0$, the PDF predicts a zero probability of having a value at x. Using Equation (3.7), the residual L has a finite value $f_n(x)^2$ for this case, even though this has no physical meaning. Shannon's entropy function (Equation 3.8) produces infinity for $p(x)=0$, a value more consistent with physical intuition. Similarly, a fixed deviation between the model and data for a small probability is more significant than the same deviation for a large probability, yet least squares does not distinguish between the two cases. A more theoretical justification of the use of Shannon's entropy is possible but beyond the scope of this report (Jaynes, 1957).

The maximum-entropy fitting procedure attempts to infer the properties of the entire population from the limited sample. Not only does the PDF reflect the shape of the frequency-distribution of the data, but it also has a range dependent upon the structure of data. For example, if data are all closely grouped at one end of the observed range, the entropy fit would interpret this as a physical limit to the property (as is illustrated in Figure 3-5 by the behavior of the fit near the parameter value 0.1). If, on the other hand, the data at the end of the range are quite scattered, the entropy fit would produce a tail on the probability distribution, implying the physical range of the data is greater than the observed range (as shown in Figure 3-5 near the value 0.8). Although the entropy fit helps in interpreting limited data sets, it does not reduce the inherent uncertainty due to small amounts of data.

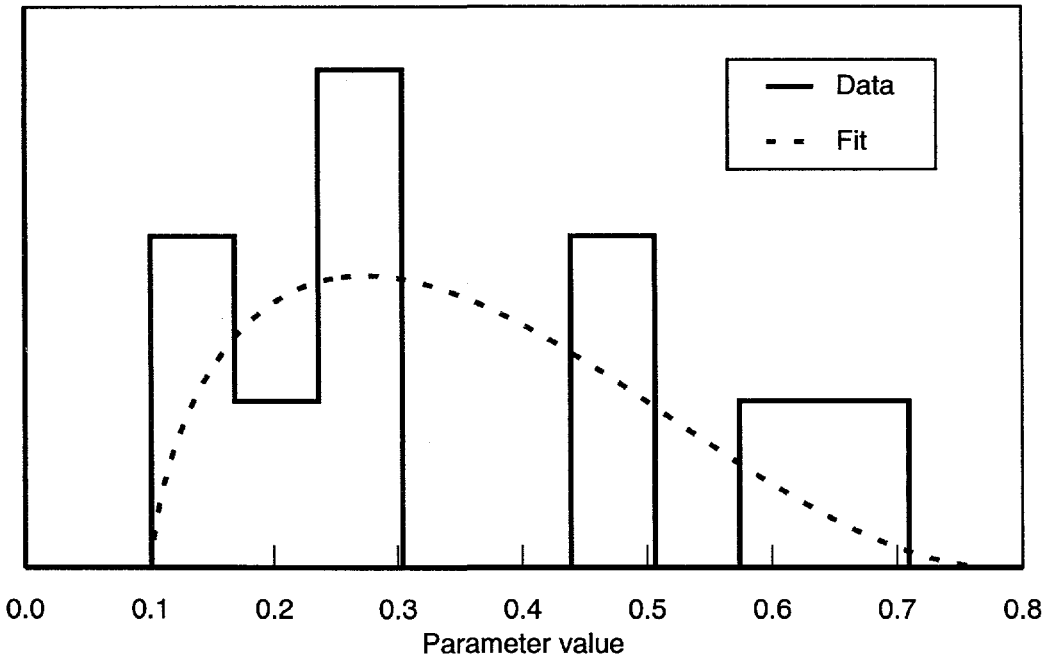

Figure 3-5. Fit to limited data using the entropy-fit routine.

The entropy fit uses nonlinear optimization to determine the best fit. Nonlinear optimization can be sensitive to the initial choices for the parameters. When the endpoints of the distribution are near the minimum and maximum of the data range, high values for the entropy and high gradients result; this sometimes causes numerical difficulties. Where such numerical difficulties exist, increasing the initial choices for the range from that of the data range circumvents the numerical problems. However, the choice of too large values for the endpoints may result in beta-function exponents that are excessively large. This also causes numerical problems.

3.1.2.3.2 Fracture parameter derivation

Limited data on fractures require a different approach to determine the modeling parameters. Only two fracture properties—frequency and orientation—are available from actual measurements of down-hole data. The remaining fracture parameters must be derived using functional relationships. Details of this derivative approach are fully described in Section 3.4.

3.1.2.3.3 Analog derivations

Because there are insufficient data, PDFs cannot be developed for bulk saturated hydraulic conductivity in three of the hydrogeologic units and for fracture orientation in six of the hydrogeologic units. In this case we select an existing hydrogeologic unit that most closely represents the hydrogeologic unit for which data are missing. Analog distributions are then created with adjustments to account for uncertainty. To make these adjustments for uncertainty, either the coefficient of variation is increased or the range is adjusted. Range adjustment is often done by setting the minimum and maximum to one or more standard deviations about the mean. This allows for more scatter around the expected value, a concession to our lack of knowledge.

3.1.2.3.4 Other considerations

In the cases where the α and β parameters of the beta function are both calculated to be less than 0 (which results in a "bathtub" shape to the PDF), we review the properties data to see if this PDF shape is physically reasonable. If it is not, the PDFs are recalculated by adjusting the range of the parameter.

Some properties (such as hydraulic conductivity) are typically distributed log-normally. Other properties have been transformed to log space if PDFs generated from the untransformed data are not well behaved. The beta distribution is able to approximate both linear and log-transformed data. Note that the logarithm of the mean of a parameter distribution is not the same value as the mean of a log-transformed distribution. Means listed for linear and log-transformed properties (such as matrix saturated hydraulic conductivity and van Genuchten parameters, etc.) given in the tables in this chapter reflect this.

3.1.3 Scaling

Once the parameters have been determined, the matrix parameters require one additional modification. Geologic materials are known to be heterogeneous but are modeled in performance-assessment analyses as being homogeneous. Therefore,

what is needed for the models is the average value of the property over the entire unit thickness. When matrix properties are determined from small core samples in a laboratory, the question that must be asked is: To what degree do the small-scale samples represent the entire hydrogeological unit? Properties values that are obtained from only a few small samples may have greater variability in the measured values (averaged over the sample) than an average taken over the entire unit. Therefore, to compensate, we reduce the variability of the parameters derived from the observed data to make them more representative of the average over the entire thickness.

The approach we use to scale parameters is an initial attempt at addressing this question. We adjust the coefficient of variation (a measure of the spread in the data) calculated for the sample to better reflect the distribution of values over the unit to be modeled. The formula we use (Freeze and Massmann, 1990) scales the coefficient of variation (CV) for either the untransformed or $\log_{10}$-transformed data to give a scaled coefficient of variation (SCV):

$$SCV = CV\sqrt{\lambda / \bar{t}}, \quad \lambda < \bar{t}, \tag{3.9}$$

where CV is the unscaled coefficient of variation, λ is the vertical correlation length and, $\bar{t}$ is the mean thickness of the entire hydrogeologic unit. Because $\bar{t}$ is greater than λ, the SCV is smaller than the CV, meaning that the variation in the mean value of the property over the entire unit thickness is reduced.

To illustrate the effect of scaling, consider the PDFs shown in Figure 3-6. These PDFs are used to represent a property such as porosity over an entire hydrogeologic unit. For the original unscaled data (the solid line in Figure 3-6), the expected value of the parameter is 0.139, with an effective range (defined as probability densities greater than about 15% of the maximum probability density) from 0.01 to 0.36. This implies that the parameter value can lie between the values 0.01 or 0.36 for the entire unit. After applying the scaling transformation, the mean of the parameter is the same (0.139), but the *Min* and *Max* values change to approximately 0.03 and 0.29 (the dashed line in Figure 3-6). Thus, the range of the PDF has narrowed and increased the probability density around the expected value.

3.2 Hydrologic units parameterized

The hydrogeologic units for which PDFs for matrix properties are derived are shown in Table 3-2. In order to perform the scaling transformation discussed above, both the vertical correlation length and the mean thicknesses of the units must be

known. The vertical correlation length is set to 30 meters based on a composite vertical porosity variogram, (λ = 40+190Sph(30); Rautman and Flint, 1992). The same SCV was used for all units because of a lack of data for the individual units. The unit thicknesses given in Ortiz *et al.* (1985) are used as the bases for scaling the data and are listed in Table 3-2. Unit thicknesses from Ortiz *et al.* are comparable to the mean unit thicknesss derived from the geostatistical simulations.

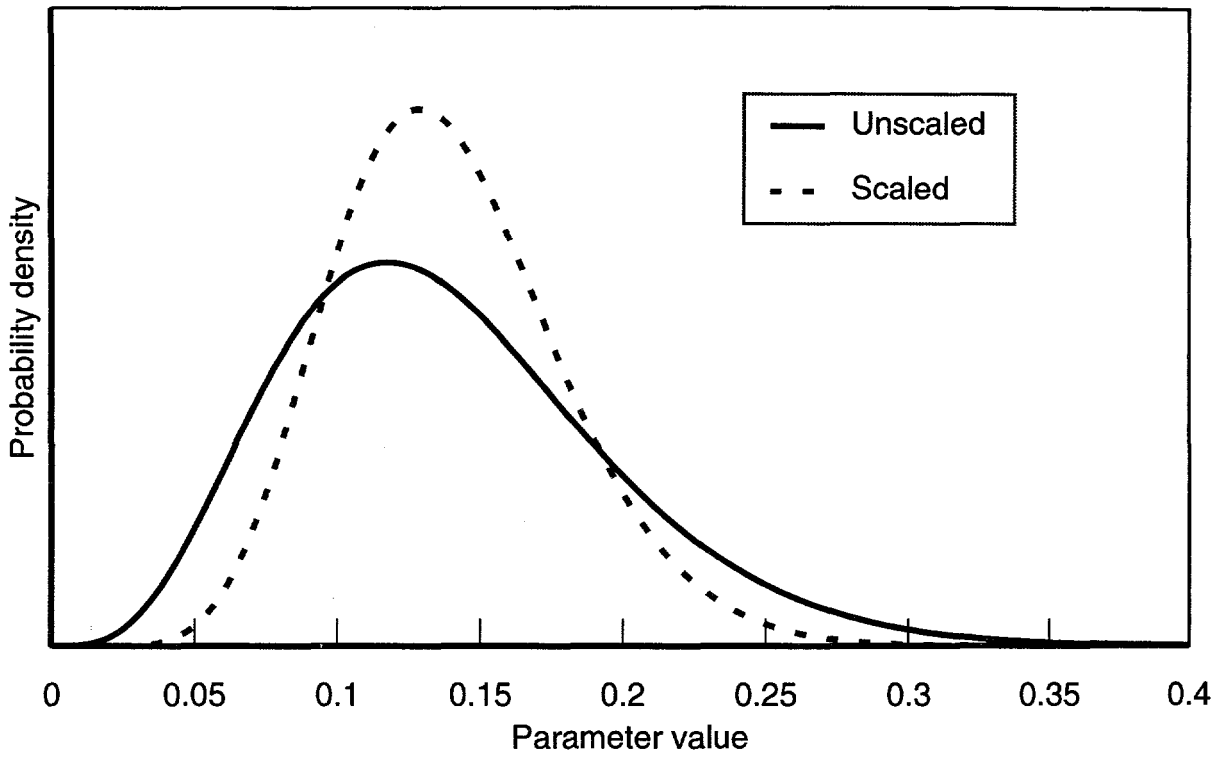

Figure 3-6. Comparison of unscaled and scaled parameter distributions.

The unsaturated flow calculations use only the units from the repository down to unit 8. Hydrogeologic unit 3 (the Topopah Spring welded), in which the potential repository is located, includes a subunit (3R) running from the base of the repository to the top of the basal vitrophyre, to properly scale the PDFs for the portion of the unit used in the modeling. Scaling is done for both the repository subunit (3R), as well as the complete Topopah Spring welded unit (3C). Scaling is done for all units with mean thicknesses greater than the 30-meter vertical correlation length.

Table 3-2. Hydrogeologic units and their mean thicknesses.

Unit	Hydrogeologic Unit and Lithology	Mean Thickness ($\bar{t}$)*
1	Tiva Canyon welded	81.00
2	Paintbrush nonwelded	39.43
3C	Topopah Spring welded–composite	237.80
3R	Topopah Spring welded–repository	61.20
4	Topopah Spring vitrophyre	14.63**
5	Calico Hills/Prow Pass nonwelded-vitric	63.99
6	Calico Hills/Prow Pass nonwelded-zeolitic	126.88
7	Prow Pass welded	†
8	Bullfrog welded	†
9	Bullfrog nonwelded	***
10	Tram welded	***

* Determined from Ortiz *et al.* (1985).
** The mean thickness is less than the vertical correlation length.
† Thicknesses for these units are not reported by Ortiz *et al.* (1985); PDFs were not scaled.
*** These units do not occur in the unsaturated-zone models.

3.2.1 Matrix parameter distributions

The following sections present compilations of data contained in the PAWDS and other sources for the matrix hydrogeologic parameters. As is discussed above, the hydrogeologic units are assumed to be homogeneous, and matrix property data have been assigned to the units without regard to the location within the units from which they were measured. At the interfaces of the units, it may occasionally be uncertain to which unit a datum belongs. After compiling the data for the unit, the minimum and maximum are determined; if there are enough data to make the calculations meaningful, the mean and variance of the data are also determined.

3.2.1.1 Porosity (ϕ)

The matrix porosity data for the ten hydrogeologic units are from the sources listed in Table 3-3. Porosity data are among the most extensive (1234 measurements available). The published values were derived by various analysis and laboratory techniques. They are: dry and saturated bulk and grain densities, gas pycnometer, buoyancy, water invasion, humidity and 105°C oven dry, and mass per volume.

Table 3-4 presents the parameters for matrix porosity data in three representations: basic statistics, beta-probability-distribution parameters, and the scaled PDF parameters. Included in the statistics for each unit are the number of data and the parameters required to generate the beta-PDFs. Because the theoretical limits of the porosity are known (i.e., porosity is defined from 0.0 to 1.0), these values are used to determine the unscaled beta-PDFs. Note that there is little effect on the PDF by overestimating the range, while underestimating the range (which commonly oc-

curs) imposes a subjective constraint on the property. Thus, the maximum and minimum for the PDFs have been adjusted beyond the limits of the observed data.

Table 3-3 Sources for matrix porosity (ϕ) data.

Source	Drillhole or Lithology	PAWDS PAN No.
Anderson (1991)	UE-25a-#4 through 7 and UE-25p #1	PA00001
Flint and Flint (1990)	Nonwelded and bedded tuffs	PA00002
Peters, *et al.* (1984)	USW GU-3 and USW G-4	PA00004
Yucca Mountain Project (1992a)	USW GU-3	PA00006
Yucca Mountain Project (1992b)	UZN-54 and UZN-55	PA00007
Rush *et al.* (1984)	USW H-1	PA00010
Lahoud *et al.* (1984)	UE-25b #1	PA00011
Weeks and Wilson (1984)	USW H-1	PA00012
Anderson (1981a)	UE-25a #1	PA00015
Anderson (1984)	USW GU-3/G3 and USW G-4	PA00016
Lin and Daily (1984)	Topopah Spring Tuff	PA00017
Knauss *et al.* (1985)	Topopah Spring Tuff	PA00018
Knauss and Peifer (1986)	Topopah Spring Tuff	PA00019
Schwartz (1990)	Unsaturated zone tuffs	PA00020
Rush *et al.* (1983)	USW H-1	PA00025
Kume and Hammermeister (1990)	USW UZ-7	PA00029

Table 3-4. Matrix porosity (ϕ) statistics, and beta and scaled beta-PDF parameters.

	Statistics					Beta Distribution Parameters				Scaled Beta-Distribution Parameters		
Unit	n	$E[x]$	CV	Min	Max	Min	Max	Alpha	Beta	SCV	Alpha	Beta
1	290	0.087	0.634	0.033	0.450	0.000	1.000	1.183	21.823	0.386	5.043	62.183
2	205	0.421	0.248	0.132	0.650	0.000	1.000	7.992	11.361	0.216	10.950	15.428
3C	300	0.139	0.412	0.004	0.480	0.000	0.368*	3.934	29.567	0.146	27.682	46.255
3R	300	0.139	0.412	0.004	0.480	0.000	1.000	3.934	29.567	0.288	9.209	62.234
4	26	0.065	0.656	0.014	0.177	0.000	1.000	1.107	29.134	–	–	–
5	117	0.331	0.271	0.097	0.510	0.000	1.000	7.775	16.720	0.186	18.093	37.555
6	127	0.306	0.209	0.141	0.470	0.050*	0.562*	14.573	34.254	0.102	32.317	32.315
7	70	0.292	0.239	0.101	0.430	0.000	1.000	11.110	28.422	–	–	–
8	26	0.165	0.361	0.058	0.231	0.000	1.000	5.243	30.601	–	–	–
9	41	0.261	0.193	0.174	0.380	0.000	1.000	18.578	54.428	–	–	–
10	32	0.191	0.306	0.018	0.280	0.000	1.000	7.445	34.691	–	–	–

* Values used for the scaled beta distribution; 0.000 and 1.000 used for the unscaled.
– These units are not scaled.

For most units, the unscaled beta-PDFs for porosity are determined using the theoretical minimum and maximum. When units 3C and 6 were scaled, the initial α and β exponents were large, resulting in numerical problems. These beta-PDFs are recalculated using as ranges multiples of the standard deviation. Using the rule of thumb devised for the TSPA-91 PDFs, ranges based on four standard deviations above and below the mean are used. This constraint has no practical effect, since virtually no area is under the PDF curves outside four standard deviations. For unit

3C, the maximum has been adjusted and the minimum remains at 0.0. For both units 3C and 6, it is likely that the maximum observed porosity values are statistical outliers; their presence has skewed the beta distributions. The choice of a maximum for unit 3C that is less than the observed maximum supports this observation.

The parameters are graphically shown in Appendix III. For those parameters that are scaled, only the scaled PDFs are shown. Comparison of a scaled and unscaled PDF in Section 3.1.1 illustrates the difference between the two distributions.

Comparing the resulting beta PDFs for porosity in this study to TSPA-9l shows significant differences. The range for both beta distributions is given by the theoretical limits (0.0 to 1.0). Consequently, differences in the PDFs arise due to differences in the means (arising from the different data sets) and differences in the coefficients of variation (arising from different assumptions about the variability of the data). Table 3-6 gives the means for the three comparable units.

Table 3-5. Comparison of expected values for matrix-porosity: TSPA-93 and TSPA-91.

Unit (Current/TSPA-91)	Porosity		Ratio: TSPA-93/TSPA-91
	TSPA-93	TSPA-91	
3R/1	0.139	0.11	1.26
4/2	0.065	0.04	1.68
5/3	0.331	0.21	1.58

Figure 3-7 compares the beta-function PDFs for the matrix porosity in the potential repository horizon (units 3R/1) for TSPA-93 and TSPA-91. The TSPA-93 distribution can be seen to have a considerably higher probability of yielding porosities above a porosity of 0.15 than does the TSPA-91 PDF. The different curve shapes result from a 26% larger expected value and 30% smaller CV. Differences of similar nature would be expected for the other two units.

3.2.1.2 Matrix rock bulk density (ρ_b)

Matrix rock bulk density values derived from matrix core samples are statistically analyzed for each of the ten hydrogeologic units. The sources for the data are listed in Table 3-6. Rock bulk density is one of the most comprehensive sets available with 2173 data for the 10 hydrogeologic units. The values are from dry, natural, and saturated states and are derived by mass-per-volume methods (both dry and saturated), mercury-displacement, buoyancy, immersion, calipered-volume, 105°C oven-dry and relative-humidity, and Archimedes-principle methods. These data are also analyzed as a comprehensive data set. Because data are very abundant for

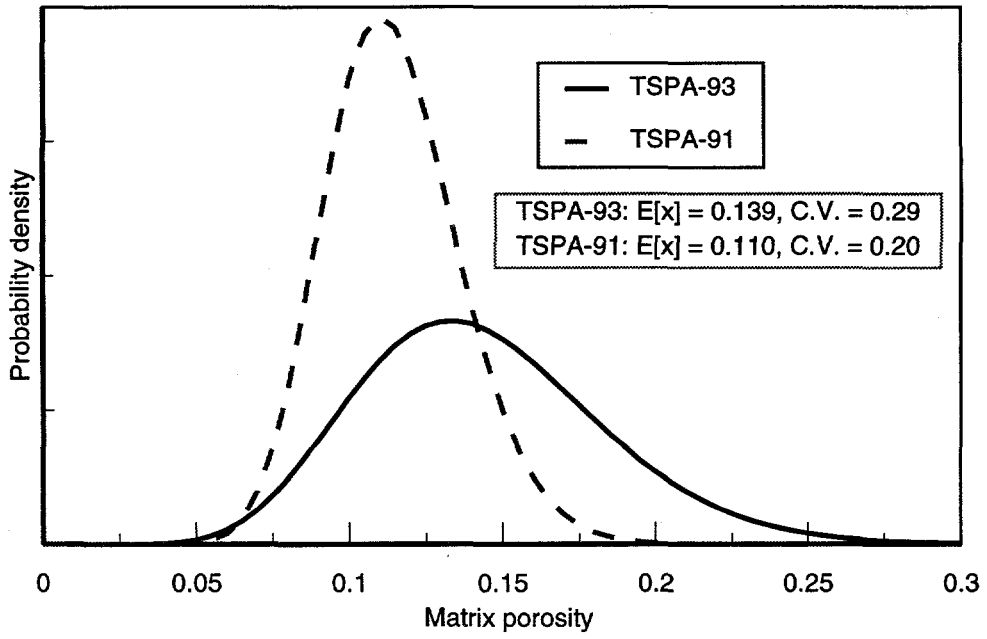

Figure 3-7. Comparison of PDFs for matrix porosity in potential repository horizon.

this property, the basic statistics (range, mean and standard deviation) can be calculated directly. Table 3-7 gives the statistics and both scaled and unscaled PDF parameters.

Table 3-6. Sources for matrix rock bulk density (ρ_b) data.

Source	Drillhole or Lithology	PAWDS PAN No.
Anderson (1991)	UE-25a-#4 through #7 and UE-25p#1	PA00001
Flint and Flint (1990)	Nonwelded and bedded tuffs	PA00002
Kume and Hammermeister (1991)	USW UZ-13	PA00003
Peters *et al.* (1984)	USW GU-3 and USW G-4	PA00004
Yucca Mountain Project (1992a)	USW GU-3	PA00006
Yucca Mountain Project (1992b)	UZN-54 and UZN-55	PA00007
Rush *et al.* (1984)	USW H-1	PA00010
Lahoud *et al.* (1984)	UE-25b #1	PA00011
Weeks and Wilson (1984)	USW H-1	PA00012
Thordarson (1983)	J-13	PA00013
Nimick *et al.* (1987)	USW G-2	PA00014
Anderson (1981a)	UE-25a #1	PA00015
Anderson (1984)	USW GU-3/G3 and USW G-4	PA00016
Lin and Daily (1984)	Topopah Spring Tuff	PA00017
Knauss *et al.* (1985)	Topopah Spring Tuff	PA00018
Knauss and Peifer (1986)	Topopah Spring Tuff	PA00019
Schwartz (1990)	Unsaturated zone tuffs	PA00020
Rutherford *et al.* (1992)	USW G-1, USW GU-3, and USW G-4	PA00021
Anderson (1981b)	UE-25a #3	PA00023
Rush *et al.* (1983)	USW H-1	PA00025
Kume and Hammermeister (1990)	USW UZ-7	PA00029

Table 3-7. Matrix rock bulk density (ρ_b) statistics, and beta and scaled beta-PDF parameters.†

Unit	Statistics					Beta-Distribution Parameters		Scaled Beta-Distribution Parameters		
	n	$E[x]$ (kg/m^3)	CV	Min (kg/m^3)	Max (kg/m^3)	Alpha	Beta	SCV	Alpha	Beta
1	380	2285	0.050	1410	2420	5.974	0.076	0.031	18.529	2.013
2	268	1419	0.197	850	2420	1.279	3.010	0.172	2.013	4.459
3C	750	2247	0.060	1360	2710	13.188	6.406	0.021	119.528	61.914
3R	750	2247	0.060	1360	2710	13.188	6.406	0.041	30.135	15.252
4	59	2308	0.026	2090	2400	2.213	0.356	–	–	–
5	199	1737	0.167	1050	2280	0.909	0.511	0.115	3.704	2.726
6	198	1746	0.110	1300	2230	1.327	1.525	0.053	10.390	11.360
7	82	1775	0.117	1440	2390	0.342	1.469	–	–	–
8	61	2260	0.071	1800	2510	1.246	0.221	–	–	–
9	92	2021	0.090	1600	2320	0.640	0.165	–	–	–
10	84	2185	0.065	1800	2470	1.551	0.889	–	–	–

– These units are not scaled.

Figure 3-8 shows the histogram of the data and the beta-function PDF for unit 3 (Topopah Spring welded). The PDF shown in Figure 3-8 is typical of the nature of the fit by a beta function to numerous data. An important characteristic of the fit is for the modes to coincide and for the widths of the peaks to be similar. The width of the PDF is controlled by the scaling transformation done (see Section 3.1.3). The modes of the two curves appear to be almost coincident; the two curves show slight skewing to the left (skewness = -1.1).

3.2.2 Matrix saturated hydraulic conductivity (K_S)

A total of 257 matrix saturated hydraulic conductivity values applicable to the modeled hydrogeologic units are used in the analysis. The sources of data for the parameter are listed in Table 3-8. Other published data (Yucca Mountain Project, 1992a), not incorporated in the PAWDS, are also part of this data set.

Table 3-8. Sources for matrix saturated hydraulic conductivity (K_S) data.

Source	Drillhole	PAWDS PAN No.
Flint and Flint (1990)	USW G-1, UE-25c #1, UE-25a #1, and UE-25a #6	PA00002
Peters *et al.* (1984)	USW G-4	PA00004
Rush *et al.* (1984)	USW H-1	PA00010
Lahoud *et al.* (1984)	UE25b #1	PA00011
Anderson (1981a)	UE25a #1	PA00015

† The values in this table differ from those presented in Table 7-4 of the TSPA-93 document (Wilson *et al.*, 1994) as a result of a review of the data. Previously, the table combined a few grain-density data with the bulk-density data for units 1, 2, 3, 5, and 7.

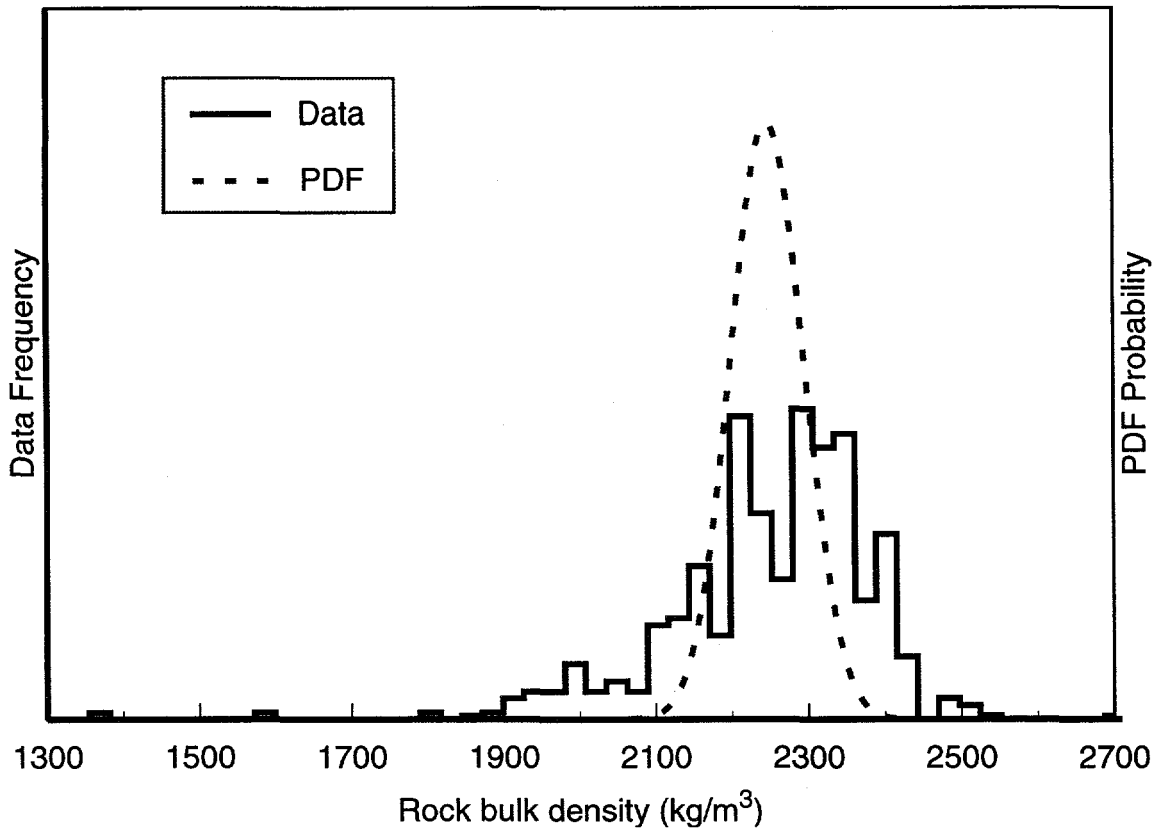

Figure 3-8. PDF fit to the rock bulk density data for unit 3 (Topopah Spring welded).

Various methods were employed in deriving K_s. For example, Rush *et al.* (1984) and Lahoud *et al.* (1984) derived values for small cores oriented both vertically and horizontally; Rush used distilled water and the constant-head technique with no application of overburden or other external pore pressures. Peters *et al.* (1984) employed the Ruska permeameter for unconfined core and Anderson (1981a) used the gas-driven and centrifuge methods to derive data.

Matrix saturated hydraulic conductivity is best represented and analyzed in log space. For this study, the data are analyzed as a beta distribution in base-10 log space. Tables 3-9a and 3-9 show the basic statistics, $\log_{10}$ statistics, and beta and scaled beta probability distribution parameters. Due to the sparseness of data, the entropy-fit routine has been used to derive the beta-function parameters. Because a nonlinear fitting procedure is sensitive to the choice of endpoints of the data range being fit, it is sometimes necessary to adjust the range to obtain reasonable beta-function PDFs. Units 1, 2, 3C, 3R, 5, 7, and 8 have been fitted with the entropy-fit routine using initial endpoints based on the ranges of the data. Unit 10 has been fitted using an initial minimum and maximum of two standard deviations (95.46% of the data

included in a normal distribution) about the mean. Units 4, 6, and 9 required initial ranges set to three standard deviations about the mean to obtain reasonable fits.

Table 3-9a. Matrix saturated hydraulic conductivity (K_S) and $\log_{10}$ statistics.

Unit	Statistics					Log_{10} Statistics			
	n	*E*[*x*] (m/s)	*CV*	Min (m/s)	Max (m/s)	E[*x*] (m/s)	*CV*	Min (m/s)	Max (m/s)
1	14	$3.86\text{x}10^{-10}$	3.32	$7.00\text{x}10^{-13}$	$4.83\text{X}10^{-9}$	-10.90	0.098	-12.16	-8.32
2	12	$5.47\text{x}10^{-7}$	1.46	$2.86\text{x}10^{-12}$	$2.35\text{x}10^{-6}$	-7.96	0.302	-11.54	-5.63
3C	66	$2.37\text{x}10^{-10}$	3.57	$3.05\text{x}10^{-13}$	$5.23\text{x}10^{-9}$	-10.71	0.084	-12.52	-8.28
3R	66	$2.37\text{x}10^{-10}$	3.57	$3.05\text{x}10^{-13}$	$5.23\text{x}10^{-9}$	-10.71	0.084	-12.52	-8.28
4	7	$2.26\text{x}10^{-11}$	1.11	$1.52\text{x}10^{-12}$	$6.95\text{x}10^{-11}$	-11.00	0.062	-11.82	-10.16
5	44	$1.82\text{x}10^{-8}$	3.27	$5.13\text{x}10^{-12}$	$2.92\text{x}10^{-7}$	-8.99	0.115	-11.29	-6.54
6	51	$1.93\text{x}10^{-10}$	3.01	$2.37\text{x}10^{-14}$	$3.14\text{x}10^{-9}$	-10.79	0.093	-13.63	-8.50
7	13	$2.58\text{x}10^{-9}$	1.28	$9.61\text{x}10^{-12}$	$8.95\text{x}10^{-9}$	-9.10	0.101	-11.02	-8.05
8	8	$4.92\text{x}10^{-10}$	0.661	$1.97\text{x}10^{-11}$	$9.26\text{x}10^{-10}$	-9.51	0.061	-10.71	-9.03
9	26	$4.20\text{x}10^{-9}$	0.950	$2.31\text{x}10^{-10}$	$1.35\text{x}10^{-8}$	-8.62	0.061	-9.64	-7.87
10	16	$1.78\text{x}10^{-9}$	1.00	$2.31\text{x}10^{-11}$	$5.79\text{x}10^{-9}$	-9.14	0.083	-10.64	-8.24

The histogram of the basic data for unit 2 (Paintbrush Tuff nonwelded) is clearly bimodal (Figure 3-9). This may occur because the matrix saturated hydraulic conductivity properties for this unit are spatially varying, or because the unit should be subdivided vertically into two units. Two values for K_S are listed in Table 3-9b. The areas under the first and second modes are 66 and 34 percent, respectively. Other parameters for unit 2 are also bimodal, as indicated in the following sections.

Table 3-9b. K_S, entropy-fit and scaled beta-PDF parameters.

Unit	Entropy Fit Distribution Parameters ($\log_{10}$)						Scaled Beta-Distribution Parameters ($\log_{10}$)		
	E[*x*] (m/s)	*CV*	Min (m/s)	Max (m/s)	Alpha	Beta	*SCV*	Alpha	Beta
1	-10.69	0.085	-12.20	-8.21	0.263	1.128	0.052	3.259	5.961
2-1st mode*	-6.42	0.081	-8.93	-3.76	10.478	11.213	0.071	14.230	15.208
2-2nd mode*	-10.75	0.076	-13.16	-6.06	4.491	9.634	0.066	6.253	13.051
3C	-10.68	0.087	-12.54	-7.97	0.980	1.875	0.031	17.491	25.854
3R	-10.68	0.087	-12.54	-7.97	0.980	1.875	0.061	3.456	5.471
4	-11.01	0.046	-12.57	-9.65	2.899	2.400	–	–	–
5	-8.96	0.116	-11.40	-5.98	1.590	2.152	0.079	5.029	6.337
6	-10.80	0.096	-14.17	-7.97	3.294	2.598	0.047	18.900	15.705
7	-9.04	0.073	-12.39	-7.95	4.567	0.807	–	–	–
8	-9.56	0.049	-10.71	-9.03	0.231	-0.431	–	–	–
9	-8.60	0.051	-10.36	-7.70	3.732	1.432	–	–	–
10	-9.12	0.069	-10.86	-8.24	0.889	-0.042	–	–	–

* Area for 1st mode is 66 %; area for second mode is 34 %.
– These units are not scaled.

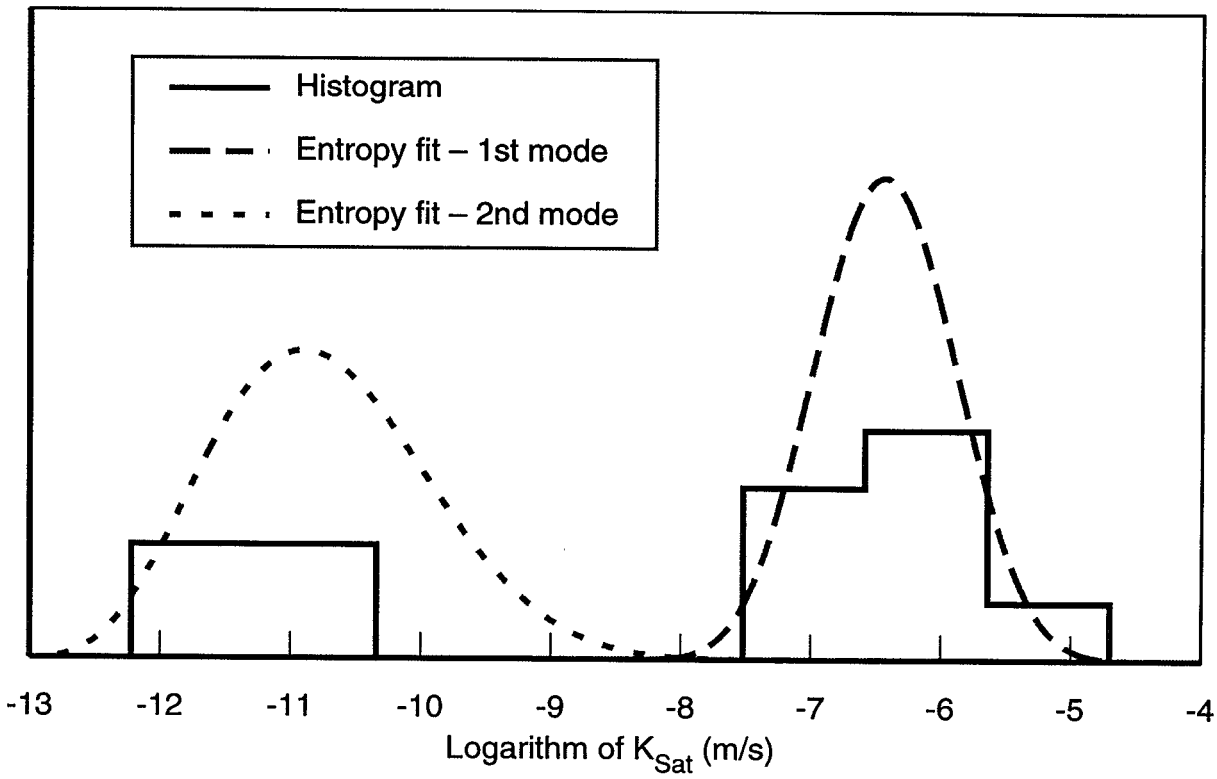

Figure 3-9. Log-transformed data and PDFs for unit 2 (Paintbrush Tuff nonwelded).

Matrix saturated hydraulic conductivity values from drillhole UE-25a #1 appear to be higher in value than for the other drillholes. Statistical tests are unable to unequivocally show that the data are different. For units 1, 3, and 6, there is a 95% confidence that the data are different; for units 2, 5, 7, and 9, the differences are not statistically significant. Therefore, the data have been included as part of the analyses. Higher conductivity values from UE-25a #1 can skew upwards the overall expected values for the distribution. Suggested causes for higher K_s in the UE-25a #1 samples are (1) increased microfracturing, since this drillhole is in the imbricate fault zone, or (2) differences in laboratory testing methods or techniques.

Substantial differences are apparent when the results of this analysis are compared with TSPA-91. The matrix saturated hydraulic conductivity PDFs in TSPA-91 were beta-distribution approximations to an exponential, while the TSPA-93 PDFs are slightly skewed unimodal curves based on log-transformed data. Table 3-10 compares the means from the two analyses for the three comparable units, and Figure 3-10 shows two examples of the PDFs for K_s in the potential repository horizon.

Table 3-10. Comparison of expected values for K_S between TSPA-93 and TSPA-91.

Unit (Current/TSPA-91)	Saturated Hydraulic Conductivity (m/s)		Ratio: TSPA-93/TSPA-91
	TSPA-93	TSPA-91	
3R/1	2.37×10^{-10}	2.00×10^{-11}	12
4/2	2.26×10^{-11}	3.01×10^{-12}	7.5
5/3	1.82×10^{-8}	7.99×10^{-11}	228

As the table shows, the values for TSPA-93 range from about ten to over 200 times larger than for TSPA-91. The range used in TSPA-91 differs from that used in this study because in the former analysis the minimum was arbitrarily defined as 0.0 for all units, and the maximum was the value the data dictated. The more comprehensive data set dictated both the minimum and maximum values for this study.

The difference between the two PDFs is quite striking. The distribution for K_S for TSPA-91 is strongly weighted toward the lower values. Very few realizations sampled from the TSPA-91 PDFs are as large as the mean used in this study.

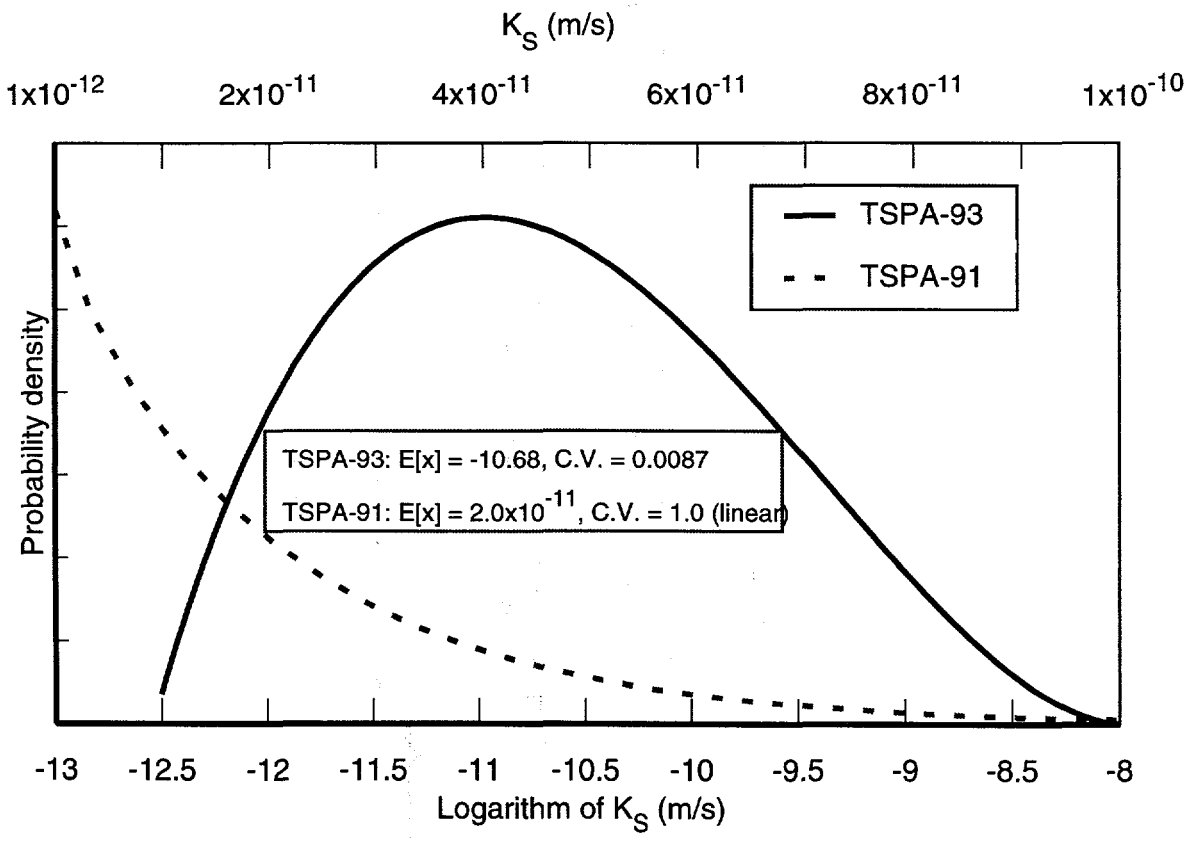

Figure 3-10. Comparison of PDFs for K_S in potential repository horizon.

3.2.3 Matrix water-retention parameters (van Genuchten model)

The van Genuchten model (van Genuchten, 1978) of water retention in unsaturated tuffs is described by an air-entry parameter (α_{vG}), a saturation/desaturation parameter (β_{vG}), and a residual-saturation parameter (S_r). These parameters are used to fit a curve of saturation (%) *vs.* pressure head (m). Other methods (gamma function, Mualem's method) are viable fitting techniques for analyzing the data, but they are not evaluated in this study for consistency with TSPA-91. Sources for the matrix water-retention parameters are listed in Table 3-11. Three of the four sources listed are not currently in the PAWDS, but they are being included.

Table 3-11. Sources for water retention parameters, (a_{vG}), (b_{vG}), and (S_r) data.

Source	Drillhole or Lithology	PAWDS PAN No.
Flint and Flint (1990)	USW G-1, USW GU-3, UE-25a #1, and UE-25a #6	PA00002
Peters *et al.* (1984)	USW GU-3 and USW G-4	NA
Rutherford *et al.* (1992)	USW G-1, USW GU-3, and USW G-4	NA
Voss (1993)	Tiva Canyon down to Calico Hills	NA

For each sample, we have derived a range of water-retention curves from the original pressure-head and saturation data from Peters *et al.* (1984), Rutherford *et al.* (1992), Flint and Flint (1990), and Voss (1993). Prior determinations of the water-retention curves have generally produced a single curve for a hydrologic unit by averaging data taken from multiple cores from that unit. For example, Peters *et al.* (1984) developed water-retention curves for each unit from the averages of two or three data sets. Where data were averaged, we chose to separate the components and produce water-retention parameters for each discrete data set.

Water-retention data are available for only units 1 through 7 and 9. Data for unit 8 (Prow Pass welded) are not available; therefore, unit 3 (Topopah Spring welded) is used as an analog for unit 8. Before determining the basic statistics and PDFs, the data are assigned to their respective hydrogeologic units. Initial determinations of the matrix air-entry and matrix saturation/desaturation parameter distributions produced beta-function PDFs that had negative exponents and are therefore "bathtub" shaped. By transforming the data to $\log_{10}$ values and employing the entropy-fit routine, satisfactory PDFs are generated for these parameters. Similar to the bimodal distribution for matrix saturated hydraulic conductivity, the air-entry parameter for unit 2 exhibits a bimodal distribution (see Appendix II). The areas for the first and second modes are 35 and 65 percent, respectively.

Matrix residual degree-of-saturation data are fit with the beta-PDF without any data transformation. Tables 3-12 and 3-13 give the entropy-fit α_{vG}, β_{vG} parameters, and Table 3-14 gives the S_r, beta-PDF parameters.

Table 3-12a. Matrix air-entry (α_{vG}) parameter statistics and $\log_{10}$ statistics.

Unit	Statistics					Log_{10} Statistics			
	n	*E*[*x*] (m^{-1})	*CV*	Min (m^{-1})	Max (m^{-1})	E[*x*] (m^{-1})	*CV*	Min (m^{-1})	Max (m^{-1})
1	19	0.0218	1.6870	0.0003	0.1338	-2.094	0.325	-3.523	-0.874
2	43	0.2485	1.4987	0.0104	1.6690	-1.134	0.636	-1.983	0.222
3C	51	0.0299	2.1728	0.0021	0.4244	-1.885	0.265	-2.678	-0.372
3R	51	0.0299	2.1728	0.0021	0.4244	-1.885	0.265	-2.678	-0.372
4	10	0.0032	0.6392	0.0002	0.0077	-2.624	0.167	-3.699	-2.114
5	24	0.0531	1.7839	0.0054	0.3752	-1.644	0.302	-2.268	-0.426
6	50	0.0193	2.1957	0.0004	0.2355	-2.270	0.275	-3.398	-0.628
7	8	0.0180	0.4319	0.0085	0.0344	-1.777	0.100	-2.071	-1.463
8	*	0.0299	2.1728	0.0021	0.4244	-1.885	0.265	-2.678	-0.372
9	6	0.0208	0.5565	0.0098	0.0356	-1.739	0.142	-2.009	-1.449

* No data; unit 8 is considered analogous to unit 3.

Table 3-12b. Matrix air-entry (α_{vG}) parameter entropy fit parameters and scaled beta-distribution parameters.

Unit	Entropy Fit Distribution Parameters ($\log_{10}$)						Scaled Beta-Distribution Parameters ($\log_{10}$)		
	E[*x*] (m^{-1})	*CV*	Min (m^{-1})	Max (m^{-1})	Alpha	Beta	*SCV*	Alpha	Beta
1	-2.102	0.327	-3.587	-0.859	0.583	0.324	0.199	4.199	3.350
2–1st mode*	-0.255	0.960	-0.744	0.235	1.500	1.500	0.837	1.129	1.129
2–2nd mode*	-1.498	0.199	-2.040	-0.764	0.474	0.995	0.174	1.070	1.803
3C	-1.868	0.274	-2.678	-0.301	0.315	1.545	0.097	11.788	23.741
3R	-1.868	0.274	-2.678	-0.301	0.315	1.545	0.192	2.038	4.878
4	-2.659	0.138	-3.755	-2.114	1.278	0.135	–	–	–
5	-1.555	0.298	-2.765	0.045	2.454	3.570	0.204	6.854	9.392
6	-2.226	0.290	-3.405	-0.504	0.576	1.301	0.141	6.977	10.647
7	-1.795	0.081	-2.071	-1.453	0.565	0.945	–	–	–
8	-1.868	0.411	-3.403	-0.301	0.525	0.556	–	–	–
9	-1.700	0.085	-2.009	-1.449	0.485	0.212	–	–	–

* Area for 1st mode is 35%; area for 2nd mode is 65%.
– These units are not scaled.

The matrix air-entry PDFs for both TSPA-91 and this study are beta functions. The values for TSPA-91 range from 0.0004 m^{-1} to 137.0 m^{-1} for all units; the minimum is within an order of magnitude of this study's values, but the maximum value is approximately four to six orders of magnitude greater. The coefficients of variation for the two studies' vary approximately by factors of 2 to 6. Table 3-15 compares the matrix air-entry parameters for the two TSPA data sets. The values in the current studies are all larger, by factors of 1.4 to more than 5.

Table 3-13a. Matrix saturation/desaturation (β_{vG}) statistics and $\log_{10}$ statistics.

Unit	Statistics					Log_{10} Statistics			
	n	$E[x]$ (m/s)	CV	Min (m/s)	Max (m/s)	E[x] (m/s)	CV	Min (m/s)	Max (m/s)
1	19	1.620	0.129	1.349	2.085	0.206	0.259	0.130	0.319
2	43	2.611	0.740	1.187	11.800	0.347	0.647	0.074	1.072
3C	51	1.793	0.395	1.155	5.363	0.233	0.523	0.063	0.729
3R	51	1.793	0.395	1.155	5.363	0.233	0.523	0.063	0.729
4	10	2.437	0.459	1.377	4.473	0.349	0.539	0.139	0.651
5	24	2.750	0.683	1.249	9.888	0.373	0.614	0.097	0.995
6	50	1.752	0.403	1.184	5.914	0.223	0.540	0.073	0.772
7	8	7.014	0.649	2.442	16.980	0.775	0.341	0.388	1.230
8	*	1.793	0.395	1.155	5.363	0.233	0.523	0.063	0.729
9	6	3.179	0.353	2.036	4.775	0.479	0.323	0.309	0.679

* No data; unit 8 is considered analogous to unit 3.

Table 3-13b. Matrix saturation/desaturation (β_{vG}) entropy fit and scaled beta-PDF parameters.

Unit	Entropy Fit Distribution Parameters ($\log_{10}$)						Scaled Beta-Distribution Parameters ($\log_{10}$)		
	$E[x]$ (m/s)	CV	Min (m/s)	Max (m/s)	Alpha	Beta	SCV	Alpha	Beta
1	0.210	0.228	0.130	0.328	0.257	0.864	0.139	3.088	5.030
2	0.375	0.558	0.074	1.080	0.147	1.673	0.487	0.603	2.759
3C	0.255	0.506	0.063	0.768	0.346	2.578	0.180	11.545	32.448
3R	0.255	0.506	0.063	0.768	0.346	2.578	0.354	2.015	7.054
4	0.348	0.400	0.101	0.777	0.628	1.835	–	–	–
5	0.391	0.510	0.095	1.020	0.182	1.519	0.349	1.881	5.116
6	0.232	0.527	0.073	0.777	0.077	2.713	0.256	4.287	17.168
7	0.770	0.270	0.369	1.240	0.554	0.832	–	–	–
8	0.255	0.557	0.063	0.768	0.057	1.825	–	–	–
9	0.445	0.257	0.238	0.778	0.630	1.631	–	–	–

– These units are not scaled.

Table 3-14. Matrix residual degree of saturation (S_r) statistics, beta, and scaled beta-distribution parameters.

Unit	Statistics					Beta-Distribution Parameters		Scaled Beta-Distribution Parameters		
	n	$E[x]$	CV	Min	Max	Alpha	Beta	SCV	Alpha	Beta
1	19	0.0212	2.5807	0.0000	1.0000	-0.8742	4.8066	0.9558	0.0502	47.4869
2	43	0.1540	1.1088	0.0000	1.0000	-0.4659	1.9342	0.8436	0.0347	4.6842
3C	51	0.0453	1.3418	0.0000	1.0000	-0.5150	9.2206	0.1693	32.2722	700.214
3R	51	0.0453	1.3418	0.0000	1.0000	-0.5150	9.2206	0.6577	1.1614	44.5525
4	10	0.1180	1.4167	0.0000	1.0000	-0.6785	1.4027	–	–	–
5	24	0.0968	1.4114	0.0000	1.0000	-0.6434	2.3273	0.6617	0.9660	17.3443
6	50	0.1207	1.4172	0.0000	1.0000	-0.6829	1.3101	0.3351	6.7103	55.1698
7	8	0.0688	0.5631	0.0000	1.0000	1.8680	37.8178	–	–	–
8	*	0.0453	1.3418	0.0000	1.0000	-0.5150	9.2206	–	–	–
9	6	0.0571	0.1855	0.0000	1.0000	0.5030	0.5030	–	–	–

* No data; unit 8 is considered analogous to unit 3.
– These units are not scaled.

Table 3-15. Comparison of expected values for matrix air-entry between TSPA-93 and TSPA-91.

Unit (TSPA93/TSPA-91)	Matrix air-entry parameter (m^{-1})		Ratio: TSPA-93/TSPA-91
	TSPA-93	TSPA-91	
3R/1	0.0299	0.0057	5.3
4/2	0.0023	0.0017	1.4
5/3	0.0531	0.0265	2.0

Because data sources for the matrix saturation/desaturation parameter are similar to those used for the air-entry parameter, it is not surprising that the differences between the two analyses are comparable. Table 3-16 compares the two analyses.

Table 3-16. Comparison of expected values for matrix saturation/ desaturation between TSPA-93 and TSPA-91.

Unit (TSPA93/TSPA-91)	Matrix saturation/desaturation parameter		Ratio: TSPA-93/TSPA-91
	TSPA-93	TSPA-91	
3R/1	1.793	1.798	1.0
4/2	2.437	1.708	1.4
5/3	2.750	2.223	1.2

The same sources of data are used in the residual degree-of-saturation analysis as are used in establishing the two water-retention parameters described above. For both studies, the ranges are set to 0.0 and 1.0. The CV in TSPA-93 is approximately a factor of 6 higher for all the comparable units. Table 3-17 compares the parameters. The fact that some values of S_r are smaller for TSPA-93 is due to accepting zero values for S_r, which skews the mean toward the lower end of the PDF range. There are no zero values in the data set for TSPA-91 (Peters *et al.*, 1984, Table A.2).

Table 3-17. Comparison of matrix residual saturation expected values between TSPA-93 and TSPA-91.

Unit (TSPA-93/TSPA-91)	Matrix Residual Saturation		Ratio: TSPA-93/TSPA-91
	TSPA-93	TSPA-91	
3R/1	0.045	0.080	0.6
4/2	0.118	0.052	2.3
5/3	0.097	0.164	0.6

3.3 Bulk hydraulic-parameter development

An effort has been made to include representations of the bulk hydraulic properties that provide a realistic view of the coupled matrix and fracture hydrology. In

the flow process, bulk saturated hydraulic conductivity (K_{bs}) and gas permeability (K_{bg}) are controlling features that dominate matrix-controlled properties.

The properties data for K_{bs} are obtained from bulk hydraulic pump tests and barometric-fluctuation measurements (which measure gas permeabilities for the vadose zone). Table 3-18 lists the sources for the drillholes. The K_{bs} values come from pump tests in drillholes USW G-4, USW H-1, USW H-3, and USW H-4, UE-25b #1, UE-25p #1, and J-13. The tests used standard techniques to derive data: pump/draw-down, pump/recovery, pump/radioactive tracer, injection, drillhole flow survey, packer injection, and swab test. Drillholes USW UZ-1 and UE-25a #4 are used for air permeability data derived from barometric fluctuations, as reported in Montazer *et al.* (1985). Where there are insufficient data available for a unit, analog units with similar lithologic and matrix properties are used. The basic data are statistically reduced and beta probability distributions produced for all hydrogeologic units.

Table 3-18. Sources for bulk saturated hydraulic conductivity (K_{bs}) and gas permeability (K_{bg}).

Source	Drillhole	PAWDS PAN No.
Rush *et al.* (1983)	USW H-1	PA00010
Lahoud *et al.* (1984)	UE-25b #1	PA00011
Thordarson (1983)	J-13	PA00013
Thordarson *et al.* (1985)	USW H-3	PA00033
Whitfield *et al.* (1985)	USW H-4	PA00034
Craig and Robison (1984)	UE-25p #1	PA00035
Lobmeyer (1986)	USW G-4	PA00037
Montazer *et al.* (1985)	USW UZ-1 and UE-25a #4	NA

The data reported in the USGS Open File Reports for the bulk saturated hydraulic conductivity data are presented as transmissivity values. These values are converted to bulk saturated hydraulic conductivities by:

$$K_{bs} = T/b, \tag{3.10}$$

where T is the transmissivity (m^2/s), and b is the thickness of the tested interval (m).

Data that are characteristic of a single hydrogeologic unit are required for our analyses. Because many of the intervals for the bulk saturated hydraulic conductivity measurements cover more than one of the hydrogeologic units, over half the data have been eliminated. The representativeness of the data from the pump testing is limited because the tests are designed to determine the hydrogeologic flow proper-

ties only in the saturated zones. For the most part, the data pertain only to the hydrogeologic units from the lower sequences of Topopah Spring downward. Only a few tests are reported above this horizon. These tests were made in drillholes located farther down-dip, where the upper units are below the water table. The hydrogeologic characteristics may differ with distance from the repository region. To supplement the information for the saturated zones and provide values at hydrogeologic units higher in the sequence in the unsaturated zone, data derived from vadose zone barometric fluctuations are used. Much of the data from these drillholes also cross hydrogeologic unit boundaries and only a limited number of observations are applicable to single hydrogeologic units. Despite these concerns, the data are used to derive PDFs, since so little other information is available.

The same general approach used for matrix PDF development is used for the bulk saturated hydraulic conductivity analyses. The results from the tabulated pump tests are sorted into the corresponding hydrogeologic units of our model. Even though we expect that the data must be transformed to log space, the usual approach (i.e., making initial beta-distribution fits to untransformed data) to analyzing and reducing the data has been taken, thereby maintaining consistency and minimizing bias. The distributions are not scaled because the data are from measurements made over unit thicknesses similar to the those in our model. For the lithologic units with unavailable data, analog or represented values are assigned (see Section 3.3.3).

3.3.1 Bulk saturated hydraulic conductivity (K_{bs})

Among the available data from pump tests in the saturated zone near Yucca Mountain, the only hydrogeologic unit information suitable for compilation comes from hydrogeologic units 6 through 10. The amount of data available for each unit ranges from four data points for unit 7 to 15 data points for unit 6. The single datum available for unit 3 is not considered useful by itself. It is, however, consistent with the values from the barometric pumping tests (see below); therefore, it has been added to that data set and considered in the subsequent evaluation. Table 3-19 shows the data as both basic statistics and log-transformed values for hydrogeologic units 6 through 10.

Analyses of the basic statistics showed that the data are highly skewed. Consequently, the statistics have been transformed to log space. The limited number of data require the use of the entropy-fit routine to determine the exponents for the beta-distribution. Table 3-19b lists the parameters for units 6 through 10.

Table 3-19a. Bulk saturated hydraulic conductivities (K_{bs}) statistics and $\log_{10}$ statistics.

Unit	Statistics					Log_{10} Statistics			
	n	*E*[*x*] (m/s)	*CV*	Min (m/s)	Max (m/s)	E[*x*] (m/s)	*CV*	Min (m/s)	Max (m/s)
6	15	2.81×10^{-6}	1.30	5.21×10^{-8}	1.35×10^{-5}	-5.93	0.114	-7.28	-4.87
7	4	5.48×10^{-5}	1.86	2.31×10^{-8}	2.08×10^{-4}	-5.69	0.304	-7.64	-3.68
8	7	8.00×10^{-6}	1.25	5.16×10^{-8}	2.50×10^{-5}	-5.63	0.163	-7.29	-4.60
9	8	2.15×10^{-7}	1.39	3.40×10^{-9}	9.26×10^{-7}	-7.04	0.103	-8.47	-6.03
10	11	5.57×10^{-6}	1.19	4.63×10^{-8}	1.76×10^{-5}	-5.75	0.155	-7.33	-4.75

Table 3-19b. Bulk saturated hydraulic conductivities beta-probability distribution parameters from an entropy fit.

Unit	Statistics *log10*					Beta-Distribution Parameters	
	n	*E*[*x*] (m/s)	*CV*	Min (m/s)	Max (m/s)	Alpha	Beta
6	15	-5.93	0.100	-7.36	-4.87	0.886	0.413
7	4	-5.73	0.188	-8.05	-2.28	1.35	2.50
8	7	-5.56	0.121	-7.82	-4.60	1.68	0.128
9	8	-7.06	0.837	-8.52	-6.03	0.941	0.367
10	11	-5.83	0.115	-7.56	-4.59	1.20	0.580

3.3.2 Bulk gas conductivity (K_{bg})

Bulk saturated hydraulic conductivity values for units 2 and 3 are developed from the data acquired by Montazer *et al.* (1985). These researchers measured air permeabilities for the unsaturated zone using measurements of barometric pumping at Yucca Mountain. As referenced by Montazer *et al.* (1985), Weeks (1978) first used this approach to measure the changes in soil-gas pressure fluctuations as climatic pressure systems move across the Yucca Mountain area. From the matrix unsaturated fluid potentials measurements, Montazer *et al.* (1985) were able to determine the soil-gas pressure fluctuations at depth and infer gas permeabilities for Yucca Mountain. The two drillholes tested, USW UZ-1 and UE-25a #4, yield results for the Tiva Canyon member down to the Topopah Spring Member. As with saturated zone-bulk saturated hydraulic conductivity testing, some measurements cross hydrogeologic unit boundaries and can not be used in the analysis.

Montazer *et al.* (1985) converted the air permeabilities to equivalent saturated hydraulic conductivity values using the viscosity and density of water at standard conditions. The results are limited but provide enough data to determine K_{bs} for units 2 and 3, the Paintbrush nonwelded and the Topopah Spring welded units, as

listed in Tables 3-20a and 3-20b. As mentioned earlier, one bulk saturated hydraulic conductivity value is included with these data for unit 3.

Table 3-20a. Barometric pumping (gas permeability) (K_{bg}) statistics expressed as bulk saturated hydraulic conductivities (K_{bs}) for units 2 and 3.

Unit	Statistics					Log_{10} Statistics			
	n	*E*[*x*] (m/s)	*CV*	Min (m/s)	Max (m/s)	E[*x*] (m/s)	*CV*	Min (m/s)	Max (m/s)
2	4	2.67×10^{-5}	1.22	2.31×10^{-7}	6.94×10^{-5}	-5.22	0.218	-6.64	-4.16
3	4	3.70×10^{-5}	1.43	7.00×10^{-6}	1.16×10^{-4}	-4.74	0.119	-5.16	-3.94

Table 3-20b. Barometric pumping (gas permeability) (K_{bg}) beta-probability distribution parameters from an entropy fit.

Unit	Beta Probability Distribution Parameters (log_{10})					Beta-Distribution Parameters	
	n	*E*[*x*] (m/s)	*CV*[*x*]	Min (m/s)	Max (m/s)	Alpha	Beta
2	4	-5.27	0.130	-6.75	-3.63	1.00	1.21
3	4	-4.74	0.068	-5.32	-3.94	0.466	1.05

The gas conductivities appear to be highly skewed, although there are little data. Thus, the gas conductivities have been converted to log_{10} values and the PDFs are calculated using the entropy fit routine. Table 3-20b provides the barometric pumping beta-probability distribution parameters. Comparing Tables 3-20a and 3-20b, it is seen that the parameters of the beta function determined from the entropy fit differ from the log_{10} statistics. This is a consequence of the entropy-fit procedure, which may expand the range of the data or change the skewness of the distribution peak, but preserves the initial structure of the data.

3.3.3 Analog bulk saturated hydraulic conductivity

There are not enough data for units 1, 4, and 5 of the model to generate PDFs for bulk saturated hydraulic conductivities. Consequently, we have created analog data by selecting from the other seven units an existing unit that most closely represents the unit with missing or no data. To account for the greater uncertainty in the properties of these analog units, we have increased the coefficient of variation to allow for more scatter around the expected value, a concession to conservatism.

Unit 1 (Tiva Canyon welded), has only one applicable published gas permeability value. Units 3 (Topopah Spring welded) and 8 (Bullfrog welded) appear to be likely analog candidates. Table 3-21 lists the comparisons of the major matrix pa-

rameters and fracture frequencies made between unit 1 and units 3 and 8. Although most parameters are similar, some differences are observed. The single K_{bs} value for unit 1 (2.31×10^{-7}) lies in the range for K_{bs} in unit 8 (Table 3-19a), but is below the minimum for unit 3 (Table 3-20a). Three geologic features between the units lead to rejection of the Bullfrog welded unit as an analog for the Tiva Canyon unit: First, the Bullfrog welded unit is much deeper in the stratigraphy and is in the saturated rather than the unsaturated zone. Second, the depth of burial of the Bullfrog would be subject to much greater lithologic stresses. Third, the saturated environment would introduce significantly different alteration and mineralization in the unit (Ortiz *et al.*, 1985). Therefore, the Topopah Spring welded is chosen as the analog to the Tiva Canyon welded unit.

Table 3-21 Hydrogeologic unit matrix, bulk-hydraulic, and fracture parameters comparison for analog bulk saturated hydraulic conductivities.

Unit Unknown Analog Candidates	Matrix				Bulk		Fracture	
	ϕ	K_s	α_{vG}	β_{vG}	ρ_b (g/cm3)	K_{bs} (m/s)	F_f* (1/m)	F_f† (1/m)
Unit 1 (TCw)	0.087	3.86×10^{-10}	0.0218	1.62	2.366	2.31×10^{-7}	4.50	7.70
Unit 3 (TSw)	0.139	2.37×10^{-11}	0.0299	1.793	2.258	3.70×10^{-5}	3.00	4.25
Unit 8 (BFw)	0.165	4.92×10^{-10}	–	–	2.26	8.00×10^{-6}	3.00	–
Unit 4 (TSwv)	0.065	2.26×10^{-11}	0.0032	2.437	2.308	–	2.50	3.40
Unit 3 (TSw)	0.139	2.37×10^{-10}	0.0299	1.793	2.258	3.70×10^{-5}	3.00	4.25
Unit 5 (CHnv/PPnv)	0.331	1.82×10^{-8}	0.0531	2.75	1.838	–	1.40	0.20
Unit 2 (PTn)	0.421	5.47×10^{-7}	0.2485	2.611	1.714	2.67×10^{-5}	1.40	1.00
Unit 6 (CHnz/PPnz)	0.306	1.93×10^{-10}	0.0193	1.752	1.746	2.81×10^{-6}	1.10	0.20

* Data are from Table 3-25 of this document.
† Data are from Lin *et al.* (1993).
– Data are either unavailable or inapplicable.

The range of barometric permeability for unit 3 is 7.00×10^{-6} m/s to 1.16×10^{-4} m/s (Table 3-20a), and the one applicable value for unit 1 is 2.31×10^{-7} m/s. Since this value is less than the minimum for unit 3, it has been chosen as the minimum value for this unit as a conservative estimate. The value 1.16×10^{-4} m/s is retained as the maximum. Using this range and a CV of one standard deviation about the mean, the entropy fit is used to generate the PDF parameters for unit 1, as listed in Table 3-22.

Unit 4 (Topopah Spring basal vitrophyre), resembles unit 3 (Topopah Spring welded). In Table 3-21, the matrix properties (porosity, saturated hydraulic conductivity, and the van Genuchten air-entry parameter) and the fracture frequency (F_f) (discussed in the following section) are all less than those of unit 3. It is assumed that the matrix properties of the bulk saturated hydraulic conductivity for unit 4 are

basically similar to those of unit 3. The difference between the units depends on fracture frequency, which is a consequence of the vitric characteristic of unit 4. To acknowledge our increased uncertainty, we have increased the coefficient of variation for unit 3 by 10%. The values generated are shown in Table 3-22.

Two possibilities exist for analogs to unit 5 (Calico Hills/Prow Pass nonwelded–vitric): unit 6, (Calico Hills/Prow Pass nonwelded-zeolitic), and unit 2, (Paintbrush nonwelded). For both analogs, the matrix and fracture frequency values are generally in close agreement. The Paintbrush nonwelded is chosen as the analog because it is not altered to zeolites and therefore physically appears to be more similar. The parameters for unit 5 are listed in Table 3-22. As for unit 4, the coefficient of variation is increased by 10% to account for increased uncertainties.

Table 3-22. Bulk saturated hydraulic conductivities (K_{bs}) parameters for units 1, 4, and 5 (based on analogs).

Unit	Statistics			Log_{10} Statistics				PDF Parameters	
	E[x] (m/s)	Min (m/s)	Max (m/s)	E[x] (m/s)	CV	Min (m/s)	Max (m/s)	Alpha	Beta
1	$1.81x10^{-5}$	$2.31x10^{-7}$	$1.16x10^{-4}$	-4.74	0.135	-6.64	-3.94	0.8978	-0.1915
4	$1.81x10^{-5}$	$4.79x10^{-6}$	$1.16x10^{-4}$	-4.74	0.074	-5.32	-3.94	0.1389	0.5930
5	$5.40x10^{-6}$	$1.78x10^{-7}$	$2.36x10^{-4}$	-5.27	0.142	-6.75	-3.63	0.5717	0.7382

Table 3-23 summarizes all the data derived for the units for K_{bs}. The table combines the parameters from aqueous K_{bs} measurements, barometric gas conductivity measurements, and the analog values.

Table 3-23. Summary of K_{bs} parameters.

Unit	Beta Probability Distribution Parameters (log_{10})					Beta-Distribution Parameters	
	n	E[x] (m/s)	CV	Min (m/s)	Max (m/s)	Alpha	Beta
1	1	-4.7424	0.1354	-6.6364	-3.9355	0.8978	-0.1915
2	4	-5.2675	0.1297	-6.7506	-3.6273	1.0015	1.2136
3	4	-4.7424	0.0677	-5.3193	-3.9355	0.4656	1.0499
4	4	-4.7424	0.0745	-5.3193	-3.9355	0.1389	0.5930
5	4	-5.2675	0.1426	-6.7506	-3.6273	0.5717	0.7382
6	15	-5.9311	0.1003	-7.3599	-4.8697	0.8862	0.4127
7	4	-5.7307	0.1884	-8.0453	-2.2818	1.3474	2.4977
8	7	-5.5563	0.1205	-7.8195	-4.6038	1.6807	0.1282
9	8	-7.0625	0.0837	-8.5240	-6.0334	0.9413	0.3670
10	11	-5.8305	0.1150	-7.5619	-4.5893	1.2035	0.5797

3.4 Fracture parameter development

Although the bulk of the continuum volume is typically occupied by the matrix rock, fractures could be important to aqueous and gaseous flow at Yucca Mountain. Fractures can exert a significant controlling influence on the hydraulic conductivity in a rock mass (Freeze and Cherry, 1979). All geologic units at Yucca Mountain display some degree of fracturing. Fractures can be grouped into two types according to the process that caused them: cooling fractures generated when the pyroclastic flows that formed Yucca Mountain cooled, and tectonic fractures caused by subsequent deformation of the tuffs (Barton *et al.*, 1989). Cooling fracture surfaces are often smoother than tectonic fractures (Barton *et al.*, 1989). Such differences could result in different hydraulic properties for the fractures, but no attempt has been made to model these properties yet. Fractures also generally fall into two orientation (dip) and frequency sets, (Spengler *et al*, 1984). The densely welded units are represented by a relatively high frequency of fractures while the nonwelded units have much lower fracture frequencies. Also the fracture orientations are generally represented by one set of high-angle fractures and a secondary group of low-angle fractures.

3.4.1 Approach

The fracture parameters required for the TSPA-93 flow and transport models are frequency, F_f, spacing, a_f, porosity, ϕ_f, van Genuchten air-entry parameter, α_{vGf}, aperture, b_f, angle/orientation, θ_f, and saturated hydraulic conductivity, K_f. Of these parameters, only two—fracture frequency and orientation—are available from actual measurements of drill-hole properties. The remainder are derived by assuming that the fractures can be modeled as a parallel array of planar joints (Snow, 1968; referenced in Freeze and Cherry, 1979; Narasimhan and Wang, 1992). Using this model of fracture flow, we can approximate K_f from bulk hydraulic conductivity (i.e., a measure of K_f and K_m combined). This approximation assumes that K_m is a minor component of K_b.

Freeze and Cherry (1979) have suggested an approach to represent fracture flow. This is a continuum approach where the fractures are effectively replaced by a representative continuum in which the spatially defined values of hydraulic conductivity, porosity, and compressibility can be assigned. This approach requires sufficiently dense fracture spacing so that Darcy's law can be considered to be valid, and it must be applied to a block of rock large enough that the volume "acts as a Darcian continuum." Then the fracture medium acts in a hydraulically similar fash-

ion as a porous medium. For fracture systems where the fracture density is extremely low, it may be necessary to analyze flow in individual fractures. Normally this approach is used where fluid pressure builds up along individual critical fractures (as may be determined by rock-mechanics analyses). To represent the fractures in a continuum approach, we use a parallel array of planar joints. An alternative approach to deriving fractures is suggested by Wang (1992). As with the Freeze and Cherry approach, this method assumes that fractures can be described by effective hydrologic properties such as permeability. This approach uses the fracture-aperture information as an analog of pore size and applies the relationship between the second moment of log saturated permeability and log pore size to calculate an effective fracture permeability. This approach offers the opportunity to estimate a more realistic range of aperture sizes; however, it also would require a substantial effort to develop as a useful tool. Consequently, for this effort, only the Freeze and Cherry approach is being used.

For this study we have accepted Freeze and Cherry's approach based on the work of Snow (1968). We assume a parallel array of fractures and consider the fracture aperture as being an effective aperture or "open area between parallel plates." Important new inputs for the development of the fracture parameters are the bulk hydraulic conductivities discussed in Section 3.3. It is assumed that the nonlinear and constrictive properties of fractures are effectively reflected in the values of the bulk hydraulic conductivity. The values developed here for fracture parameters are therefore hydraulic apertures and not actual measured aperture sizes.

The approach presented here assumes that the fractures approximate parallel plates oriented in the directions described in the Yucca Mountain drill hole logs. Fractures in the field usually are not horizontal and are therefore not normal to a vertical drillhole. Fracture frequencies for the Yucca Mountain data are therefore corrected for the variable fracture angles.

3.4.2 Available fracture data

Fracture properties are tabulated from four drillholes: USW G-1, USW GU-3, USW G-4, and UE 25a #1. Other researchers have performed similar fracture studies, and the drillholes selected are based on the four drillholes that Lin *et al.* (1993) incorporated in their fracture analysis. The holes selected bound the potential repository area and provide a limited but geographically broad distribution of fracture frequencies representing the potential repository area. Other drillholes have

fracture frequency information but, partly due to resource limitations, are not included in this study.

It is recognized that the current fracture count methods are not a true representation of the *in situ* properties of Yucca Mountain. This is due to poor core recovery, missing core, and fracture analysis of the core, which bias the data to lower fracture counts. To resolve this bias, several method are used to correct for the low fracture counts. Methods related to inverse core recovery and rock quality designation, might aid in assigning more correct fracture counts to the missing core sections. It is beyond the current scope of this study to pursue these methods.

Table 3-24. Sources for fracture frequency and orientation data.

Source	Drillhole	PAWDS PAN No*
Spengler *et al.* (1981)	USW G-1	NA*
Spengler *et al.* (1984)	USW G-4	NA*
Spengler *et al.* (1979)	UE-25a #1	NA*
Scott and Castellanos (1984)	USW GU-3	NA*

*Pending inclusion into the PAWDS

We have determined the fracture frequencies for each of the ten hydrogeologic units from the lithologic logs for each hole. Fracture-orientation data are only available for units 1, 2, 3, and 5. The data consist of the fracture count (number/m) and the fracture orientation (dip angles).

3.4.3 Frequency (F_f)

Fracture frequencies are determined from the down-hole fracture-count data for drillholes USW G-1, USW G-4, USW GU-3, and UE-25a #1. The data are reported as the number of fractures per 10-foot interval down the drillholes. They have been converted to number of fractures per 1-meter interval and grouped according to hydrogeologic unit.

The basic statistics for the fracture frequencies all have coefficients of variation that are near 1.0 (Table 3-25). By definition, the exponential distribution has a CV of 1.0; therefore, we assume that all the distributions can be represented by beta-function PDFs that approximate exponential distributions. For the exponential distribution, the minimum is zero and the maximum is infinity. To approximate an exponential PDF by a beta function requires that the maximum be set to a value less than infinity, so 30 times the mean value has been chosen. The resulting beta distribution is reasonably close to the desired exponential (see the TSPA-91 document for a discussion of the approximation of an exponential by a beta function). Because the

maximum is a constant multiplicative factor of the mean, the alpha and beta exponents for *all* the hydrogeologic units are the same. Table 3-25 lists the statistics and the approximated beta-distribution exponents for fracture frequency.

Table 3-25. Fracture frequency (F_f) statistics and beta-distribution approximation of the exponential.

Unit	Statistics					Approximated Exponential Distribution Parameters				
	n	*E*[*x*] (m^{-1})	*CV*	Min (m^{-1})	Max (m^{-1})	*CV*	Min (m^{-1})	Max (m^{-1})	Alpha	Beta
1	57	4.5	0.7	0.3	14.8	1.00	0.00	135.00	-0.067	26.067
2	12	1.4	0.8	0.7	3.9	1.00	0.00	42.00	-0.067	26.067
3	323	3.0	1.0	0.2	23.3	1.00	0.00	90.00	-0.067	26.067
4	23	2.5	0.7	0.3	6.2	1.00	0.00	75.00	-0.067	26.067
5	59	1.4	0.9	0.2	4.9	1.00	0.00	42.00	-0.067	26.067
6	70	1.1	1.1	0.2	7.5	1.00	0.00	33.00	-0.067	26.067
7	33	1.0	0.8	0.3	4.3	1.00	0.00	30.00	-0.067	26.067
8	77	3.0	0.8	0.3	10.8	1.00	0.00	90.00	-0.067	26.067
9	43	1.0	0.7	0.3	2.6	1.00	0.00	30.00	-0.067	26.067
10	71	1.3	0.8	0.3	4.6	1.00	0.00	39.00	-0.067	26.067

3.4.4 Orientation (θ_f)

Fracture-orientation data are only available for units 1, 2, 3, and 5. These four units with data are used as analogs for the remaining units where there are no data. (Unit 10 is not considered because it lies below the water table and was not part of the modeling domain). The basic statistics for degree of welding and fracture frequency are used to select analogs for missing fracture-orientation data. Table 3-26 provides comparisons between the missing units and the analog units. Unit 3 is used as an analog for units 4 and 8 because all three are welded units, and the fracture frequency for unit 3 is similar to the frequencies for units 4 and 8. Fracture frequencies for the other units differ from those for units 3, 4, and 8. Unit 6 is considered analogous to unit 5 because both are nonwelded units and both units were deposited during the same ash-flow event. The main difference between the two is that unit 6 has been zeolitized (Broxton *et al.*, 1986; Ortiz *et al.*, 1985). The fracture frequencies of the two units are similar. Units 7 and 9 are considered analogous to unit 2 based on the similar expected values of their fracture frequencies. If only the binary welded designation (welded *vs.* nonwelded) is considered, no analog would be obvious for unit 7.

The orientations are compiled as numbers of fractures falling in each 10-degree increment between 0 and 90 degrees from vertical. Table 3-27 summarizes the statistics and the beta-PDF exponents for the nine units.

Table 3-26. Analog units used for fracture orientation (θ_f) of missing units.

Missing Unit	Analog Unit	Fracture Frequency: Missing Unit (m^{-1})	Fracture Frequency: Analog Unit (m^{-1})	Degree of Welding: Analog Unit	Degree of Welding: Missing Unit
4	3C	2.5	3.0	Welded	Welded
8	3C	3.0	3.0	Welded	Welded
6	5	1.1	1.5	Nonwelded	Nonwelded
7	2	1.0	1.4	Welded	Welded
9	2	1.0	1.4	Nonwelded	Nonwelded

Table 3-27. Fracture angle/orientation (θ_f) statistics and beta-PDF parameters.

Unit	Basic Statistics					Beta-Distribution Parameters	
	n	$E[x]$ (degrees)	CV	Min (degrees)	Max (degrees)	Alpha	Beta
1	300	48.900	0.546	0.000	90.000	-0.010	-0.168
2	100	41.400	0.702	0.000	90.000	-0.365	-0.255
3	399	58.183	0.478	0.000	90.000	-0.100	-0.508
4	399	58.183	0.478	0.000	90.000	-0.100	-0.508
5	400	57.650	0.474	0.000	90.000	-0.043	-0.463
6	400	57.650	0.474	0.000	90.000	-0.043	-0.463
7	100	41.400	0.702	0.000	90.000	-0.365	-0.255
8	399	58.183	0.478	0.000	90.000	-0.100	-0.508
9	100	41.400	0.702	0.000	90.000	-0.365	-0.255

Fracture orientations in the YMP Reference Information Base (DOE, 1993) for welded tuffs have predominantly near-vertical dip angles, with a secondary grouping that is nearly horizontal. For the hydrogeologic units used in this study, the fracture orientations also follow this trend, although the distributions generated are not as strongly bimodal. Figure 3-11 is a rose diagram showing the distribution of fracture orientations for unit 2 (Pah Canyon nonwelded). Because the fracture orientations are grouped at high and low angles, the probability distribution is "bathtub shaped". A typical PDF for unit 2 (Pah Canyon nonwelded) is shown in Figure 3-12.

3.4.5 Derived parameters

Fractures are modeled as a parallel array of planar fractures; this assumption permits the determination of fracture-model parameters that cannot be measured (i.e., spacing, hydraulic aperture, porosity, hydraulic conductivity, and air entry parameter) in terms of the ones that are (bulk saturated hydraulic conductivity, fracture frequency, and fracture orientation). The relationship between porosity and bulk saturated hydraulic conductivity established by Snow (1968), as cited by

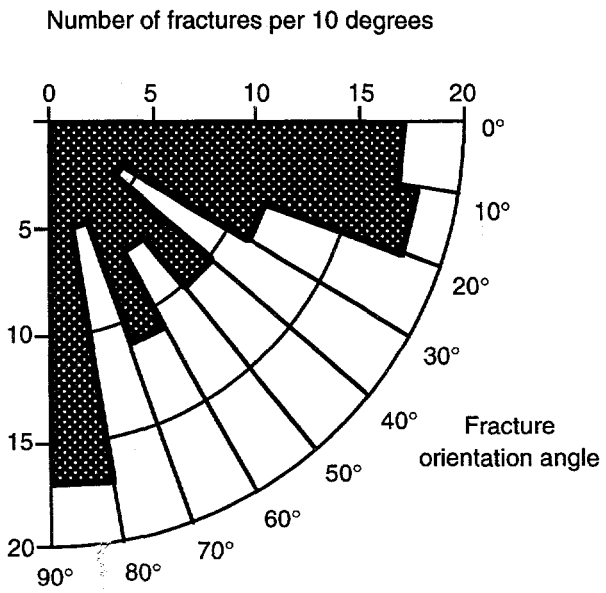

Figure 3-11. Rose diagram for fracture orientations for unit 2.

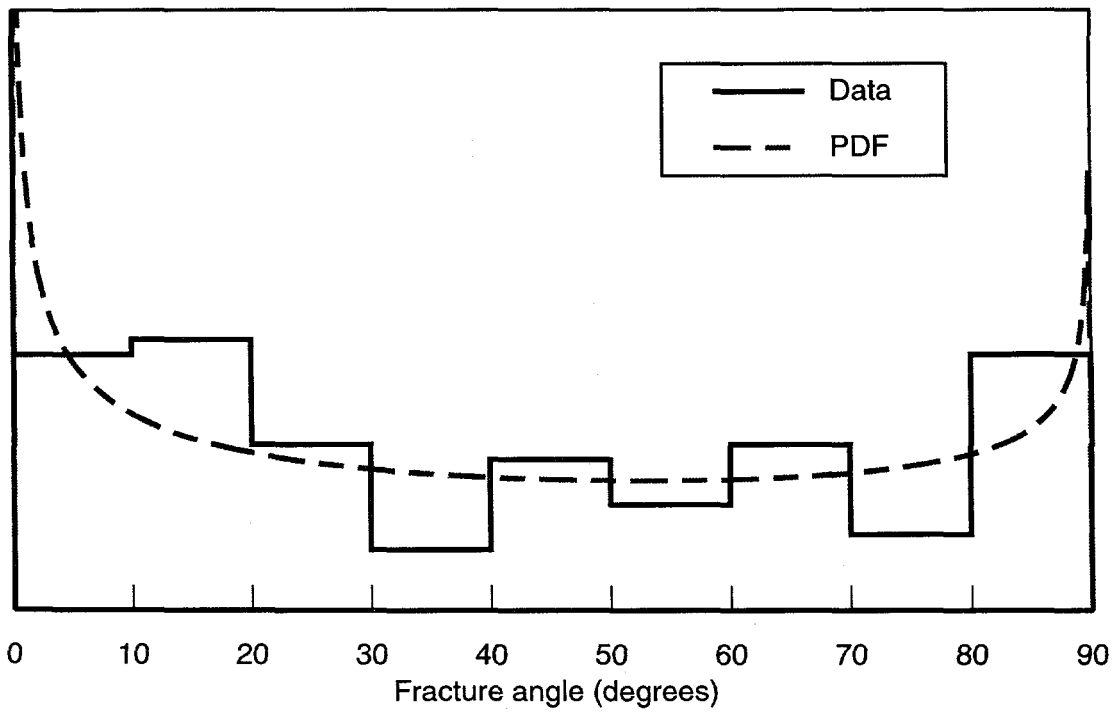

Figure 3-12. PDF for fracture orientations for unit 2 (Pah Canyon nonwelded).

Freeze and Cherry (1979), gives the fracture porosity ϕ_f and the permeability k (in m^2) for an array of parallel planar fractures:

$$\phi_f = N_p b_f, \text{ and} \tag{3.11}$$

$$k = N_p b_f^3 / 12, \tag{3.12}$$

where b_f (m) is the hydraulic aperture, and N_p (m^{-1}) is number of fractures per unit distance (specified normal to the plane of the fractures). Freeze and Cherry state that "a permeability k, [calculated with Equation (3.12)], can be considered as the permeability of an equivalent porous medium; one that acts hydraulically like the fractured rock."

Note that this formula models parallel-plate fractures with N_p fractures per unit distance normal to the fractures. The fractures intersected by a drillhole may be oriented in any direction, so the number of fractures per unit distance measured along the drillhole, Ff, differs from the number used in Equation (3.13), N_p, whenever the fracture orientations are not horizontal. (The drillholes are assumed to be vertical for this analysis.) The number of fractures per unit distance normal to the plane of the fractures is therefore given by

$$N_p = N / cos(\theta_f), \tag{3.13}$$

where θ_f is the fracture orientation. Figure 3-13 illustrates how two different measured numbers of fractures, Ff, at different angles, θ, are the result of the same number of fractures per unit distance, N_p.

Parallel-plate fracture spacing (a_f) is given by:

$$a_f = 1 / N_p \text{ , or} \tag{3.14}$$

$$a_f = cos(\theta_f) / N. \tag{3.15}$$

The bulk permeability (k) is related to bulk saturated hydraulic conductivity (K_{bs}) by the viscosity and density of the fluid; at 20°C and at sea level the conversion factor is K_{bs} (m/s) = k x 1.022×10^{-7}(m^2) (Gerhart and Gross, 1985). Substituting for N_p and K_{bs}, the fracture hydraulic aperture can then be calculated by substitution in Equation (3.12):

$$b_f = \sqrt[3]{\frac{12 K_{bs} \cos(\theta_f)}{1.022 x 10^{-7} N}}. \tag{3.16}$$

Substituting Equation (3.15) into Equation (3.16) gives:

$$b_f = \sqrt[3]{1.226 x 10^{-6} K_{bs} a_f}. \tag{3.17}$$

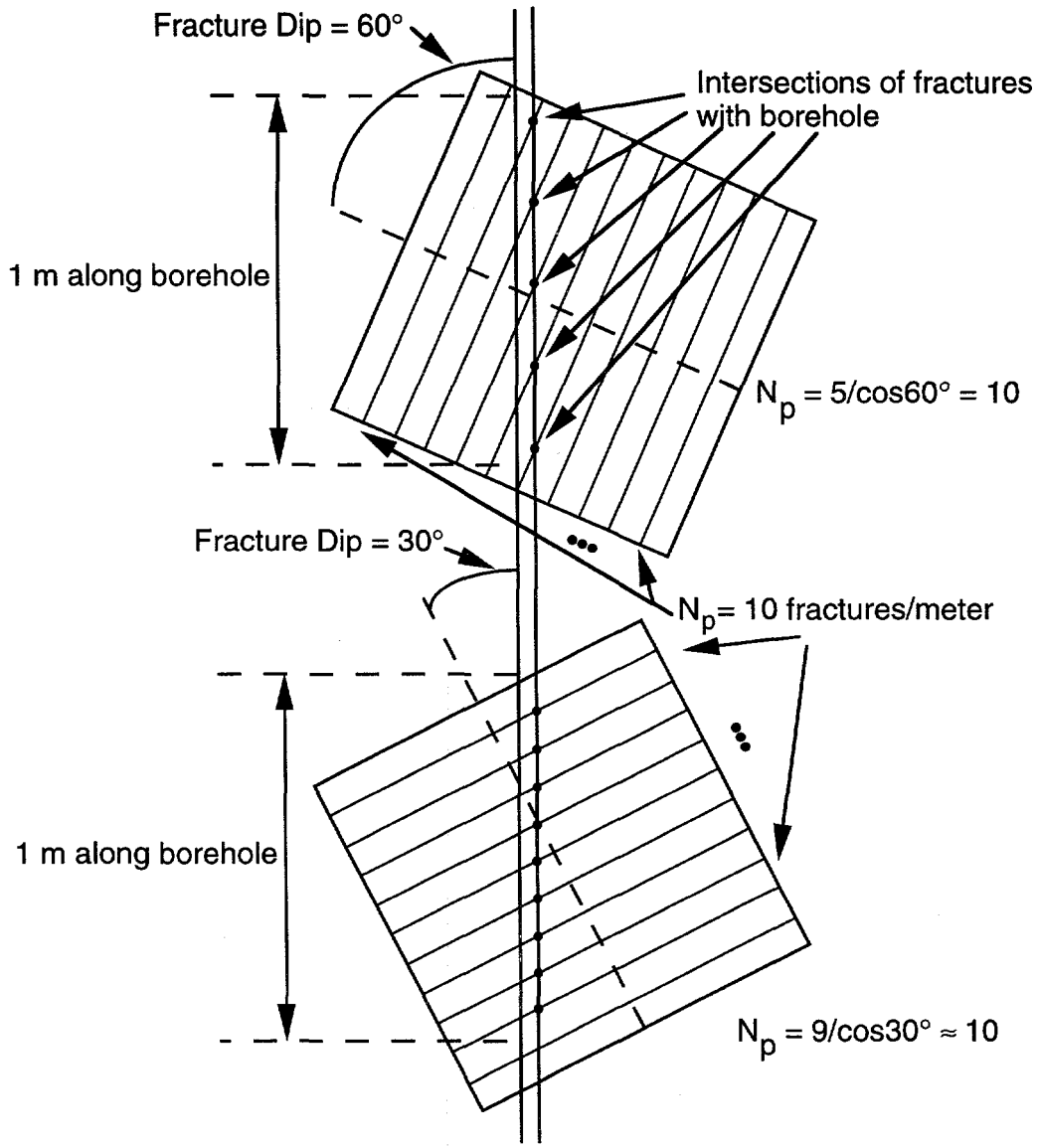

Figure 3-13. Illustration of the calculation of the number of fractures/unit distance for two observed fracture densities and orientation angles.

Substituting Equation (3.17) into Equation (3.11) gives fracture porosity in terms of observed fracture frequency and hydraulic aperture:

$$\phi_f = \frac{Nb_f}{\cos(\theta_f)}. \tag{3.18}$$

Lastly, fracture hydraulic conductivity, K_f, is calculated from

$$K_f = \frac{K_{bs}}{\phi_f}. \tag{3.19}$$

With these relations, the required fracture parameters can be determined for use in the flow and transport models. To obtain distributions of the derived fracture parameters, a computer routine developed at SNL randomly samples 100 values of K_{bs}, F_f, and θ_f from the probability distribution for these properties, and then calculates 100 values of the derived parameters based on the above equations. The following subsections discuss the individual parameters.

3.4.6 Spacing (a_f)

Fracture spacings for the nine units are calculated from Equation (3.15). A set of 100 values is computed from randomly sampled inputs, and the basic statistics are then derived. The statistical data and the beta-distribution parameters are presented in Table 3-28.

Comparing the expected value with the minimum and maximum in the table shows that the distribution of fracture spacings is strongly skewed toward low values (close spacings). Figure 3-14 illustrates this for unit 7 (the one with the greatest range), showing that although most values are grouped near 0 m spacing, a few are very large.

Table 3-28. Fracture-spacing statistics and beta-distribution parameters.

Unit	Basic Statistics					Beta-Distribution Parameters	
	n	$E[x]$ (m)	CV	Min (m)	Max (m)	Alpha	Beta
1	100	0.618	2.776	2.0×10^{-4}	13.444	-0.9222	0.6170
2	100	2.222	2.674	6.0×10^{-4}	43.907	-0.9178	0.5416
3	100	0.740	3.147	3.0×10^{-6}	19.878	-0.9400	0.5514
4	100	0.888	3.147	4.0×10^{-6}	23.854	-0.9400	0.5514
5	100	1.618	3.096	2.0×10^{-5}	42.465	-0.9378	0.5715
6	100	2.059	3.096	2.0×10^{-5}	54.046	-0.9377	0.5718
7	100	3.111	2.674	8.0×10^{-4}	61.469	-0.9178	0.5416
8	100	0.740	3.147	3.0×10^{-6}	19.878	-0.9400	0.5514
9	100	3.111	2.674	8.0×10^{-4}	61.469	-0.9182	0.5279

3.4.7 Hydraulic aperture (b_f)

Hydraulic apertures are calculated with Equation (3.17) for 100 randomly generated values for hydrogeologic units 1 through 9. Eight of the units exhibit similar sized mean apertures; their expected values range from approximately 100 to 200 microns. Unit 9 is the exception; its value is somewhat smaller (60 microns), consistent with lithologic overburden compaction and slight healing of the fractures.

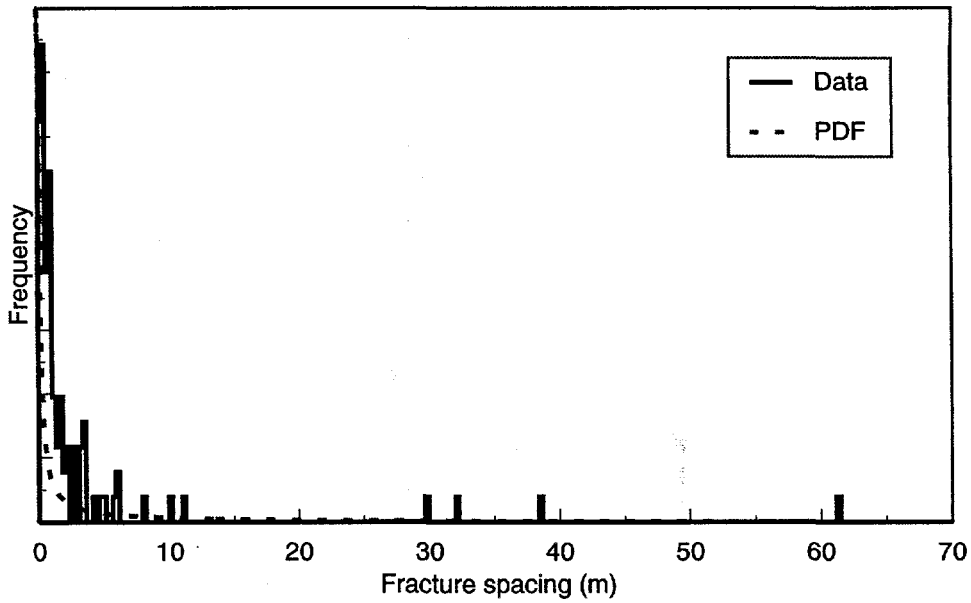

Figure 3-14. Distribution of fracture spacings for unit 7 (Prow Pass welded).

The hydraulic-aperture parameter is developed as a beta-distribution function. Table 3-29 lists the statistics and the beta-distribution parameters.

Table 3-29. Hydraulic aperture (b_f) statistics and beta-distribution parameters.

Unit	Statistics					Beta-Distribution Parameters	
	n	$E[x]$ (μm)	CV	Min (μm)	Max (μm)	Alpha	Beta
1	100	181	0.73	253	980	0.012	4.193
2	100	206	1.04	24.5	1640	-0.475	3.146
3	100	180	0.85	6.4	1190	-0.053	4.510
4	100	192	0.88	7.1	1320	-0.100	4.491
5	100	179	1.24	11.7	1760	-0.582	2.951
6	100	108	1.00	6.2	858	-0.338	3.881
7	100	203	1.66	11.8	2380	-0.785	1.450
8	100	103	1.00	4.3	800	-0.320	3.803
9	100	55.7	0.88	7.1	371	-0.285	3.644

3.4.8 Fracture porosity (ϕf)

Fracture porosity is a function of the fracture frequency and the hydraulic aperture. Starting with the 100 values for apertures computed in the previous section, PDFs for fracture porosity are then calculated from Equation (3.18). Since Equation (3.18) has $cos(\theta_f)$ in the denominator, fracture angles near 90° (i.e., vertical) predict very large values for ϕ_f. To compensate for this, the highest of the 100 sampled values for θ_f have been eliminated. The porosities predicted by the omitted values include several above 1.0. (High fracture porosities are not necessarily phys-

ically unreasonable; the likelihood of a vertical drillhole intersecting a vertical fracture is small unless the fracture density—and thus the fracture porosity—is very high.) Some near-vertical fracture orientations are included in the data. Because the values calculated for ϕ_f span several orders of magnitude, the higher values skew the data; consequently, the data have been transformed to $\log_{10}$ space. The parameters for the log-transformed data are given in Table 3-30.

Table 3-30. Fracture porosity (θ_f) statistics, $\log_{10}$ statistics and beta-distribution parameters.

	Statistics					Log_{10} Statistics				Beta-Distribution Parameters	
Unit	n	$E[x]$	CV	Min	Max	$E[x]$	CV	Min	Max	Alpha	Beta
1	99	$1.38\text{x}10^{-3}$	1.20	$6.63\text{x}10^{-5}$	$1.08\text{x}10^{-2}$	-3.063	0.140	-4.179	-1.966	1.815	1.805
2	99	$4.12\text{x}10^{-4}$	1.47	$1.50\text{x}10^{-5}$	$4.43\text{x}10^{-3}$	-3.631	0.127	-4.825	-2.354	1.982	2.189
3	99	$2.75\text{x}10^{-3}$	2.18	$5.00\text{x}10^{-4}$	$4.25\text{x}10^{-2}$	-2.999	0.190	-4.301	-1.371	1.457	2.072
4	99	$2.44\text{x}10^{-3}$	2.18	$4.30\text{x}10^{-5}$	$3.74\text{x}10^{-2}$	-3.053	0.187	-4.367	-1.427	1.483	2.072
5	99	$9.98\text{x}10^{-4}$	2.18	$1.47\text{x}10^{-5}$	$1.38\text{x}10^{-2}$	-3.438	0.169	-4.834	-1.860	1.594	1.932
6	99	$4.84\text{x}10^{-4}$	2.07	$8.46\text{x}10^{-6}$	$6.69\text{x}10^{-3}$	-3.725	0.151	-5.073	-2.174	1.608	2.001
7	99	$2.78\text{x}10^{-4}$	2.06	$6.41\text{x}10^{-6}$	$4.91\text{x}10^{-3}$	-3.897	0.136	-5.193	-2.309	1.843	2.484
8	99	$1.55\text{x}10^{-3}$	2.31	$2.17\text{x}10^{-5}$	$2.54\text{x}10^{-2}$	-3.284	0.183	-4.664	-1.596	1.451	1.998
9	99	$8.06\text{x}10^{-5}$	1.35	$3.22\text{x}10^{-6}$	$6.92\text{x}10^{-4}$	-4.323	0.105	-5.493	-3.160	1.811	1.794

3.4.9 Fracture hydraulic conductivity (K_f)

Based on the model described in Section 3.4.1, we can approximate K_f from the bulk hydraulic conductivity, K_{bs}, because the latter is a combination of the matrix and fracture conductivities. Fracture hydraulic conductivity is calculated as a function of saturated bulk conductivity and fracture frequency using Equation (3.19). From the 100 values sampled for K_{bs} and ϕ_f, fracture hydraulic conductivities are computed. Values are transformed to log space; the beta-distribution parameters are given in Table 3-31.

Darcy flow is an average over the entire cross-section considered; i.e., it is characterized by bulk saturated conductivity. To determine fracture conductivity from bulk conductivity, the matrix flow is subtracted from the averaged total flow to get the fracture component. Since bulk conductivity generally is dominated by the fracture component by several orders of magnitude (except for some nonwelded hydrogeologic units), matrix flow can be ignored in these calculations for the sake of simplicity. Thus, the formula for computing fracture conductivity is given by Equation 3.19, relating the bulk and fracture conductivities.

Table 3-31. Fracture hydraulic conductivity (K_f) statistics, $\log_{10}$ statistics, and beta-distribution parameters.

Unit	Statistics					Log_{10} Statistics				Beta-Distribution Parameters	
	n	$E[x]$ (m/s)	CV	Min (m/s)	Max (m/s)	$E[x]$ (m/s)	CV	Min (m/s)	Max (m/s)	Alpha	Beta
1	100	$4.06\text{x}10^{-2}$	2.20	$5.21\text{x}10^{-4}$	$7.84\text{x}10^{-1}$	-1.732	0.300	-3.282	-0.104	3.082	3.289
2	100	$7.14\text{x}10^{-2}$	3.38	$4.89\text{x}10^{-4}$	$2.21\text{x}10^{0}$	-1.724	0.378	-3.310	0.344	1.910	2.794
3	100	$4.57\text{x}10^{-2}$	2.73	$3.30\text{x}10^{-5}$	$1.16\text{x}10^{0}$	-1.804	0.369	-4.480	0.065	5.046	3.223
4	100	$5.30\text{x}10^{-2}$	2.86	$4.06\text{x}10^{-5}$	$1.43\text{x}10^{0}$	-1.753	0.380	-4.390	0.154	4.991	3.332
5	100	$6.54\text{x}10^{-2}$	4.13	$1.12\text{x}10^{-4}$	$2.54\text{x}10^{0}$	-1.931	0.398	-3.951	0.405	2.244	2.751
6	100	$1.91\text{x}10^{-2}$	3.33	$3.17\text{x}10^{-5}$	$6.03\text{x}10^{-1}$	-2.298	0.310	-4.496	-0.220	3.112	2.888
7	100	$1.26\text{x}10^{-1}$	4.65	$1.13\text{x}10^{-4}$	$4.60\text{x}10^{0}$	-1.961	0.438	-3.946	0.665	1.616	2.461
8	100	$1.74\text{x}10^{-2}$	3.19	$1.53\text{x}10^{-5}$	$5.24\text{x}10^{-1}$	-2.372	0.331	-4.816	-0.281	2.939	2.370
9	100	$4.48\text{x}10^{-3}$	2.77	$4.16\text{x}10^{-5}$	$1.13\text{x}10^{-1}$	-2.818	0.219	-4.380	-0.948	2.028	2.626

3.4.10 Water retention air-entry (α_{vGf}) parameter

The fracture air-entry parameter (α_{vG_f}) of the van Genuchten model is derived from the fracture aperture b_f by the method of Wang and Narasimhan (1985). This method assumes that we can apply capillary theory to model a set of parallel, smooth-wall fractures:

$$\alpha_{vG_f} = \frac{b_f}{(2\gamma\cos(\theta_{ls})/\rho g)}, \tag{3.20}$$

where γ is surface tension, ρ is fluid density, g is gravitational acceleration, and θ_{ls} is the contact angle between the liquid surface and solid surface. Values of $\theta_{ls} = 0°$, $\gamma = 0.072$ kg/sec^2, $\rho = 1000$ kg/m^3, and $g = 9.8$ m/sec^2 are used in Equation 3.20 to calculate α_{vG_f} in units of m^{-1}. The denominator of the equation is a constant, ($1.47\text{x}10^{-5}$ m^2), so the fracture aperture statistics given in Table 3-29 are divided by this value to compute α_{vG_f}. Since the distribution being generated is essentially that of the fracture aperture, all other parameters (i.e., n, CV, and beta-distribution exponents) are the same. Table 3-32 gives the parameters.

Because fracture parameters were derived differently for TSPA-91, only two parameters can be compared to this study—fracture saturated hydraulic conductivity (K_f) and the van Genuchten fracture air-entry (α_{vG_f}) parameter. In TSPA-91 both parameters are modeled as beta distributions; in this study; K_f is modeled as a beta distribution approximating an exponential, and the van Genuchten fracture air-entry parameter is modeled as a normal beta distribution.

Table 3-32. Fracture air-entry parameter basic statistics and beta-PDF parameters.

Unit	Basic Statistics					Beta Distribution Parameters	
	n	$E[x]$ (m^{-1})	CV	Min (m^{-1})	Max (m^{-1})	Alpha	Beta
1	100	12.3	0.73	1.7	66.7	0.012	4.193
2	100	14.0	1.04	1.7	111.6	-0.475	3.146
3	100	12.2	0.85	0.4	81.0	-0.053	4.510
4	100	13.1	0.88	0.5	89.8	-0.100	4.491
5	100	12.2	1.24	0.8	119.8	-0.582	2.951
6	100	7.3	1.00	0.4	58.4	-0.338	3.881
7	100	13.8	1.66	0.8	162.0	-0.785	1.450
8	100	7.0	1.00	0.3	54.4	-0.320	3.803
9	100	3.8	0.88	0.5	25.2	-0.285	3.644

The fracture properties for this study are modeled by the parallel-plate approximation discussed in Section 3.4.1. The near-vertical fracture orientations in this study data set result in PDFs for fracture hydraulic conductivity that are weighted toward higher values. In TSPA-91 a composite-porosity model was used in which the fracture is assumed to have the hydraulic properties of sand. Fracture characteristics for all the TSPA-91 units were the same. Table 3-33 compares the fracture parameters.

Table 3-33. Comparison of expected values for fracture parameters between TSPA-91 and this study.

Unit (Current/TSPA-91)	Fracture Hydraulic Conductivity (m/s)		Ratio: Current/TSPA-91
	Current	TSPA-91	
3R/1	4.57×10^{-2}	8.25×10^{-5}	550
4/2	5.30×10^{-2}	8.25×10^{-5}	640
5/3	6.54×10^{-2}	8.25×10^{-5}	790
	Fracture Air-Entry Parameter		
3R/1	12.2	14.5	0.8
4/2	13.1	14.5	0.9
5/3	12.2	14.5	0.8

The significance of the differences between the TSPA-91 and the PDFs developed for this study depends on the sensitivity of the hydrogeologic models to the parameters.

3.5 Parameter correlations

Thus far, the PDFs of hydrogeologic properties have been discussed individually, but correlations among them could be important as well. For this reason, the data from the PAWDS are examined to determine whether correlations exist. For most of the parameters, data are not complete enough to calculate meaningful correlation coefficients, but a correlation analysis is conducted between matrix porosity and matrix saturated hydraulic conductivity. As more data become available, other correlations will be examined.

The Latin Hypercube Sampler (LHS) program (Iman and Shortencarrier, 1984), which generates stochastic parameter realizations for the aqueous-transport simulations, accepts correlations among parameters being sampled. Spearman rank-correlation analyses provide the correlation constraints to the LHS. The correlation analyses are done separately for each hydrogeologic unit; correlations are significant if the Spearman two-sided significance level is less than 0.05. As Table 3-34 shows, there is not a clear-cut pattern of either correlation or lack thereof.

Although the significance level for unit 7 is greater than 0.05, the correlation coefficient implies a fairly high correlation among the data pairs; we assume that the correlation coefficient takes precedence. We therefore consider the parameters of the unit to be correlated.

Table 3-34. Spearman rank correlations for matrix porosity and saturated hydraulic conductivity.

Unit	Data Pairs	Spearman Rank Correlation Coefficient	Two-Sided Significance Level	Correlation Significant?
1	10	-0.308	0.387	no
2	8	0.929	0.000	yes
3	25	0.467	0.019	yes
4	4	-0.400	0.600	no
5	16	0.744	0.000	yes
6	17	0.159	0.541	no
7	6	0.771	0.072	yes
8	5	-0.300	0.624	no
9	13	0.121	0.694	no
10	7	0.000	1.000	no

4.0 Summary and Discussion

A hydrogeologic modeling domain and parameter working data set (the PAWDS) have been systematically developed for total-system and other performance-assessment analyses at the potential Yucca Mountain repository site. The model domain is designed to provide a stochastic representation of the uncertainties and variabilities of the hydrogeologic units and parameters. The working data set consists of statistical parameter distribution functions derived from properties values.

The model domain is created from geostatistical simulations of rock types at the site. The geostatistical model uses the degree of welding of the rocks as a measure of differences in hydrologic properties. The model assumes that the rocks are either welded or nonwelded. Additional detail was deterministically included to account for variation in the hydrologic properties of the Prow Pass welded and Prow Pass vitric and zeolitic nonwelded units.

The PAWDS was initially developed for TSPA and other performance-assessment analyses. The PAWDS contains both raw data and interpreted parameter sets. The data set is designed to provide consistency in the manipulation of the data from the raw observations to the final parameter PDFs. In addition, the PAWDS provides traceability of data, linking the data used to develop the PDFs with the original data sources. The PAWDS contains one of the most comprehensive data sets of the geologic and hydrogeologic parameters available for performance-assessment analyses. The working data set is complementary to the YMP/GENISES database because it takes properties data from the YMP database and interprets them for PA applications. The interpreted data are then available to the YMP database to supplement their raw and interpreted data.

4.1 Discussion and Recommendations

Although an attempt has been made to obtain as complete a data set as possible, the degree of completeness in the drillhole logs and related information varies. The highest concentration of drillhole data comes from the northeast area of the potential Yucca Mountain repository; the southern and particularly the western repository area lack coverage. If further modeling shows a sensitivity to data values, more drillholes may be needed to fill in the gaps in stratigraphic detail and hydrogeologic data.

Some of the hydrogeologic data, such as porosity and bulk density, are very extensive. PDFs for these data are directly produced and are fairly representative of the model domain. Other data are not as dense and require additional interpretation to produce credible PDFs. Some properties data are quite sparse, and only through extrapolation and simulation could PDFs be developed. The variances of the PDFs were adjusted to reflect the differences in the range of values expected because of the differences in scale between direct properties measurements and site-scale modeling.

There are far fewer fracture data available, and there are none for fracture hydraulic properties such as conductivity. Fracture hydraulic parameters were developed analytically from the two observed fracture properties (frequency and orientation) in combination with bulk saturated hydraulic conductivity values. Fracture hydrologic properties were calculated by assuming that fracture flow obeys a parallel-plate model. Using derived fracture parameters is a less-than-optimal procedure, especially since future emphasis for performance assessments will be on fast-path flow processes.

Two immediate solutions to the lack of fracture-parameter data are to secure additional direct measurements of properties or to pursue alternative methods to develop parameters in a manner that inspires an acceptable level of confidence. Better data or methods to determine fracture frequency, orientation, aperture, and conductivities are of particular interest. Some adaptation of Wang's (1992) approach (Section 3.4.1) may also provide an alternative method.

Bulk properties from pumping or aquifer tests have been incorporated for the first time to account for the larger controls on fluid flow outside the matrix property domain. Statistical parameters have been derived from hydraulic transmissivities for bulk conductivities. These properties will be evaluated for their influence on or sensitivity to the resulting flow models. Some bulk property data from aquifer tests produced results that are not incorporated into this analysis because the test data crossed stratigraphic boundaries and could not be separated by units.

The bulk parameters should include the effects of structural controls such as fractures and their cumulative hydrologic effects. One area not addressed in this analysis is that of fault properties. Studies that can characterize their hydraulic properties would aid in modeling the localized effects of major structural elements in the repository area.

The current and future performance-assessment efforts will help to assess the adequacy of hydrogeologic data. As discussed earlier in this report, the availability

and quantity of data vary considerably. For the matrix properties there are considerable data that allow for the development of quite robust PDFs. Future performance assessments must conduct sensitivity studies to evaluate the adequacy of the direct and scaled matrix PDFs before recommending the amount of additional data to be collected. For fracture data, the development of alternative conceptual models for fast-path flow will undoubtedly require additional data-gathering efforts. These should also include additional data, of the type discussed in this report, to increase our confidence in the predictions of the models in which they are currently used (the composite-porosity model).

It is likely that more data could change the outcome of performance assessment calculations. But before more data are sought through either field examination or laboratory analysis, sensitivity studies should be undertaken to determine which parameters if any would significantly be affected by the inclusion of additional data.

This page left intentionally blank.

References

Anderson, L. A., 1981a, "Rock Property Analysis of Core Samples from the Calico Hills UE25a-3 Borehole, Nevada Test Site, Nevada," *USGS/OFR-81-1337*, U.S. Geological Survey, Denver, CO. (SRX.86087.4164)

Anderson, L. A., 1981b, "Rock Property Analysis of Core Samples from the Yucca Mountain UE25a-1 Borehole, Nevada Test Site, Nevada," *USGS/OFR-81-1338*, U.S. Geological Survey, Denver, CO. (NNA.870406.0031)

Anderson, L. A., 1984, "Rock Property Measurements on Large-Volume Core Samples from Yucca Mountain USW GU-3/G-3 and USW G-4 Boreholes, Nevada Test Site, Nevada," *USGS/OFR-84-552*, U.S. Geological Survey, Denver, CO. (NNA.870323.0195)

Anderson, L. A., 1991, "Results of Rock Property Measurements Made on Core Samples from Yucca Mountain Boreholes, Nevada Test Site, Nevada," Part 1: Boreholes UE25A-4, -5, -6, and 7; Part 2: Borehole UE25p#1, *USGS/OFR-90-474*, U.S. Geological Survey, Denver, CO. (NNA.910411.0081)

Arkin, H., and R. R. Colton, 1970, *Statistical Methods*, Harper & Row, New York, NY. (MOL.940805.0098)

Barnard, R. W., and H. A. Dockery, editors, 1991, "Technical Summary of the Performance Assessment Calculational Exercises for 1990 (PACE-90)," Volume 1: Nominal Configuration Hydrogeologic Parameters and Calculational Results, *SAND90-2726*, Sandia National Laboratories, Albuquerque, NM, and Livermore, CA. (NNA.910523.0001)

Barnard, R. W., M. L. Wilson, H. A. Dockery, J. H. Gauthier, P. G. Kaplan, R. R. Eaton, F. W. Bingham, and T. H. Robey, 1992, "TSPA 1991: An Initial Total-System Performance Assessment for Yucca Mountain," *SAND91-2795*, Sandia National Laboratories, Albuquerque, NM. (NNA.920630.0033)

Barton, C., W. R Page, and T. L. Morgan, 1989, "Fractures in Outcrops in the Vicinity of Drill Hole USW G-4, Yucca Mountain, Nevada, Data Analysis and Compilation," *USGS-OFR-89-92*, U.S. Geological Survey, Denver, CO. (NNA.900108.0155)

Bentley, C. B., J. H. Robinson, and R. W. Spengler, 1983, "Geohydrologic Data for Test Well USW H-5, Yucca Mountain Area, Nye County, Nevada," *USGS/OFR-83-853*, U.S. Geological Survey, Denver, CO. (NNA.870519.0098)

Broxton, D. E., R. G. Warren, R. C. Hagan, and G. Leudemann, 1986, "Chemistry of Diagenetically Altered Tuffs at a Potential Nuclear Waste Repository, Yucca Mountain, Nye County, Nevada, *LA-10802-MS*, Los Alamos National Laboratory, Los Alamos, NM. (NNA.890327.0036)

Buesch, D. C., J. E. Nelson, R. P. Dickerson, and R. W. Spengler, 1993, "Development of 3-D Lithostratigraphic and Confidence Models at Yucca Mountain, Nevada," High level Radioactive Waste Management Proceedings at the Forth International Conference, April 26-30, American Nuclear Society, La Grange Park, IL, p. 943. (NNA.931214.0104)

Byers, F. M., Jr., W. J. Carr, P. P. Orkild, W. D. Quinlivan, and K. A. Sargent, 1976, "Volcanic Suites and Related Cauldrons of Timber Mountain–Oasis Valley Caldera Complex, Southern Nevada," *USGS Professional Paper 919*, U.S. Geological Survey, Denver, CO. (NNA.870406.0239)

Craig, R. W., and J. H. Robison, 1984, "Geohydrology of Rocks Penetrated by Test Well UE-25p No.†1, Yucca Mountain Area, Nye County, Nevada," *USGS/WRI-84-4248*, U.S. Geological Survey, Denver, CO. (NNA.890905.0209)

Department of Energy (DOE), 1984, "Nuclear Waste Policy Act of 1982; General Guidelines for the Recommendation of Sites for the Nuclear Waste Repositories; Final Siting Guidelines," *Code of Federal Regulations*, Title 10, Part 960, U.S. Department of Energy, Washington, DC. (NNA.870506.0140)

Department of Energy (DOE), 1988a, "Core Photographs of USW G-4," PAN AM-DNA Photo, Negative No. W 088 through W 195, U.S. Department of Energy, Mercury, NV. (NNA.931112.0075)

Department of Energy (DOE), 1988b, "Core Photographs of UE25a #1," PAN AM-DNA Photo, Negative No. W 217 through W 301, U.S. Department of Energy, Mercury, NV. (NNA.931112.0075)

Department of Energy (DOE), 1988c, "Core Photographs of USW G-1," PAN AM-DNA Photo, Negative No. W 554 through W 742, U.S. Department of Energy, Mercury, NV. (NNA.931112.0075)

Department of Energy (DOE), 1988d, "Core Photographs of UE25b-1H," PAN AM-DNA Photo, Negative No. W 800 through W 883, U.S. Department of Energy, Mercury, NV. (NNA.931112.0075)

Department of Energy (DOE), 1988e, "Core Photographs of USW GU-3/G-3," PAN AM-DNA Photo, Negative No. W 1096 through W 1282, U.S. Department of Energy, Mercury, NV. (NNA.931112.0075)

Department of Energy (DOE), 1988f, "Core Photographs of UE25a #5," PAN AM-DNA Photo, Negative No. W 1448 through W 1461, U.S. Department of Energy, Mercury, NV. \(NNA.931112.0075)

Department of Energy (DOE), 1988g, "Core Photographs of USW H#1," PAN AM-DNA Photo, Negative No. W 1466 through W 1479, U.S. Department of Energy, Mercury, NV. (NNA.931112.0075)

Department of Energy (DOE), 1988h, "Core Photographs of UE25a #6," PAN AM-DNA Photo, Negative No. W 1482 through W 1493, U.S. Department of Energy, Mercury, NV. (NNA.931112.0075)

Department of Energy (DOE), 1988i, "Core Photographs of UE25a #4," PAN AM-DNA Photo, Negative No. W 1530 through W 1545, U.S. Department of Energy, Mercury, NV. (NNA.931112.0075)

Department of Energy (DOE), 1988j, "Site Characterization Plan, Yucca Mountain Site, Nevada Research and Development Area, Nevada," *DOE/RW-0199*, U.S. Department of Energy, Washington, DC. (HQO.881201.0002)

Department of Energy (DOE), 1988k, "Yucca Mountain Project Site Atlas," *YMP/88-21*, U.S. Department of Energy, Las Vegas, NV. (NNA.890428.0364)

Department of Energy (DOE), 1989a, "Core Photographs of USW H-6," PAN AM-DNA Photo, Negative No. W 1549 through W 1558, U.S. Department of Energy, Mercury, NV. (NNA.931112.0075)

Department of Energy (DOE), 1989b, "Core Photographs of UE25a #7," PAN AM-DNA Photo, Negative No. W 1560 through W 1592, U.S. Department of Energy, Mercury, NV. (NNA.931112.0075)

Department of Energy (DOE), 1989c, "Core Photographs of USW H-1," PAN AM-DNA Photo, Negative No. W 1602 through W 1635, U.S. Department of Energy, Mercury, NV. (NNA.931112.0075)

Department of Energy (DOE), August 20, 1992, "Core Photographs of UE25 UZ-16," Photo, Negative No. C-SM-216-1 through C-SM-216-22 OUS (boxes 1 through 64), U.S. Department of Energy, Mercury, NV. (NNA.931112.0075)

Department of Energy (DOE), 1993, "The Yucca Mountain Site Characterization Project—Reference Information Base, Version 4, Revision 7," *YMP/CC-0002*, U.S. Department of Energy, Las Vegas, NV. (NNA.930517.0092)

Deutsch, C. V. and A. G. Journel, 1992, "GSLIB: Geostatistical Software Library and User's Guide", Oxford University Press, New York. (NNA.930507.0081)

Dudley, A. L. , R. R. Peters, J. H. Gauthier, M. L. Wilson, M. S. Tierney, and E. A. Klavetter, 1988, "Total System Performance Assessment Code (TOSPAC) Volume 1: Physical and Mathematical Bases," *SAND85-0002*, Sandia National Laboratories, Albuquerque, NM. (NNA.881202.0211)

Environmental Protection Agency (EPA), 1985, "Environmental Radiation Protection Standards for Management and Disposal of Spent Nuclear Fuel, High-Level, and Transuranic Radioactive Wastes," *Code of Federal Regulations*, Title 40, Part 191. (HQS.880517.3264)

Flint, L. E., and A. L. Flint, 1990, "Preliminary Permeability and Water-Retention Data for Nonwelded and Bedded Tuff Samples, Yucca Mountain Area, Nye County, Nevada," *USGS/OFR-90-569*, U.S. Geological Survey, Denver, CO. (NNA.920225.0002)

Freeze, R. A., and J. A. Cherry, 1979, *Groundwater*, Prentice-Hall, Englewood Cliffs, NJ. (NNA.870406.0444)

Freeze, R. A., and J. Massmann, 1990, "Hydrogeological Decision Analysis. 1: A Framework," Groundwater, 28, pp. 738–766. (NNA.910306.0143)

Gerhart, P. M., and R. J. Gross, 1985, *Fundamentals of Fluid Mechanics*, Addison-Wesley, Reading, MA. (NNA.940303.0056)

Gogg, J. T., and J. R. A. Mott, 1992, *Improve Quality and Productivity with Simulation*, JMI Consulting Group, Palos Verdes, CA. (NNA.940509.0029)

Harr, M. E., 1987, *Reliability-Based Design in Civil Engineering*, McGraw-Hill, New York, NY. (NNA.890713.0149)

Huijbregts, C. and A. Matheron, 1971, *Universal Kriging-An Optimal Approach to Trend Surface Analysis, In Decision Making in the Mineral Industry*, Canadian Institute of Mining and Metallurgy, Special Volume 12, pp. 159–169. (MOL.19940714.0115)

Iman, R. L., and M. J. Shortencarrier, 1984, "A FORTRAN-77 Program and User's Guide for the Generation of Latin Hypercube and Random Samples for Use with Computer Models," *SAND83-2365*, Sandia National Laboratories, Albuquerque, NM. (NNA.900117.0157)

Jaynes, E. T., 1957, "Informational Theory and Statistical Mechanics II," *Phys. Rev.*, **108**, pp. 171–190. (NNA.910306.0127)

Journel, A. G., and Ch. J. Huijbregts, 1978, *Mining Geostatistics*, Academic Press, New York, NY. (NNA.900919.0192)

Journel, A. G., 1993, "Nonparametric Estimation of Spatial Distributions," *Math. Geol.*, **15**:445–468. (NNA.891114.0349)

Knauss, K. G., W. J. Beiriger, D. W. Peifer, and A. J. Piwinskii, 1985, "Hydrothermal Interaction of Solid Wafers of Topopah Spring Tuff with J-13 Water and Distilled Water at 90, 150, and 250°C, Using Dickson-type, Gold-bag Rocking Autoclave," *UCRL-53645*, Lawrence Livermore National Laboratory, Livermore, CA. (NNA.900207.0282)

Knauss, K. G., and D. W. Peifer, 1986, "Reaction of Vitric Topopah Spring Tuff and J-13 Ground Water Under Hydrothermal Conditions Using Dickson-type, Gold-bag Rocking Autoclaves," *UCRL-53795*, Lawrence Livermore National Laboratory, Livermore, CA. (NNA.891102.0117)

Krumbein, W. C., and F. A. Graybill, 1965, *An Introduction to Statistical Models in Geology,* McGraw-Hill, New York, NY. (HQZ.870301.7475)

Kume, J., and D. P. Hammermeister, 1990, "Geohydrologic Data from Test Hole USW UZ-7, Yucca Mountain Area, Nye County, Nevada, *USGS/OFR-88-465, U.S.* Geological Survey, Denver, CO. (NNA.900312.0300)

Kume, J., and D. P. Hammermeister, 1991, "Geohydrologic Data from Drill-bit Cuttings and Rotary Cores from Test Hole USW UZ-13, Yucca Mountain Area, Nye County, Nevada," *USGS/OFR-90-362,* U.S. Geological Survey, Denver, CO. (NNA.901015.0196)

Lahoud, R. G., D. H. Lobmeyer, and M. S. Whitfield, Jr., 1984, "Geohydrology of Volcanic Tuff Penetrated by Test Well UE-25b No. 1, Yucca Mountain, Nye County, Nevada," *USGS/WRI-84-4253,* U.S. Geological Survey, Denver, CO, and Fenix and Scisson, Inc., Mercury, NV. (NNA.890511.0117)

Lin, W., and W. Daily, 1984, "Transport Properties of Topopah Spring Tuff," *UCRL-53602,* Lawrence Livermore National Laboratory, Livermore, CA. (NNA.891026.0025)

Lin, M., M. P. Hardy, and S. J. Bauer, 1993, "Fracture Analysis and Rock Quality Designation Estimation for the Yucca Mountain Site Characterization Project," *SAND92-0449,* Sandia National Laboratories, Albuquerque, NM. (NNA.921204.0012)

Lobmeyer, D. H., 1986, "Geohydrology of Rocks Penetrated by Test Well USW G-4, Yucca Mountain, Nye County, Nevada," *USGS/WRIR-86-4015,* U.S. Geological Survey, Denver, CO. (NNA.890918.0510)

Lobmeyer, D. H., M. S. Whitfield, Jr., R. G. Lahoud, and L. Bruckheimer, 1983, "Geohydrologic Data for Test Well UE-25b No. 1, Nevada Test Site, Nye County, Nevada," *USGS/OFR-83-855,* U.S. Geological Survey, Denver, CO, and Fenix and Scisson, Inc., Mercury, NV. (NNA.890922.0285)

Loskot, C. L., and D. P. Hammermeister, 1992, "Geohydrologic Data from Test Holes UE-25 UZ #4 and UE-25 UZ #5, Yucca Mountain Area, Nye County, Nevada," *USGS/OFR-90-369,* U.S. Geological Survey, Denver, CO. (NNA.911219.0001)

Montogolou, A. and J. Wilson, 1982, *The Turning-Bands Method for Simulation of Random Fields Using Line Generation by a Special Method,* Water Resources Research, 18, p. 5. (NNA.930330.0027)

Montazer, P., E. P. Weeks, F. Thamir, S. N. Yard, and P. B. Hofrichter, 1985, "Monitoring the Vadose Zone in Fractured Tuff, Yucca Mountain, Nevada," *Proceedings of NWWA Conference on Characterization and Monitoring of the Vadose (Unsaturated) Zone,* National Water Well Association, Worthington, OH. (NNA.900924.0023)

Muller, D. C., and J. E. Kibler, 1984, "Preliminary Analysis of Geophysical Logs from Drill Hole UE-25p No. 1, Yucca Mountain, Nye County, Nevada," *USGS/OFR-84-649*, U.S. Geological Survey, Denver, CO. (HQS.8805017.1353)

Narasimhan, T. N., and J. S. Y. Wang, 1992, "Conceptual, Experimental, and Computational Approaches to Support Performance Assessment of Hydrology and Chemical Transport at Yucca Mountain," *SAND89-7018*, Sandia National Laboratories, Albuquerque, NM. (NNA.920710.0121)

Nelson, P. H., D. C. Muller, U. Schimschal, and J. E. Kibler, 1991, "Geophysical Logs and Core Measurements from Forty Boreholes at Yucca Mountain, Nevada," *Geophysical Investigations MAP GP-1001*, U.S. Geological Survey, Denver, CO. (NNA.920211.0022)

Nimick, F. B., R. G. Van Buskirk, and A. F. McFarland, 1987, "Uniaxial and Triaxial Compression Test Series, Topopah Spring Member from USW G-2, Yucca Mountain Nevada," *SAND85-0703*, Sandia National Laboratories, Albuquerque, NM. (NNA.891019.0289)

Ortiz, T. S., R. L. Williams, F. B. Nimick, B. C. Whittet, and D. L. South, 1985, "Three-Dimensional Model of Reference Thermal/Mechanical and Hydrological Stratigraphy at Yucca Mountain, Southern Nevada," *SAND84-1076*, Sandia National Laboratories, Albuquerque, NM. (NNA.891019.0289)

Peters, R. R., E. A. Klavetter, I. J. Hall, S. C. Blair, P. R. Heller, and G. W. Gee, 1984, "Fracture and Matrix Hydrogeologic Characteristics of Tuffaceous Materials from Yucca Mountain, Nye County, Nevada," *SAND84-1471*, Sandia National Laboratories, Albuquerque, NM. (NNA.870407.0036)

Rautman, C. A., and A. L. Flint, 1992, "Deterministic Geologic Processes and Stochastic Modeling," in *Proceedings of the Third International High Level Radioactive Waste Management Conference, April 12-16, 1992, Las Vegas, NV*, pp 1617–1624, American Nuclear Society (ANS), La Grange Park, IL; American Society of Civil Engineers (ASCE), New York, NY. (NNA.920505.0069)

Rautman, C. A., and T. H. Robey, 1994, "Development of Stochastic Indicator Models of Lithology, Yucca Mountain, Nevada," in, *Proceedings of the Fifth Annual International High Level Waste Conference, May 22–26*, 1994, *Las Vegas, Nevada*, pp. 1797–2815, American Nuclear Society, La Grange Park, IL. (NNA.940629.0015)

Rush, F. E., W. Thordarson, and L. Bruckheimer, 1983, "Geohydrologic and Drill-Hole Data for Test Well USW H-1, Adjacent to the Nevada Test Site, Nye County, Nevada," *USGS/OFR-83-141*, U.S. Geological Survey, Reston, VA. (NNA.870519.0103)

Rush, F. E., W. Thordarson, and D. G. Pyles, 1984, "Geohydrology of Test Well USW H-1, Yucca Mountain, Nye County, Nevada," *USGS/WRIR-84-4032*, U.S. Geological Survey, Denver, CO. (NNA.870518.0067)

Rutherford, B. M., I. J. Hall, R. R. Peters, R. G. Easterling, and E. A. Klavetter, 1992, "Statistical Analysis of Hydrologic Data for Yucca Mountain," *SAND87-2380,* Sandia National Laboratories, Albuquerque, NM. (NNA.910822.0001)

Schwartz, B. M., 1990, SNL Yucca Mountain Project Data Report: Density and Porosity Data for Tuffs from the Unsaturated Zone at Yucca Mountain, Nevada," *SAND88-0811,* Sandia National Laboratories, Albuquerque, NM. (NNA.900108.0028)

Scott, R. B., R. W. Spengler, S. Diehl, A. R. Lappin, and M. P. Chornack, 1983, "Geologic Character of Tuffs in the Unsaturated Zone at Yucca Mountain, Southern Nevada," *Role of the Unsaturated Zone in Radioactive and Hazardous Waste Disposal,* Ann Arbor Science, Ann Arbor, MI, pp. 289–335. (NNA.870406.0034)

Scott, R. B., and J. Bonk, 1984, "Preliminary Geologic Map of Yucca Mountain, Nye County, Nevada with Geologic Sections," *USGS/OFR-84-494,* U.S. Geological Survey, Denver, CO. (HQS.880517.1443)

Scott, R. B., and M. Castellanos, 1984, "Stratigraphic and Structural Relations of Volcanic Rocks in Drill Holes USW GU-3 and USW G-3, Yucca Mountain, Nye County, Nevada," *USGS/OFR-84-491,* U.S. Geological Survey, Denver, CO. (NNA.890804.0017)

Shannon, C. E., 1948, "The Mathematical Theory of Communication," *Bell Sys. Tech. J.,* 27, pp. 379–423. (NNA.910306.0126)

Snow, D. T., 1968, "Rock Fracture Spacing, Openings, and Porosities," *J. Soil Mech. Found. Div.,* Proc. Amer. Soc. Civil Engrs., pp. 73–91. (HQZ.870227.2751)

Spengler, R. W., D. C. Muller, and R. B. Livermore, 1979, "Preliminary Report on the Geology and Geophysics of Drill Hole UE25a-1, Yucca Mountain, Nevada Test Site," *USGS/OFR-79-1244,* U.S. Geological Survey, Denver, CO. (HQS.880517.1491)

Spengler, R. W., and J. G. Rosenbaum, 1980, "Preliminary Interpretations of Geologic Results Obtained from Boreholes UE25a-4, -5, -6, and -7, Yucca Mountain, Nevada Test Site," *USGS/OFR-80-929,* U.S. Geological Survey, Reston, VA. (NNA.890823.0106)

Spengler, R. W., F. M. Byers, Jr., and J. B. Warner, 1981, "Stratigraphy and Structure of Volcanic Rocks in Drill Hole USW-G1, Yucca Mountain, Nye County, Nevada," *USGS/OFR-81-1349, DOE/ET/44802/T4,* U.S. Geological Survey, Denver, CO. (HQS.880517.1492)

Spengler, R. W., M. P. Chornack, D. C. Muller, and J. E. Kibler, 1984, "Stratigraphic and Structural Characteristics of Volcanic Rocks in Core Hole USW G-4, Yucca Mountain, Nye County, Nevada," *USGS/OFR-84-789,* U.S. Geological Survey, Denver, CO. (NNA.870519.0105)

Thordarson, W., 1983, "Geohydrologic Data and Test Results from Well J-13, Nevada Test Site, Nye County, Nevada," *USGS/WRIR-83-4171,* U.S. Geological Survey, Denver, CO. (HQS.880517.1849)

Thordarson, W., F. E. Rush, R. W. Spengler, and S. J. Wadell, 1984, "Geohydrologic and Drill-Hole Data for Test Well USW H-3, Yucca Mountain, Nye County, Nevada," *USGS/OFR-84-149*, U.S. Geological Survey, Denver, CO. (NNA.870406.0056)

Thordarson, W., F. E. Rush, and S. J. Wadell, 1985, "Geohydrology of Test Well USW H-3, Yucca Mountain, Nye County, Nevada," *USGS/WRI-84-4272*, U.S. Geological Survey, Lakewood, CO. (SRX.850418-0031)

Van Genuchten, T., 1978, Calculating the Unsaturated Hydraulic Conductivity with a New Closed-Form Analytical Model, *Water Resources Bulletin*, Princeton University Press, Princeton University, Princeton, NJ. (HQS.880517.1859)

Voss, C., 1992a, Letter to P. Kaplan SNL, Subject: Transfer of Test Case Data—Attachment A: Composite Transect Dataset: Includes Representative Samples from Surface Outcrop Studies with Data on Porosity, Bulk Density, and Sorptivity, Saturated Hydraulic Conductivity, and Moisture Retention, dated June 15, 1992, Golder Associates, Inc., Redmond, WA. (MOL.19941021.0001)

Voss, C., 1992b, Letter to P. Kaplan SNL, Subject: Transfer of Test Case Data—Attachment B: USW GU-3 Core Analyses, 69 Samples from Topopah Spring Shardy Base (1263.8 ft) to Prow Pass Partially Welded (1883.5 ft), with Measurements of Porosity, Bulk Density, Sorptivity, and Saturated Conductivity, dated June 15, 1992, Golder Associates, Inc., Redmond, WA. (MOL.19941021.0001)

Voss, C., 1992c, Letter to T. Robey, SNL, Subject: Additional Data For Yucca Mountain Test Case—Attachment 3: USW UZN-53 Core Data, dated October 30, 1992, Golder Associates, Inc., Redmond, WA. (MOL.19941021.0002)

Voss, C., 1993, Letter to T. Robey, SNL, Subject: Moisture Retention Curves for Outcrop Samples; Physical Property Data for 11 core samples from USW UZN-53, Golder Associates, Inc., Redmond, WA. (NNA.940113.0033)

Wang, J. S. Y. and T. N. Narasimhan, 1985, "Hydrologic Mechanisms Governing Fluid Flow in Partially Saturated, Fractured, Pourous Tuff at Yucca Mountain," *SAND84-7202*, Sandia National Laboratories, Albuquerque, NM. (NNA.870407.0209)

Wang, J. S. Y., 1992, "Variation of Hydrologic Parameters of Tuff and Soil", in, *Proceedings of the Third Annual International High Level Waste Conference, April 12–16, 1992, Las Vegas, Nevada,* pp. 727–731, American Nuclear Society, La Grange Park, IL. (MOL.19950223.00676)

Weeks, E. P., 1978, "Field Determination of Vertical Permeability to Air," U.S. Geological Survey Professional Paper 1051, Washington, DC, 41pp. (HQS.880517.1930)

Weeks, E. P., and W. E. Wilson, 1984, "Preliminary Evaluation of Hydrologic Properties of Cores of Unsaturated Tuff, Test Well USW H-1, Yucca Mountain, Nevada," *USGS/WRI-84-4193*, U.S. Geological Survey, Denver, CO. (NNA.870407.0037)

Whitfield, M. S., Jr., W. Thordarson, and E. P. Eshom, 1984, "Geohydrologic and Drill-Hole Data for Test Well USW H-4, Yucca Mountain, Nye County, Nevada," *USGS/OFR-84-449,* U.S. Geological Survey, Denver, CO. (NNA.870407.0317)

Whitfield, M. S., Jr., E. P. Eshom, W. Thordarson, and D. H. Schaefer, 1985, "Geohydrology of Rocks Penetrated by Test Well USW H-4, Yucca Mountain, Nye County, Nevada," *USGS/WRI-85-4030,* U.S. Geological Survey, Denver, CO, and Fenix and Scisson, Inc., Mercury, NV. (NNA.870407.0328)

Whitfield, M. S., Jr., W. Thordarson, D. P. Hammermeister, and J. B. Warner, 1990, "Drilling and Geohydrologic Data for Test Hole USW UZ-1, Yucca Mountain, Nye County, Nevada," *USGS/OFR 90-354,* U.S. Geological Survey, Denver, CO. (NNA.900622.0450)

Whitfield, M. S., Jr., C. M. Cope, and C. L. Loskot, 1993, "Borehole and Geohydrologic Data for Test Hole USW UZ-6, Yucca Mountain Area, Nye County, Nevada," *USGS/OFR 92-28,* U.S. Geological Survey, Denver, CO. (NNA.920123.0088)

Wilson, M. L., J. H. Gauthier, R. W. Barnard, G. E. Barr, H. A. Dockery, E. Dunn, R. R. Eaton, D. C. Guerin, N. Lu, M. J. Martinez, R. Nilson, C. A. Rautman, T. H. Robey, B. Ross, E. E. Ryder, A. R. Schenker, S. A. Shannon, L. H. Skinner, W. G. Halsey, J. D. Gansemer, L. C. Lewis, A. D. Lamont, I. R. Triay, A. Meijer, and D. E. Morris, "Total-System Performance Assessment for Yucca Mountain — SNL Second Iteration (TSPA-1993)," *SAND93-2675,* Vols. 1 and 2, Sandia National Laboratories, Albuquerque, NM. (NNA.940112.0123)

Wittwer, C. S., G. S. Bodvarsson, M. P. Chornack, A. L. Flint, B. D. Lewis, R. W. Spengler, and C. A. Rautman, 1992, "Design of a Three-Dimensional Site Scale Model for the Unsaturated Zone at Yucca Mountain, Nevada," High-Level Radioactive Waste Management, Proceedings of the Third International Conference, April 12–16, 1992, American Nuclear Society, La Grange Park, IL, p.262. (NNA.930125.0071)

Yucca Mountain Project, 1992a, "Data Resulting from Data Acquisition," *Technical Data Information Form,* (DTN: GS920508312231.011)

Yucca Mountain Project, 1992b, "Data Resulting from Data Acquisition," *Technical Data Information Form,* (DTN: GS920508312231.012)

Yucca Mountain Site Characterization Project, 1993, "Preliminary Field Composite Borehole Log, UE-25 UZ Number 16," April 14, 1993. (NNA.930427.0129)

Appendix I

Drill Hole Data

This page left intentionally blank.

Introduction

Most of the information reviewed in producing the simplified model stratigraphy for TSPA-93 came from the drill hole lithologic logs and geophysical logs. The results of that review, and analysis of the data available for the 22 drill holes and one supplemental drill hole (USW GU3-G3), are shown in the appendix tables.

The lithologic log was the primary source of information for all of the drill holes except WT-2, and the geophysical log supplemented or collaborated in supporting the interpretations. The primary distinction for categorizing the units is welded or nonwelded, as discussed in the text. The secondary distinction for categorizing degree of welding, the relative degree of the amplitude shift for each respective log, was derived from a qualitative review of the geophysical logs. Some designations of units as welded or nonwelded were based on very limited information, and the choice was inferred. In these instances, the choice is followed by the symbol **(?)** to indicate that the classification is questionable.

The caliper log had the most weight in determining the degree of welding. This log shows a smooth, nonvarying trace as the drill hole moves down through moderately welded and densely welded sequences. On encountering a nonwelded sequence, the drill hole widens in diameter and the log exhibits an erratic trace.

The values in the density logs (DBC and DBDCN) are almost always low in bedded tuffs and nonwelded to poorly welded ash flow tuffs; they increase as welding becomes moderate or dense. The values in the resistivity logs (R-LN, R-SN, RDIEL, and RILD) are similar in many respects to those in the density logs but are low where zeolites and clays are abundant (Nelson *et al.*, 1985). The amplitude shifts of all other logs were noted but not relied on for correlating degree of welding.

To determine the true thickness of the hydrostratigraphic units at Yucca Mountain, the drill holes must intersect the units orthogonally. At the potential repository the dip of the beds is about 6 degrees, and drill hole deviations are no more than several degrees. The resulting angle between each unit and the drill hole is small, so correction to true hydrostratigraphic thickness is unnecessary for most of the Yucca Mountain drill holes (Nelson *et al.*, 1985).

IDENTIFICATION NUMBERS FOR STRATUM TYPE

0	unsimulated sequence
1	welded sequence
2	nonwelded sequence
3	Prow Pass welded sequence
6	alluvium (not simulated in model)
-1	bottom of drill hole

UE25a #1 STRATIGRAPHY

Coordinates: E-566350.0, N-764900.2, ground elevation 3934.00 ft (DOE, 1988s)

Sources: litholog–Spengler *et al.* (1979); geophysical log–Nelson *et al.* (1991); core photographs–DOE (1988b)

Elevation (ft)	ID	Depth to top of unit (ft)	Stratigraphic Unit: lithology (methods)
3934.00	6	0.00	alluvium (litholog, low gamma ray)
3904.00	1	30.00	Tiva Canyon: welded (litholog, photolog, moderate gamma ray increase, smooth caliper)
3739.00	2	195.00	Tiva Canyon: nonwelded-vitric (litholog, photolog, moderate gamma ray decrease, moderate caliper increase)
3664.00	2	270.00	Topopah Spring: nonwelded-vitric (litholog, photolog)
3658.40	1	275.60	Topopah Spring: welded (litholog, photolog, moderate caliper decrease, low core porosity, high core dry bulk density and core grain density)
2661.00	1	1273.00	Topopah Spring: welded-vitrophyre (litholog, photolog, low caliper, high borehole compensated density)
2616.80	2	1317.20	Topopah Spring: nonwelded-devitrified (litholog, photolog, large decrease in borehole compensated density)
2570.10	2	1363.90	Calico Hills: nonwelded-zeolitic (litholog, photolog, moderate caliper increase, moderate decrease in borehole compensated density, moderate thermal neutron increase)
2098.30	2	1835.70	Prow Pass: nonwelded-devitrified (litholog, photolog, moderate spontaneous potential increase, stable borehole compensated density and delta-t and waveform compressional velocity)
1984.20	3	1949.80	Prow Pass: welded (litholog, photolog, moderate spontaneous potential decrease, moderate borehole compensated density increase, moderate increase in delta-t and waveform compressional velocity, moderate increase in short normal and long normal resistivity, moderate thermal neutron increase)
1920.00	2	2014.00	Prow Pass: nonwelded-devitrified (litholog, photolog, moderate spontaneous potential increase, moderate decrease in borehole compensated density, moderate delta-t and waveform compressional velocity decrease, moderate decrease in long normal and short normal resistivity, moderate thermal neutron decrease)
1824.50	3	2109.50	Prow Pass: welded (litholog, photolog, moderate spontaneous potential decrease, moderate borehole compensated density increase, moderate increase in delta-t and waveform compressional velocity, moderate short normal resistivity increase, moderate long normal resistivity decrease, moderate thermal neutron increase)
1812.00	2	2122.00	Prow Pass: nonwelded-devitrified (litholog, photolog, moderate spontaneous potential increase, moderate borehole compensated density decrease, moderate decrease in delta-t and waveform compressional velocity, moderate short normal resistivity decrease, moderate long normal resistivity increase, moderate thermal neutron decrease)

UE25a #1 STRATIGRAPHY (continued)

Elevation (ft)	ID	Depth to top of unit (ft)	Stratigraphic Unit: lithology (methods)
1600.80	2	2333.20	Bullfrog Member: nonwelded-devitrified (litholog, photolog, moderate gamma ray increase, moderate spontaneous potential decrease, moderate decrease in delta-t and waveform compressional velocity, moderate short normal resistivity increase, moderate long normal resistivity decrease, moderate thermal neutron increase)
1433.40	-1	2500.60	bottom

UE25a #4 STRATIGRAPHY

Coordinates: E-564472.0, N-767972.0, ground elevation 4101.0 ft (Nelson *et al.*, 1991)

Sources: litholog–Spengler and Rosenbaum (1980); geophysics–Nelson *et al.* (1991); core photographs–DOE (1988q)

Elevation (ft)	ID	Depth to top of unit (ft)	Stratigraphic Unit: lithology (methods)
4101.00	6	0.00	alluvium: (litholog, high caliper - erratic, low borehole compensated density, low epithermal neutron)
4071.00	1	30.00	Tiva Canyon: moderately to densely welded-devitrified (litholog, moderate spontaneous potential increase, moderate gamma ray decrease, large caliper decrease, moderate borehole compensated density increase, moderate increase in short normal and long normal resistivity, moderate epithermal neutron increase)
3980.00	2	121.00	Tiva Canyon: partially welded-nonwelded-vitric (litholog, photolog, moderate caliper spike increase, deep induction resistivity spike, epithermal neutron spike)
3950.30	2	150.70	bedded tuff: nonwelded-vitric (litholog, gamma ray spike, borehole compensated density spike, deep induction resistivity spike, epithermal neutron spike)
3948.30	2	152.70	Yucca Mtn: nonwelded-vitric (litholog, photolog, moderate gamma ray increase, moderate decrease in borehole compensated density, moderate deep induction resistivity increase, moderate epithermal neutron increase)
3921.80	2	179.20	bedded tuff: nonwelded-vitric (litholog, photolog, slight caliper increase, gamma ray spike, borehole compensated density spikes, moderate increase in deep induction resistivity)
3910.00	2	191.00	Pah Canyon: nonwelded-vitric, some argillic (litholog, photolog, moderate caliper decrease, moderate gamma ray decrease, moderate borehole compensated density decrease, moderate deep induction resistivity increase, moderate epithermal neutron decrease)
3826.30	2	274.70	bedded tuff: nonwelded-vitric (litholog, moderate caliper increase, moderate gamma ray decrease, moderate borehole compensated density increase, moderate decrease in deep induction resistivity, moderate short normal and long normal resistivity decrease, magnetic susceptibility spike)
3821.00	2	280.00	Topopah Spring: nonwelded-vitric (litholog, photolog, moderate caliper increase, moderate gamma ray decrease, moderate borehole compensated density decrease, moderate short normal and long normal resistivity decrease, moderate epithermal neutron decrease, magnetic susceptibility spike)
3784.20	1	316.80	Topopah Spring: welded-vitrophyre (litholog, photolog, moderate caliper decrease, moderate gamma ray increase, large borehole compensated density increase, moderate increase in deep induction resistivity, moderate short normal and long normal resistivity increase, moderate magnetic susceptibility increase)

UE25a #4 STRATIGRAPHY (continued)

Elevation (ft)	ID	Depth to top of unit (ft)	Stratigraphic Unit: lithology (methods)
3781.00	1	320.00	Topopah Spring: densely welded-devitrified (litholog, photolog, gamma ray spike, high borehole compensated density, deep induction resistivity spike, moderate epithermal neutron decrease, moderate magnetic susceptibility decrease)
3601.00	-1	500.00	bottom

UE25a #5 STRATIGRAPHY

Coordinates: E-564755.1, N-766956.4, ground elevation 4056.50 ft (DOE, 1988s)

Sources: litholog–Spengler and Rosenbaum (1980); geophysics–Nelson *et al.* (1991); core photographs–DOE (1988h)

Elevation (ft)	ID	Depth to top of unit (ft)	Stratigraphic Unit: lithology (methods)
4056.50	6	0.00	alluvium (litholog, erratic caliper, low borehole compensated density, low epithermal neutron, low magnetic susceptibility)
3966.50	1	90.00	Tiva Canyon: densely welded-devitrified (litholog, photolog, low caliper - deflects lower at 118 ft, high borehole compensated density)
3928.50	2	128.00	Tiva Canyon: nonwelded-partially welded-vitric (litholog, photolog, moderate caliper increase, moderate gamma ray increase, moderate decrease in borehole compensated density, moderate deep induction resistivity decrease, moderate epithermal neutron decrease)
3917.90	2	138.60	Yucca Mtn: nonwelded-vitric (litholog, photolog, moderate caliper increase, moderate gamma ray decrease, moderate decrease in borehole compensated density, moderate deep induction resistivity decrease, magnetic susceptibility spike)
3889.50	2	167.00	bedded tuff: nonwelded-vitric (litholog, photolog, moderate caliper decrease, moderate gamma ray increase, moderate spontaneous potential decrease, moderate borehole compensated density increase, moderate increase in deep induction resistivity, slight epithermal neutron increase, moderate magnetic susceptibility decrease)
3871.20	2	185.30	Pah Canyon: nonwelded-vitric (litholog, photolog, moderate gamma ray increase, moderate borehole compensated density decrease, greater deep induction resistivity, moderate epithermal neutron increase, moderate magnetic susceptibility decrease)
3826.90	2	229.60	bedded tuff: nonwelded-vitric (litholog, photolog, moderate gamma ray decrease, moderate spontaneous potential increase, moderate borehole compensated density increase, moderate decrease in deep induction resistivity, moderate short normal and long normal resistivity decrease, moderate magnetic susceptibility decrease)
3819.40	2	237.10	Topopah Spring: nonwelded-vitric (litholog, moderate gamma ray increase, moderate spontaneous potential decrease, moderate borehole compensated density decrease, moderate increase in deep induction resistivity, moderate short normal and long normal resistivity increase, moderate epithermal neutron increase, moderate magnetic susceptibility decrease)
3788.50	2	268.00	Topopah Spring: nonwelded-moderately welded-vitric (litholog, photolog, slight caliper increase, moderate gamma ray increase, moderate decrease in spontaneous potential, large increase in borehole compensated density, moderate deep induction resistivity increase, moderate short normal and long normal resistivity increase, moderate epithermal neutron increase, moderate magnetic susceptibility increase)

UE25a #5 STRATIGRAPHY (continued)

Elevation (ft)	ID	Depth to top of unit (ft)	Stratigraphic Unit: lithology (methods)
3779.50	1	277.00	Topopah Spring: densely welded-vitrophyre (litholog, photolog, slight caliper decrease, moderate gamma ray decrease, moderate increase in spontaneous potential, large borehole compensated density increase, moderate deep induction resistivity increase, moderate increase in short normal and long normal resistivity, moderate epithermal neutron increase, moderate magnetic susceptibility increase)
3777.50	1	279.00	Topopah Spring: densely welded-devitrified (litholog, photolog, caliper spike, moderate gamma ray decrease, moderate increase in spontaneous potential, moderate borehole compensated density decrease, moderate deep induction resistivity increase, moderate short normal and long normal resistivity increase, moderate epithermal neutron decrease, large decrease in magnetic susceptibility)
3569.50	-1	487.00	bottom

UE25a #6 STRATIGRAPHY

Coordinates: E-564500.7, N-765899.5, ground elevation 4052.90 ft (DOE, 1988s)

Sources: litholog–Spengler and Rosenbaum (1980); geophysics–Nelson *et al.* (1991); core photographs–DOE (1988j)

Elevation (ft)	ID	Depth to top of unit (ft)	Stratigraphic Unit: lithology (methods)
4052.90	6	0.00	alluvium (litholog, low gamma ray, low epithermal neutron)
4032.90	1	20.00	Tiva Canyon: densely and welded-devitrified (litholog, photolog, moderate gamma ray increase, moderate to high borehole compensated density, moderate to high deep induction resistivity, low induced polarization and magnetic susceptibility)
3949.90	1	103.00	Tiva Canyon: partially-moderately welded-devitrified (litholog, photolog, moderate caliper decrease, moderate gamma ray decrease, high spontaneous potential, moderate borehole compensated density decrease, moderate decrease in deep induction resistivity, moderate short normal and long normal resistivity decrease, moderate epithermal neutron decrease, moderate magnetic susceptibility decrease)
3929.80	2	123.10	Tiva Canyon: non-partially welded-vitric (litholog, photolog, moderate caliper increase, moderate gamma ray decrease, moderate borehole compensated density decrease, moderate decrease in deep induction resistivity, moderate short normal resistivity increase, moderate epithermal neutron decrease, moderate magnetic susceptibility increase, moderate decrease in induced polarization)
3908.70	2	144.20	bedded tuff: nonwelded-argillic (litholog, photolog, moderate caliper increase, moderate gamma ray decrease, moderate increase in spontaneous potential, moderate borehole compensated density increase, moderate increase in deep induction resistivity, moderate short normal resistivity increase, moderate epithermal neutron increase, moderate epithermal neutron increase, moderate magnetic susceptibility increase)
3903.60	2	149.30	Yucca Mtn member: nonwelded-vitric (litholog, photolog, moderate caliper decrease, moderate gamma ray increase, moderate increase in spontaneous potential, moderate borehole compensated density decrease, moderate increase in deep induction resistivity, moderate short normal resistivity increase, moderate epithermal neutron increase, moderate magnetic susceptibility decrease, moderate induced polarization increase)
3883.60	2	169.30	bedded tuff: nonwelded-vitric (litholog, moderate caliper decrease, moderate gamma ray decrease, moderate increase in spontaneous potential, moderate borehole compensated density decrease, moderate deep induction resistivity increase, moderate short normal resistivity increase, moderate epithermal neutron decrease, moderate increase in magnetic susceptibility, moderate induced polarization decrease)

UE25a #6 STRATIGRAPHY (continued)

Elevation (ft)	ID	Depth to top of unit (ft)	Stratigraphic Unit: lithology (methods)
3864.70	2	188.20	Pah Canyon member: nonwelded-vitric (litholog, photolog, moderate caliper decrease, moderate decrease in spontaneous potential, moderate gamma ray decrease, moderate borehole compensated density increase, moderate deep induction resistivity decrease, moderate short normal resistivity increase, moderate epithermal neutron decrease, moderate increase in magnetic susceptibility, moderate induced polarization decrease)
3825.90	2	227.00	Topopah Spring: nonwelded-vitric (litholog, photolog, moderate caliper decrease, moderate gamma ray increase, moderate decrease in spontaneous potential, moderate borehole compensated density increase, moderate deep induction resistivity increase, moderate short normal and long normal resistivity increase, moderate epithermal neutron increase, moderate decrease in magnetic susceptibility, moderate induced polarization increase)
3811.20	1	241.70	Topopah Spring: densely welded-vitrophyre (lithology, photolog, moderate caliper decrease, moderate gamma ray increase, moderate decrease in spontaneous potential, large increase in borehole compensated density, moderate deep induction resistivity increase, moderate short normal and long normal resistivity increase, large epithermal neutron increase, moderate increase in magnetic susceptibility, moderate induced polarization decrease)
3806.90	1	246.00	Topopah Spring: densely welded-devitrified (litholog, photolog, moderate caliper decrease, moderate gamma ray increase, moderate decrease in spontaneous potential, slight decrease in borehole compensated density, moderate deep induction resistivity increase, moderate short normal and long normal resistivity increase, moderate induced polarization decrease, moderate decrease in magnetic susceptibility)
3552.90	-1	500.00	bottom

UE25a #7 STRATIGRAPHY

Coordinates: E-565468.5, N-766249.9, ground elevation 4004.60 ft (DOE, 1988s)

Sources: litholog–Spengler and Rosenbaum (1980); geophysics–Nelson *et al.* (1991); core photographs–DOE (1989b)

Elevation (ft)	ID	Depth to top of unit (ft)	Stratigraphic Unit: lithology (methods)
4004.60	6	0.00	alluvium (litholog, photolog, high caliper, low to erratic borehole compensated density, low epithermal neutron, low magnetic susceptibility)
3851.60	1	153.00	Tiva Canyon: densely welded-devitrified (litholog, photolog, moderate caliper decrease, moderate gamma ray decrease, moderate borehole compensated density increase, moderate deep induction resistivity decrease, moderate decrease in short normal and long normal resistivity, moderate epithermal neutron decrease, moderate increase in magnetic susceptibility, moderate induced polarization decrease)
3831.10	2	173.50	Tiva Canyon: partially-nonwelded-vitric (litholog, photolog, moderate caliper decrease, moderate gamma ray increase, moderate increase in spontaneous potential, moderate borehole compensated density decrease, moderate deep induction resistivity decrease, moderate short normal and long normal resistivity decrease, moderate epithermal neutron decrease, moderate increase in magnetic susceptibility, moderate induced polarization decrease)
3814.60	2	190.00	bedded tuff: nonwelded-argillic (litholog, photolog, geophysical log stratigraphic breaks obscure logs)
3810.40	2	194.20	Yucca Mtn member: nonwelded-vitric (litholog, slight caliper increase, moderate gamma ray decrease, moderate increase in spontaneous potential, moderate borehole compensated density decrease, moderate decrease in deep induction resistivity, moderate short normal resistivity decrease, moderate long normal resistivity increase, moderate epithermal neutron decrease, moderate decrease in magnetic susceptibility)
3791.70	2	212.90	bedded tuff: nonwelded-vitric (litholog, photolog, slight caliper increase, moderate gamma ray decrease, moderate increase in spontaneous potential, moderate borehole compensated density decrease)
3784.40	2	220.20	Pah Canyon member: nonwelded-vitric (litholog, slight caliper increase, moderate gamma ray decrease, moderate increase in spontaneous potential, moderate borehole compensated density decrease, moderate deep induction resistivity decrease, moderate short normal and long normal resistivity decrease, moderate epithermal neutron decrease, moderate increase in magnetic susceptibility)

UE25a #7 STRATIGRAPHY (continued)

Elevation (ft)	ID	Depth to top of unit (ft)	Stratigraphic Unit: lithology (methods)
3738.80	2	265.80	bedded tuff: nonwelded-argillic (litholog, photolog, moderate caliper increase, moderate gamma ray increase, moderate increase in spontaneous potential, moderate borehole compensated density increase, moderate deep induction resistivity decrease, moderate short normal and long normal resistivity decrease, moderate epithermal neutron increase, moderate increase in magnetic susceptibility, moderate induced polarization decrease)
3731.90	2	272.70	Topopah Spring: partially and nonwelded-vitric (litholog, photolog, moderate caliper decrease, moderate gamma ray decrease, moderate increase in spontaneous potential, moderate borehole compensated density decrease, moderate deep induction resistivity increase, moderate short normal and long normal resistivity increase, moderate decrease in magnetic susceptibility, moderate induced polarization decrease)
3700.10	1	304.50	Topopah Spring: densely welded-vitrophyre (litholog, photolog, smooth caliper, large gamma ray increase, moderate decrease in spontaneous potential, large increase in borehole compensated density, moderate deep induction resistivity increase, moderate short normal and long normal resistivity increase, large epithermal neutron increase, moderate thermal neutron increase, large increase in magnetic susceptibility, large induced polarization increase)
3696.60	1	308.00	Topopah Spring: densely and moderately welded-devitrified (litholog, photolog, smooth caliper, moderate gamma ray increase, moderate decrease in spontaneous potential, slight decrease in borehole compensated density, moderate deep induction resistivity increase, moderate short normal and long normal resistivity increase, moderate induced polarization decrease, moderate decrease in magnetic susceptibility)
3504.60	1	500.00	Topopah Spring: densely welded (low caliper, bottom of lithologic description)
3307.60	1	697.00	Topopah Spring: welded (?) (USW G-4 geophysical log and lithologs, photolog, smooth caliper, moderate gamma ray decrease, moderate increase in spontaneous potential, moderate short normal and long normal resistivity increase, large thermal neutron decrease)
3130.60	1	874.00	Topopah Spring: moderately welded (?) (USW G-4 geophysical log and lithologs, photolog, moderate gamma ray decrease, moderate decrease in spontaneous potential, moderate short normal and long normal resistivity decrease, moderate thermal neutron decrease)
3002.60	-1	1002.00	bottom

UE25b #1 STRATIGRAPHY

Coordinates: E-566416.4, N-765243.4, ground elevation 3939.00 ft (DOE, 1988s)

Sources: litholog–Lobmeyer *et al.* (1983); geophysics–Nelson *et al.* (1991); core photographs–DOE (1988d)

Elevation (ft)	ID	Depth to top of unit (ft)	Stratigraphic Unit: lithology (methods)
3939.00	6	0.00	alluvium (litholog, erratic caliper)
3789.06	1	149.94	Tiva Canyon: welded (litholog, moderate caliper decrease)
3729.02	2	209.98	Tiva Canyon: nonwelded-vitric (litholog, slight caliper increase)
3699.16	2	239.84	Pah Canyon and bedded tuffs: nonwelded-vitric (litholog, erratic caliper)
3664.05	1	274.95	Topopah Spring: welded-vitrophyre (litholog, slight caliper increase)
3659.13	1	279.87	Topopah Spring: welded-vitric (litholog, photolog, moderate caliper decrease, moderate potassium spectral log increase, moderate thorium spectral log increase)
2643.99	1	1295.01	Topopah Spring: welded-vitrophyre (litholog, moderate caliper decrease, moderate borehole compensated density increase, moderate epithermal neutron spike decrease, moderate deep induction resistivity spike decrease)
2608.88	1	1330.12	Topopah Spring: welded-vitric (litholog, slight caliper increase, moderate borehole compensated density decrease, moderate epithermal neutron decrease)
2588.87	2	1350.13	Topopah Spring and bedded tuff: nonwelded-?zeolitic? (litholog, moderate increase in spontaneous potential, moderate borehole compensated density increase, moderate potassium spectral log increase, moderate deep induction resistivity decrease, moderate epithermal neutron increase)
2553.76	2	1385.24	Calico Hills: nonwelded-zeolitic (litholog, photolog from 1571 ft and below to 1591 ft, moderate decrease in spontaneous potential, slight decrease in borehole compensated density, moderate deep induction resistivity decrease, moderate potassium spectral log decrease)
2069.81	2	1869.19	Prow Pass: nonwelded-zeolitic (litholog, photolog from 1900 ft and below, moderate increase in spontaneous potential, moderate borehole compensated density increase, moderate increase in delta-t and waveform compressional velocity, moderate deep induction resistivity decrease, moderate short normal resistivity decrease, moderate potassium spectral log decrease)
1967.12	3	1971.88	Prow Pass: welded-devitrified (litholog, photolog, moderate caliper decrease, moderate borehole compensated density increase, moderate compensated neutron porosity decrease, moderate increase in delta-t and waveform compressional velocity, moderate deep induction resistivity increase, moderate short normal resistivity increase, moderate decrease in radioactive tracer flow log)

UE25b #1 STRATIGRAPHY (continued)

Elevation (ft)	ID	Depth to top of unit (ft)	Stratigraphic Unit: lithology (methods)
1894.28	2	2044.72	Prow Pass: nonwelded-devitrified (litholog, photolog, moderate caliper increase, moderate decrease in spontaneous potential, moderate borehole compensated density decrease, moderate compensated neutron porosity increase, moderate decrease in delta-t and waveform compressional velocity, moderate deep induction resistivity decrease, moderate short normal resistivity decrease, moderate potassium spectral log decrease)
1804.05	3	2134.95	Prow Pass: welded-devitrified (litholog, photolog, moderate caliper decrease, moderate increase in spontaneous potential, moderate borehole compensated density increase, moderate compensated neutron porosity decrease, moderate increase in delta-t and waveform compressional velocity, moderate waveform shear velocity increase, moderate deep induction resistivity increase, moderate short normal resistivity increase)
1708.58	2	2230.42	Prow Pass: nonwelded-devitrified and zeolitic (litholog, photolog, moderate borehole compensated density decrease, moderate compensated neutron porosity increase, moderate decrease in delta-t and waveform compressional velocity, moderate decrease in waveform shear velocity, moderate deep induction resistivity decrease, moderate short normal resistivity decrease)
1577.66	2	2361.34	Bullfrog Member: nonwelded-devitrified and vapor phase alteration (litholog, photolog, slight caliper increase, moderate decrease in waveform shear velocity, moderate decrease in delta-t and waveform compressional velocity, moderate deep induction resistivity increase, moderate short normal resistivity increase)
1341.10	1	2597.90	Bullfrog Member: welded-devitrified (litholog, photolog, slight caliper increase, moderate increase in spontaneous potential, slight increase in delta-t and waveform compressional velocity and waveform shear velocity, moderate potassium spectral log increase, moderate decrease in radioactive tracer flow log)
1156.06	2	2782.94	Bullfrog Member and bedded tuff: nonwelded-zeolitic (litholog, photolog, large decrease in spontaneous potential, moderate borehole compensated density decrease, moderate compensated neutron porosity increase, waveform shear velocity and delta-t and waveform compressional velocity spikes, moderate deep induction resistivity decrease, moderate short normal resistivity decrease, moderate potassium spectral log decrease)
1056.31	2	2882.69	Tram Member: nonwelded-zeolitic (litholog, photolog, moderate increase in spontaneous potential, slight increase in borehole compensated density, moderate decrease in waveform shear velocity and delta-t and waveform compressional velocity, moderate decrease in deep induction and short normal resistivity)

UE25b #1 STRATIGRAPHY (continued)

Elevation (ft)	ID	Depth to top of unit (ft)	Stratigraphic Unit: lithology (methods)
993.32	2	2945.68	Tram Member: nonwelded-devitrified (litholog, photolog, large increase in spontaneous potential, moderate borehole compensated density increase, moderate compensated neutron porosity decrease, moderate increase in waveform shear velocity and delta-t and waveform compressional velocity, moderate deep induction resistivity increase, moderate short normal resistivity increase, moderate increase in potassium spectral log)
786.62	1	3152.38	Tram Member: welded-devitrified (litholog, photolog, slight caliper decrease, moderate borehole compensated density increase, moderate compensated neutron porosity decrease, moderate increase in waveform shear velocity and delta-t and waveform compressional velocity, net decrease in deep induction resistivity and short normal resistivity)
578.60	2	3360.40	Tram Member and bedded tuff: nonwelded-zeolitic (litholog, photolog, moderate decrease in spontaneous potential, slight decrease in borehole compensated density and slight increase in compensated neutron porosity, moderate decrease in deep induction resistivity and short normal resistivity)
-21.50	1	3960.50	Lithic Ridge: welded-devitrified (litholog, photolog, moderate increase in spontaneous potential, moderate caliper decrease, moderate potassium spectral log increase)
-61.20	-1	4000.20	bottom

USW G-1 STRATIGRAPHY

Coordinates: E-561000.0, N-770500.2, ground elevation 4348.60 ft (DOE, 1988s)

Sources: litholog–Spengler *et al.* (1981); geophysics–Nelson *et al.* (1991); core photographs–DOE (1988c)

Elevation (ft)	ID	Depth to top of unit (ft)	Stratigraphic Unit: lithology (methods)
4348.6	6	0.0	alluvium, surface
4288.6	2	60.0	Paintbrush Tuff: nonwelded, litholog description
4078.6	1	270.0	Topopah Spring: welded, litholog description
3061.6	1	1287.0	Topopah Spring: vitrophyre, litholog description, photo log - dark gray to black core/appearance
3006.2	1	1342.4	Topopah Spring: vitric, litholog, photolog - decrease in glassy appearance, more brown in color than black, geophysical log - high grain and bulk density, very low porosity
2988.1	2	1360.5	Topopah Spring: nonwelded vitric; litholog description, photolog change, geophysical log compensated neutron porosity, borehole compensated density, long normal and short normal resistivity, thermal neutron all decrease, very low porosity
2954.3	2	1394.3	Topopah Spring: nonwelded, zeolitic, litholog, geophysical log - porosity increase, bulk and grain density decrease, photolog - color change, gray to more orange matrix and texture finer
2923.1	2	1425.5	Calico Hills nonwelded zeolitized; litholog, geophysical log, etc., stabilize at lower values, porosity increase to about 30-35%
2547.1	2	1801.5	Prow Pass, partially welded, devitrified; litholog, indication in geophysical log at 1790.0 increasing grain density, increasing dry bulk density and porosity increases, photolog at 1800-1800.5 core becomes more uniform and fewer light colored pumice fragments (upper 24 ft zeolitic and argillic)
2482.0	3	1866.6	Prow Pass, partially-moderately welded, devitrified, litholog, increasing core grain density
2473.6		1875.0	WT
2372.1	2	1976.5	Prow Pass, partially welded, devitrified, litholog
2274.7	3	2073.9	Prow Pass, partially-moderately welded, devitrified
2196.6	2	2152.0	Prow Pass bedded, devitrified and zeolitized; litholog, photolog - change color to more reds, increase fragments, geophysical log - grain and bulk density decrease, porosity increase
2175.6	2	2173.0	Bullfrog Member, nonwelded, devitrified, litholog, core grain density, core dry bulk density decreasing porosity
2030.7	2	2317.9	Bullfrog Member partially welded, litholog description, geophysical log grain density, dry bulk density, saturated bulk density all significant increase, porosity decrease, photolog does not provide any obvious indication

USW G-1 STRATIGRAPHY (continued)

Elevation (ft)	ID	Depth to top of unit (ft)	Stratigraphic Unit: lithology (methods)
1901.6	1	2447.0	Bullfrog Member: moderately welded, devitrified
1747.0	2	2601.6	Bullfrog Member: bedded, litholog description, photolog color and texture change
1709.2	1	2639.4	Tram Member: ashflow, partially to moderately welded and zeolitized, litholog, photolog - subtle change in appearance, goes from mottled with small fragments (pumice) to more uniform matrix with fewer fragments
1265.6	2	3083.0	Tram Member: partially welded, slightly-moderately zeolitic
826.6	2	3522.0	Tram Member: flow breccia nonwelded (bedded), litholog, abrupt change in color, lithic fragments, very lithic rich, dark ash flow to light colored sandstone looking sequence
790.4	2	3558.2	flow breccia, nonwelded, devitrified, litholog
423.5	2	3925.1	flow breccia, nonwelded, devitrified, litholog
402.8	1	3945.8	Lithic Ridge well indurated, argillic and zeolitic; litholog, photolog does not provide obvious break
-572.1	2	4920.7	nonwelded (moderately indurated), litholog, photolog color and texture change, lighter color (less red, more green), indication of bedding, fewer lithic fragments
-591.6	0	4940.2	ashflow/bedded, moderately welded, litholog, photolog - indication of old paleo surface with reworked fragments, color change from tan to more green hue, increase in lithic fragments
-652.5	0	5001.1	ashflow/bedded, litholog
-960.7	0	5309.3	ashflow, tuffaceous sandstone, litholog
-1651.4	-1	6000.0	bottom

USW G-3/GU-3 STRATIGRAPHY

Coordinates: E-558483.1, N-752779.8, dirt pad elevation 4856.50 ft (DOE, 1988s)

Sources: litholog–Scott and Castellanos (1984); geophysics–Nelson *et al.* (1991); core photographs–DOE (1988f)

Elevation (ft)	ID	Depth to top of unit (ft)	Stratigraphic Unit: lithology (methods)
4856.50	1	0.00	Tiva Canyon: welded
4482.79	2	373.71	Tiva Canyon: nonwelded-vitric (litholog, photolog, moderate caliper increase, moderate gravimeter decrease, moderate deep induction resistivity increase, moderate thermal neutron decrease)
4428.66	1	427.84	Topopah Spring: welded (litholog, photolog, moderate caliper decrease, moderate deep induction resistivity increase, moderate thermal neutron increase)
3669.20	1	1187.30	Topopah Spring: vitrophyre (welded) (litholog, photolog, caliper smoothed, moderate gravimeter decrease, moderate deep induction resistivity increase, thermal neutron spike)
3587.61	1	1268.89	Topopah Spring: welded (photolog, litholog, moderate caliper increase, moderate gravimeter decrease, moderate deep induction resistivity decrease, moderate thermal neutron increase)
3562.65	2	1293.85	Topopah Spring: Calico Hills and Prow Pass: nonwelded-vitric (photolog, moderate caliper increase, deep induction resistivity, moderate thermal neutron decrease)
3255.40	1	1601.10	Prow Pass: welded (partially welded to 1755 ft below surface, welded below) (photolog, litholog, moderate caliper decrease, moderate gravimeter increase, moderate deep induction resistivity increase, moderate thermal neutron decrease)
2868.20	2	1988.30	Prow Pass and Bullfrog Member: nonwelded (to partially welded)-vitric (litholog, photolog, moderate caliper increase)
2756.66	1	2099.84	Bullfrog Member: welded (litholog, photolog, moderate caliper decrease, moderate gravimeter increase, moderate deep induction resistivity decrease)
2310.08	2	2546.42	Bullfrog Member: nonwelded-vitric (litholog, photolog, some geophysical logs stop at 2200 ft below surface)
2290.76	1	2565.74	Bullfrog Member: welded (litholog, photolog)
2239.31	2	2617.19	Bullfrog Member and Tram Member: nonwelded (to partially welded)-vitric (litholog, photolog)
1961.87	1	2894.63	Tram Member: welded (litholog, photolog)
1634.23	1	3222.27	Tram Member: vitrophyre (welded) (litholog, photolog)
1628.98	1	3227.52	Tram Member: welded (litholog, photolog)
1011.20	2	3845.30	Tram Member: nonwelded (to partially welded)-zeolitic (litholog, photolog)
979.93	1	3876.57	Tram Member and Lithic Ridge: welded (litholog, photolog)
879.93	2	3976.57	Lithic Ridge: nonwelded-zeolitic (litholog, photolog)
-14.47	2	4870.97	Lithic Ridge: nonwelded-zeolitic (litholog, photolog)
-43.02	1	4899.52	Lithic Ridge: welded (litholog, photolog)
-174.55	-1	5031.05	bottom

USW G-4 STRATIGRAPHY

Coordinates: E-563081.6, N-765807.1, dirt pad elevation 4166.90 ft (DOE, 1988s)

Sources: litholog–Spengler, *et al.* (1984); geophysics–Nelson *et al.* (1991); core photographs–DOE (1988a)

Elevation (ft)	ID	Depth to top of unit (ft)	Stratigraphic Unit: lithology (methods)
4166.90	6	0.00	alluvium (litholog)
4136.90	1	30.00	Tiva Canyon: moderately and densely welded-devitrified (litholog, photolog, high spontaneous potential, low caliper, high borehole compensated density, high gravimeter, low thermal neutron, moderate potassium spectral log increase, moderate thorium spectral log increase)
4048.90	2	118.00	Tiva Canyon and bedded tuff: partially and nonwelded-vitric (litholog, photolog, moderate caliper increase, moderate decrease in spontaneous potential, moderate gravimeter decrease, moderate borehole compensated density decrease, moderate thermal neutron decrease, potassium spectral log spike, thorium spectral log spike)
3998.70	2	168.20	Pah Canyon: nonwelded-vitric (litholog, photolog, moderate caliper increase, moderate increase in spontaneous potential, moderate borehole compensated density decrease, moderate gravimeter decrease, moderate potassium spectral log increase, moderate thorium spectral log decrease)
3978.90	2	188.00	bedded tuff: nonwelded-vitric and vitrophyric (litholog, photolog, high caliper, moderate borehole compensated density decrease, moderate gravimeter decrease, moderate thermal neutron decrease, moderate potassium spectral log decrease, moderate thorium spectral log decrease)
3938.90	2	228.00	Topopah Spring: nonwelded-vitric (litholog, photolog, moderate caliper decrease, moderate decrease in spontaneous potential, moderate gravimeter increase, moderate borehole compensated density increase, moderate thermal neutron increase, moderate potassium spectral log increase, moderate thorium spectral log increase)
3927.90	1	239.00	Topopah Spring: densely welded-vitrophyre (litholog, photolog, moderate borehole compensated density increase, moderate gravimeter increase, moderate thermal neutron decrease, moderate potassium spectral log decrease, moderate thorium spectral log increase)
3924.10	1	242.80	Topopah Spring: densely welded (caprock) - devitrified (litholog, photolog, moderate caliper decrease, moderate decrease in spontaneous potential, moderate borehole compensated density increase, moderate gravimeter increase, moderate thermal neutron increase, moderate potassium spectral log increase, moderate thorium spectral log increase)
3901.40	1	265.50	Topopah Spring: moderately to densely welded-vapor phase crystallization (litholog, photolog, moderate borehole compensated density decrease, moderate gravimeter decrease, moderate thermal neutron decrease, moderate potassium spectral log increase)

USW G-4 STRATIGRAPHY (continued)

Elevation (ft)	ID	Depth to top of unit (ft)	Stratigraphic Unit: lithology (methods)
3889.10	1	277.80	Topopah Spring: moderately to densely welded (caprock) - devitrified (litholog, photolog, moderate caliper decrease, moderate decrease in spontaneous potential, moderate borehole compensated density decrease, moderate gravimeter decrease, moderate thermal neutron decrease, moderate potassium spectral log increase)
3886.90	2	280.00	Topopah Spring: nonwelded to partially welded-vapor phase crystallization (litholog, photolog, moderate caliper decrease, moderate increase in spontaneous potential, moderate borehole compensated density increase, moderate thermal neutron increase, moderate potassium spectral log increase)
3882.40	1	284.50	Topopah Spring: moderately to densely welded-devitrified (litholog, photolog, moderate borehole compensated density decrease, moderate thermal neutron increase, moderate potassium spectral log increase, moderate thorium spectral log increase)
2873.90	1	1293.00	Topopah Spring: moderately to densely welded-argillic and zeolitic (?) (litholog, photolog, moderate caliper decrease, moderate borehole compensated density increase, moderate potassium spectral log decrease)
2850.30	1	1316.60	Topopah Spring: densely welded-vitrophyre (litholog, photolog, moderate caliper increase, moderate borehole compensated density increase, moderate thermal neutron increase, moderate potassium spectral log increase)
2821.50	1	1345.40	Topopah Spring: moderately welded-vitric (litholog, photolog, moderate caliper decrease, moderate borehole compensated density decrease, moderate thermal neutron increase, moderate potassium spectral log increase)
2813.30	2	1353.60	Topopah Spring: partially welded-vitric (litholog, photolog indicate welding to 1362.1 ft, moderate decrease in borehole compensated density, moderate gravimeter decrease, moderate potassium spectral log increase)
2789.10	2	1377.80	Topopah Spring: partially welded-zeolitic and vitric (litholog, photolog, moderate caliper increase, moderate gravimeter decrease, moderate borehole compensated density decrease)
2760.10	2	1406.80	Topopah Spring/bedded tuff: nonwelded-zeolitic (litholog, photolog, moderate gravimeter decrease, moderate borehole compensated density decrease, moderate deep induction resistivity decrease)
2757.50	2	1409.40	Calico Hills: nonwelded-vitric (slightly zeolitic) (litholog, photolog, borehole compensated density, moderate gravimeter decrease, moderate deep induction resistivity increase, moderate potassium spectral log increase, moderate thorium spectral log increase)
2742.40	2	1424.50	Calico Hills: nonwelded-zeolitic (litholog, photolog, moderate caliper decrease, moderate borehole compensated density increase, moderate deep induction resistivity decrease)

USW G-4 STRATIGRAPHY (continued)

Elevation (ft)	ID	Depth to top of unit (ft)	Stratigraphic Unit: lithology (methods)
2405.50	2	1761.40	Prow Pass: nonwelded-zeolitic (litholog, photolog, moderate caliper 1 increase, moderate decrease in spectral gamma total count, moderate borehole compensated density decrease, moderate gravimeter decrease, moderate deep induction resistivity increase, moderate short normal increase, moderate thermal neutron decrease, potassium spectral log spike)
2389.30	2	1777.60	Prow Pass: nonwelded-devitrified (slightly zeolitic and argillic) (litholog, photolog, moderate deep induction resistivity increase, moderate short normal increase, moderate potassium spectral log decrease, moderate thorium spectral log decrease)
2374.50	2	1792.40	Prow Pass: nonwelded-vapor phase crystallization-argillic (litholog, photolog, moderate increase in spectral gamma total count, moderate compensated neutron porosity decrease, moderate gravimeter increase, moderate borehole compensated density decrease, moderate decrease in delta-t and waveform compressional velocity, moderate deep induction resistivity increase, moderate short normal increase, moderate thermal neutron increase, large potassium spectral log increase)
2296.90	2	1870.00	Prow Pass: partially welded [welding] "increases from unit above")-devitrified (litholog indicates partial welding, geophysical log indicates moderate welding by moderate gravimeter increase, moderate borehole compensated density increase)
2212.30	2	1954.60	Prow Pass: nonwelded to partially welded-devitrified and zeolitic (litholog, photolog, caliper spike, spectral gamma total count spike, spontaneous potential spike, moderate borehole compensated density decrease, moderate compensated neutron porosity decrease, moderate deep induction resistivity decrease, moderate short normal decrease, moderate potassium spectral log decrease)
1929.40	2	2237.50	Prow Pass/bedded tuff: nonwelded-zeolitic (litholog, photolog, moderate caliper increase, moderate increase in spectral gamma total count, moderate increase in delta-t and waveform compressional velocity, moderate potassium spectral log increase)
1922.70	2	2244.20	Bullfrog Member: partially welded-devitrified (litholog, photolog, moderate caliper decrease, moderate decrease in spectral gamma total count, moderate borehole compensated density decrease, moderate compensated neutron porosity decrease, moderate decrease in delta-t and waveform compressional velocity, moderate deep induction resistivity increase, moderate short normal increase, moderate thermal neutron increase, moderate potassium spectral log increase)
1796.90	1	2370.00	Bullfrog Member: moderately welded-devitrified (litholog, photolog, slight caliper decrease, moderate borehole compensated density increase, moderate deep induction resistivity decrease, moderate short normal decrease)

USW G-4 STRATIGRAPHY (continued)

Elevation (ft)	ID	Depth to top of unit (ft)	Stratigraphic Unit: lithology (methods)
1769.10	2	2397.80	Bullfrog Member: nonwelded and partially welded-devitrified (litholog, photolog, moderate caliper increase, moderate decrease in spectral gamma total count, moderate borehole compensated density decrease, moderate decrease in delta-t and waveform compressional velocity, moderate potassium spectral log decrease)
1607.90	1	2559.00	Bullfrog Member: moderately to densely welded-devitrified (litholog, photolog indicate moderately to densely welded at 2559 ft -- correlates with geophysical log, moderate caliper decrease, moderate increase in spectral gamma total count, moderate gravimeter increase, moderate borehole compensated density increase, moderate increase in delta-t and waveform compressional velocity, moderate increase in waveform shear velocity, moderate short normal increase, moderate potassium spectral log increase)
1486.60	2	2680.30	Bullfrog Member: partially welded-argillic (litholog, photolog, moderate caliper increase, moderate increase in spectral gamma total count, moderate gravimeter decrease, moderate borehole compensated density decrease, moderate compensated neutron porosity increase, moderate decrease in delta-t and waveform compressional velocity, moderate deep induction resistivity decrease, moderate short normal decrease, moderate thermal neutron decrease, moderate potassium spectral log decrease)
1471.30	2	2695.60	Bullfrog Member: nonwelded and partially welded-zeolitic (litholog, photolog, moderate caliper decrease, moderate increase in spectral gamma total count, moderate borehole compensated density increase, moderate increase in delta-t and waveform compressional velocity, moderate thermal neutron decrease, moderate potassium spectral log decrease)
1433.60	2	2733.30	Bullfrog Member/bedded tuff: nonwelded-argillic and zeolitic (litholog, photolog, moderate increase in spectral gamma total count, moderate gravimeter increase, moderate borehole compensated density increase, moderate increase in waveform shear velocity, moderate deep induction resistivity decrease, moderate short normal decrease, moderate potassium spectral log increase)
1411.30	2	2755.60	Tram Member: nonwelded-devitrified (litholog, photolog, moderate decrease in spectral gamma total count, moderate borehole compensated density decrease, moderate gravimeter decrease, moderate deep induction resistivity increase, moderate short normal increase, moderate thermal neutron decrease, moderate potassium spectral log decrease)
1404.60	2	2762.30	Tram Member: nonwelded-zeolitic (litholog, photolog, moderate caliper 1 increase, moderate decrease in spectral gamma total count, moderate decrease in waveform shear velocity, moderate decrease in delta-t and waveform compressional velocity, moderate thermal neutron decrease, moderate potassium spectral log decrease)
1168.10	1	2998.80	Tram Member: moderately welded-vitrified (litholog, photolog, moderate caliper 1 decrease)
1165.90	-1	3001.00	bottom

USW H-1 STRATIGRAPHY

Coordinates: E-562388.0, N-770254.3, ground elevation 4274.40 ft (DOE, 1988s)

Sources: geophysics–Nelson *et al.* (1991); lithologs–Rush *et al.* (1983), and Spengler *et al.* (1981); core photographs–DOE(1988i & 1989c)

Elevation (ft)	ID	Depth to top of unit (ft)	Stratigraphic Unit: lithology (methods)
4274.40	2	0.00	Tiva Canyon, Yucca Mtn, and Topopah Spring: nonwelded-vitric (litholog, photolog, moderate caliper increase, moderate gravimeter decrease)
3949.40	1	325.00	Topopah Spring: welded (litholog, photolog, moderate caliper decrease, moderate gravimeter increase)
2948.40	1	1326.00	Topopah Spring: vitrophyre (G-1 and H-1 lithologs, photolog, moderate caliper increase, moderate gravimeter increase, epithermal neutron smoothed)
2887.40	1	1387.00	Topopah Spring: welded (G-1 litholog, caliper spike, moderate deep induction resistivity decrease, moderate short normal resistivity decrease, epithermal neutron spike)
2869.40	2	1405.00	Topopah Spring: nonwelded-vitric (G-1 litholog, moderate increase in spectral gamma total count, moderate decrease in deep induction resistivity and short normal resistivity spikes, moderate epithermal neutron spike decrease, moderate increase in proton total magnetic field spike and smoothed)
2816.40	2	1458.00	Topopah Spring: nonwelded-zeolitic (G-1 and H-1 lithologs, moderate gravimeter decrease, moderate decrease in delta-t and waveform compressional velocity, moderate deep induction resistivity decrease, moderate short normal resistivity decrease, moderate epithermal neutron spike decrease)
2784.40	2	1490.00	Calico Hills: nonwelded (?) zeolitic (?) (H-1 litholog, moderate gravimeter decrease, moderate decrease in delta-t and waveform compressional velocity, moderate increase in proton total magnetic field)
2417.35	2	1857.05	Prow Pass: nonwelded (?) zeolitic (?) (H-1 litholog and photolog, moderate caliper increase, moderate gravimeter decrease, moderate borehole compensated density decrease, moderate deep induction resistivity increase, moderate short normal resistivity increase, moderate increase in proton total magnetic field)
2356.40	3	1918.00	Prow Pass: welded (H-1 and G-1 lithologs, photolog, moderate gravimeter increase, moderate borehole compensated density increase, moderate increase in deep induction resistivity spike, moderate increase in short normal and long normal resistivity spikes, potassium spectral log spike)

USW H-1 STRATIGRAPHY (continued)

Elevation (ft)	ID	Depth to top of unit (ft)	Stratigraphic Unit: lithology (methods)
2222.40	2	2052.00	Prow Pass: nonwelded (to partially welded) (H-1 and G-1 lithologs, photolog, moderate gamma ray increase, moderate caliper increase, moderate gravimeter decrease, moderate borehole compensated density decrease, moderate deep induction resistivity decrease, moderate decrease in short normal and long normal resistivity, moderate epithermal neutron decrease, moderate decrease in proton total magnetic field)
2134.40	3	2140.00	Prow Pass: welded (H-1 and G-1 lithologs, photolog, moderate caliper decrease, moderate increase in delta-t and waveform compressional velocity, moderate deep induction resistivity increase, moderate increase in short normal and long normal resistivity, large decrease in radioactive tracer flow log 1)
2006.40	2	2268.00	Prow Pass: nonwelded-zeolitic (G-1 and H-1 lithologs, moderate decrease in delta-t and waveform compressional velocity, moderate decrease in waveform shear velocity, moderate thermal neutron increase, moderate increase in potassium spectral log spike, moderate thorium spectral log increase, large increase in radioactive tracer flow log 1)
1954.73	2	2319.67	Bullfrog Member: nonwelded-zeolitic (litholog, photolog)
1740.40	1	2534.00	Bullfrog Member: welded (G-1 and H-1 lithologs, photolog, moderate caliper decrease, moderate gravimeter increase, moderate borehole compensated density increase, very large decrease in radioactive tracer flow log 1)
1583.98	2	2690.42	Bullfrog Member: nonwelded-zeolitic (litholog, photolog)
1408.40	1	2866.00	Bullfrog Member and Tram Member: welded (to partially welded) (litholog, photolog)
655.46	2	3618.94	Tram Member: nonwelded-zeolitic (litholog, photolog)
-676.63	1	4951.03	older tuffs: welded (litholog, photolog)
-1726.55	-1	6000.95	bottom

USW H-3 STRATIGRAPHY

Coordinates: E-558452.0, N-756542.0, elevation 4866.38 ft (DOE, 1988s)

Sources: litholog–Thordarson *et al.* (1984); geophysical logs–Nelson *et al.* (1991)

Elevation (ft)	ID	Depth to top of unit (ft)	Stratigraphic Unit: lithology (methods)
4866.38	1	0.00	Tiva Canyon: welded, litholog description only
4516.30	2	350.08	Tiva Canyon/Paintbrush Tuff: nonwelded, litholog description, geophysical log change in amplitude of borehole compensated density with less amplitude of waveform, slight increase in resistivity and thermal neutron values
4424.43	1	441.95	Topopah Spring: welded, litholog description, spectral gamma total count decrease at very top of unit, caliper width increase, character of the borehole compensated density waveform and relatively high values, high resistivity values, nature of the thermal neutron waveform
3672.42	1	1193.96	Topopah Spring: vitrophyre, litholog description, extreme increase in resistivity to offscale, marked epithermal neutron decrease
3614.35	2	1252.03	Topopah Spring: vitric, ashflow, nonwelded to moderately welded, litholog description, gradual decrease in both caliper and spectral gamma plots total count, change to smoother and higher values in borehole density waveform, decreasing resistivity
3474.25	2	1392.13	Calico Hills: ashflow, litholog description, gradual decrease in resistivity to bottom of unit, gradual increase in borehole compensated density
3379.43	2	1486.95	Prow Pass: nonwelded, vitric, litholog description, geophysical log, smoothness of caliper and spectral gamma total count, for first 130 ft, square wave nature of borehole compensated density, gradual decrease in resistivity
3162.23	2	1704.15	Prow Pass: nonwelded, zeolitic, litholog description, geophysical log has inflection for borehole compensated density, resistivity, epithermal neutron, potassium spectral log
2966.35	2	1900.3	Bedded/top Bullfrog Member: nonwelded-partially welded, zeolitic, litholog description, increase in spectral gamma total count and caliper, square wave nature of borehole compensated density, marked increase in resistivity, and gradual increase in epithermal neutron and potassium spectral values
2926.32	2	1940.06	Bullfrog Member: ashflow, partially welded, litholog description only
2866.28	1	2000.1	Bullfrog Member: densely welded, devitrified, litholog description, geophysical log, loss of square wave nature of borehole compensated density waveform
2543.10	2	2323.28	Bullfrog Member: ashflow, nonwelded-partially welded, devitrified, litholog description, geophysical log spectral total count and borehole compensated density traces smooth out, increase in resistivity and thermal neutron values

USW H-3 STRATIGRAPHY (continued)

Elevation (ft)	ID	Depth to top of unit (ft)	Stratigraphic Unit: lithology (methods)
2417.11	2	2449.27	Bedded, zeolitic, litholog description, geophysical log, small deflection downward on resistivity and upward on epithermal neutron
2389.22	2	2477.16	Tram Member: ashflow, nonwelded, devitrified, litholog description, geophysical log, bottom of deflections noted at 2417.11 ft
1876.08	2	2990.3	Tram Member: partially-moderately welded, zeolitic, litholog description only
1856.39	1	3009.99	Tram Member: partially-moderately welded, zeolitic, litholog description only
1796.35	1	3070.03	Tram Member: ashflow, moderately welded, devitrified, litholog description; geophysical log, spectral gamma total count decreases, spontaneous potential increases, neutron porosity and borehole compensated density both decrease, as well as velocity, resistivity, thermal neutron and potassium waveforms. Total magnetic field peaks at this depth. Geophysical log, stairstep deflection for spectral gamma total count, all deflections noted at 1796.35 ft, return to relatively smooth trace from deflections
1784.21	1	3082.17	Tram Member: ashflow, moderately welded, zeolitic, litholog description only
1748.12	2	3118.26	Tram Member: partially welded, devitrified, litholog description only
1506.31	2	3360.07	Tram Member: partially welded, zeolitic, litholog description only
866.84	-1	3999.54	bottom

USW H-4 STRATIGRAPHY

Coordinates: E-563911.1, N-761643.6, elevation 4097.64 ft (DOE 1988s)

Sources: litholog–Whitfield *et al.* (1984); geophysics–Nelson *et al.* (1991)

Elevation (ft)	ID	Depth to top of unit (ft)	Stratigraphic Unit: lithology (methods)
4097.64	1	0.0	Land surface, Tiva Canyon welded (litholog)
3923.64	2	174.0	Tiva Canyon and Paintbrush Tuff: nonwelded-vitric (litholog)
3845.64	1	252.0	Topopah Spring: welded (?) (litholog, moderate increase in borehole compensated density, moderate deep induction resistivity increase)
2912.64	1	1185.0	Topopah Spring: welded-vitrophyre (litholog, moderate caliper increase, moderate deep induction resistivity decrease, moderate epithermal neutron decrease, moderate decrease in potassium spectral log, thorium spectral log, and uranium spectral log)
2880.64	2	1217.0	Topopah Spring: nonwelded-vitric (litholog, moderate deep induction resistivity decrease, moderate epithermal neutron decrease)
2785.54	2	1312.1	Calico Hills: nonwelded-zeolitic (litholog, moderate borehole compensated density increase, moderate deep induction resistivity decrease, moderate epithermal neutron decrease)
2457.64	2	1640.0	Prow Pass: partially welded (litholog, moderate borehole compensated density increase, moderate deep induction resistivity increase, epithermal neutron spike)
2441.44	2	1656.2	Prow Pass: nonwelded-zeolitic (litholog, moderate borehole compensated density increase, moderate deep induction resistivity increase, epithermal neutron spike)
2142.54	2	1955.1	Prow Pass: partially welded (litholog, moderate caliper decrease, moderate borehole compensated density increase, moderate long normal and short normal resistivity increase, moderate increase in thorium spectral log and uranium spectral log)
1834.44	2	2263.2	Prow Pass: nonwelded-zeolitic (litholog, moderate increase in long normal and short normal resistivity, moderate potassium spectral log increase, moderate borehole compensated density increase)
1822.64	1	2275.0	Bullfrog Member: welded (litholog, moderate caliper decrease, moderate borehole compensated density increase, moderate increase in short normal and long normal resistivity)
1453.48	2	2644.2	zeolitic
1433.47	1	2664.2	Tram Member: welded
755.61	2	3342.0	zeolitic
278.56	1	3819.0	Lithic Ridge: welded
97.45	-1	4000.2	bottom

USW H-5 STRATIGRAPHY

Coordinates: N-766634.3, E-558908.7, elevation 4850.80 ft (DOE, 1988s)

Sources: litholog–Bentley *et al* (1983); geophysical log–Nelson *et al.* (1991)

Elevation (ft)	ID	Depth to top of unit (ft)	Stratigraphic Unit: lithology (methods)
4850.96	1	0.0	Tiva Canyon: welded, lithologic log, ashflow, densely welded, devitrified; geophysical log, density high, resistivity moderately high, potassium plateau
4441.16	2	409.8	Paintbrush Tuff and top 25 ft Topopah Spring: nonwelded, lithologic log, bedded, ashfall or flow nonwelded, vitric, geophysical log density decreases, resistivity decreases to moderate level, epithermal neutron stabilizes at low value, potassium low, total magnetic field plateau
4283.02	1	567.9	Topopah Spring: welded, lithologic log, ashflow densely welded, devitrified; geophysical log, density very hashy but uniform, epithermal neutron uniform
3268.86	1	1582.1	Topopah Spring: vitrophyre, lithologic log, ashflow densely welded vitrophyre; geophysical log, borehole compensated density changes character, smoother, higher density, resistivity characterization changes - higher value; both resistivity and epithermal neutron show kick to lower values just above welded to vitric interface, could be indication of paleo weathered zone
3196.02	2	1654.9	Bottom 170 ft of Topopah Spring below vitrophyre and Calico Hills: vitric, lithologic log, first 55.45 ft Topopah Spring ashflow tuff, below Calico Hills, ashflow vitric; geophysical log, density log decreases, character change
2970.95	2	1880.0	Calico Hills: zeolitic, lithologic log, ashfall (?) zeolitic; geophysical log, increase in borehole compensated density, decrease in resistivity, total count, spectral gamma decreases
2905.98	2	1945.0	Prow Pass: nonwelded vitric; lithologic log, ashflow; geophysical log, decrease in density and total magnetic field, slight increase in resistivity
2880.07	2	1970.9	Prow Pass: partially welded, devitrified; lithologic log, ashflow, devitrified
2725.85	2	2125.1	Lower Prow Pass: nonwelded, zeolitic; lithologic log, ashflow, zeolitized; geophysical log, spectral gamma total count shows dip, short rise followed by low swing in borehole compensated density
2587.72	1	2263.2	Bullfrog Member: partially to moderately welded, devitrified; lithologic log, ashflow; geophysical log, compensated borehole density signal changes character, loses smoothness, resistivity increases
2137.90	2	2713.1	bedded tuff: lithologic log, reworked; geophysical log only slight indications in resistivity; quick peak then dip
2108.70	1	2742.3	Tram Member: ashflow, moderately welded, devitrified; litholog only
1530.91	2	3320.1	Tram Member: zeolitic; litholog only, partially welded
850.76	-1	4000.2	bottom

USW UZ-1 STRATIGRAPHY

Coordinates: E-560220.8, N-771275.8 (DOE, 1988s), ground elevation 4424.36 ft (Whitfield *et al.*, 1990), casing elevation 4426.20 ft (DOE, 1988s)

Sources: litholog–Whitfield *et al.* (1990); geophysics–Nelson *et al.* (1991)

Elevation (ft)	ID	Depth to top of unit (ft)	Stratigraphic Unit: lithology (methods)
4424.36	6	0.00	alluvium (litholog, low spectral gamma total count, high dielectric, low epithermal neutron)
4384.36	2	40.00	Yucca Mtn: moderately welded-devitrified (litholog, moderate increase in spectral gamma total count, moderate epithermal neutron increase, moderate potassium spectral log increase, moderate thorium spectral log increase)
4356.44	2	67.92	Yucca Mtn and bedded tuff: nonwelded-vitric (litholog, moderate decrease in spectral gamma total count, moderate dielectric resistivity increase, moderate deep induction resistivity decrease, moderate epithermal neutron decrease, moderate potassium spectral log decrease, moderate thorium spectral log decrease)
4319.37	2	104.99	Pah Canyon and bedded tuff: nonwelded-vitric (litholog, moderate caliper decrease, moderate increase in spectral gamma total count, moderate borehole compensated density decrease, moderate deep induction resistivity increase, moderate epithermal neutron decrease, moderate potassium spectral log increase, moderate thorium spectral log decrease)
4169.43	2	254.93	Topopah Spring: nonwelded-vitric (litholog, moderate decrease in spectral gamma total count, moderate caliper decrease, moderate borehole compensated density increase, moderate deep induction resistivity decrease)
4149.41	1	274.95	Topopah Spring: partially to moderately welded-vitric (litholog, moderate caliper decrease, moderate increase in spectral gamma total count, moderate borehole compensated density increase, moderate increase spike in dielectric resistivity, moderate deep induction resistivity increase, large dielectric resistivity increase spike, moderate epithermal neutron increase, moderate potassium spectral log decrease, moderate thorium spectral log increase)
4141.21	1	283.15	Topopah Spring: densely welded-vitrophyre (litholog, moderate caliper decrease, moderate increase in spectral gamma total count, large increase in borehole compensated density, moderate deep induction resistivity increase, large dielectric resistivity decrease, moderate epithermal neutron increase, moderate potassium spectral log increase)
4137.27	1	287.09	Topopah Spring: moderately to densely welded-devitrified (litholog, low caliper, moderate borehole compensated density increase, moderate deep induction resistivity decrease, low dielectric resistivity, moderate epithermal neutron increase, moderate potassium spectral log decrease)
3209.41	1	1214.95	"Samples not available below 1215 ft." (litholog)
3154.36	-1	1270.00	bottom

UE25 UZ-4 STRATIGRAPHY

Coordinates: E-566139.2, N-768715.7, ground elevation 3938.51 ft (Loskot and Hammermeister, 1992)

Source: litholog–Loskot and Hammermeister (1992)

Elevation (ft)	ID	Depth to top of unit (ft)	Stratigraphic Unit: lithology (methods)
3938.51	6	0.00	alluvium (litholog)
3899.50	1	39.01	Tiva Canyon: moderately to densely welded (?) (litholog)
3867.51	2	71.00	Tiva Canyon: partially to nonwelded-argillic (litholog)
3852.81	2	85.70	bedded tuff: nonwelded (?) (litholog)
3832.50	2	106.01	Yucca Mtn: nonwelded-vitric (litholog)
3784.86	2	153.65	bedded tuff: nonwelded-vitric (litholog)
3764.62	2	173.89	Pah Canyon: nonwelded-vitric (litholog)
3643.55	2	294.96	bedded tuff: nonwelded (?) (litholog)
3605.49	1	333.02	Topopah Spring: welded (?) tuff (litholog)
3591.71	1	346.80	Topopah Spring: densely welded-glassy (litholog)
3571.50	-1	367.01	bottom

UE25 UZ-5 STRATIGRAPHY

Coordinates: E-566135.24, N-768590.98, ground elevation 3951.60 ft (Loskot and Hammermeister, 1992)

Source: litholog–Loskot and Hammermeister (1992)

Elevation (ft)	ID	Depth to top of unit (ft)	Stratigraphic Unit: lithology (methods)
3951.60	6	0.00	alluvium-colluvial material (text, p. 2)
3885.59	1	66.01	Tiva Canyon: densely and moderately welded-devitrified (litholog)
3861.60	2	90.00	Tiva Canyon: partially-nonwelded-vitric (litholog)
3833.58	2	118.02	bedded tuff: ash-fall, unconsolidated-vitric (litholog)
3829.58	2	122.02	Yucca Mtn: partially and nonwelded-vitric (litholog)
3785.58	2	166.02	bedded tuff: nonwelded-unconsolidated-vitric (litholog)
3775.61	2	175.99	bedded tuff: nonwelded-poorly consolidated-vitric (litholog)
3761.60	2	190.00	Pah Canyon: partially and nonwelded-vitric and argillic (litholog)
3640.59	2	311.01	bedded tuff: nonwelded, moderately-highly indurated, zeolitic (?), moderately and partly consolidated (litholog)
3618.58	2	333.02	Topopah Spring: nonwelded-zeolitic (?) and argillic (litholog)
3607.59	2	344.01	Topopah Spring: nonwelded-vitric, slightly argillic (litholog)
3597.58	1	354.02	Topopah Spring: densely welded-vitrophyre (litholog)
3593.58	1	358.02	Topopah Spring: densely welded-devitrified (litholog)
3588.59	-1	363.01	bottom

USW UZ-6 STRATIGRAPHY

Coordinates: E-558325.0, N-759731.0, ground elevation 4924.50 ft (DOE, 1988s)

Sources: litholog–Whitfield *et al.* (1993); geophysical–Nelson *et al.* (1991)

Elevation (ft)	ID	Depth to top of unit (ft)	Stratigraphic Unit: lithology (methods)
4924.50	1	0.00	Tiva Canyon: welded-devitrified (H-3 litholog, moderate decrease in spectral gamma total count spike, moderate potassium spectral log increase, moderate thorium spectral log increase, moderate increase in vertical magnetic field)
4543.50	2	381.00	Tiva Canyon, bedded tuff and Topopah Spring-top: nonwelded-vitric (H-3 litholog, erratic caliper, moderate increase in spectral gamma total count, low borehole compensated density)
4470.50	1	454.00	Topopah Spring: welded-devitrified (H-3 litholog, moderate caliper decrease, moderate increase in spectral gamma total count, moderate borehole compensated density increase, slight increase in deep induction resistivity and dielectric resistivity, moderate potassium spectral log increase, epithermal neutron off-line)
3614.50	1	1310.00	Topopah Spring: welded-vitrophyre (H-3 litholog, moderate, smooth caliper decrease, large increase in borehole compensated density, slight decrease in epithermal neutron spike, moderate potassium spectral log decrease, moderate increase in magnetic susceptibility, moderate decrease in vertical magnetic field)
3549.50	1	1375.00	Topopah Spring: welded-vitric (H-3 litholog, moderate caliper decrease, moderate borehole compensated density decrease, moderate decrease in dielectric resistivity, moderate epithermal neutron decrease, moderate potassium spectral log decrease, moderate increase in magnetic susceptibility, moderate decrease in vertical magnetic field)
3090.50	2	1834.00	Prow Pass: nonwelded-zeolitic (erratic caliper, spectral gamma total count spike, moderate borehole compensated density decrease, moderate epithermal neutron increase, moderate potassium spectral log decrease, moderate increase in magnetic susceptibility, vertical magnetic field spike)
3037.50	-1	1887.00	bottom

USW UZ-7 STRATIGRAPHY

Coordinates: E-562911.3, N-760836.1, ground elevation 4169.30 ft (DOE, 1988s)

Source: litholog–Kume and Hammermeister (1990)

Elevation (ft)	ID	Depth to top of unit (ft)	Stratigraphic Unit: lithology (methods)
4169.30	6	0.00	alluvium (litholog)
4147.28	1	22.02	Tiva Canyon: moderately-densely welded-devitrified (litholog)
4079.30	2	90.00	Tiva Canyon: partially welded-nonwelded-vitric (litholog)
4055.29	2	114.01	bedded tuff: nonwelded-vitric (litholog)
4035.89	2	133.41	Pah Canyon: nonwelded-vitric (litholog)
4031.50	2	137.80	bedded tuff: nonwelded-vitric (litholog)
4009.29	2	160.01	Topopah Spring: nonwelded-vitric (litholog)
3997.28	1	172.02	Topopah Spring: welded-vitrophyre (litholog)
3991.80	1	177.50	Topopah Spring: densely-moderately welded-devitrified (litholog)
3962.79	-1	206.51	bottom

UE25 UZ-16 STRATIGRAPHY

Coordinates: E-564857.5, N-760535.0, ground elevation 4000.0 ft (DOE, 1988s)

Source: YM Site Characterization Project (1993)

Elevation (ft)	ID	Depth to top of unit (ft)	Stratigraphic Unit: lithology (methods)
4042.00	6	0.00	alluvium (borehole log)
4002.30	1	39.70	Tiva Canyon: densely welded-devitrified (borehole log)
3901.30	2	140.70	Tiva Canyon-bedded tuff: nonwelded-breccia zone (borehole log)
3897.50	1	144.50	Tiva Canyon: moderately-densely welded-vitric (borehole log)
3893.40	2	148.60	Top of shardy base: nonwelded (?) (borehole log)
3888.40	2	153.60	Tiva Canyon: nonwelded-vitric (borehole log)
3812.70	1	229.30	Topopah Spring: moderately welded-vitrophyre (borehole log)
3810.30	1	231.70	Topopah Spring: moderately welded-vitric (borehole log)
3713.40	1	328.60	Topopah Spring: densely welded-devitrified (borehole log)
2999.00	1	1043.00	ashflow tuff: welded (?)-vitric and zeolitic (borehole log)
2930.80	1	1111.20	Topopah Spring: welded-vitrophyre (borehole log)
2876.40	2	1165.60	bedded tuff: partially welded (?) (borehole log and projected stratigraphy)
2772.00	2	1270.00	Calico Hills: nonwelded (?) (projected stratigraphy)
2457.00	2	1585.00	Prow Pass: partially welded (?) (projected stratigraphy)
2407.00	-1	1686.20	bottom

USW UZN-53 STRATIGRAPHY

Coordinates: E-564236.86, N-760095.86, ground elevation 4055.64 ft (Voss, 1992c)

Source: litholog–Voss (1992c)

Elevation (ft)	ID	Depth to top of unit (ft)	Stratigraphic Unit: lithology (methods)
4055.64	6	0.00	alluvium (assumed)
4053.04	1	2.60	Tiva Canyon: welded-lower lithophysal/hackly (litholog)
4008.14	1	47.50	Tiva Canyon: welded-hackly (litholog)
3975.54	1	80.10	Tiva Canyon: welded-columnar (litholog)
3915.54	2	140.10	Tiva Canyon: nonwelded-columnar (litholog)
3902.84	2	152.80	Paintbrush Tuff: non-mod. welded shardy base (litholog, USW UZN-54 litholog)
3873.64	2	182.00	bedded tuff: nonwelded (litholog)
3834.24	2	221.40	Topopah Spring: nonwelded (litholog)
3825.64	2	230.00	Topopah Spring: moderately welded-caprock (litholog, USW UZN-54 litholog)
3822.24	-1	233.40	bottom

USW UZN-54 STRATIGRAPHY

Coordinates: E-564262.2, N-760272.0, collar elevation: 4045.8 ft

Sources: litholog–Voss (1992a)

Elevation (ft)	ID	Depth to top of unit (ft)	Stratigraphic Unit: lithology (methods)
4045.80	6	0.00	alluvium (litholog)
4026.90	1	18.90	Tiva Canyon: welded-lower lithophysae/hackly (litholog)
3995.80	1	50.00	Tiva Canyon: welded-hackly (litholog)
3978.30	1	67.50	Tiva Canyon: welded-columnar (litholog)
3910.60	1	135.20	Tiva Canyon: mod. welded-columnar (litholog)
3900.40	2	145.40	Paintbrush Tuff: moderately welded-nonwelded-shardy base (litholog)
3865.80	2	180.00	bedded tuff: nonwelded (litholog)
3850.90	2	194.90	Topopah Spring: nonwelded (litholog)
3825.00	2	220.80	Topopah Spring: nonwelded-pumice flow (litholog)
3818.20	1	227.60	Topopah Spring: moderately welded-caprock (litholog)
3813.30	1	232.50	Topopah Spring: densely welded-caprock (litholog)
3801.10	-1	244.70	bottom

USW UZN-55 STRATIGRAPHY

Coordinates: E-564248.3, N-760502.9, collar elevation 4072.4 ft (IGIS, CAVE, 1992)

Source: litholog–Voss (1992a)

Elevation (ft)	ID	Depth to top of unit (ft)	Stratigraphic Unit: lithology (methods)
4072.40	6	0.00	Alluvium (litholog)
4070.10	1	2.30	Tiva: welded-hackly (litholog)
3980.10	1	92.30	Tiva: welded-columnar (litholog)
3927.40	1	145.00	Tiva: moderately welded-columnar (litholog)
3895.00	2	177.40	Paintbrush: moderately welded-shardy base (litholog)
3859.80	2	212.60	Bedded Tuff: nonwelded (litholog)
3849.90	2	222.50	Topopah Sp.: nonwelded (litholog)
3827.40	1	245.00	Topopah Sp.: welded-vitric, caprock (litholog)
3822.40	1	250.00	Topopah Sp.: welded, caprock (litholog)
3817.10	-1	255.30	Bottom

USW WT-2 STRATIGRAPHY

Coordinates: E-561923.6, N-760660.5, casing elevation 4269.70 ft (DOE, 1988s)

General Comment: Due to no lithologic log for USW WT-2, hole was evaluated by using geophysical log for WT-2 and comparing both the geophysical and lithologic logs for USW H-4 and relating the geophysical information between the two holes.

Source: For WT-2, Muller and Kibler (1984); USW H-4, Nelson *et al.* (1991); lithologic log for H-4 from Whitfield *et al.* (1984)

Elevation (ft)	ID	Depth to top of unit (ft)	Stratigraphic Unit: lithology (methods)
4270.0	1	0.0	Tiva Canyon: welded, geophysical log, caliper, density high, seismic velocity, 2-3K m/s
4070.0	2	200.0	Paintbrush Tuff: nonwelded, geophysical log, caliper increased diameter, dielectric constant low, resistivity low, gamma ray low, epithermal neutron low, density low.
4002.0	2	268.0	Topopah Spring: nonwelded, vitric, as above, similar nonwelded sequence
3990.0	1	280.0	Topopah Spring: densely-moderately welded, devitrified, geophysical log, resistivity moderately high, character of density trace; very variable and spiky
3080.0	1	1190.0	Topopah Spring: vitrophyre, geophysical log, caliper - hole becomes larger in diameter, contrary to expected trend, but is similar to H-4; resistivity increases, epithermal neutron increases
3042.0	2	1228.0	Topopah Spring: partially welded-nonwelded, vitric, geophysical log, general decrease in density and epithermal neutron
2968.0	2	1302.0	Calico Hills: nonwelded-partially welded, devitrified and zeolitized, geophysical log, resistivity decreases, dielectric constant increases, epithermal neutron decreases, density decreases
2675.0	2	1595.0	Prow Pass: nonwelded, zeolitized and devitrified, geophysical log, high resistivity first 100 ft sequence, resistivity decreases on down
2210.0	-1	2060.0	bottom

Appendix II

Representative Cross-Sections from the Three-Dimensional Geostatistical Model

This page left intentionally blank.

Northing 769520

Northing 765520

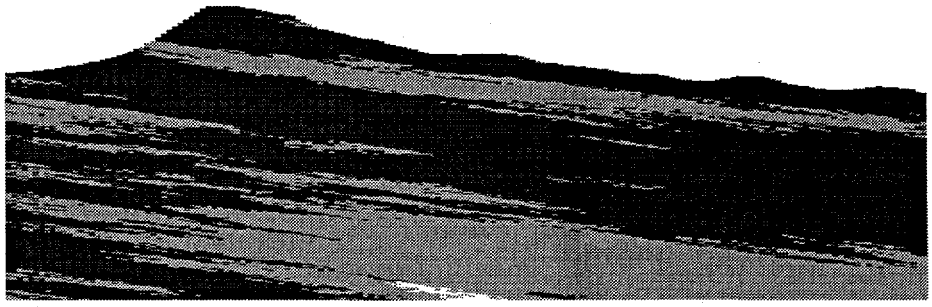

Northing 761620

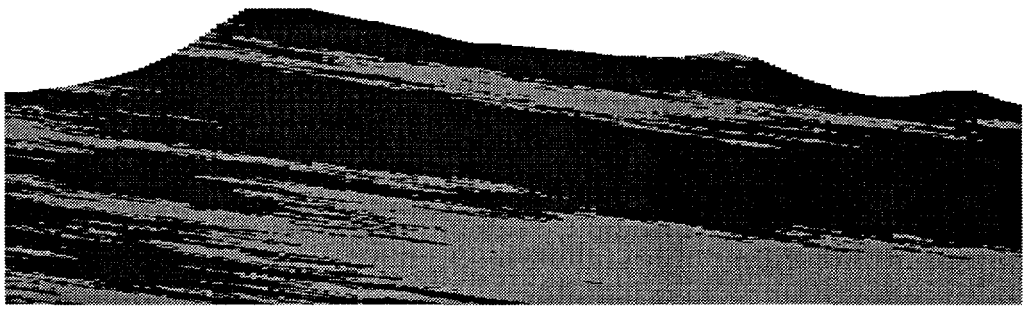

Northing 757620

Welded
Nonwelded
Prow Pass Welded

Northing 769520

Northing 765520

Northing 761620

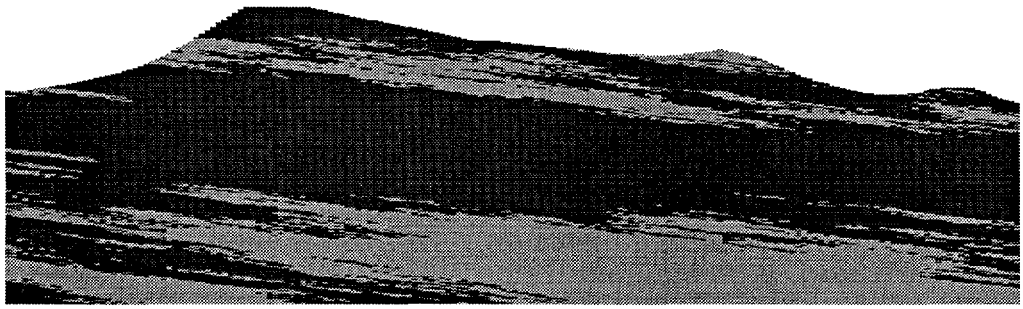

Northing 757620

Welded
Nonwelded
Prow Pass Welded

Northing 769520

Northing 765520

Northing 761620

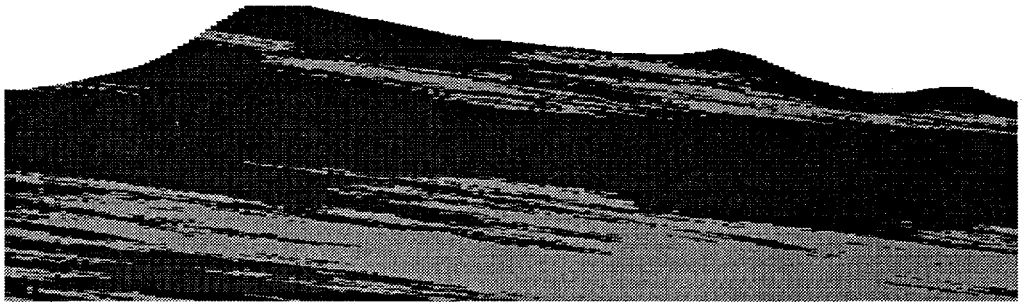

Northing 757620

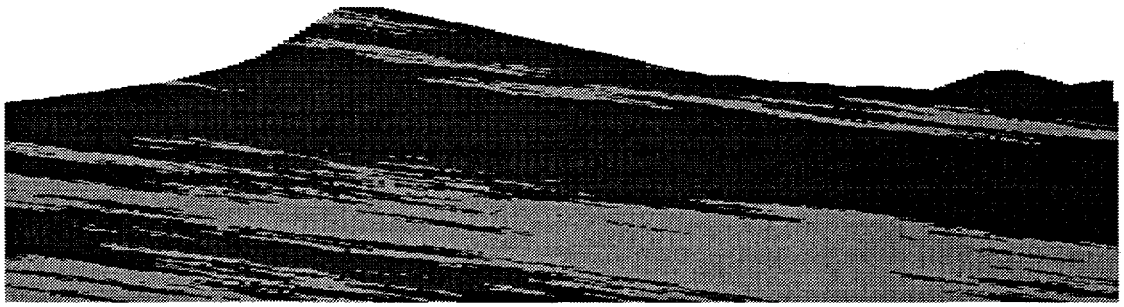

Welded
Nonwelded
Prow Pass Welded

Northing 769520

Northing 765520

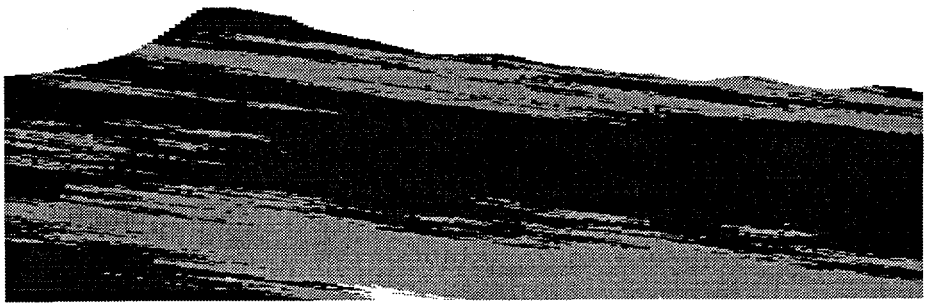

Northing 761620

Northing 757620

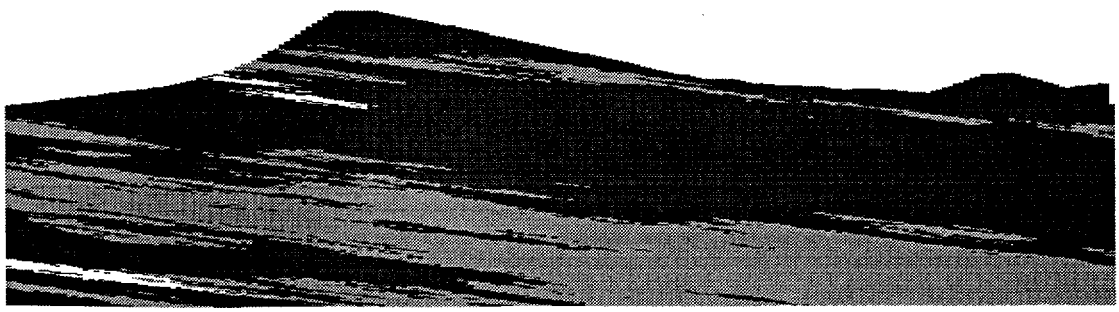

Welded
Nonwelded
Prow Pass Welded

Northing 769520

Northing 765520

Northing 761620

Northing 757620

Welded
Nonwelded
Prow Pass Welded

Northing 769520

Northing 765520

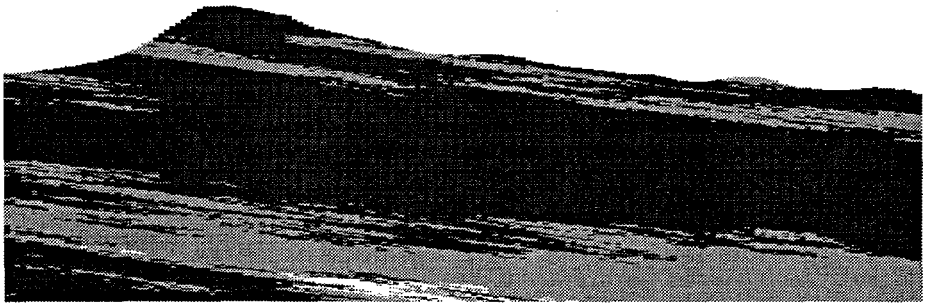

Northing 761620

Northing 757620

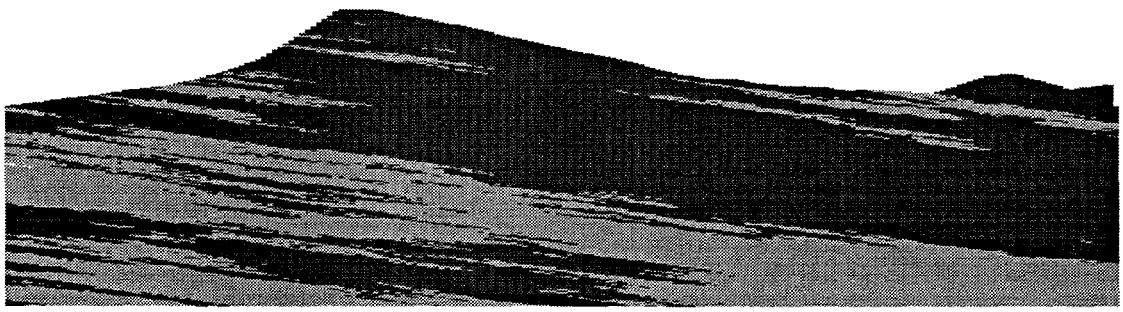

Welded
Nonwelded
Prow Pass Welded

Northing 769520

Northing 765520

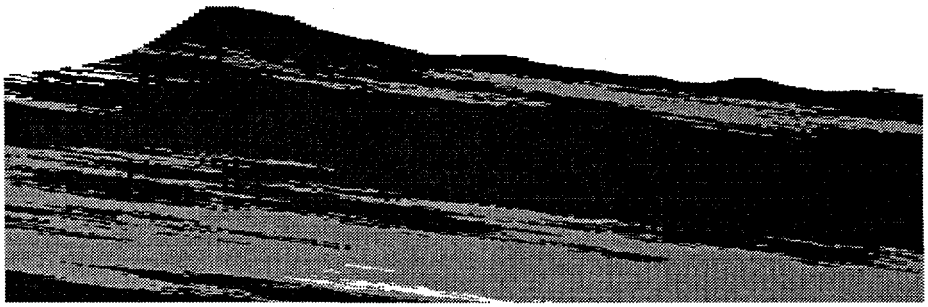

Northing 761620

Northing 757620

Welded
Nonwelded
Prow Pass Welded

Northing 769520

Northing 765520

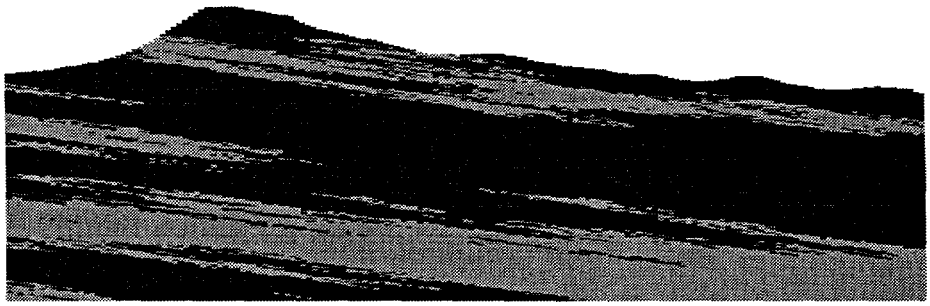

Northing 761620

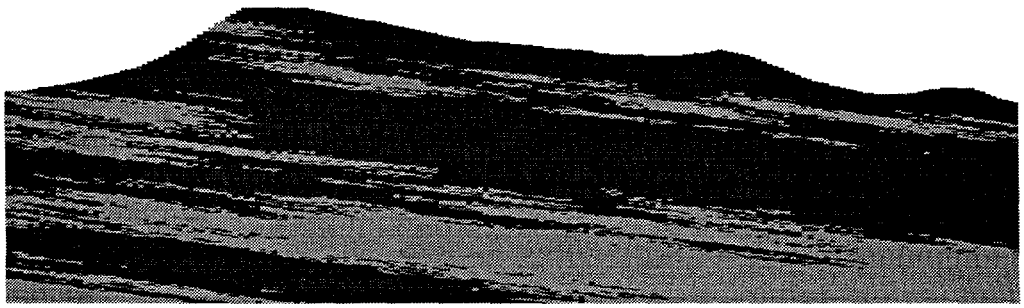

Northing 757620

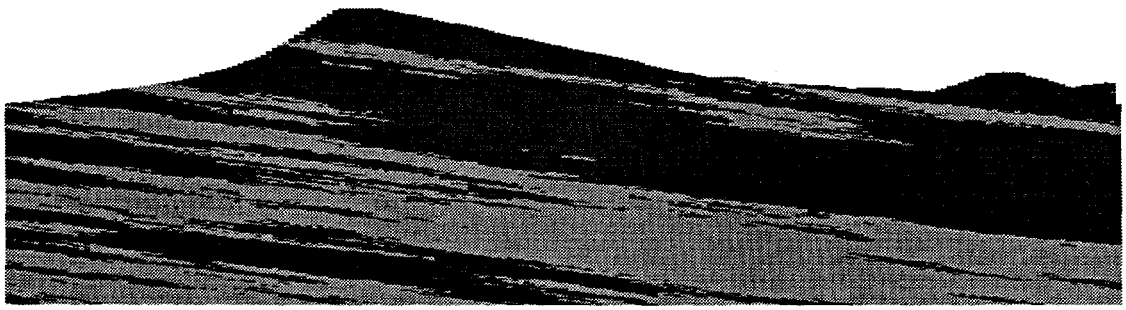

Welded
Nonwelded
Prow Pass Welded

Northing 769520

Northing 765520

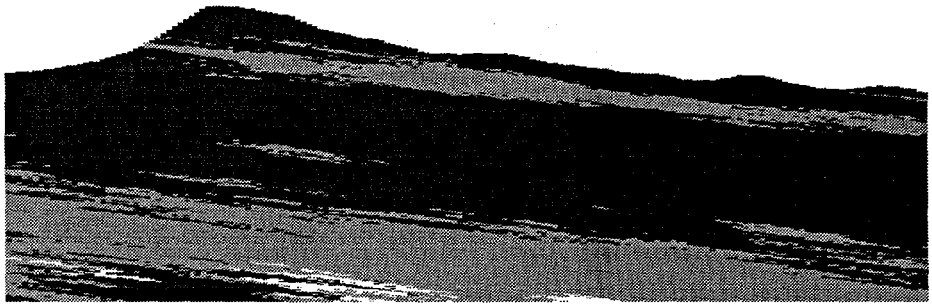

Northing 761620

Northing 757620

Welded
Nonwelded
Prow Pass Welded

Northing 769520

Northing 765520

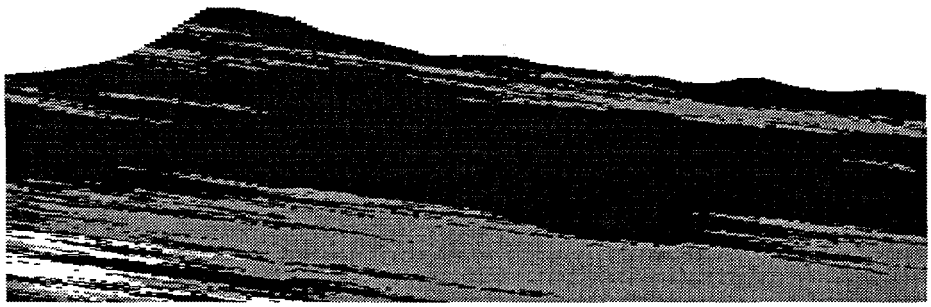

Northing 761620

Northing 757620

Welded
Nonwelded
Prow Pass Welded

Appendix III

Property-Value Histograms with Parameter PDFs

This page left intentionally blank.

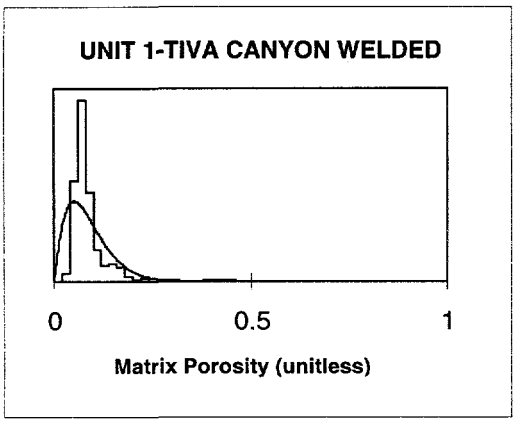
UNIT 1-TIVA CANYON WELDED
0
0.5
1
Matrix Porosity (unitless)

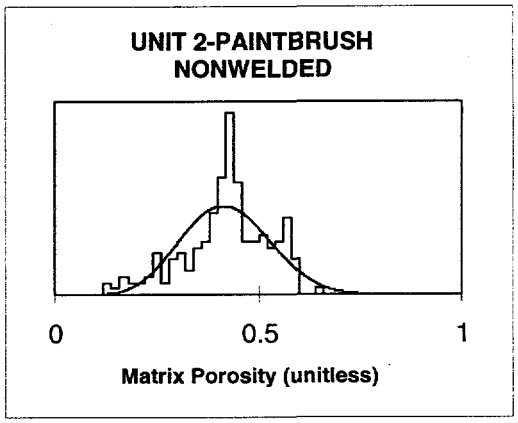
UNIT 2-PAINTBRUSH NONWELDED
0
0.5
1
Matrix Porosity (unitless)

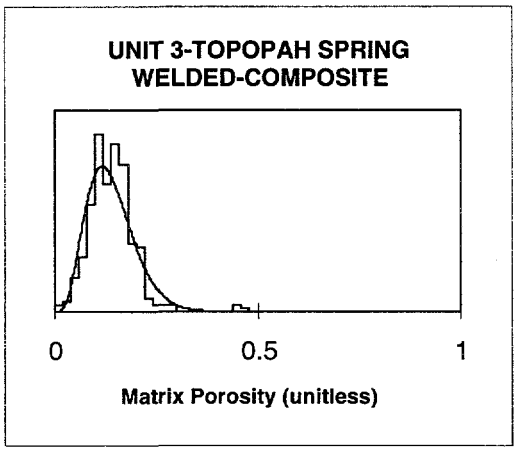
UNIT 3-TOPOPAH SPRING WELDED-COMPOSITE
0
0.5
1
Matrix Porosity (unitless)

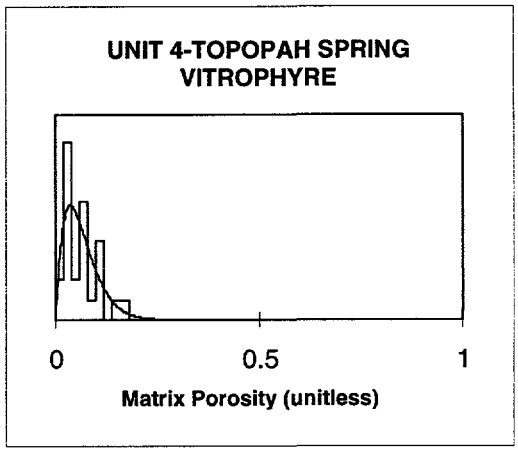
UNIT 4-TOPOPAH SPRING VITROPHYRE
0
0.5
1
Matrix Porosity (unitless)

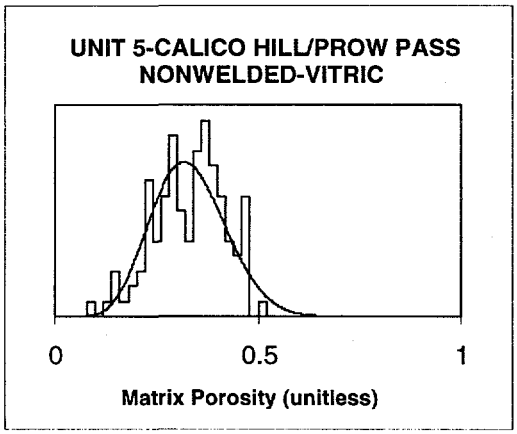
UNIT 5-CALICO HILL/PROW PASS NONWELDED-VITRIC
0
0.5
1
Matrix Porosity (unitless)

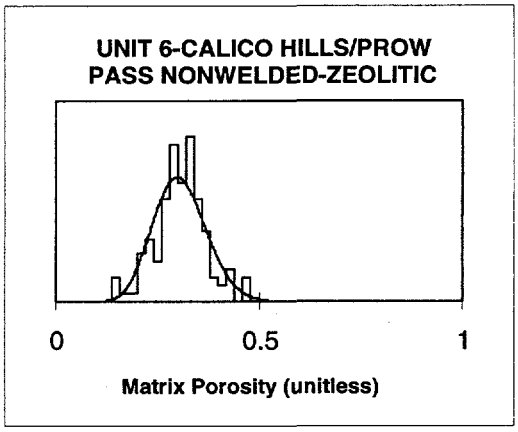
UNIT 6-CALICO HILLS/PROW PASS NONWELDED-ZEOLITIC
0
0.5
1
Matrix Porosity (unitless)

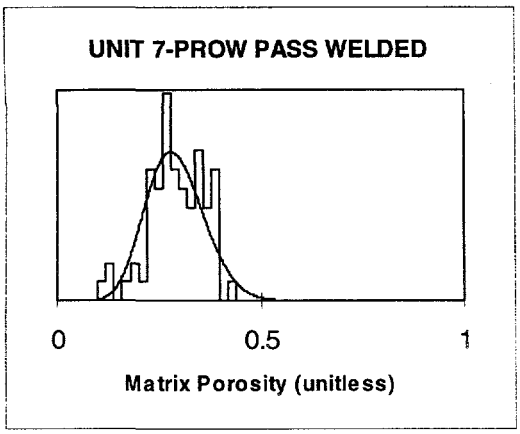
UNIT 7-PROW PASS WELDED
0
0.5
1
Matrix Porosity (unitless)

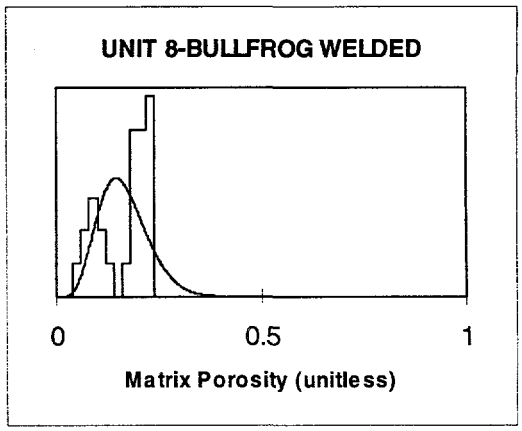
UNIT 8-BULLFROG WELDED
0
0.5
1
Matrix Porosity (unitless)

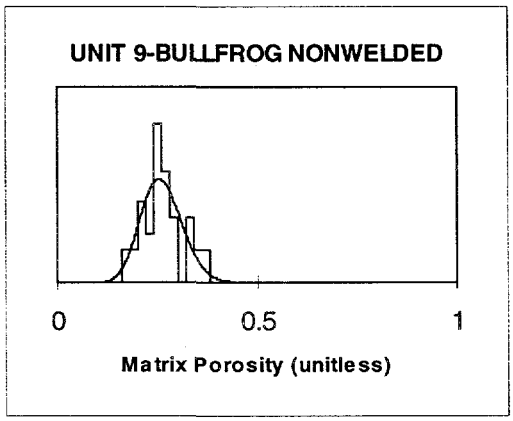
UNIT 9-BULLFROG NONWELDED
0
0.5
1
Matrix Porosity (unitless)

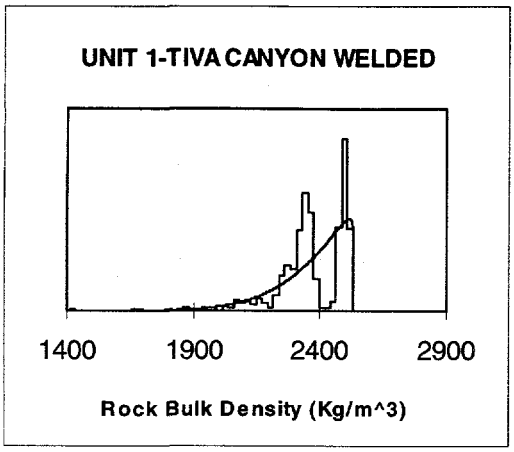
UNIT 1-TIVA CANYON WELDED
1400
1900
2400
2900
Rock Bulk Density (Kg/m^3)

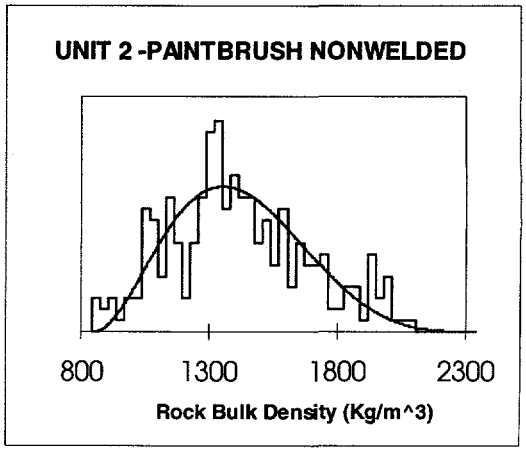
UNIT 2 -PAINTBRUSH NONWELDED
800
1300
1800
2300
Rock Bulk Density (Kg/m^3)

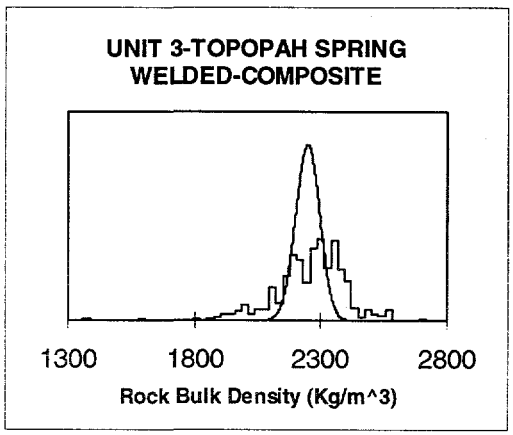
UNIT 3-TOPOPAH SPRING
WELDED-COMPOSITE
1300
1800
2300
2800
Rock Bulk Density (Kg/m^3)

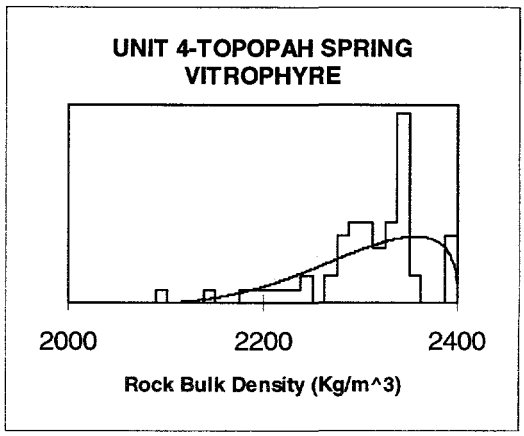
UNIT 4-TOPOPAH SPRING
VITROPHYRE
2000
2200
2400
Rock Bulk Density (Kg/m^3)

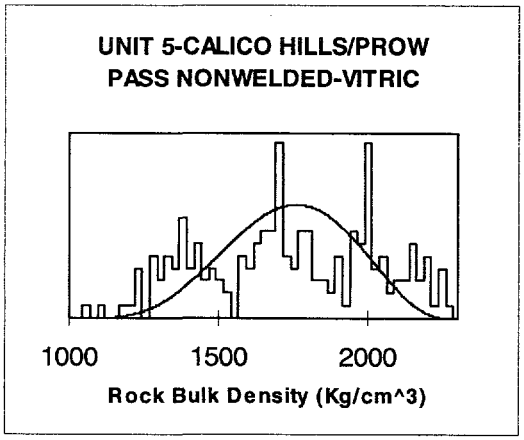
UNIT 5-CALICO HILLS/PROW
PASS NONWELDED-VITRIC
1000
1500
2000
Rock Bulk Density (Kg/cm^3)

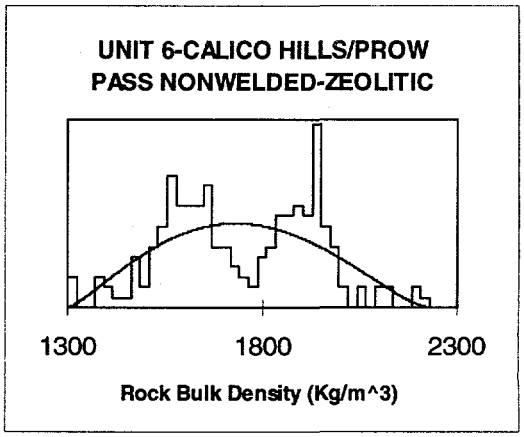
UNIT 6-CALICO HILLS/PROW
PASS NONWELDED-ZEOLITIC
1300
1800
2300
Rock Bulk Density (Kg/m^3)

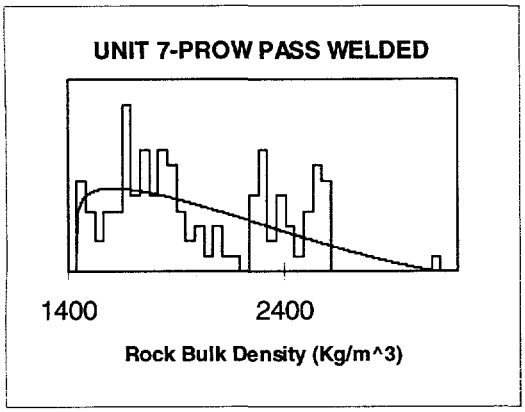
UNIT 7-PROW PASS WELDED
1400
2400
Rock Bulk Density (Kg/m^3)

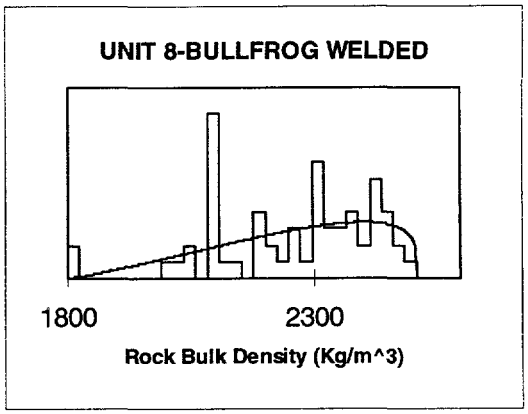
UNIT 8-BULLFROG WELDED
1800
2300
Rock Bulk Density (Kg/m^3)

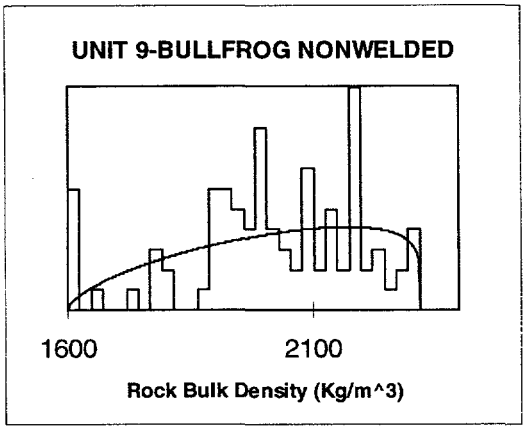
UNIT 9-BULLFROG NONWELDED
1600
2100
Rock Bulk Density (Kg/m^3)

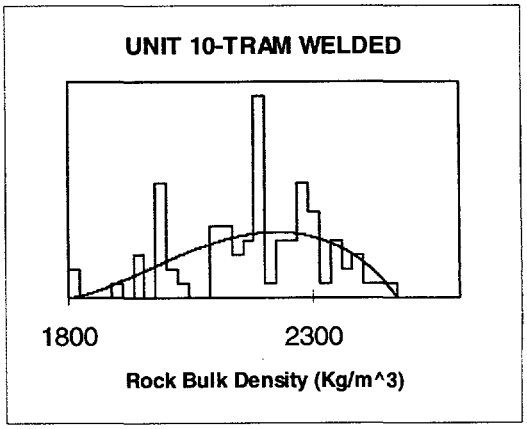
UNIT 10-TRAM WELDED
1800
2300
Rock Bulk Density (Kg/m^3)

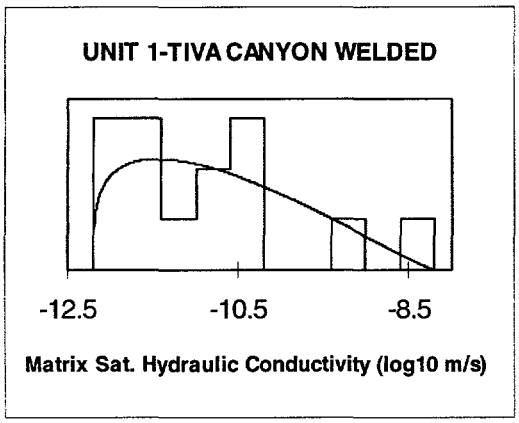
UNIT 1-TIVA CANYON WELDED
-12.5
-10.5
-8.5
Matrix Sat. Hydraulic Conductivity (log10 m/s)

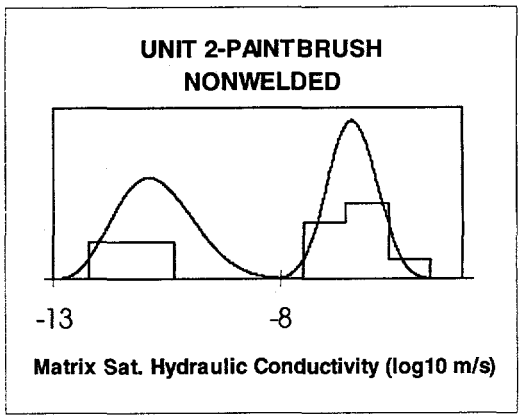
UNIT 2-PAINTBRUSH NONWELDED
-13
-8
Matrix Sat. Hydraulic Conductivity (log10 m/s)

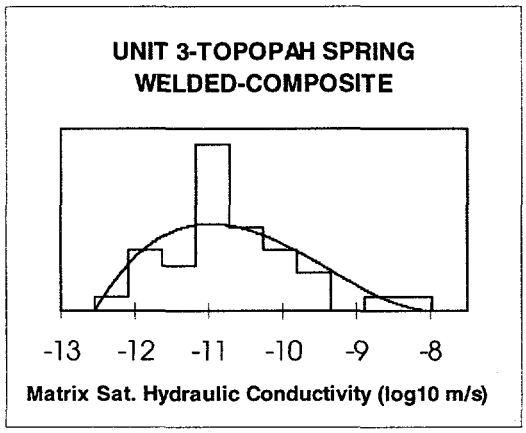
UNIT 3-TOPOPAH SPRING WELDED-COMPOSITE
-13
-12
-11
-10
-9
-8
Matrix Sat. Hydraulic Conductivity (log10 m/s)

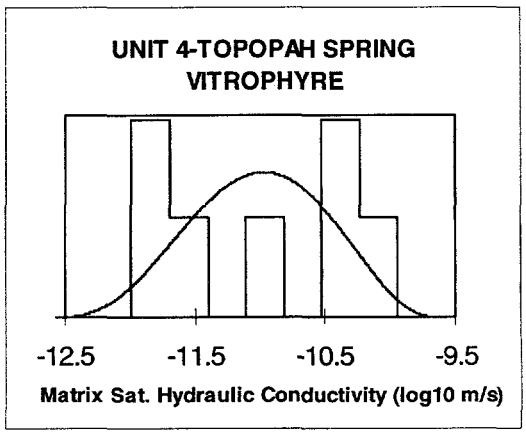
UNIT 4-TOPOPAH SPRING VITROPHYRE
-12.5
-11.5
-10.5
-9.5
Matrix Sat. Hydraulic Conductivity (log10 m/s)

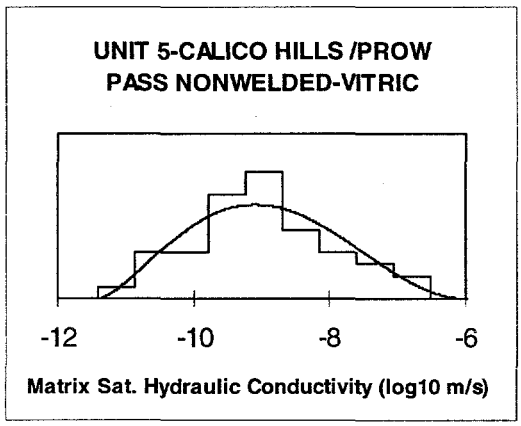
UNIT 5-CALICO HILLS /PROW PASS NONWELDED-VITRIC
-12
-10
-8
-6
Matrix Sat. Hydraulic Conductivity (log10 m/s)

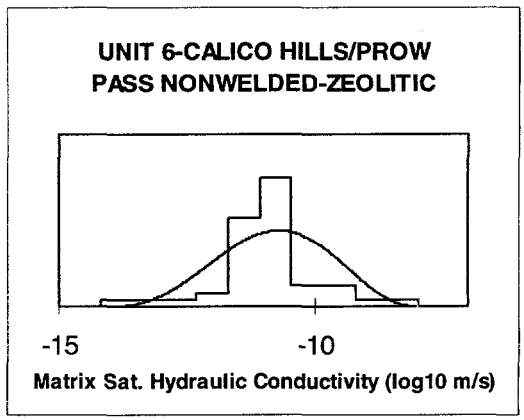
UNIT 6-CALICO HILLS/PROW PASS NONWELDED-ZEOLITIC
-15
-10
Matrix Sat. Hydraulic Conductivity (log10 m/s)

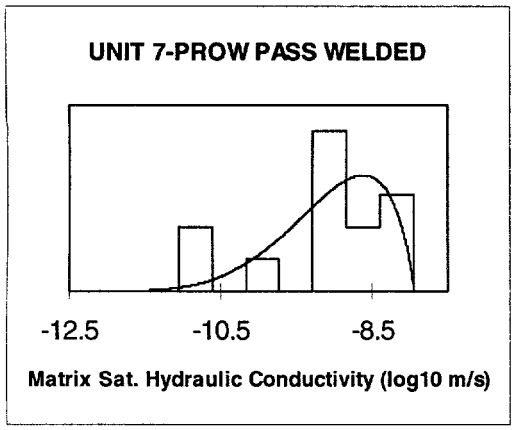
UNIT 7-PROW PASS WELDED
-12.5
-10.5
-8.5
Matrix Sat. Hydraulic Conductivity (log10 m/s)

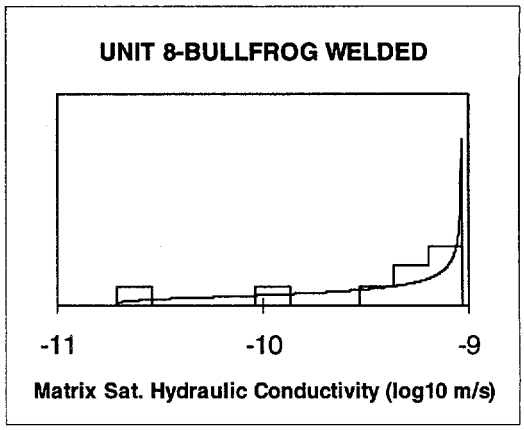
UNIT 8-BULLFROG WELDED
-11
-10
-9
Matrix Sat. Hydraulic Conductivity (log10 m/s)

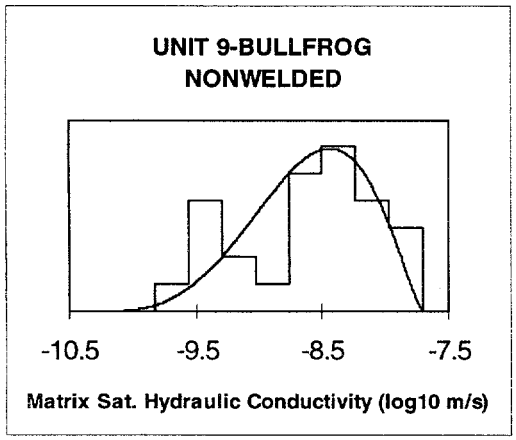
UNIT 9-BULLFROG
NONWELDED
-10.5
-9.5
-8.5
-7.5
Matrix Sat. Hydraulic Conductivity (log10 m/s)

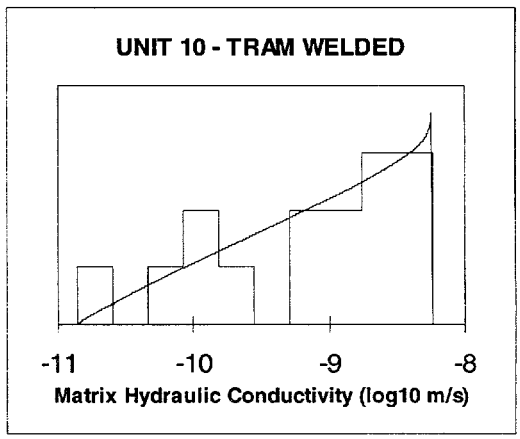
UNIT 10 - TRAM WELDED
-11
-10
-9
-8
Matrix Hydraulic Conductivity (log10 m/s)

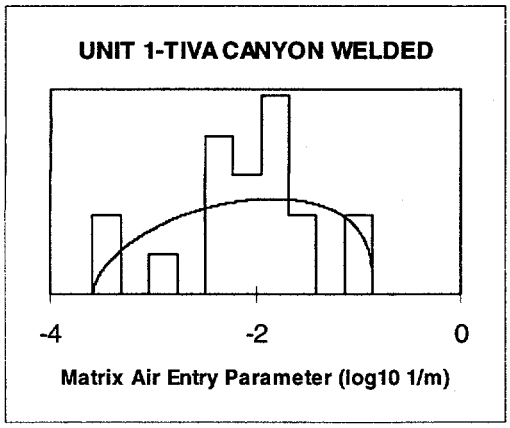
UNIT 1-TIVA CANYON WELDED
-4
-2
0
Matrix Air Entry Parameter (log10 1/m)

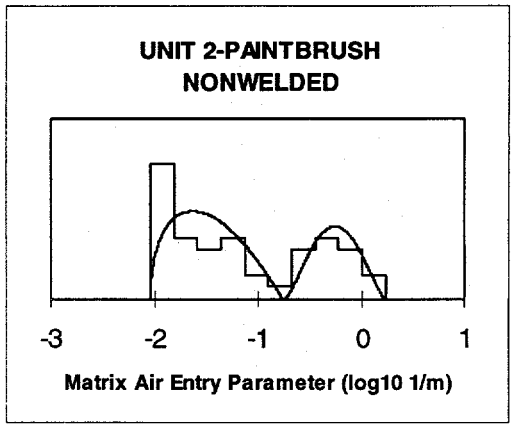
UNIT 2-PAINTBRUSH NONWELDED
-3
-2
-1
0
1
Matrix Air Entry Parameter (log10 1/m)

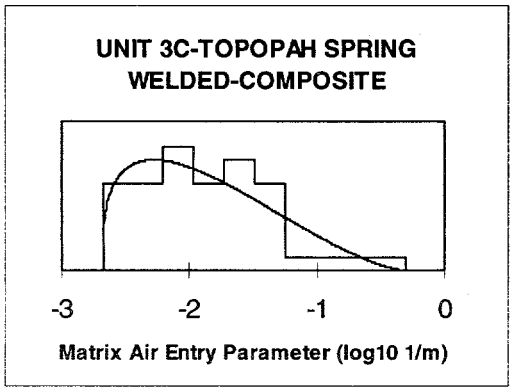
UNIT 3C-TOPOPAH SPRING WELDED-COMPOSITE
-3
-2
-1
0
Matrix Air Entry Parameter (log10 1/m)

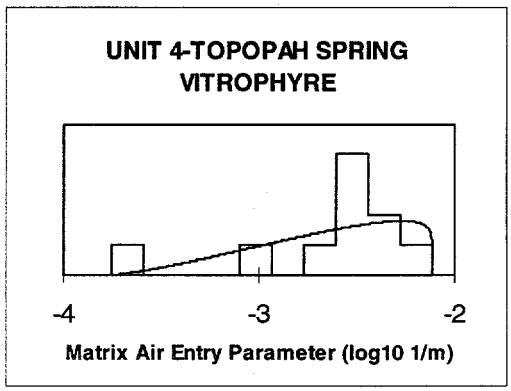
UNIT 4-TOPOPAH SPRING VITROPHYRE
-4
-3
-2
Matrix Air Entry Parameter (log10 1/m)

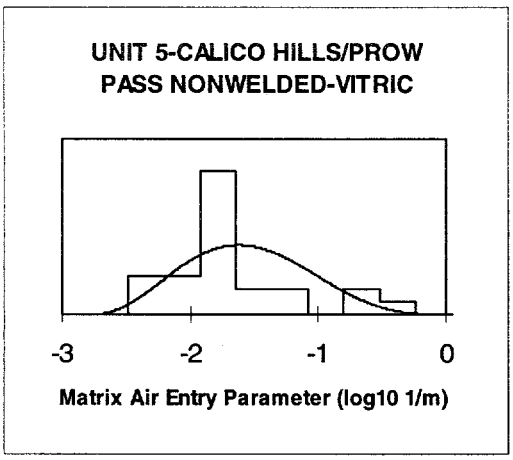
UNIT 5-CALICO HILLS/PROW PASS NONWELDED-VITRIC
-3
-2
-1
0
Matrix Air Entry Parameter (log10 1/m)

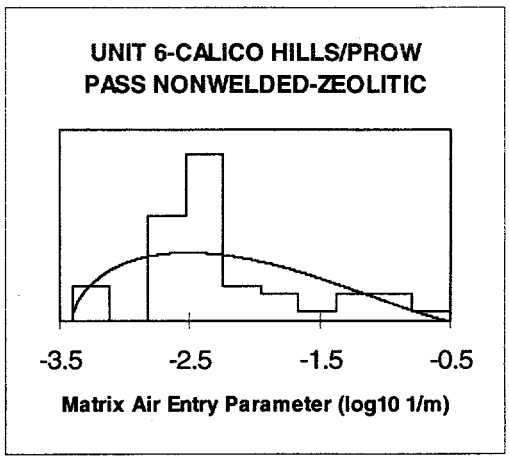
UNIT 6-CALICO HILLS/PROW PASS NONWELDED-ZEOLITIC
-3.5
-2.5
-1.5
-0.5
Matrix Air Entry Parameter (log10 1/m)

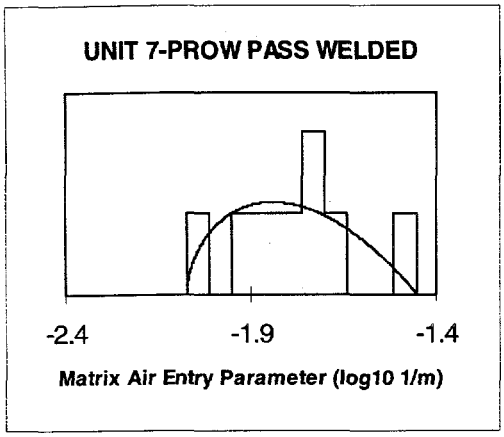
UNIT 7-PROW PASS WELDED
-2.4
-1.9
-1.4
Matrix Air Entry Parameter (log10 1/m)

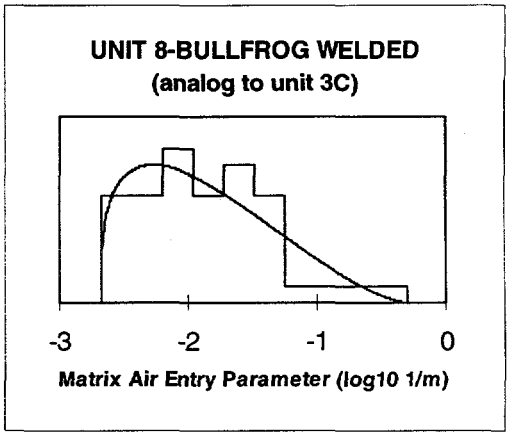
UNIT 8-BULLFROG WELDED
(analog to unit 3C)
-3
-2
-1
0
Matrix Air Entry Parameter (log10 1/m)

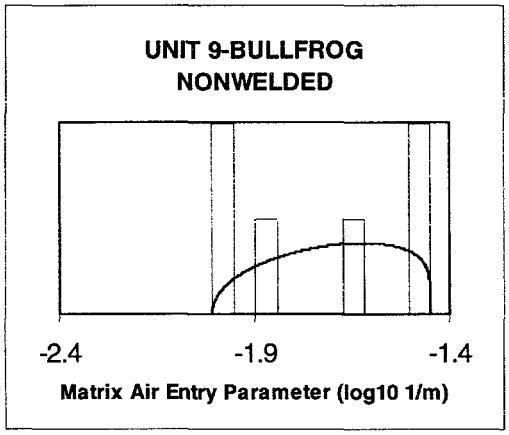
UNIT 9-BULLFROG
NONWELDED
-2.4
-1.9
-1.4
Matrix Air Entry Parameter (log10 1/m)

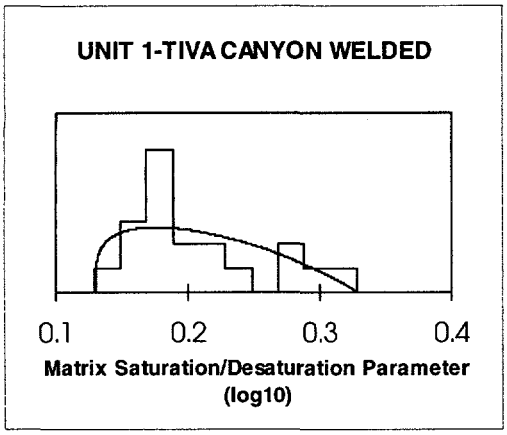
UNIT 1-TIVA CANYON WELDED
0.1
0.2
0.3
0.4
Matrix Saturation/Desaturation Parameter
(log10)

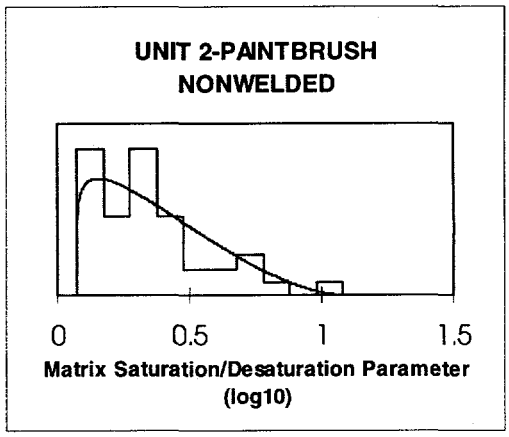
UNIT 2-PAINTBRUSH
NONWELDED
0
0.5
1
1.5
Matrix Saturation/Desaturation Parameter
(log10)

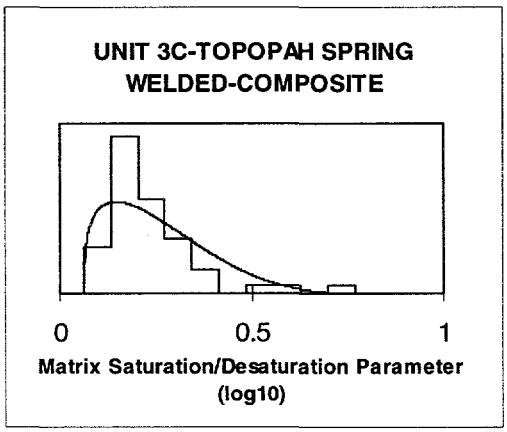
UNIT 3C-TOPOPAH SPRING
WELDED-COMPOSITE
0
0.5
1
Matrix Saturation/Desaturation Parameter
(log10)

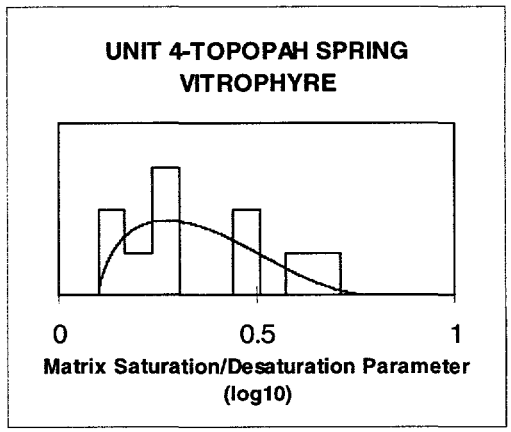
UNIT 4-TOPOPAH SPRING
VITROPHYRE
0
0.5
1
Matrix Saturation/Desaturation Parameter
(log10)

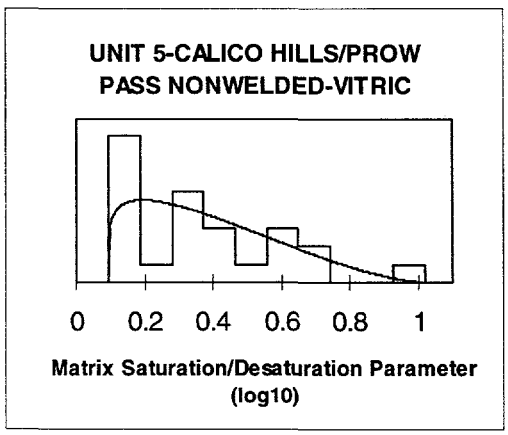
UNIT 5-CALICO HILLS/PROW
PASS NONWELDED-VITRIC
0
0.2
0.4
0.6
0.8
1
Matrix Saturation/Desaturation Parameter
(log10)

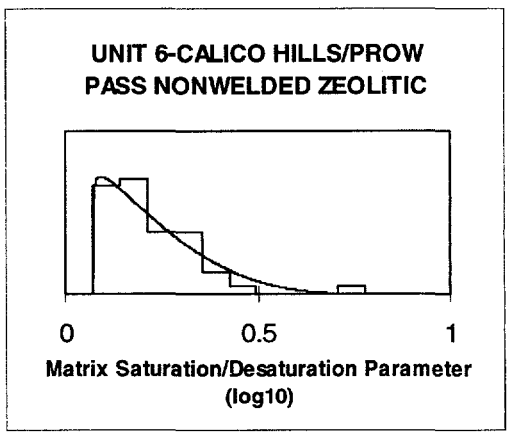
UNIT 6-CALICO HILLS/PROW
PASS NONWELDED ZEOLITIC
0
0.5
1
Matrix Saturation/Desaturation Parameter
(log10)

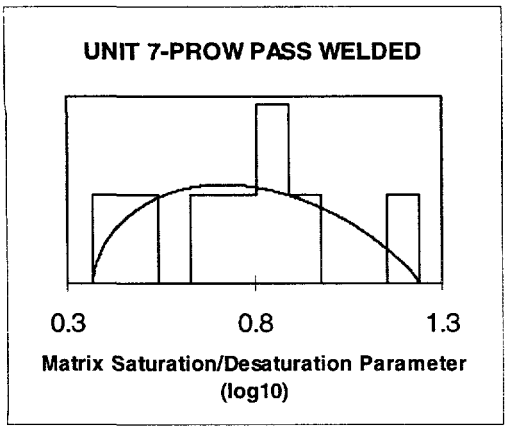
UNIT 7-PROW PASS WELDED
0.3
0.8
1.3
Matrix Saturation/Desaturation Parameter
(log10)

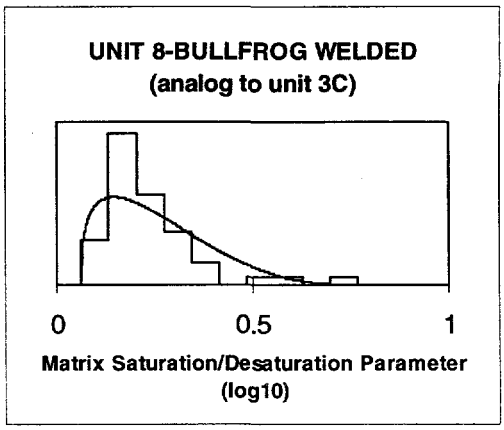
UNIT 8-BULLFROG WELDED
(analog to unit 3C)
0
0.5
1
Matrix Saturation/Desaturation Parameter
(log10)

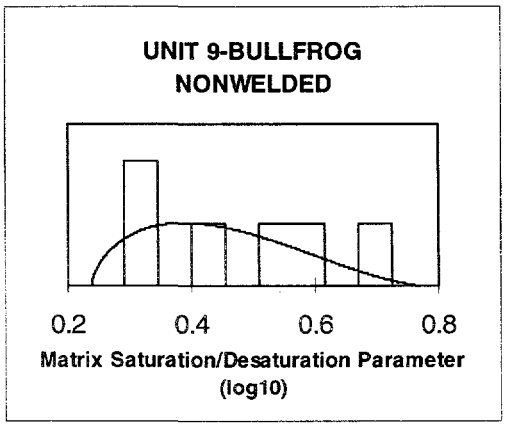
UNIT 9-BULLFROG
NONWELDED
0.2
0.4
0.6
0.8
Matrix Saturation/Desaturation Parameter
(log10)

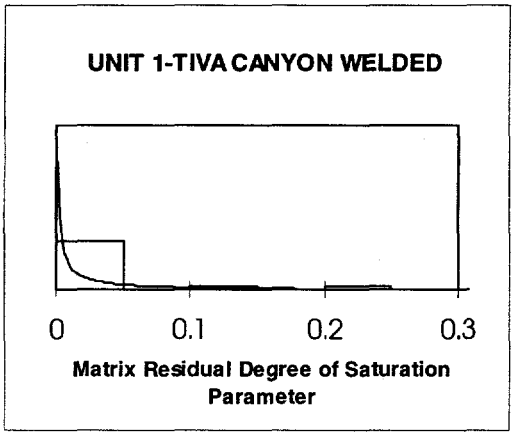
UNIT 1-TIVA CANYON WELDED
0
0.1
0.2
0.3
Matrix Residual Degree of Saturation Parameter

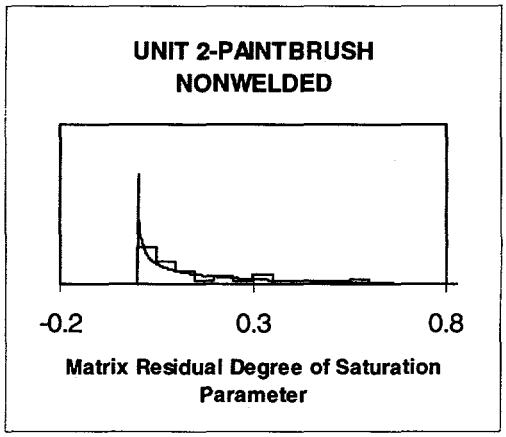
UNIT 2-PAINTBRUSH NONWELDED
-0.2
0.3
0.8
Matrix Residual Degree of Saturation Parameter

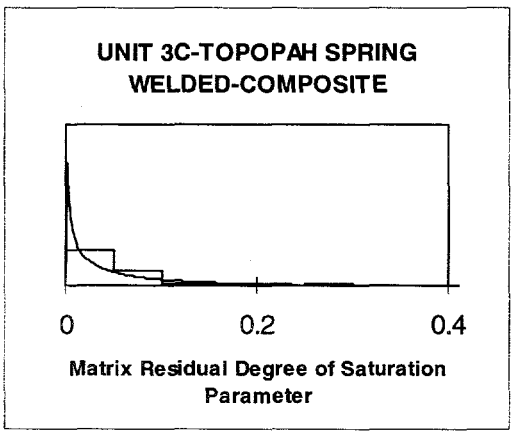
UNIT 3C-TOPOPAH SPRING WELDED-COMPOSITE
0
0.2
0.4
Matrix Residual Degree of Saturation Parameter

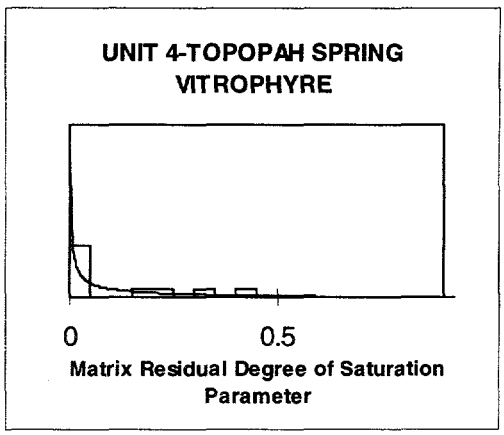
UNIT 4-TOPOPAH SPRING VITROPHYRE
0
0.5
Matrix Residual Degree of Saturation Parameter

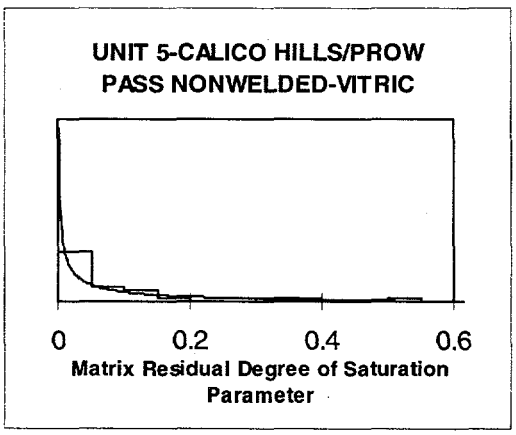
UNIT 5-CALICO HILLS/PROW PASS NONWELDED-VITRIC
0
0.2
0.4
0.6
Matrix Residual Degree of Saturation Parameter

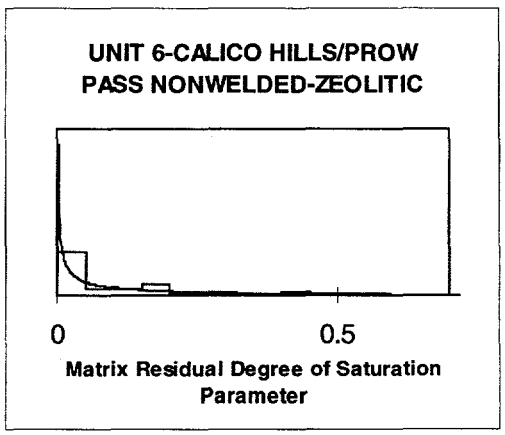
UNIT 6-CALICO HILLS/PROW PASS NONWELDED-ZEOLITIC
0
0.5
Matrix Residual Degree of Saturation Parameter

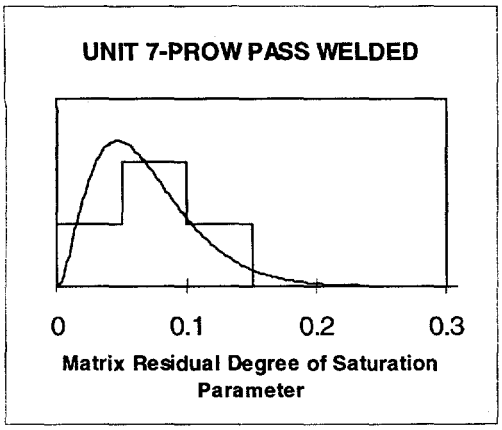
UNIT 7-PROW PASS WELDED
0
0.1
0.2
0.3
Matrix Residual Degree of Saturation Parameter

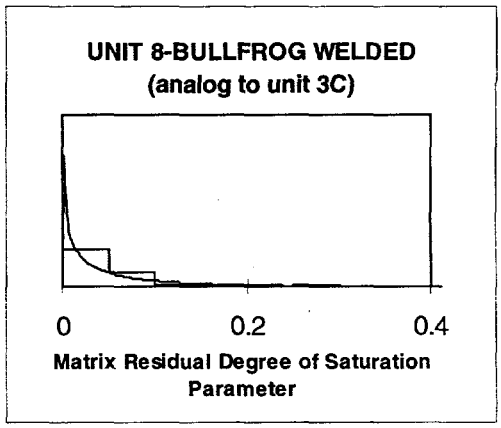
UNIT 8-BULLFROG WELDED
(analog to unit 3C)
0
0.2
0.4
Matrix Residual Degree of Saturation Parameter

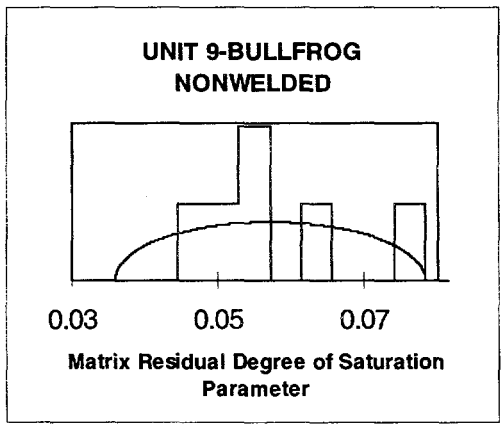
UNIT 9-BULLFROG
NONWELDED
0.03
0.05
0.07
Matrix Residual Degree of Saturation Parameter

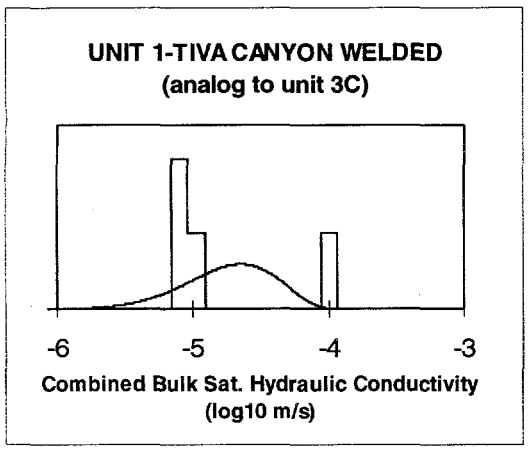
UNIT 1-TIVA CANYON WELDED
(analog to unit 3C)
-6
-5
-4
-3
Combined Bulk Sat. Hydraulic Conductivity
(log10 m/s)

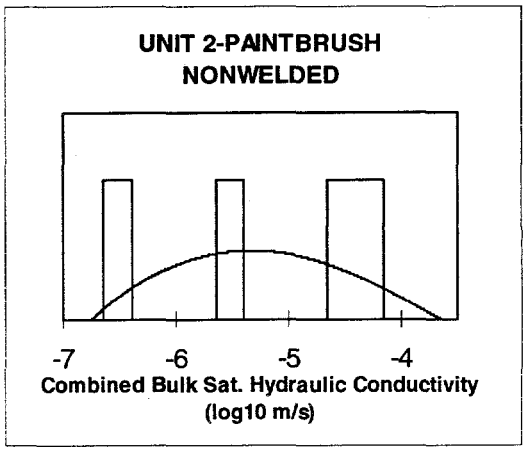
UNIT 2-PAINTBRUSH
NONWELDED
-7
-6
-5
-4
Combined Bulk Sat. Hydraulic Conductivity
(log10 m/s)

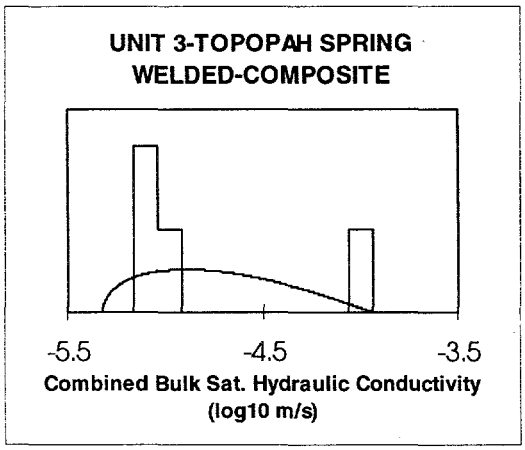
UNIT 3-TOPOPAH SPRING
WELDED-COMPOSITE
-5.5
-4.5
-3.5
Combined Bulk Sat. Hydraulic Conductivity
(log10 m/s)

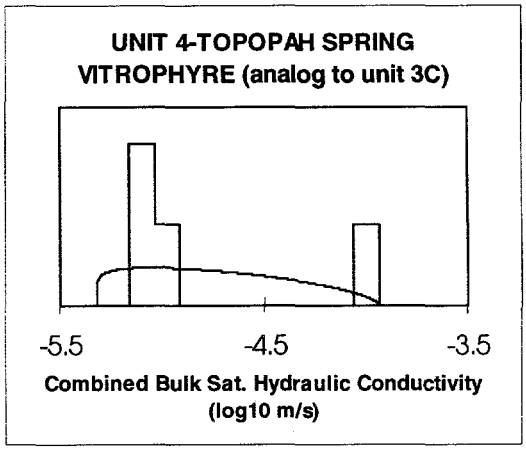
UNIT 4-TOPOPAH SPRING
VITROPHYRE (analog to unit 3C)
-5.5
-4.5
-3.5
Combined Bulk Sat. Hydraulic Conductivity
(log10 m/s)

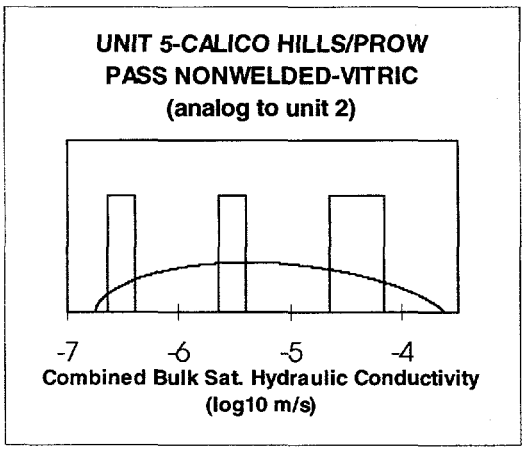
UNIT 5-CALICO HILLS/PROW
PASS NONWELDED-VITRIC
(analog to unit 2)
-7
-6
-5
-4
Combined Bulk Sat. Hydraulic Conductivity
(log10 m/s)

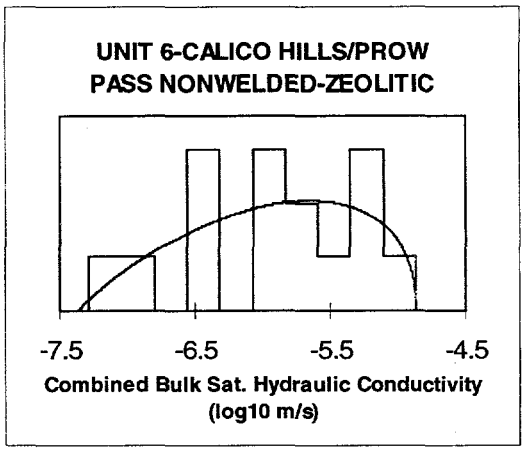
UNIT 6-CALICO HILLS/PROW
PASS NONWELDED-ZEOLITIC
-7.5
-6.5
-5.5
-4.5
Combined Bulk Sat. Hydraulic Conductivity
(log10 m/s)

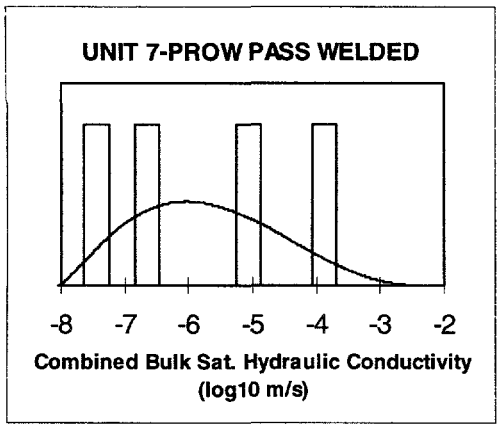
UNIT 7-PROW PASS WELDED
-8 -7 -6 -5 -4 -3 -2
Combined Bulk Sat. Hydraulic Conductivity
(log10 m/s)

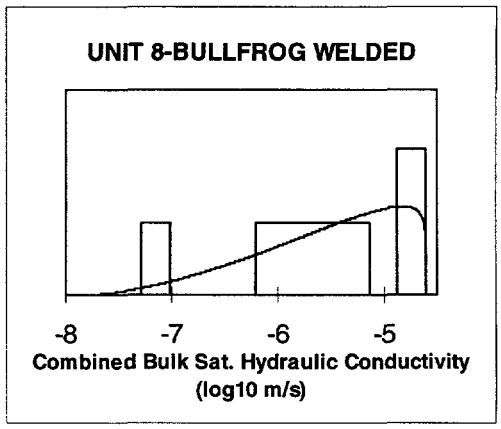
UNIT 8-BULLFROG WELDED
-8 -7 -6 -5
Combined Bulk Sat. Hydraulic Conductivity
(log10 m/s)

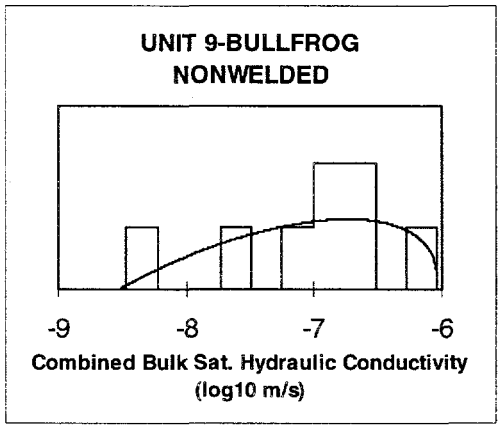
UNIT 9-BULLFROG
NONWELDED
-9 -8 -7 -6
Combined Bulk Sat. Hydraulic Conductivity
(log10 m/s)

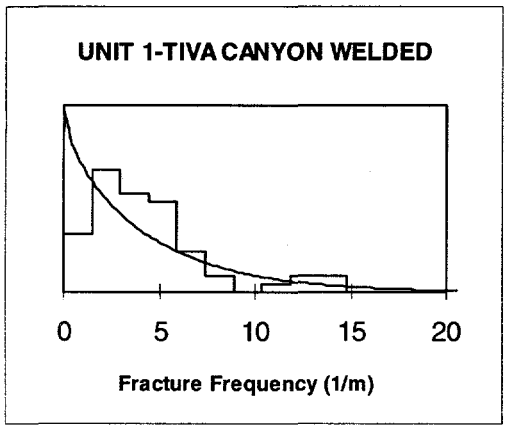
UNIT 1-TIVA CANYON WELDED
0
5
10
15
20
Fracture Frequency (1/m)

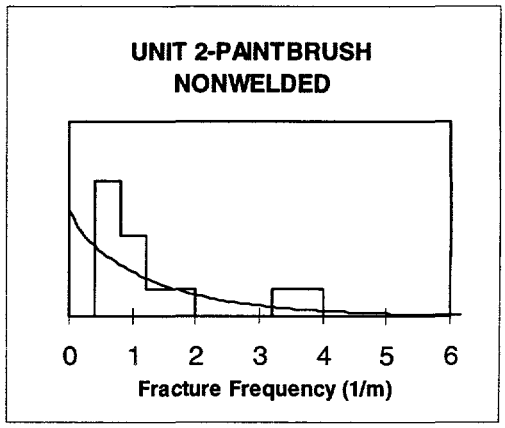
UNIT 2-PAINTBRUSH NONWELDED
0
1
2
3
4
5
6
Fracture Frequency (1/m)

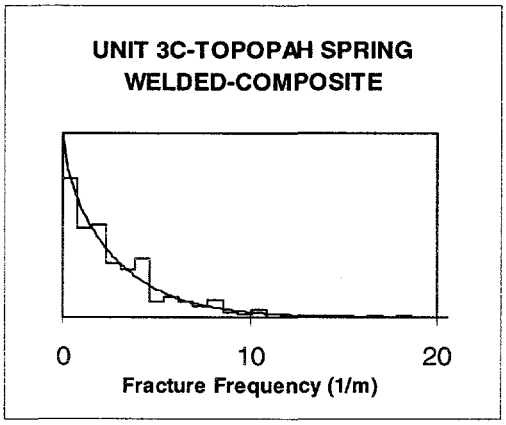
UNIT 3C-TOPOPAH SPRING WELDED-COMPOSITE
0
10
20
Fracture Frequency (1/m)

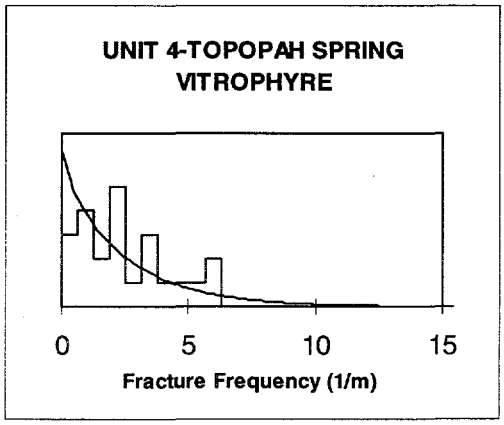
UNIT 4-TOPOPAH SPRING VITROPHYRE
0
5
10
15
Fracture Frequency (1/m)

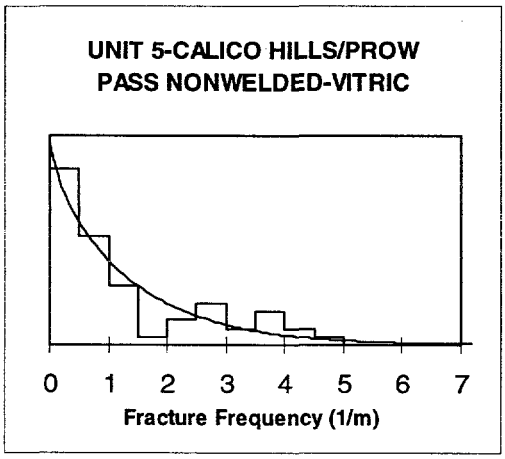
UNIT 5-CALICO HILLS/PROW PASS NONWELDED-VITRIC
0
1
2
3
4
5
6
7
Fracture Frequency (1/m)

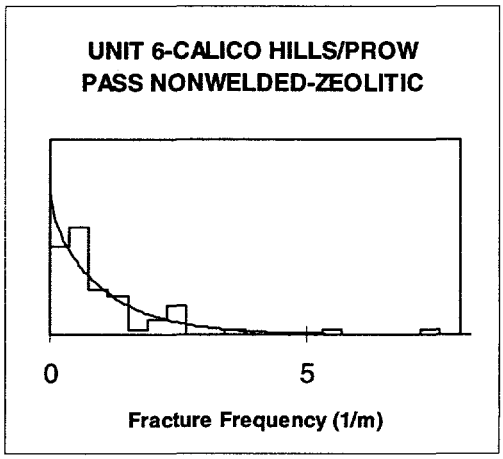
UNIT 6-CALICO HILLS/PROW PASS NONWELDED-ZEOLITIC
0
5
Fracture Frequency (1/m)

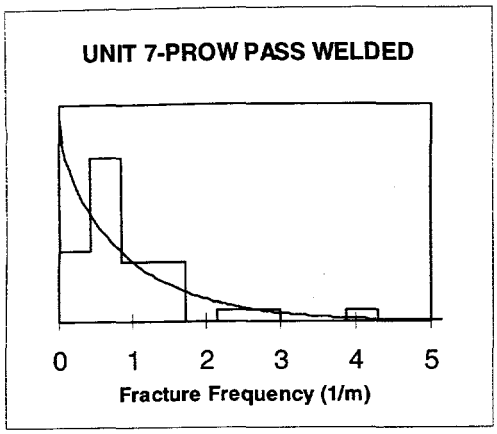
UNIT 7-PROW PASS WELDED
0 1 2 3 4 5
Fracture Frequency (1/m)

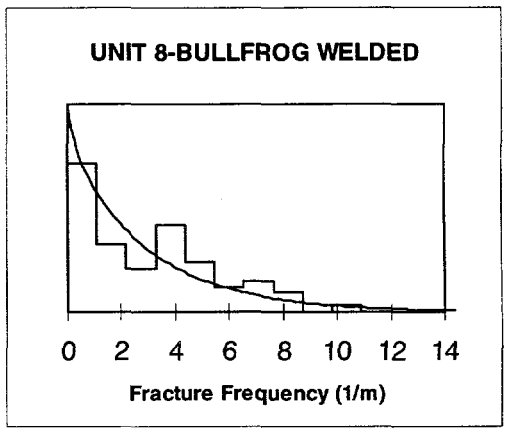
UNIT 8-BULLFROG WELDED
0 2 4 6 8 10 12 14
Fracture Frequency (1/m)

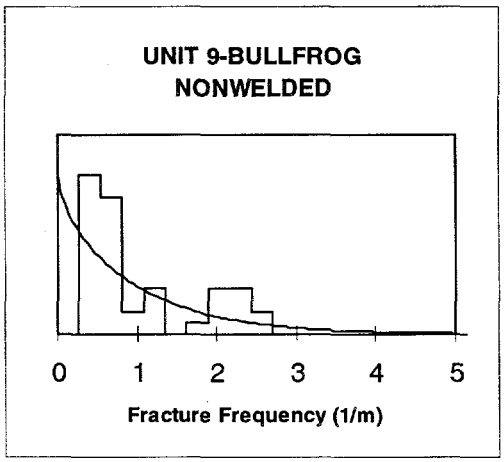
UNIT 9-BULLFROG
NONWELDED
0 1 2 3 4 5
Fracture Frequency (1/m)

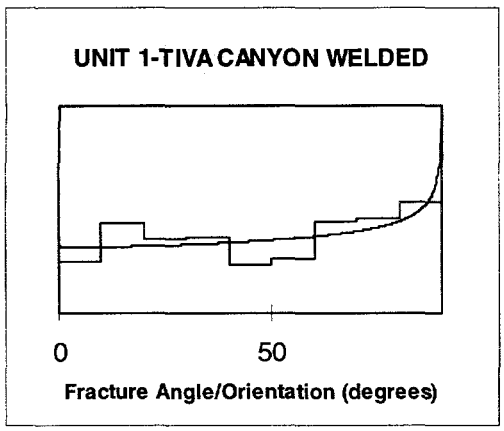
UNIT 1-TIVA CANYON WELDED
0
50
Fracture Angle/Orientation (degrees)

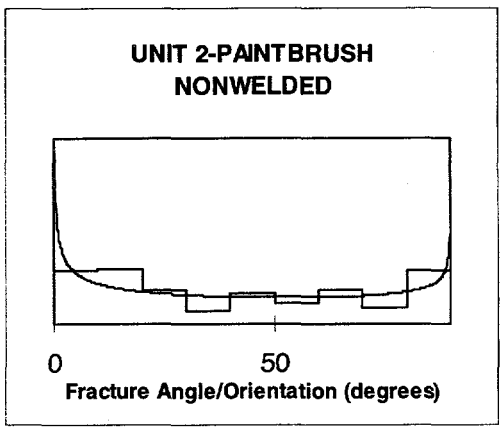
UNIT 2-PAINTBRUSH NONWELDED
0
50
Fracture Angle/Orientation (degrees)

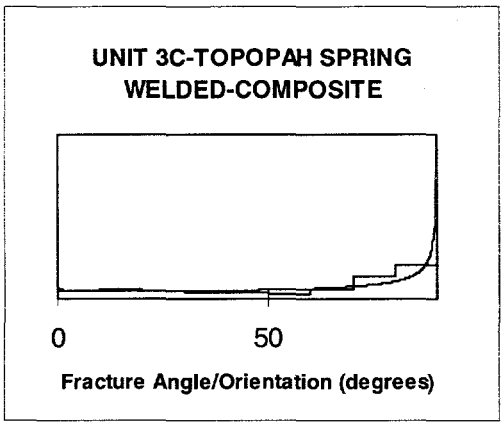
UNIT 3C-TOPOPAH SPRING WELDED-COMPOSITE
0
50
Fracture Angle/Orientation (degrees)

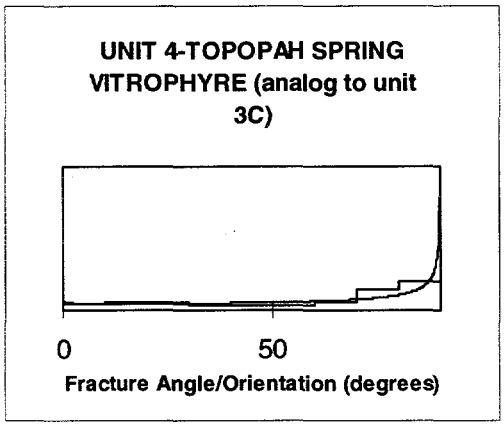
UNIT 4-TOPOPAH SPRING VITROPHYRE (analog to unit 3C)
0
50
Fracture Angle/Orientation (degrees)

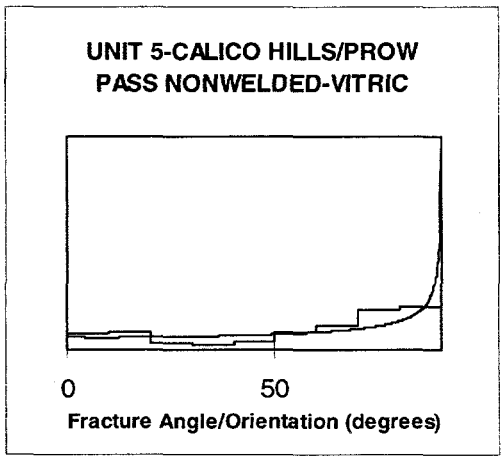
UNIT 5-CALICO HILLS/PROW PASS NONWELDED-VITRIC
0
50
Fracture Angle/Orientation (degrees)

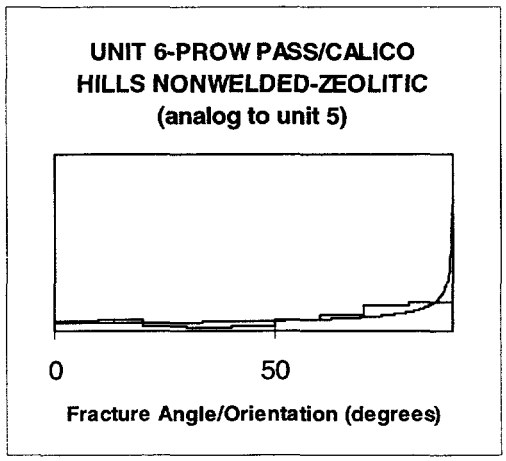
UNIT 6-PROW PASS/CALICO HILLS NONWELDED-ZEOLITIC (analog to unit 5)
0
50
Fracture Angle/Orientation (degrees)

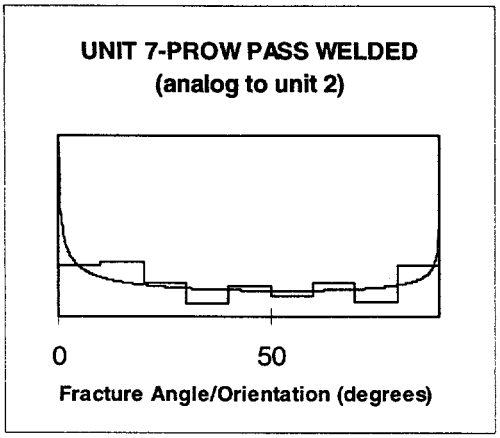
UNIT 7-PROW PASS WELDED
(analog to unit 2)
0
50
Fracture Angle/Orientation (degrees)

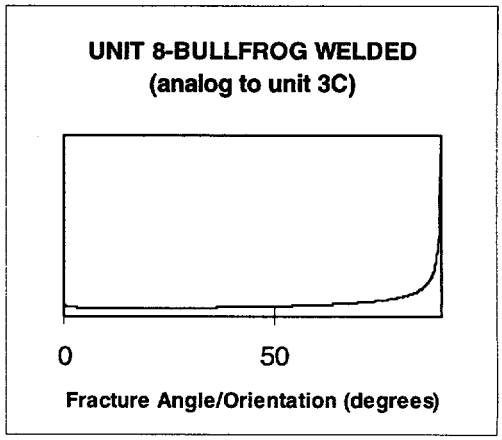
UNIT 8-BULLFROG WELDED
(analog to unit 3C)
0
50
Fracture Angle/Orientation (degrees)

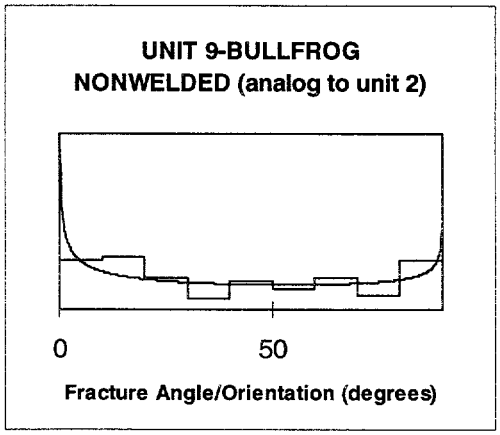
UNIT 9-BULLFROG
NONWELDED (analog to unit 2)
0
50
Fracture Angle/Orientation (degrees)

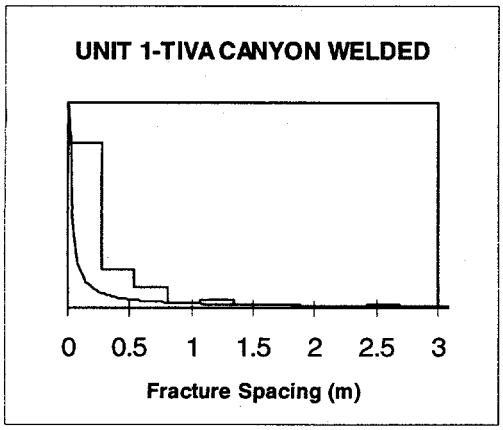
UNIT 1-TIVA CANYON WELDED
0 0.5 1 1.5 2 2.5 3
Fracture Spacing (m)

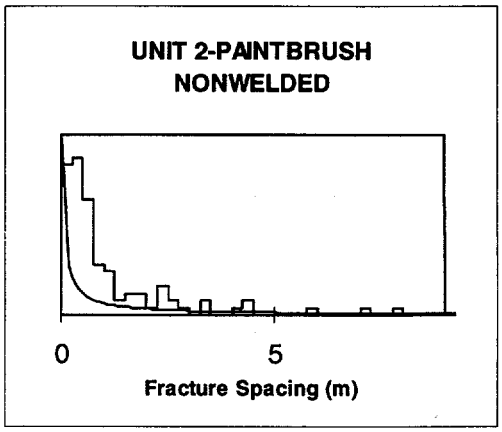
UNIT 2-PAINTBRUSH NONWELDED
0 5
Fracture Spacing (m)

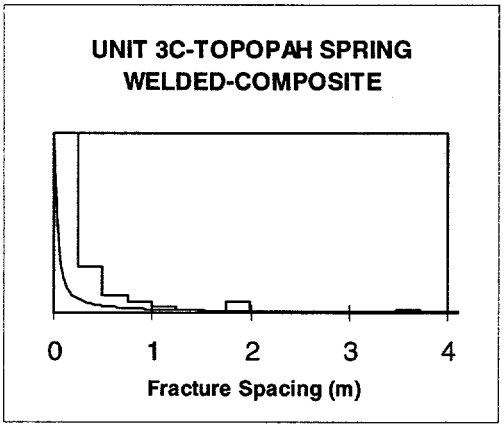
UNIT 3C-TOPOPAH SPRING WELDED-COMPOSITE
0 1 2 3 4
Fracture Spacing (m)

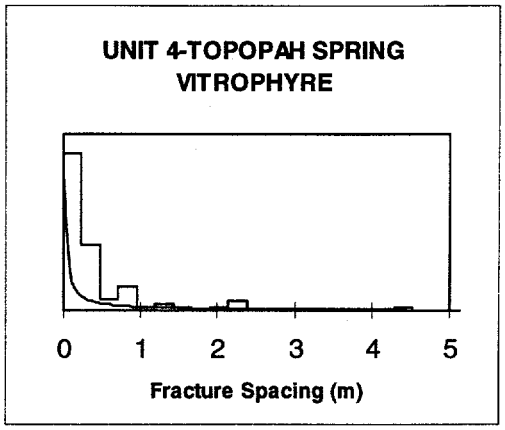
UNIT 4-TOPOPAH SPRING VITROPHYRE
0 1 2 3 4 5
Fracture Spacing (m)

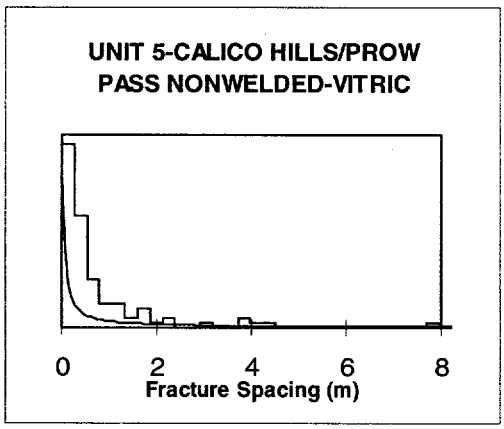
UNIT 5-CALICO HILLS/PROW PASS NONWELDED-VITRIC
0 2 4 6 8
Fracture Spacing (m)

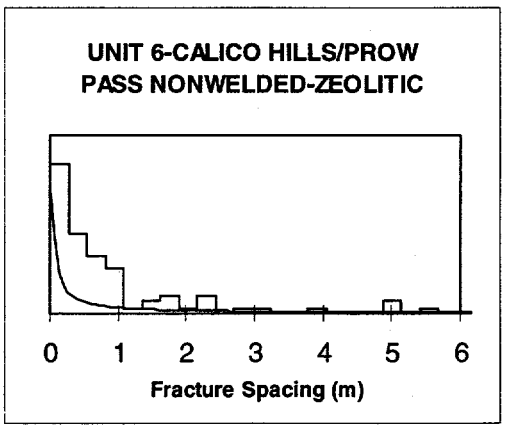
UNIT 6-CALICO HILLS/PROW PASS NONWELDED-ZEOLITIC
0 1 2 3 4 5 6
Fracture Spacing (m)

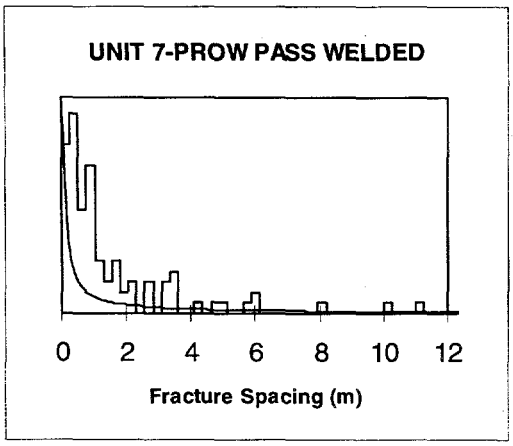
UNIT 7-PROW PASS WELDED
0 2 4 6 8 10 12
Fracture Spacing (m)

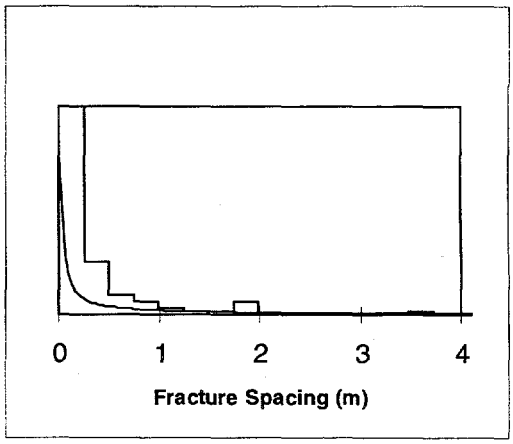
0 1 2 3 4
Fracture Spacing (m)

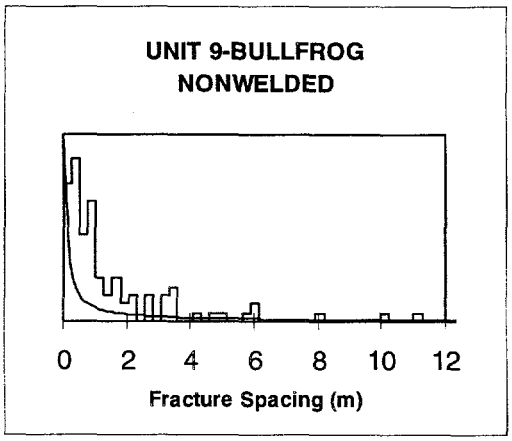
UNIT 9-BULLFROG
NONWELDED
0 2 4 6 8 10 12
Fracture Spacing (m)

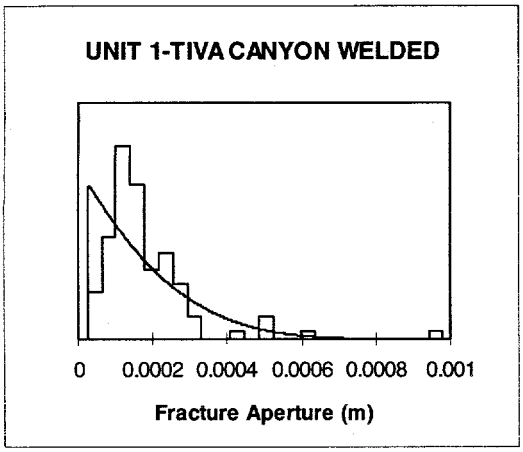
UNIT 1-TIVA CANYON WELDED
0
0.0002
0.0004
0.0006
0.0008
0.001
Fracture Aperture (m)

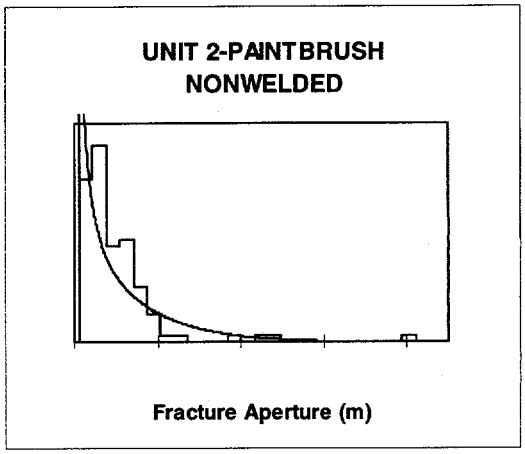
UNIT 2-PAINTBRUSH NONWELDED
Fracture Aperture (m)

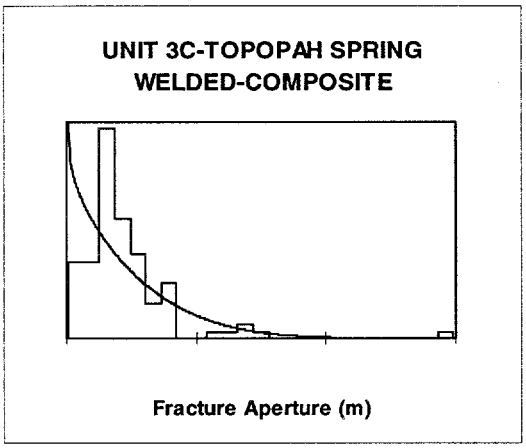
UNIT 3C-TOPOPAH SPRING WELDED-COMPOSITE
Fracture Aperture (m)

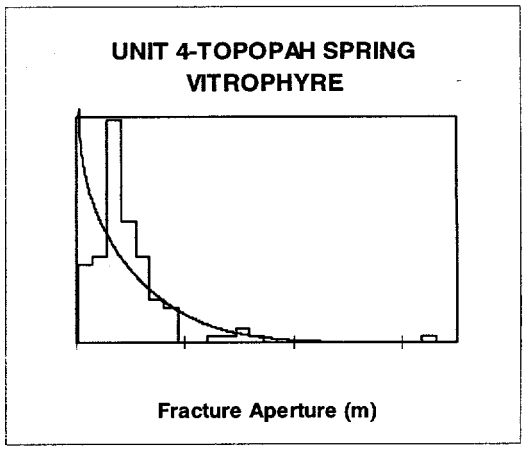
UNIT 4-TOPOPAH SPRING VITROPHYRE
Fracture Aperture (m)

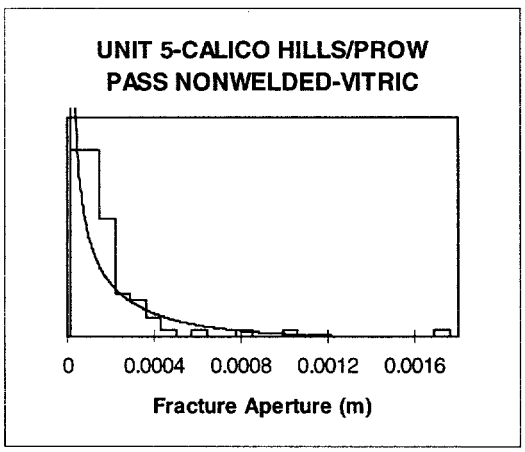
UNIT 5-CALICO HILLS/PROW PASS NONWELDED-VITRIC
0
0.0004
0.0008
0.0012
0.0016
Fracture Aperture (m)

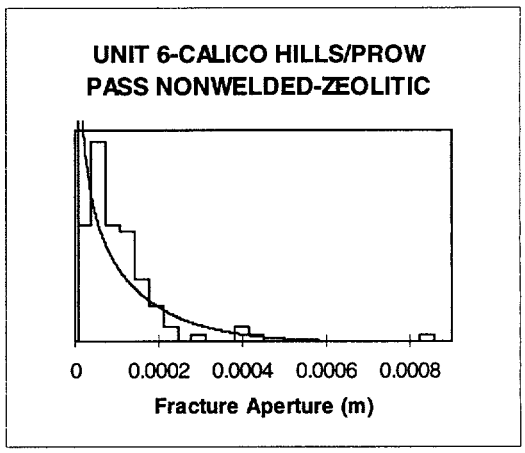
UNIT 6-CALICO HILLS/PROW PASS NONWELDED-ZEOLITIC
0
0.0002
0.0004
0.0006
0.0008
Fracture Aperture (m)

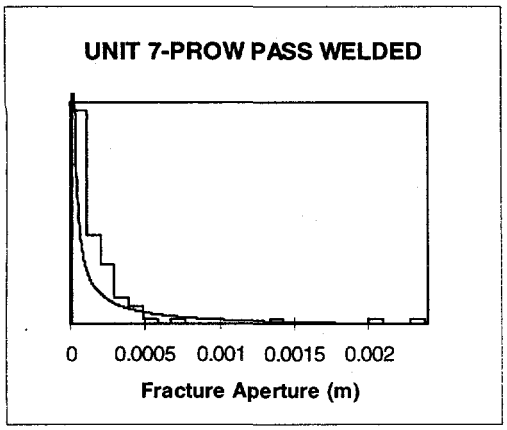
UNIT 7-PROW PASS WELDED
0
0.0005
0.001
0.0015
0.002
Fracture Aperture (m)

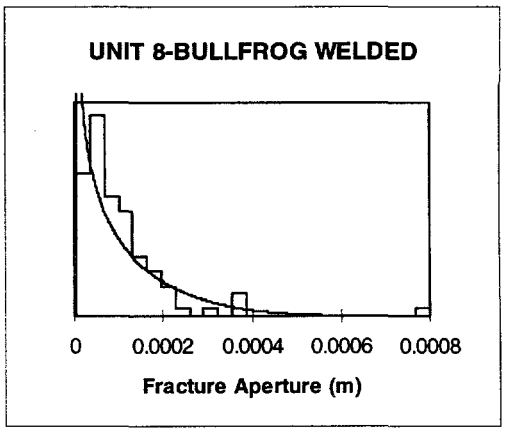
UNIT 8-BULLFROG WELDED
0
0.0002
0.0004
0.0006
0.0008
Fracture Aperture (m)

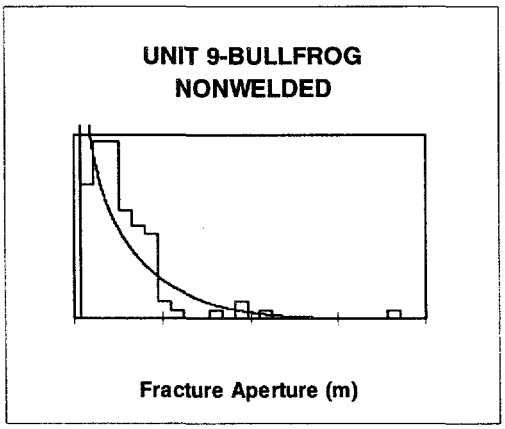
UNIT 9-BULLFROG
NONWELDED
Fracture Aperture (m)

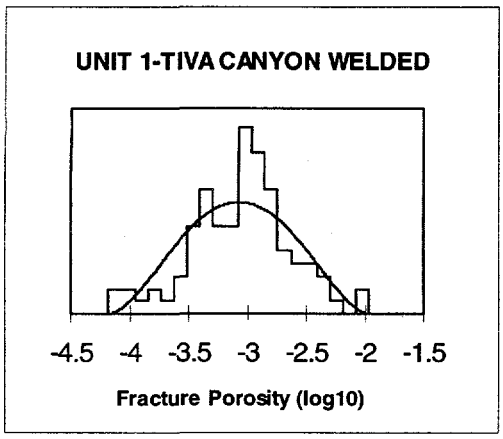
UNIT 1-TIVA CANYON WELDED
-4.5 -4 -3.5 -3 -2.5 -2 -1.5
Fracture Porosity (log10)

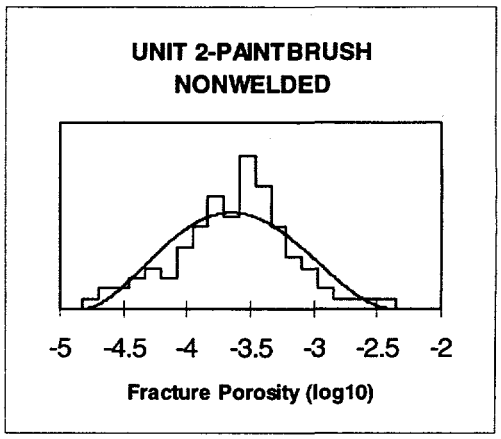
UNIT 2-PAINTBRUSH NONWELDED
-5 -4.5 -4 -3.5 -3 -2.5 -2
Fracture Porosity (log10)

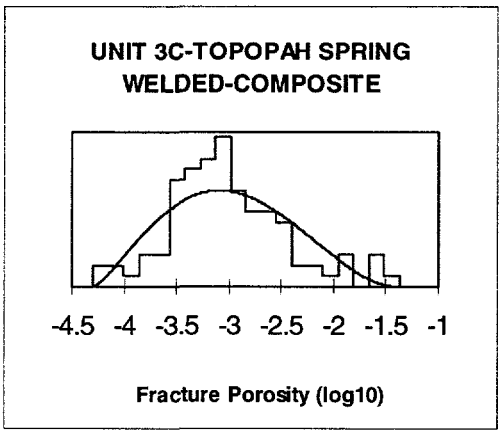
UNIT 3C-TOPOPAH SPRING WELDED-COMPOSITE
-4.5 -4 -3.5 -3 -2.5 -2 -1.5 -1
Fracture Porosity (log10)

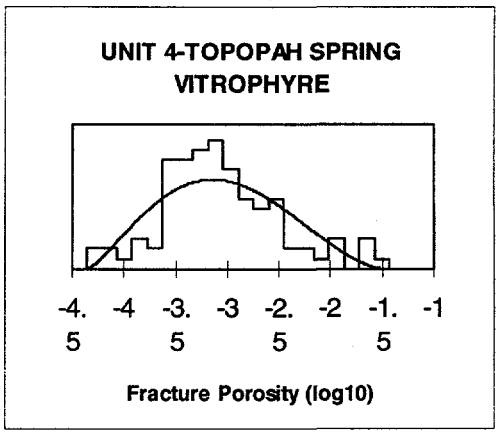
UNIT 4-TOPOPAH SPRING VITROPHYRE
-4.5 -4 -3.5 -3 -2.5 -2 -1.5 -1
Fracture Porosity (log10)

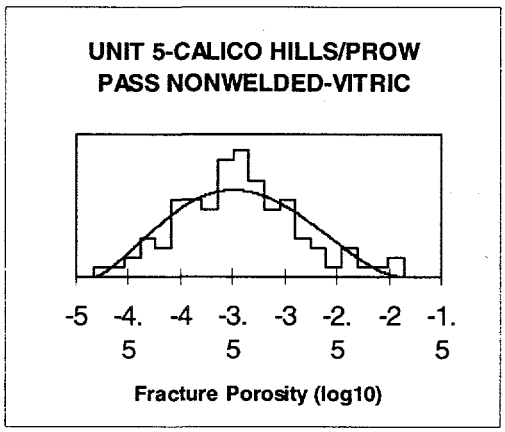
UNIT 5-CALICO HILLS/PROW PASS NONWELDED-VITRIC
-5 -4.5 -4 -3.5 -3 -2.5 -2 -1.5
Fracture Porosity (log10)

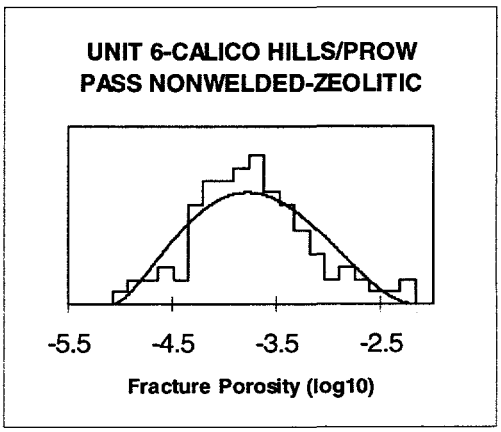
UNIT 6-CALICO HILLS/PROW PASS NONWELDED-ZEOLITIC
-5.5 -4.5 -3.5 -2.5
Fracture Porosity (log10)

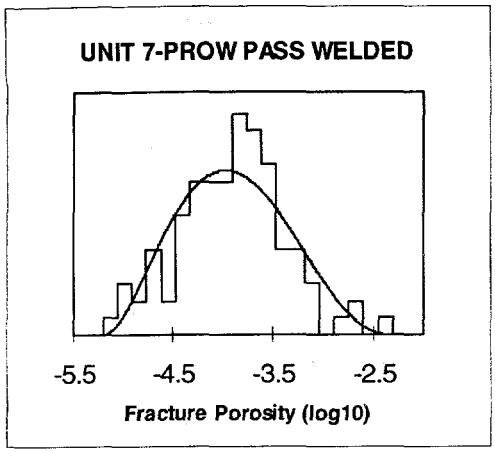
UNIT 7-PROW PASS WELDED
-5.5
-4.5
-3.5
-2.5
Fracture Porosity (log10)

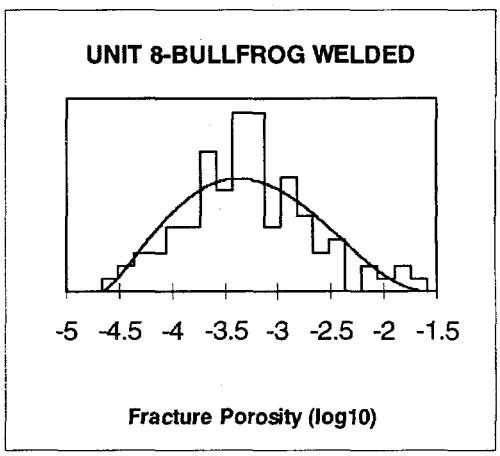
UNIT 8-BULLFROG WELDED
-5
-4.5
-4
-3.5
-3
-2.5
-2
-1.5
Fracture Porosity (log10)

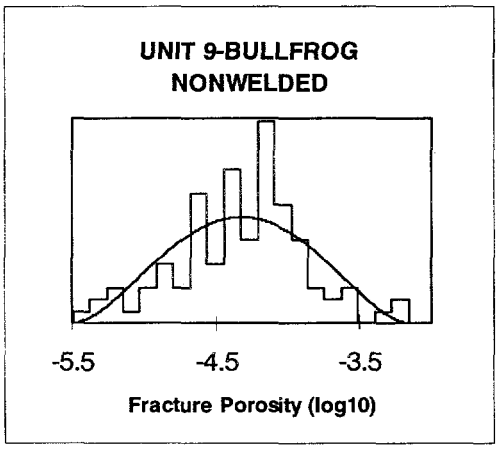
UNIT 9-BULLFROG
NONWELDED
-5.5
-4.5
-3.5
Fracture Porosity (log10)

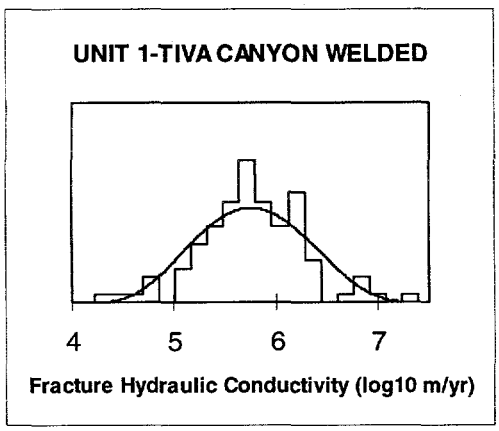
UNIT 1-TIVA CANYON WELDED
4
5
6
7
Fracture Hydraulic Conductivity (log10 m/yr)

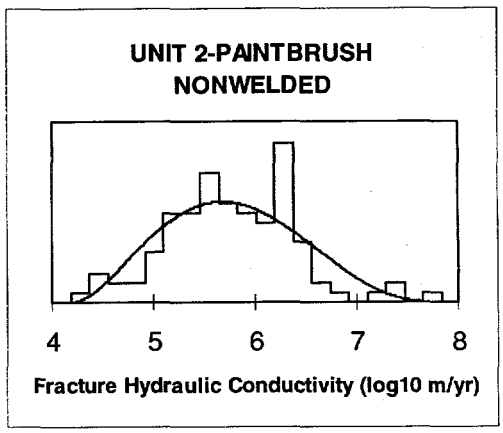
UNIT 2-PAINTBRUSH
NONWELDED
4
5
6
7
8
Fracture Hydraulic Conductivity (log10 m/yr)

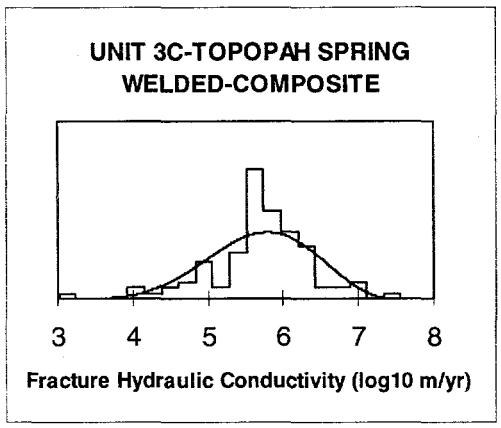
UNIT 3C-TOPOPAH SPRING
WELDED-COMPOSITE
3
4
5
6
7
8
Fracture Hydraulic Conductivity (log10 m/yr)

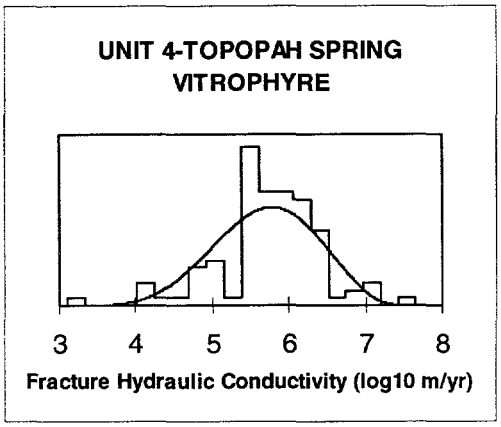
UNIT 4-TOPOPAH SPRING
VITROPHYRE
3
4
5
6
7
8
Fracture Hydraulic Conductivity (log10 m/yr)

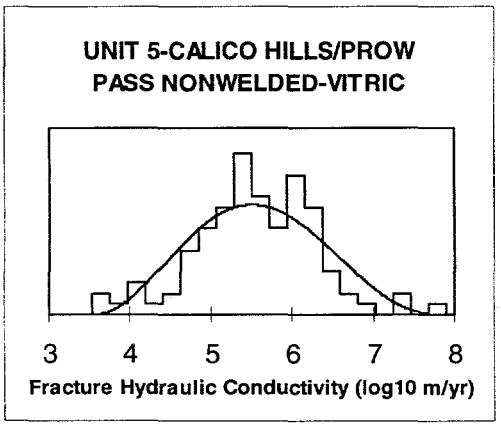
UNIT 5-CALICO HILLS/PROW
PASS NONWELDED-VITRIC
3
4
5
6
7
8
Fracture Hydraulic Conductivity (log10 m/yr)

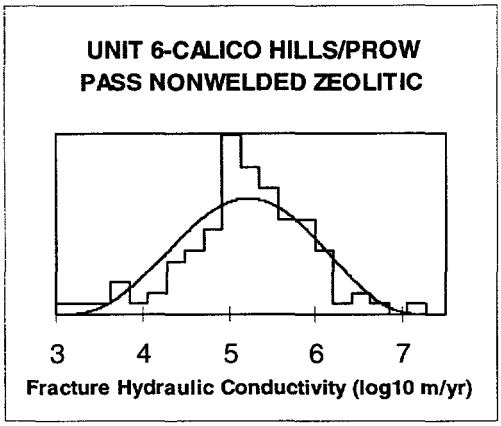
UNIT 6-CALICO HILLS/PROW
PASS NONWELDED ZEOLITIC
3
4
5
6
7
Fracture Hydraulic Conductivity (log10 m/yr)

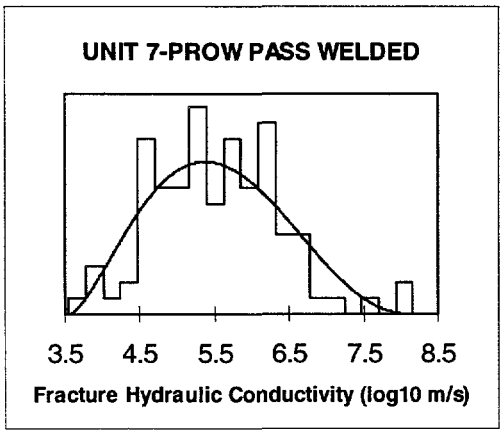
UNIT 7-PROW PASS WELDED
3.5
4.5
5.5
6.5
7.5
8.5
Fracture Hydraulic Conductivity (log10 m/s)

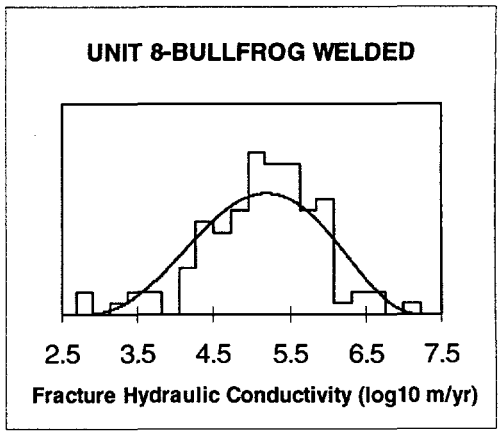
UNIT 8-BULLFROG WELDED
2.5
3.5
4.5
5.5
6.5
7.5
Fracture Hydraulic Conductivity (log10 m/yr)

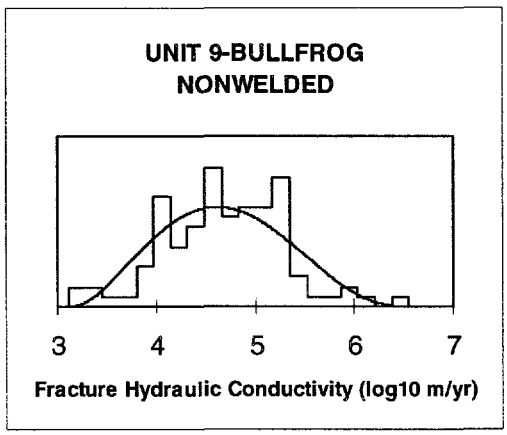
UNIT 9-BULLFROG
NONWELDED
3
4
5
6
7
Fracture Hydraulic Conductivity (log10 m/yr)

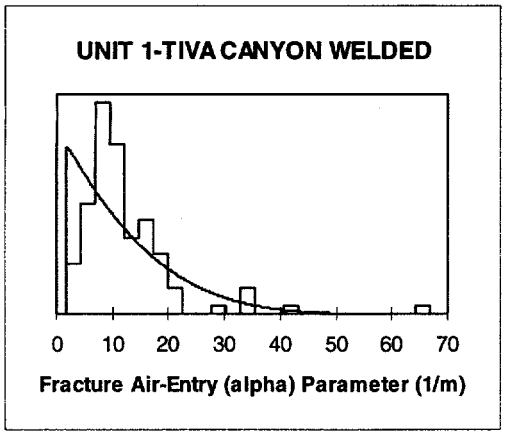
UNIT 1-TIVA CANYON WELDED
0 10 20 30 40 50 60 70
Fracture Air-Entry (alpha) Parameter (1/m)

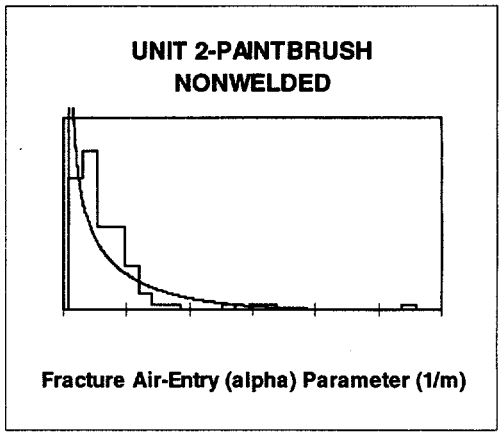
UNIT 2-PAINTBRUSH NONWELDED
Fracture Air-Entry (alpha) Parameter (1/m)

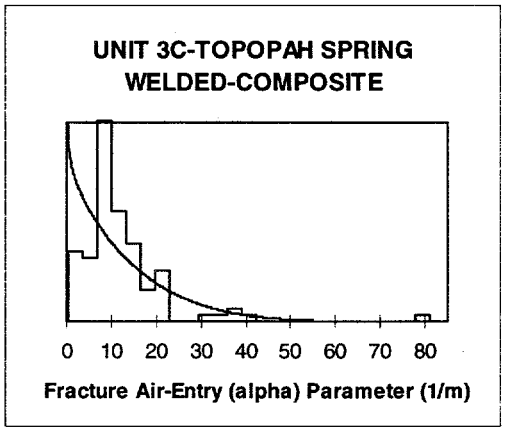
UNIT 3C-TOPOPAH SPRING WELDED-COMPOSITE
0 10 20 30 40 50 60 70 80
Fracture Air-Entry (alpha) Parameter (1/m)

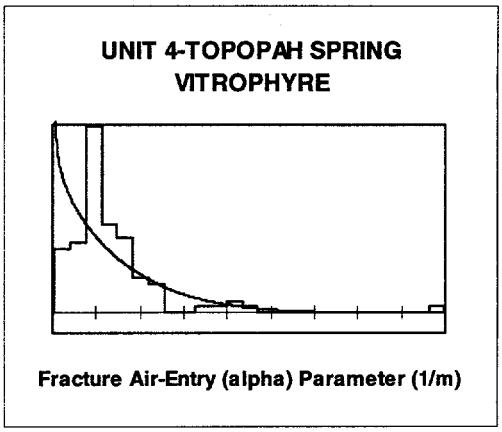
UNIT 4-TOPOPAH SPRING VITROPHYRE
Fracture Air-Entry (alpha) Parameter (1/m)

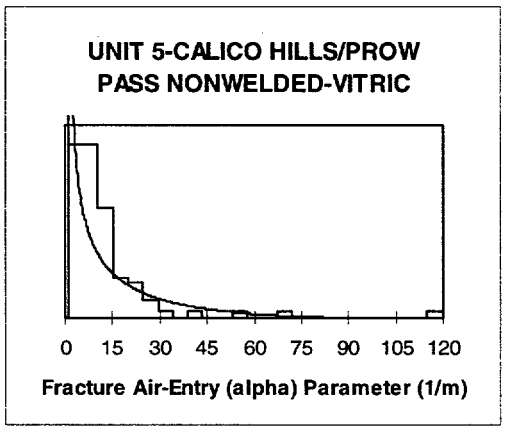
UNIT 5-CALICO HILLS/PROW PASS NONWELDED-VITRIC
0 15 30 45 60 75 90 105 120
Fracture Air-Entry (alpha) Parameter (1/m)

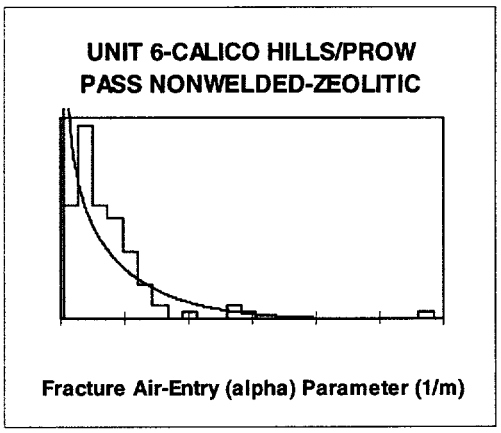
UNIT 6-CALICO HILLS/PROW PASS NONWELDED-ZEOLITIC
Fracture Air-Entry (alpha) Parameter (1/m)

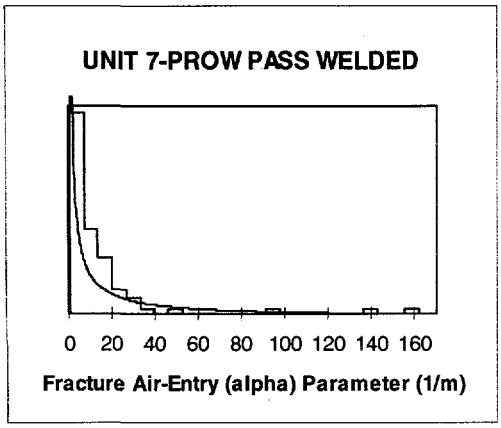
UNIT 7-PROW PASS WELDED
0 20 40 60 80 100 120 140 160
Fracture Air-Entry (alpha) Parameter (1/m)

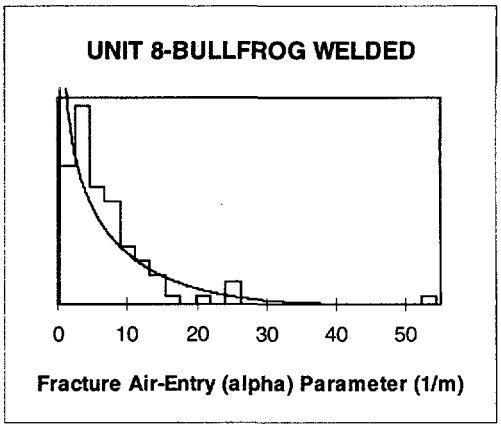
UNIT 8-BULLFROG WELDED
0 10 20 30 40 50
Fracture Air-Entry (alpha) Parameter (1/m)

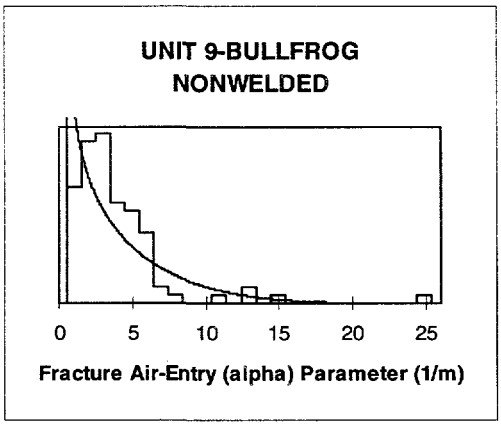
UNIT 9-BULLFROG
NONWELDED
0 5 10 15 20 25
Fracture Air-Entry (alpha) Parameter (1/m)

APPENDIX IV

Information from the Reference Information Base
Used in this Report:

References to fracture frequency and orientation are reported in the Reference Information Base are contained in this report.

Candidate Information for the
Reference Information Base:

This report contains candidate information for the Reference Information Base.

Candidate Information for the
Geographic Nodal Information Study and Evaluation System:

This report contains candidate information for the Geographic Nodal Information Study and Evaluation System. The information for GENISES is the proabability distribution functions developed from the hydrogeologic-properties data in tables 3-4, 3-7, 3-9a and b, 3-12a and b, 3-13a and b, 3-14, 3-19a and b, 3-20a and b, 3-21, 3-22, 3-23, 3-25, 3-27, 3-28, 3-29, 3-30, 3-31, and 3-32.

YUCCA MOUNTAIN SITE CHARACTERIZATION PROJECT

UC814 - DISTRIBUTION LIST

1 D. A. Dreyfus (RW-1)
Director
OCRWM
US Department of Energy
1000 Independence Avenue SW
Washington, DC 20585

1 L. H. Barrett (RW-2)
Acting Deputy Director
OCRWM
US Department of Energy
1000 Independence Avenue SW
Washington, DC 20585

1 S. Rousso (RW-40)
Office of Storage and Transportation
OCRWM
US Department of Energy
1000 Independence Avenue SW
Washington, DC 20585

1 R. A. Milner (RW-30)
Office of Program Management
and Integration
OCRWM
US Department of Energy
1000 Independence Avenue SW
Washington, DC 20585

1 D. R. Elle, Director
Environmental Protection Division
DOE Nevada Field Office
US Department of Energy
P.O. Box 98518
Las Vegas, NV 89193-8518

1 T. Wood (RW-14)
Contract Management Division
OCRWM
US Department of Energy
1000 Independence Avenue SW
Washington, DC 20585

4 Victoria F. Reich, Librarian
Nuclear Waste Technical Review Board
1100 Wilson Blvd., Suite 910
Arlington, VA 22209

5 Wesley Barnes, Project Manager
Yucca Mountain Site Characterization
Office
US Department of Energy
P.O. Box 98608--MS 523
Las Vegas, NV 89193-8608

1 Director
Office of Public Affairs
DOE Nevada Operations Office
US Department of Energy
P.O. Box 98518
Las Vegas, NV 89193-8518

8 Technical Information Officer
DOE Nevada Operations Office
US Department of Energy
P.O. Box 98518
Las Vegas, NV 89193-8518

1 P. K. Fitzsimmons, Technical Advisor
Office of Assistant Manager for
Environmental Safety and Health
DOE Nevada Operations Office
US Department of Energy
P.O. Box 98518
Las Vegas, NV 89193-8518

1 J. A. Blink
Deputy Project Leader
Lawrence Livermore National Laboratory
101 Convention Center Drive
Suite 820, MS 527
Las Vegas, NV 89109

2 J. A. Canepa
Technical Project Officer - YMP
N-5, Mail Stop J521
Los Alamos National Laboratory
P.O. Box 1663
Los Alamos, NM 87545

1 Repository Licensing & Quality
Assurance
Project Directorate
Division of Waste Management
US NRC
Washington, DC 20555

1 Senior Project Manager for Yucca
Mountain
Repository Project Branch
Division of Waste Management
US NRC
Washington, DC 20555

1 NRC Document Control Desk
Division of Waste Management
US NRC
Washington, DC 20555

1 Chad Glenn
NRC Site Representative
301 E Stewart Avenue, Room 203
Las Vegas, NV 89101

1 E. P. Binnall
Field Systems Group Leader
Building 50B/4235
Lawrence Berkeley Laboratory
Berkeley, CA 94720

1 Center for Nuclear Waste
Regulatory Analyses
6220 Culebra Road
Drawer 28510
San Antonio, TX 78284

2 W. L. Clarke
Technical Project Officer - YMP
Attn: YMP/LRC
Lawrence Livermore National Laboratory
P.O. Box 5514
Livermore, CA 94551

1 V. R. Schneider
Asst. Chief Hydrologist -- MS 414
Office of Program Coordination
and Technical Support
US Geological Survey
12201 Sunrise Valley Drive
Reston, VA 22092

1 J. S. Stuckless, Chief
Geologic Studies Program
MS 425
Yucca Mountain Project Branch
US Geological Survey
P.O. Box 25046
Denver, CO 80225

1 N. Z. Elkins
Deputy Technical Project Officer
Los Alamos National Laboratory
Mail Stop 527
101 Convention Center Drive, #820
Las Vegas, NV 89109

2 L. S. Costin, Acting
Technical Project Officer - YMP
Sandia National Laboratories
Organization 6313, MS 1325
P.O. Box 5800
Albuquerque, NM 87185

1 Ray Wallace
US Geological Survey
106 National Center
12201 Sunrise Valley Drive
Reston, VA 22092

1 L. R. Hayes
Technical Project Officer
Yucca Mountain Project Branch
MS 425
US Geological Survey
P.O. Box 25046
Denver, CO 80225

1 A. L. Flint
US Geological Survey
MS 721
P.O. Box 327
Mercury, NV 89023

1 R. E. Lewis
Yucca Mountain Project Branch
MS 425
US Geological Survey
P.O. Box 25046
Denver, CO 80225

1 D. Zesiger
US Geological Survey
101 Convention Center Drive
Suite 860, MS 509
Las Vegas, NV 89109

2 L. D. Foust
Nevada Site Manager
TRW Environmental Safety Systems
101 Convention Center Drive
Suite P-110, MS 423
Las Vegas, NV 89109

1 C. E. Ezra
YMP Support Office Manager
EG&G Energy Measurements Inc.
MS V-02
P.O. Box 1912
Las Vegas, NV 89125

1 E. L. Snow, Program Manager
Roy F. Weston, Inc.
955 L'Enfant Plaza SW
Washington, DC 20024

1 Technical Information Center
Roy F. Weston, Inc.
955 L'Enfant Plaza SW
Washington, DC 20024

1 Technical Project Officer - YMP
US Bureau of Reclamation
Code D-3790
P.O. Box 25007
Denver, CO 80225

1 B. T. Brady
Records Specialist
US Geological Survey
MS 421
P.O. Box 25046
Denver, CO 80225

1 M. D. Voegele
Technical Project Officer - YMP
M&O/SAIC
101 Convention Center Drive
Suite 407
Las Vegas, NV 89109

1 Paul Eslinger, Manager
PASS Program
Pacific Northwest Laboratories
P.O. Box 999
Richland, WA 99352

1 A. T. Tamura
Science and Technology Division
OSTI
US Department of Energy
P.O. Box 62
Oak Ridge, TN 37831

1 P. J. Weeden, Acting Director
Nuclear Radiation Assessment Div.
US EPA
Environmental Monitoring Sys. Lab
P.O. Box 93478
Las Vegas, NV 89193-3478

1 ONWI Library
Battelle Columbus Laboratory
Office of Nuclear Waste Isolation
505 King Avenue
Columbus, OH 43201

1 C. H. Johnson
Technical Program Manager
Agency for Nuclear Projects
State of Nevada
Evergreen Center, Suite 252
1802 N. Carson Street
Carson City, NV 89710

1 John Fordham, Deputy Director
Water Resources Center
Desert Research Institute
P.O. Box 60220
Reno, NV 89506

1 The Honorable Cyril Schank
Chairman
Churchill County Board of
Commissioners
190 W. First Street
Fallon, NV 89406

1 T. Hay, Executive Assistant
Office of the Governor
State of Nevada
Capitol Complex
Carson City, NV 89710

3 R. R. Loux
Executive Director
Agency for Nuclear Projects
State of Nevada
Evergreen Center, Suite 252
1802 N. Carson Street
Carson City, NV 89710

1 Brad R. Mettam
Inyo County Yucca Mountain
Repository Assessment Office
P. O. Drawer L
Independence, CA 93526

1 Lander County Board of Commissioners
315 South Humbolt Street
Battle Mountain, NV 89820

1 Vernon E. Poe
Office of Nuclear Projects
Mineral County
P.O. Box 1600
Hawthorne, NV 89415

1 Les W. Bradshaw
Program Manager
Nye County Nuclear Waste Repository
Project Office
P.O. Box 1767
Tonopah, NV 89049

1 Florindo Mariani
White Pine County Coordinator
P. O. Box 135
Ely, NV 89301

1 Judy Foremaster
City of Caliente Nuclear Waste
Project Office
P.O. Box 158
Caliente, NV 89008

1 Philip A. Niedzielski-Eichner
Nye County Nuclear Waste
Repository Project Office
P.O. Box 221274
Chantilly, VA 22022-1274

1 Dennis Bechtel, Coordinator
Clark County Nuclear Waste Div.
500 S. Grand Central Parkway
Suite 3012
Las Vegas, NV 89155-1751

1 Juanita D. Hoffman
Nuclear Waste Repository
Oversight Program
Esmeralda County
P.O. Box 490
Goldfield, NV 89013

1 Eureka County Board of Commissioners
Yucca Mountain Information Office
P.O. Box 714
Eureka, NV 89316

1 Economic Development Dept.
City of Las Vegas
400 E. Stewart Avenue
Las Vegas, NV 89101

1 Community Planning & Development
City of North Las Vegas
P.O. Box 4086
North Las Vegas, NV 89030

1 Community Development & Planning
City of Boulder City
P.O. Box 61350
Boulder City, NV 89006

1 Commission of European Communities
200 Rue de la Loi
B-1049 Brussels
BELGIUM

2 Librarian
YMP Research & Study Center
MS 407
P.O. Box 98521
Las Vegas, NV 89193-8521

1 Amy Anderson
Argonne National Laboratory
Building 362
9700 S. Cass Avenue
Argonne, IL 60439

1 Glenn Van Roekel
Director of Community Development
City of Caliente
P.O. Box 158
Caliente, NV 89008

1 G. S. Bodvarsson
Head, Nuclear Waste Department
Lawrence Berkeley Laboratory
1 Cyclotron Road, MS 50E
Berkeley, CA 94720

1 Michael L. Baughman
Intertech Services Corp.
P.O. Box 93537
Las Vegas, NV 89193

1 Clarence R. Allen
Nuclear Waste Technical Review Board
1000 E. California Blvd.
Pasadena, CA 91106

1 Donald Langmuir
Nuclear Waste Technical Review Board
109 S. Lookout Mountain Circle
Golden, CO 80401

1 Russell McFarland
Nuclear Waste Technical Review Board
100 Wilson Blvd., Suite 910
Arlington, VA 22209

1 John E. Cantlon, Chairman
Nuclear Waste Technical Review Board
1795 Bramble Drive
East Lansing, MI 48823

1 John J. McKetta
Nuclear Waste Technical Review Board
Department of Chemical Engineering
CRE Building 1450
Austin, TX 78712-1062

1 Leon Reiter
Nuclear Waste Technical Review Board
100 Wilson Blvd., Suite 910
Arlington, VA 22209

1 Victor Palciauskas
Nuclear Waste Technical Review Board
100 Wilson Blvd., Suite 910
Arlington, VA 22209

1 Dwayne Chesnut
Lawrence Livermore National Laboratory
P.O. Box 808
MS L202
Livermore, CA 94551

1 Thomas A. Buscheck
Lawrence Livermore National Laboratory
P.O. Box 808
MS L206
Livermore, CA 94551

1 Ning Lu
US Geological Survey
P.O. Box 25046
Denver Federal Center
Lakewood, CO 80225

1 Dwight Hoxie
US Geological Survey
101 Convention Center Drive
Suite 860
Las Vegas, NV 89109

1 Edward Kwicklis
US Geological Survey
P.O. Box 25046
Denver Federal Center
Lakewood, CO 80225

1 William Dudley
US Geological Survey
P.O. Box 25046
MS 425
Denver, CO 80225

1 R. R. Luckey
US Geological Survey
Building 53
Denver Federal Center
Room H2314/MS 5421
Denver, CO 80225

1 A. B. Gureghian
Center for Nuclear Waste
Regulatory Analyses
6220 Culebra Road
San Antonio, TX 78228-0510

1 Dr. William M. Murphy
Center for Nuclear Waste
Regulatory Analyses
Southwest Research Institute
6220 Culebra Road
San Antonio, TX 78238-5166

1 Michael J. Apted
Intera Information Technologies, Inc.
3609 S. Wadsworth Blvd, Suite 500
Denver, CO 80235

1 Wei Zhou
Intera Information Technologies, Inc.
3609 S. Wadsworth Blvd, Suite 500
Denver, CO 80235

1 R. W. Nelson
M&O/INTERA
101 Convention Center Drive
Suite P110
Las Vegas, NV 89109

1 Jerry McNeish
M&O/INTERA
MS 423
101 Convention Center Drive
Las Vegas, NV 89109

1 Srikanta Mishra
M&O/INTERA
MS 423
101 Convention Center Drive
Las Vegas, NV 89109

1 C. Thomas Statton
Yucca Mountain Project
M&O/WCFS
MS 423
101 Convention Center Drive
Las Vegas, NV 89109

1 Suresh Pahwa
M&O/INTERA
6850 Austin Center Blvd.
Suite 300
Austin, TX 78731

1 Robert Andrews
M&O/INTERA
MS 423
101 Convention Center Drive
Las Vegas, NV 89109

1 Darren Jolley
M&O/INTERA
MS 423
101 Convention Center Drive
Las Vegas, NV 89109

1 Yanyong Xiang
M&O/INTERA
MS 423
101 Convention Center Drive
Las Vegas, NV 89109

1 Dave Sevougian
M&O/INTERA
MS 423
101 Convention Center Drive
Las Vegas, NV 89109

1 Frank Tsai
Yucca Mountain Project
M&O/WCFS
MS 423
101 Convention Center Drive
Las Vegas, NV 89109

1 Jim Duguid
M&O/INTERA
2650 Park Tower Drive
Suite 800
Vienna, VA 22180

1 Ines Triay
Los Alamos National Laboratory
MS CST-7
P.O. Box 1663
Los Alamos, NM 87545

1 Dr. June Fabryka-Martin
Los Alamos National Laboratory
MS J-514
P.O. Box 1663
Los Alamos, NM 87545

1 George Zyvoloski
Los Alamos National Laboratory
MS F-665
P.O. Box 1663
Los Alamos, NM 87545

1 Andy Wolfsburg
Los Alamos National Laboratory
MS EES-5
P.O. Box 1663
Los Alamos, NM 87545

1 Johan Andersson
SKI
Division of Nuclear Waste
Sehlstedtgatan II
Box 27106
S-102 52 Stockholm
SWEDEN

1 Richard Codell
US Nuclear Regulatory Commission
MS 4-H-3
Washington, DC 20555

1 Norman A. Eisenberg
US Nuclear Regulatory Commission
MS 4-H-3
Washington, DC 20555

1 Claudia Newbury
Yucca Mountain Project Office
US Department of Energy
P.O. Box 98608
MS 523
Las Vegas, NV 89193-8518

1 J. Russell Dyer
Yucca Mountain Project Office
US Department of Energy
P.O. Box 98608
MS 425
Las Vegas, NV 89193-8518

5 Eric Smistad
Yucca Mountain Project
US Department of Energy
MS 523
101 Convention Center Drive
Las Vegas, NV 89109

1 Susan B. Jones
Yucca Mountain Project
US Department of Energy
MS 523
101 Convention Center Drive
Las Vegas, NV 89109

1 Abraham Van Luik
Yucca Mountain Project
US Department of Energy
101 Convention Center Drive
Las Vegas, NV 89109

1 April V. Gil
Yucca Mountain Project
US Department of Energy
MS 523
101 Convention Center Drive
Las Vegas, NV 89109

1 Ardyth Simmons
Yucca Mountain Project
US Department of Energy
MS 523
101 Convention Center Drive
Las Vegas, NV 89109

1 Tom Bjerstedt
Yucca Mountain Project
US Department of Energy
MS 523
101 Convention Center Drive
Las Vegas, NV 89109

1 Scott Sinnock
TRW
101 Convention Center Drive
Suite P110
Las Vegas, NV 89109

1	Jean Younker TRW 101 Convention Center Drive Suite P110 Las Vegas, NV 89109		MS	
		2	1330	C. B. Michaels, 6352 100/12541/SAND94-0244/QA
		20	1330	WMT Library, 6352
		1	9018	Central Technical Files, 8523-2
		5	0899	Technical Library, 13414
		1	0619	Print Media, 12615
1	Dr. John Kessler Nuclear Power Division EPRI P.O. Box 10412 Palo Alto, CA 94303-0813	2	0100	Document Processing, 7613-2 for DOE/OSTI
		1	0835	R. R. Eaton, 1513
		1	1320	M. D. Siegel, 6119
		1	1324	P. D. Davies, 6115
		1	1324	C. A. Rautman, 6115
		1	1324	C. Ho, 6115
		1	1325	R. E. Finley, 6313
		1	1325	J. Pott, 6313
		1	1325	E. E. Ryder, 6313
		1	1325	S. R. Sobolik, 6313
		1	1326	H. A. Dockery, 6312
		10	1326	R. W. Barnard, 6312
		1	1326	G. E. Barr, 6312
		1	1326	J. H. Gauthier, 6312
		1	1326	T. H. Robey, 6312
		1	1326	L. H. Skinner, 6312
		1	1326	W. G. Perkins, 6312
		10	1326	A. R. Schenker, 6312
		1	1326	S. A. Shannon, 6312
		1	1326	M. L. Wilson, 6312
		1	1347	D. G. Guerin, 7582
		1	1399	M. C. Brady, 6314
		1	1399	F. J. Schelling, 6314
1	Per-Eric Ahlstrom Research Director Swedish Nuclear Fuel and Waste Management Company Box 5864 S-102 48 Stockholm, SWEDEN			
1	W. A. Seddon AECL Technologies 9210 Corporate Blvd. Suite 410 Rockville, MD 20850			
1	Yvonne Tsang Lawrence Berkeley Laboratory Earth Sciences Division 1 Cyclotron Road Berkeley, CA 94720			
1	Karsten Pruess Lawrence Berkeley Laboratory Earth Sciences Division 1 Cyclotron Road Berkeley, CA 94720			
1	Joseph Wang Lawrence Berkeley Laboratory Earth Sciences Division 1 Cyclotron Road Berkeley, CA 94720			
1	W. W. L. Lee Environmental Evaluation Group 7007 Wyoming NE Suite F-2 Albuquerque, NM 87109			
1	Dr. Martin Mifflin Waster Resources Center Desert Research Center 2505 Chandler Ave., Suite 1 Las Vegas, NV 89120			
1	Leo Scully Los Alamos Technical Associates 2400 Louisiana Blvd., NE Building 1, Suite 400 Albuquerque, NM 87110			